Landscape Evolution in Namibia and Antarctica: Quantifying Denudation Rates Using *In-Situ* Cosmogenic Isotope Analysis

by

Hermione Anne Phoebe Cockburn

Submitted for the Degree of Doctor of Philosophy

The University of Edinburgh

1998

Declaration of Originality

I hereby declare that the work presented in this thesis has been carried out by myself, except where due acknowledgement is made, and has not been submitted for any other degree.

Hermione A. P. Cockburn

Acknowledgements

The work presented in this thesis was supported principally by NERC studentship GT4/93/8/G but also by NERC grant GR3/9128 (D.E. Sugden and M. A. Summerfield) and GR9/01730 (M. A. Summerfield). Additional funding was gratefully received from the Carnegie Trust for the Universities of Scotland and the Department of Geography, University of Edinburgh.

I would like to offer sincere thanks to Mike Summerfield for supervision, guidance and encouragement throughout the preparation of this thesis. Many, many thanks are also due to Michele Seidl as an unofficial second supervisor, motivator and friend.

My work has benefited from numerous discussions and comments from Alastair Fleming, Sarah Metcalfe, Paul Bishop, Alun Hubbard, Susan Ivy-Ochs, Ross Purves, David Sugden, Bob Finkel, Rob Ellam, and Rachel Oxburgh. I would like to thank them all for their time and patience, but of course any errors in the thesis are entirely my own.

In the Department of Geography I would like to thank the following people for their encouragement and support: Alun Hubbard, Jane Boygle, Malcolm Murray, Anthony Newton, Mike Bentley, Sarah Davies, Nick Spedding, Simon Zisman, Alastair Borthwick, Fran Taylor.

Prior to sample preparation at the Department of Geography, University of Edinburgh, it was necessary to set up a suitable laboratory. This included design of a room with an appropriate level of cleanliness and purchase of all the equipment needed from a new pure-water system right down to the last custom made quartz vial. The procedure began with submission of funding proposals that resulted in a £15,000 equipment grant from the Faculty of Social Sciences as well as £40,000 for renovation of an existing laboratory. I would like to thank Sarah Metcalfe for overseeing the laboratory renovation and my thanks to her and Andy Dugmore for assistance and support and to Bob McCulloch and Chris Minty for their input.

Some sample preparation was carried out at the Scottish Universities Research and Reactor Centre, East Kilbride. I would like to thank Rob Ellam, Tony Fallick, Fin Stuart, Julian Jocelyn, Gawen Jenkins and Susan Waldren and the technical staff of the Isotope Geoscience Group for their help and advice. Susan Ivy-Ochs, Michael Ochs and Peter Kubik are thanked for their help and kindness during sample measurement at ETH. Bob Finkel is gratefully acknowledged for AMS measurement at LLNL, and Fin Stuart and Tibor Dunai at Vrije Universiteit, Amsterdam for ^{21}Ne analysis.

The Geological Survey of Namibia is gratefully acknowledged for logistical support during two field seasons in central Namibia. I would especially like to thank Brian Hoal, Bruce Groenewald, Wulf Hergenberger and Raphael Simahima. I would also like to acknowledge the Ministry of Wildlife, Conservation and Tourism in Namibia for permitting me to work in the Namib-Naukluft Park. Excellent field assistance was provided by Imogen Russon and Alastair Fleming.

During my visit to Lamont-Doherty Earth Observatory of Columbia University, Rachel Oxburgh and Gideon Henderson made me feel very welcome and it was a pleasure to be part of the Department of Geochemistry, if only for a short while. Michele Seidl is thanked for showing me how to do Be and Al sample preparation and thanks also to Neil Shubin and Mick Seidl for hospitality during my visits to the United States.

I would like to offer enormous thanks to Jonathan Peltenburg for helping me so much and offering never ending support over the last three years. I am also especially grateful for the support and encouragement I have received from my parents, family and friends, without which I could not have completed this thesis.

Abstract of Thesis

Quantifying denudation rates is fundamental to understanding the way landscapes evolve. Such data are required to constrain numerical models of long-term landscape evolution, the development of which is outrunning our ability to constrain them empirically. *In-situ* cosmogenic isotope analysis is a valuable addition to the range of techniques currently available to measure denudation rates and is especially useful in providing information over periods of 10^3 - 10^6 a. *In-situ* cosmogenic ^{10}Be, ^{26}Al and ^{21}Ne concentrations from locations in central Namibia and the Transantarctic Mountains, Antarctica have been used to investigate rates of landscape change in passive margin settings and contrasting hot and cold arid conditions.

Concentrations of cosmogenic ^{10}Be and ^{26}Al in quartz separated from 14 samples from the Gamsberg in central Namibia have been measured using accelerator mass spectrometry. The Gamsberg is a flat-topped residual forming part of the Great Escarpment of central Namibia. Rates of summit denudation range from 0.2 to 0.8 m Ma^{-1} and rates of slope retreat have been ~10 m Ma^{-1} over the past 0.04 to 1.5 Ma. The data indicate that backwearing is much more significant than downwearing but that summit denudation is occurring. Low rates of escarpment retreat of ~10 m Ma^{-1} are incompatible with the idea that retreat from the coast has been at a uniform rate since rifting occurred ~130 Ma BP. The data are consistent with geological evidence and data from apatite fission track thermochronology that suggest that the escarpment retreated rapidly soon after rifting but has not retreated significantly during the Tertiary.

Measurements of cosmogenic ^{10}Be and ^{26}Al from three granite bornhardts on the coastal plain of Namibia seaward of the Great Escarpment in the arid/hyper-arid central Namib Desert indicate mean rates of summit lowering ranging from 2.2 to 6.3 m Ma^{-1} over the past 1-3 x 10^5 a. Low variability in estimated denudation rates between the sampling sites and the long-term persistence of an arid climate implies that a rate of summit lowering of ~5 m Ma^{-1} has characterised bedrock exposures in the central Namib for at least the past 10 Ma, and possibly throughout much of the Cenozoic. The complex exposure history of some samples appears to be due to the mode of inselberg weathering and mass wasting.

Cosmogenic ^{10}Be, ^{26}Al and ^{21}Ne denudation rate estimates from high-elevation surfaces and rectilinear slopes in the Dry Valleys region of Antarctica suggest very slow rates of denudation of <1 m Ma^{-1} for at least the past 2-5 Ma. The rates from all three isotopes for each sample are generally consistent and where paired isotopic data are available exposure histories appear to be simple. The data are fully compatible with existing cosmogenic isotope data and independent evidence from the region that imply minimal landscape modification and a polar, hyper-arid climate since the late Miocene. The data support a hypothesis that the East Antarctic Ice Sheet has been essentially stable over this period rather than experiencing significant fluctuations as recently as the Pliocene.

It has been demonstrated that *in-situ* cosmogenic isotope analysis can provide previously unobtainable data on denudation rates over timescales intermediate between short-term process studies and long-term estimates from techniques such as thermochronology. Used in conjunction with other techniques, cosmogenic isotopes analysis has significant potential for evaluating controls on denudation rates in a range of geomorphic settings and constraining models of long-term landscape evolution.

Table of Contents

page number

List of Figures

page number

Chapter 5:

Chapter 6:

List of Tables

Chapter 1:

Introduction

1.1 Aim of Thesis

The overall aim of this thesis is to quantify rates of denudation using *in-situ* cosmogenic isotope analysis. In order to investigate landscape evolution in passive continental margin settings, the technique is applied to the tectonically similar, but climatically contrasting, hot and cold arid locations of central Namibia and the Dry Valleys region of the Transantarctic Mountains, Antarctica.

1.2 The Importance of Denudation Rates

Quantification of denudation rates is fundamental to an understanding of the way landscapes evolve. However, constraining rates of denudation over time scales applicable to landscape evolution (10^5-10^7 a) remains one of the greatest challenges to geomorphology. Denudation is a key component of all landscape change given that geomorphic evolution is, essentially, a result of weathering and erosion in some parts of the landscape and deposition in other parts, operating against a background setting of tectonic and climatic controls. Although denudation is sometimes used as a synonym for erosion, it is used here in a broader sense to include all processes that result in the wearing down or progressive lowering of the Earth's surface including: weathering; erosion; mass wasting; and transportation (Jackson, 1997). A knowledge of denudation rates at a variety of different spatial and temporal scales is desirable for a number of reasons, including: 1) discovering what rates characterise certain environments and therefore to assess the relative importance of controlling variables; 2) assessing the relative importance of surface processes operating on different morphological elements of the landscape; 3) evaluating styles of landscape development, for example, the relationship between downwearing and backwearing in relief reduction; 4) quantifying the denudational component of global mass balance studies; and 5) constraining the antiquity of landscapes and assessing how long they might survive. In geomorphology over the past ~15 years there has been renewed interest in

long-term landscape evolution coupled with a growing concern that, within this context, it is important to be able to link short-term, relatively small-scale studies with macroscale ideas (Thomas and Summerfield, 1987; Summerfield, 1996a; Sugden *et al.,* 1997). Part of the reason for this has been the realisation that denudation can play a key role in moderating tectonic mechanisms, and possibly climate, through the isostatic response of the crust to sediment loading and denudational unloading (Fig. 1.1), (Molnar and England, 1990; Gilchrist *et al.,* 1994a). As a result, linking of surface and tectonic processes is becoming increasingly important in landscape modelling both in passive and active tectonic settings (Gilchrist and Summerfield, 1990; Koons, 1989; Beaumont *et al.,* 1992). A particular concern currently facing geomorphologists is that the sophistication of numerical models of long-term landscape development, such as those described by Beaumont *et al.* (1998), is outrunning our ability to constrain surface process rates over geologically meaningful periods of time and hence to assess the adequacy of such models.

Direct assessment of denudation is, in general, problematic because the essence of the mechanism is to remove the evidence that it has occurred and to deposit this evidence over a poorly defined, often large area. The problem becomes increasingly marked over longer periods of time. Bishop (1998, p. 8) has recently summed up the problem, in the context of constraining landscape evolution, by posing the question: "how do we handle the methodological question of reconstructing the history of denudational terrains....when the central element of this history....involves the destruction of the evidence (the evidence of past landforms)?". This is particularly true of passive continental margins which comprise a large proportion of the Earth's continental margins (Summerfield, 1991a). Accumulations of sediment up to 10 km thick located in offshore basins surrounding these margins attest to the dominant role of onshore denudation in their evolution (Allen and Allen, 1990). However, a lack of knowledge regarding the pattern, timing and rate of this denudation has meant that, in some regions, traditional explanations of landscape evolution have persisted largely unchallenged (Gilchrist, 1995). This is particularly true of southern Africa (King, 1962, 1983; Twidale, 1992) where models remain quantitatively deficient. New models of passive margin evolution, both conceptual and quantitative, which conflict with traditional viewpoints (Gilchrist and Summerfield, 1990; Kooi and Beaumont, 1994, 1996; Tucker and Slingerland, 1994), require improved empirical constraints over relevant time scales in order to allow validation and gain credibility.

In arid environments, rates of denudation are poorly constrained. Arid climates are often characterised by infrequent, but high magnitude, storm events and resulting denudational processes can be very effective, especially as they are enhanced by a general lack of vegetation

(Cooke *et al.*, 1993). However, as denudation events are episodic in nature, overall rates of denudation have been hard to measure by traditional techniques, which commonly monitor sediment yields over short periods of time only. It has been suggested that rates of landscape change in arguably the world's most consistently hyper-arid, polar environment of the Dry Valleys region of the Transantarctic Mountains in Antarctica were much greater during the Pliocene than they are today, due to the combined effects of climatic change and tectonic uplift (Webb *et al.*, 1984; Barrett *et al.*, 1992). A sound assessment of the range of rates in both hot and cold arid regions linked with an evaluation of how long these processes have been operating, is required to resolve such controversies and for a full appreciation of landscape evolution in arid locations.

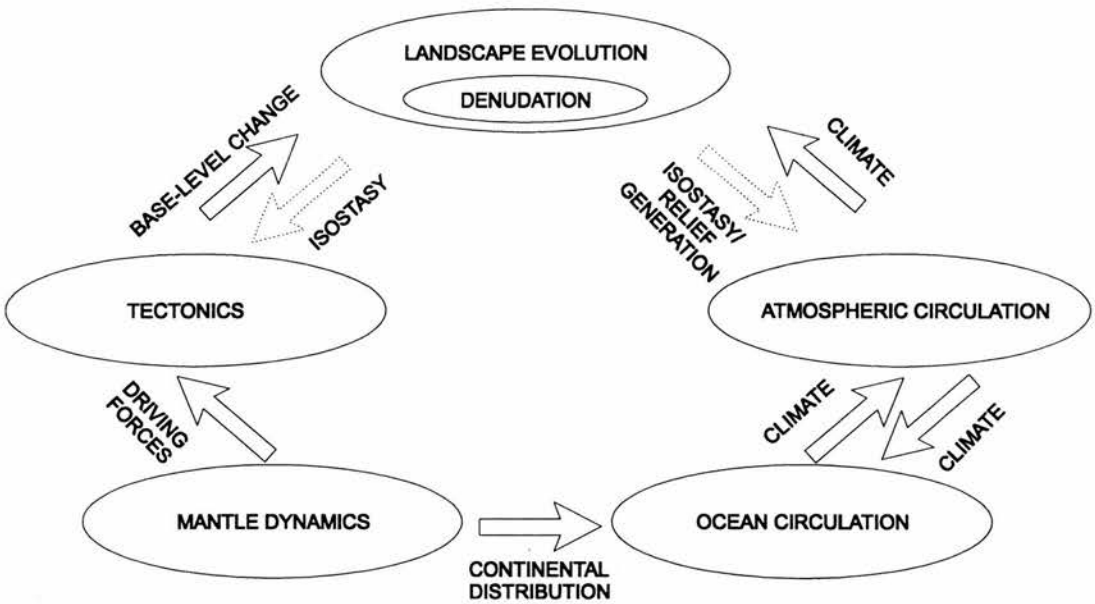

Figure 1.1: Factors influencing denudation and landscape evolution at the macro-scale. The diagram illustrates that the interaction between tectonics, atmospheric circulation and landscape evolution are not simple cause and effect relationships due to the influence of denudation and isostatic rebound (after Beaumont et al., 1998).

1.3 Quantification of Denudation Rates

Since the pioneering days of geomorphic thought, denudation has been a key issue (Chorley *et al.*, 1964). Early protagonists such as Hutton (1785) and Lyell (1830) were concerned with rates of landscape development and essentially advocated slow continuous rates of change in contrast to the alternative view of the time that catastrophic events had shaped the landscape, not as is

often quoted, with respect to biblical events such as Noah's flood, but based on more scientific, empirical arguments for sudden geological events (Gould, 1977). However, as geomorphology developed into a distinct discipline in the late Nineteenth and early Twentieth Centuries it became increasingly concerned with the long-term, morphological development of entire landscapes and less concerned with rates of change. The widespread popularity of the cyclic approach to landscape analysis of Davis (1899) and his disciples (at least in the English speaking world), and the encompassing assumptions about how long such cycles of erosion require (~10^6 - 10^7 a), precluded studies specifically concerned with rates of processes (Gilchrist and Summerfield, 1994). Of course there were some exceptions, most of which addressed the operation of processes over short periods of time such as soil erosion and coastal erosion which have social impacts (Goudie, 1995).

In the 1960s, geomorphology experienced a marked shift away from the grand Davisian style of landscape analysis towards a strong emphasis on studies of surface processes, which were invariably concerned with much more limited temporal and spatial scales. Many reasons for this have been suggested, but the most likely are a lack of satisfaction with the treatment of process by the evolutionary models as well as the emergence of new, quantitative techniques (Saunders and Young, 1983). Also highly significant was the lack of a coherent tectonic framework of the classical approach, combined with the development of tectonic theory in other disciplines (Gilchrist and Summerfield, 1994), as well as a perceived relevance of modern process studies to engineering and landscape management (Goudie, 1995). The transition from form to process as the central theme in geomorphology resulted in numerous attempts to assess localised process rates, particularly surface processes on slopes as well as rates of total denudation, and to link these rates to controlling variables such as climate (e.g. Langbein and Schumm, 1958). There was an understandable tendency for studies to be concentrated in dynamic areas which resulted in a bias against making measurement in situations where little activity was apparent (Goudie, 1995). Consequently, not many studies were carried out in arid locations.

Over 300 publications dating from the early 1960s to the early 1980s, which resulted from the transition to a process paradigm in geomorphology, were compiled by Saunders and Young (1983). Although specific surface processes such as creep and solifluction had had significant attention, in terms of landscape evolution, the results of total denudation are most relevant here. The overall conclusion of the studies was that badland environments and steep glaciated areas had the highest overall rates of denudational processes. The small number of studies in arid environments meant that only a minimum typical rate of 10 m Ma^{-1} (equivalent to mm ka^{-1}) could

be estimated. In semi-arid environments, which included most badland sites, measured rates ranged from 100 to 1000 m Ma^{-1} (Saunders and Young, 1983).

The most widely used technique to estimate rates of total denudation over short time scales has been to monitor the load of rivers and assign a depth or rate of denudation to the total catchment area, be it a first order stream or a continental scale drainage basin. This has also included the use of sedimentation in reservoirs behind dams. There are however, several problems inherent with such an approach (Saunders and Young, 1983; Goudie, 1995):

1. River load data not only include denudation from the catchment slopes but also river bed and bank erosion, therefore mean rates cannot easily be translated to catchment lowering rates.
2. Many records have referred to suspended load only whereas the dissolved load can be significant and the ratio of dissolved to suspended load varies greatly between catchments. Also little account is usually taken of bed load. Non-denudational components to river loads have rarely been subtracted from measurements.
3. Temporal variation in the discharge of load requires longer-term monitoring than is usually carried out. The sediment delivery ratio suffers from high variability and the sediment can be stored for indeterminate periods of time before release.
4. A high proportion of rivers have been subjected to human influences and therefore modern sediment load data can be atypical of the past.

Despite these problems, this approach is generally regarded as the most viable method for linking variations in denudation rates to specific controlling variables (Summerfield, 1991a). A recent compilation by Summerfield and Hulton (1994), which has tried to address some of the problems outlined above, has emphasised the importance of basin relief and runoff rather than the more traditional viewpoint that climate is the key variable for determining of rates of denudation.

As already mentioned, the past ~15 years has seen some re-emergence of the longer-term perspective within geomorphology. In other branches of the earth sciences there has been a dramatic development in geophysical modelling and new geochronometric techniques for understanding long-term, large-scale landscape evolution (Beaumont *et al.*, 1998). An important realisation has been that denudation and topographic development is not simply an effect of tectonic mechanisms but, through the mechanism of isostasy and the response of crustal stress patterns to unloading, denudation can actually play a key role in moderating tectonic forces (Fig. 1.1). Although still evolving, the interface between earth science disciplines is becoming

increasingly blurred and has led to greater requirements for empirical data relevant to landscape evolution, such as denudation rates, over long time-scales (Merritts and Ellis, 1994; Summerfield, 1996a). The greatest limitation with using present-day measurements of denudation as a basis for understanding long-term landscape evolution is the short period of time over which they apply. There is an implicit assumption that the recurrence interval of the most important denudation events within a system is within the monitoring period. However, if a major low frequency, high magnitude event which determines peak denudation for the catchment or slope under investigation, does not occur then short term data will be misleading. Extrapolation of data of this kind poses further problems because of potential changes in the overall rate of denudation through time, for example, due to a change in climate. So that geomorphic processes can be incorporated into long-term models, there is a need for the limited temporal and spatial scales that geomorphologists have tended to work with over the past few decades to be re-focused (Kirkby, 1994). For long-term rates, over periods of time $>10^3$ a, it is necessary to examine evidence for denudation using other techniques.

Several of the techniques available to monitor denudation on longer time scales than the analysis of modern sediment yields have resulted from new technological developments in the past twenty years. These can be divided into three principal categories: 1) geochronometric techniques; 2) analysis of continental sediments, both on and offshore in sedimentary basins; and 3) thermochronology. Geochronometric techniques, such as K-Ar and $^{40}Ar/^{39}Ar$ dating of volcanic rocks, have led to significantly more age control in onshore landscape assemblages and sedimentary sequences. Identification of dated material at a certain distance away from a feature or at a certain depth in a deposit can provide data on rates of denudation. In south east Australia Cenozoic basalt flows have provided an excellent chronological framework for studies of channel development and landscape evolution (Young and McDougall, 1982; Bishop, 1988; Bishop and Goldrick, 1998; Nott, 1996a, b). Similarly in Hawaii, Seidl *et al.* (1994) investigated bedrock river incision and benefited from well constrained incision rates into dated basalt flows. Other dating techniques such as thermoluminescence also potentially provide age control of stratigraphic markers within onshore sedimentary sequences (Stokes *et al.*, 1997). Obviously these techniques rely on the presence of datable material of significant age that can be closely correlated with landforms or denudation events. This is not always possible, particularly in landscapes dominated by denudation such as passive margins.

A large majority of continental sediments end up in offshore basins, analysis of which is the second method that can successfully be used to monitor long-term rates of denudation. The

growth in analysis of the off-shore sedimentary record has stemmed from developments in drilling and seismic mapping around the world since the 1960s. Rust and Summerfield (1990) and Poag and Sevon (1989) have successfully investigated the denudational history of the south-west African margin and the US Atlantic margin off the Appalachians. The major problem with this technique is that the evidence is spread over a large area and the catchment area for sediment supply is poorly constrained. Subtle changes in drainage networks can lead to dramatic effects in sediment supply to offshore basins, but the signal may be misinterpreted because of the numerous possible reasons for such an effect.

The third technique available, thermochronology, is perhaps the most valuable of existing techniques to investigate long-term denudation (Summerfield, 1996a) and has advantages over the others in that it does not rely on chronological markers and is more site specific than sediment analysis. The technique provides information on the cooling history of the upper 3-4 km of the crust which can been interpreted in terms of denudation provided geothermal temperature gradients can be constrained (Brown *et al.,* 1994). Apatite fission track thermochronology has provided useful insights into the large-scale denudation history of landscapes in passive margin settings including south-west Africa (Brown, 1992; Brown *et al.,* 1990, 1998) and the Transantarctic Mountains (Fitzgerald, 1992; Gleadow and Fitzgerald, 1987; Fitzgerald *et al.,* 1986).

Of the long-term techniques described above, a common problem faced by all of them, is their relatively insensitive nature. The minimum time scale over which thermochronological data are useful for constraining denudation is on the order of 10^7 a. One advantage they do have is that they all integrate the magnitude/frequency problem by providing average rates over long-time scales. As such, they offer an invaluable means for comparing present-day denudation rates with those in the geological past (Summerfield and Hulton, 1994; Summerfield, 1996a).

1.4 *In-Situ* Cosmogenic Isotope Analysis

In-situ cosmogenic isotope analysis is a relatively new technique that can provide a number of quantitative constraints on the exposure histories of rocks based on the 'dwell time' of material now exposed at the surface (Nishiizumi *et al.,* 1993; Bierman, 1994; Cerling and Craig, 1994). These include estimation of site-specific denudation rates on time scales of 10^4 - 10^6 a (Lal, 1991) and, as such, the technique offers the geomorphologist a valuable new tool with which to assess rates of landscape change. Analysis of cosmogenic nuclides (literally, produced by cosmic

rays) has been carried out on meteorites for many years, but it was not until relatively recently that developments were made in analytical techniques that permitted measurement of the small abundances of nuclides found *in situ* at the Earth's surface (Elmore and Phillips, 1987; Finkel and Suter, 1993). Although still in its infancy and subject to some uncertainties that remain to be clarified (Gosse *et al.,* 1996), the technique has been successfully applied in a small number of applications to constrain denudation rates in a variety of geomorphic settings (Nishiizumi *et al.,* 1991; Brown *et al.,* 1995; Bierman and Turner, 1995; Summerfield *et al.,* 1998a). In applications of this type, the *in-situ* cosmogenic technique is best used in simple, well understood geomorphic settings with plenty of exposed bedrock available for sampling. It is therefore appropriate to use in arid environments which often have a high proportion of soil and vegetation-free rock slopes and surfaces. Unlike techniques such as fission track thermochronology, it is well suited to the lower end of the magnitude spectrum, i.e. rates <100 m Ma^{-1}, because the concentration of *in-situ*-produced cosmogenic nuclides (which form the basis of the technique) is enhanced in more slowly eroding rock surfaces. Compared to some techniques which use a short-term monitoring approach, it overcomes magnitude/frequency problems to a certain extent because rate estimates from cosmogenic isotope analysis are necessarily integrated over a time period between 10^3 a and 10^6 a, depending on the denudation rate and isotope used. However, the accuracy of the rates determined from cosmogenic isotope analysis depends on the validity of assumptions regarding the style of denudational processes acting on the sampled surface. Therefore, the technique offers advantages in some respects, but it is also subject to limitations of different kinds.

One of the major problems with constraining rates of landscape evolution at present is the disparity between the temporal and spatial scales of denudation rate data from modern surface process studies and long-term, regional-scale estimates from other techniques described above. A key benefit of cosmogenic isotope analysis is that it provides data on an intermediate time scale between these two contrasting scales of investigation. This issue has been recently pointed out by Summerfield (1996a, p. 214): "The technique thus neatly fills the gap between present-day and historical denudation rate data, and the long-term estimates provided by thermochronology and offshore sediment volumes". Given that as many lines of independent evidence as possible are desirable in reconstructing landscape evolution (Bishop, 1998), the addition of a technique in a new 'temporal niche' is an exciting development. Although as yet untested, the coupling of results of cosmogenic isotope analysis with estimates of denudation rates at difference temporal scales is likely to increase dramatically the usefulness of the technique in constraining landscape evolution. In this respect, the technique also offers practical potential in solving the long-

standing problem faced by geomorphologists of linking short-term process studies into studies of long-term landscape evolution (Sugden *et al.*, 1997).

Bishop (1998) has recently proposed that although significant advances have been made in providing information on rates of landscape change, the reconstruction of previous morphology is a key issue in research on long-term landscape evolution that remains problematic. It should be noted however, that not only does cosmogenic isotope analysis offer a temporal advantage over existing reconstructions of rates, it also offers the potential to constrain modes of landscape development by providing information on relative rates of denudation of specific morphological elements in a single landscape. This is not possible, over time scales relevant to landscape evolution, using previously mentioned long-term perspective techniques because of the large spatial scale over which they apply. Because short term process studies are commonly also associated with more limited spatial scales than the long-term techniques, cosmogenic isotope analysis provides a further advantage in that it offers site specific data over a comparatively long time scale.

1.5 Objectives and Organisation of Thesis

The specific objectives of the thesis are as follows:

1) To evaluate and review the use of cosmogenic isotopes in geomorphology, with particular reference to the potential to determine denudation rates.

2) To apply the technique to contrasting landscape elements in central Namibia and the Dry Valleys region of Antarctica for the specific purposes of:

a) Estimating a rate of retreat for the Great Escarpment in central Namibia.
b) Assessing rates of denudation of bornhardts in the central Namib Desert.
c) Determining rates of landscape change in the Dry Valleys region of Antarctica.

The objectives of this thesis are as much concerned with evaluating the potential of cosmogenic isotope analysis to measure denudation rates as with the provision of quantitative data on an intermediate time-scale to assist our understanding of landscape evolution. At the initiation of research in 1993, there were very few examples of cosmogenic isotope analysis that had been interpreted in terms of denudation rates, although the possibility had been discussed since the late

1980s. To date, there are still only a limited number of publications on denudation rate estimation. For these reasons, the thesis begins with a detailed review of the technique and its application in geomorphology in Chapter 2. Because the technique is relatively new and the chemical procedures involved in sample preparation are far from routine, field and analytical methods are described in detail in Chapter 3 rather than being assigned to an appendix. The three principal applications (2a,b,c listed above) are presented consecutively in Chapters 4, 5 and 6. All three involve the analysis of *in-situ* cosmogenic ^{10}Be and ^{26}Al in quartz samples. Because the applications are essentially separate from each other, each contains detailed background material on the relevant research framework. In Chapter 4, cosmogenic isotope analysis is applied to the problem of escarpment retreat across passive continental margins. Denudation rate estimates from the Gamsberg, a prominent feature of the Great Escarpment in central Namibia, are presented. Chapter 5 details an investigation of bornhardts in the central Namib Desert, chosen not only to monitor rates of denudation in an arid environment but also to provide an overall assessment of the relative rate of denudation on the coastal plain of Namibia below the Great Escarpment. In Chapter 6, denudation rate estimates from *in-situ* cosmogenic ^{21}Ne as well as ^{10}Be and ^{26}Al are presented for some sites in the Dry Valleys region of Antarctica within the broad framework of the East Antarctic Ice Sheet stability debate. The final chapter, Chapter 7, includes a synthesis of the findings of the preceding three chapters as well as identification of areas for future research and a list of major conclusions of the thesis. Information about the samples described in Chapters 4, 5 and 6 are given in Appendix A and publications to date on work contained within the thesis are included in Appendix B.

Chapter 2:

In-Situ Cosmogenic Isotope Analysis and Its Use in Geomorphology

---

2.1 Introduction

Over the past 12 years, *in-situ* cosmogenic isotope analysis has been developed as a geomorphological technique. As will be shown in this chapter it represents an exciting opportunity for geomorphologists to address fundamental issues with a new approach. The technique uses the *in-situ* accumulations of cosmic-ray-produced nuclides detectable in the upper layers of rock surfaces to assess the exposure history of those rocks. The technique is virtually unique in that it can provide information on the exposure history of rock surfaces over significant periods of time directly rather than by association with deposits or other chronological markers (section 1.4). The information obtained can be in terms of either an 'age' related to an exposure event or a denudation rate. It is important to appreciate that each of these interpretations is an end-member in a full range of possibilities and requires strict limiting assumptions to be valid. In general, the denudation scenario is more applicable than exposure age determination given the ubiquitous nature of weathering and erosion on exposed rock. Cosmogenic isotope analysis should not therefore be seen merely as a dating technique but rather a "set of tools" with which to explore geomorphic histories (Nishiizumi *et al.*, 1993, p. 423).

Cosmic rays from the sun and galactic sources continuously bombard the Earth's atmosphere and surface. The incoming cosmic radiation is strongly attenuated by reactions with atmospheric particles and most of the incoming energy is dissipated before reaching the troposphere. However, a small proportion of cosmic rays reach the Earth's surface where nuclear interactions with terrestrial matter produce cosmogenic nuclides *in situ* and alter the isotopic concentration of surface material down to a depth of approximately one to two meters (Fig. 2.1). The rate of cosmic ray reactions at the Earth's surface is several hundred times smaller than in the atmosphere, but the availability of targets for certain isotopes is very limited in the atmosphere compared to terrestrial matter such as rock and therefore surface production is significant (Lal and Peters, 1967). Cosmogenic isotopes are produced in a range of locations and materials

including extraterrestrial matter such as meteorites, terrestrial matter such as rock, soil and ice as well as in the Earth's atmosphere (Fig. 2.1). Nuclides produced in the atmosphere, termed meteoric nuclides, can become incorporated into surface terrestrial matter, for example via precipitation, but these have not been produced *in situ* and therefore must be classified separately from those formed directly in rocks. Figure 2.2 demonstrates the full extent of cosmogenic nuclide production and the wide range of potential applications. It is clear that the application of *in-situ*-produced cosmogenic isotopes in rocks is just one part of a spectrum of possibilities but is the sole focus of this chapter.

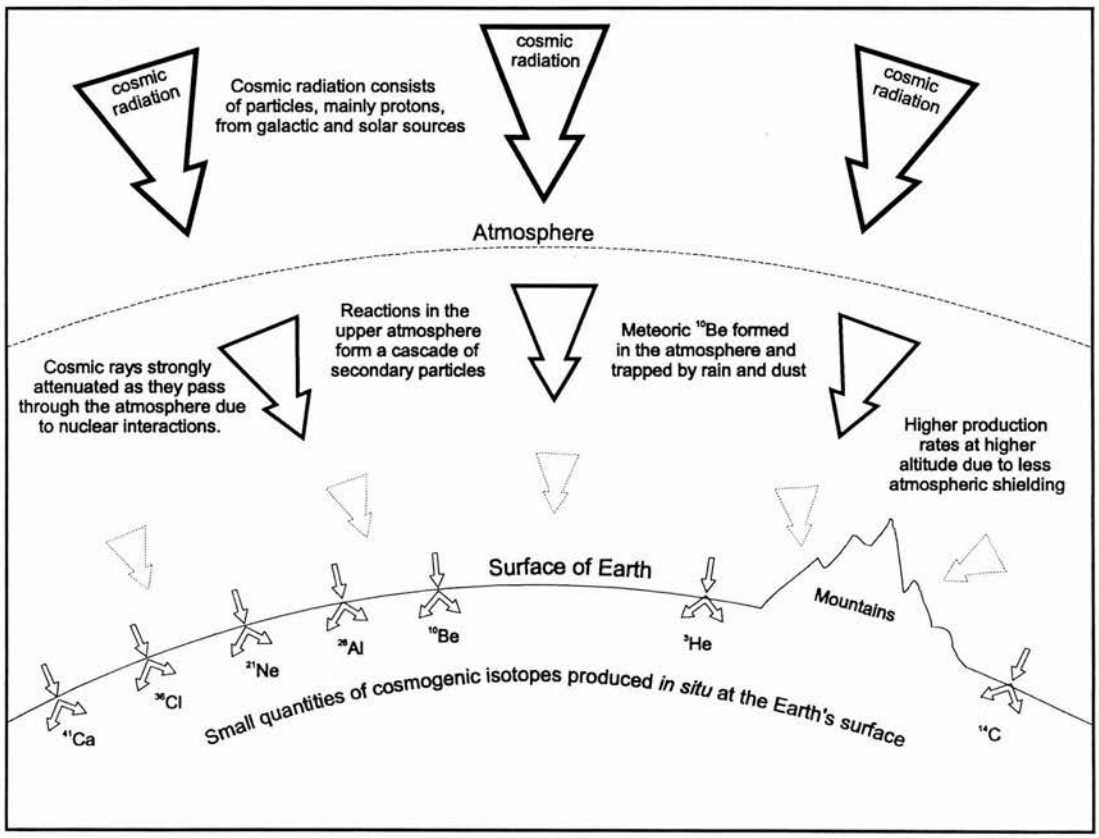

Figure 2.1: Schematic representation of the basis of the cosmogenic technique. Incoming cosmic radiation is attenuated as it passes through the atmosphere. Small amounts of cosmogenic isotopes are formed in situ at the Earth's surface and accumulate through time.

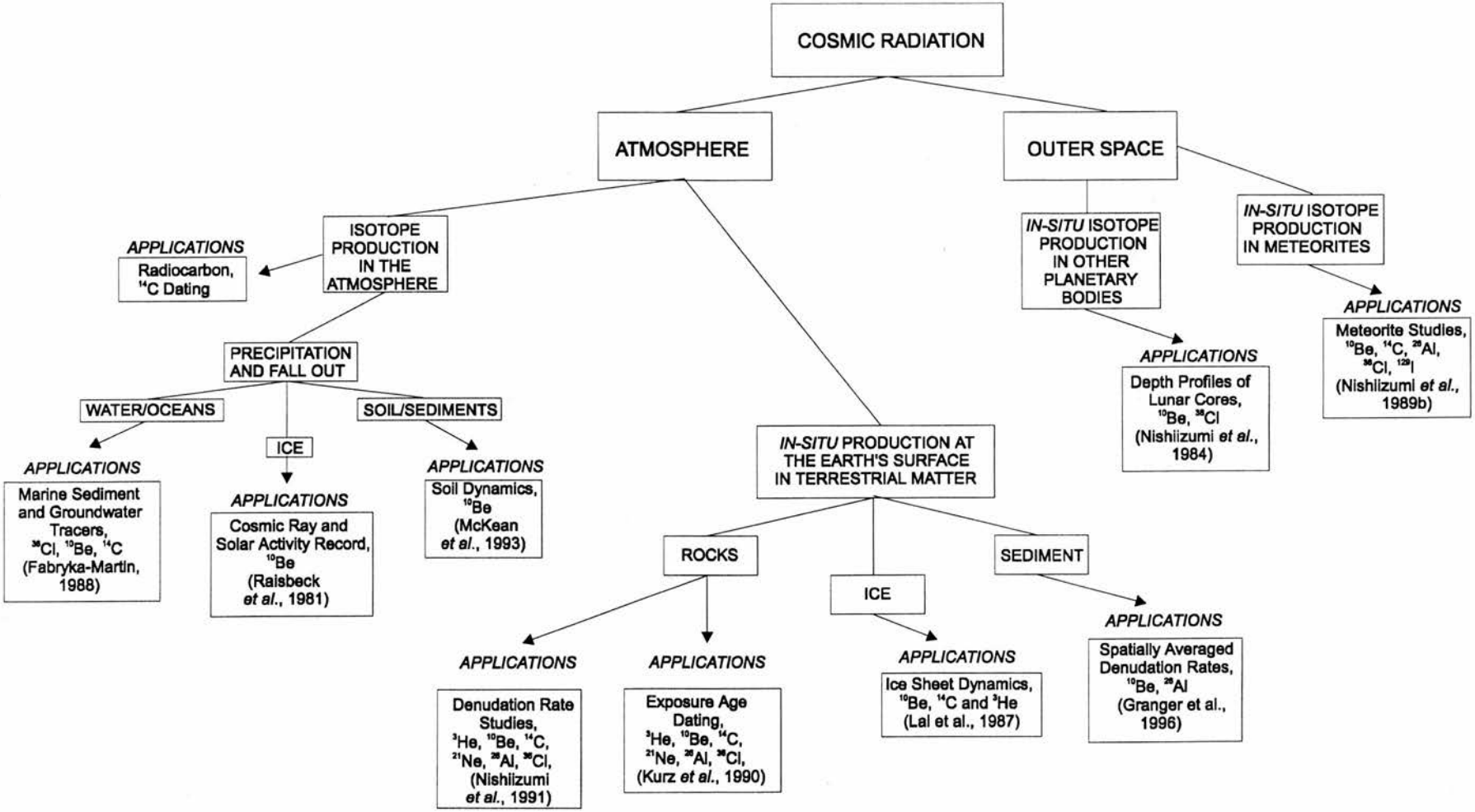

Figure 2.2: "Root" diagram showing the many branches of cosmogenic isotope analysis including analysis of in-situ-produced isotopes in terrestrial rocks. (For details of the other applications refer to the studies listed in the relevant box and references therein.)

Although the potential to use concentrations of *in-situ*-produced cosmogenic isotopes to explore geomorphic processes was first identified by Davis and Schaeffer (1955), it was not until the late 1970s that developments were made in accelerator mass spectrometry (AMS) and conventional mass spectrometry that enabled measurement of both radioactive and stable nuclides with sufficient sensitivity and accuracy for geomorphic applications (Elmore and Phillips, 1987; Finkel and Suter, 1993). In the last five years there has been a large increase in the number of *in-situ* cosmogenic studies and a shift from those concerned with the systematics of the technique to those concerned with geomorphic problems (Cerling and Craig, 1994). However, there are still inherent uncertainties, particularly with production rates, and refinement of the technique refinement an important research topic. A number of useful review papers (Dorn and Phillips, 1991; Bierman, 1994; Cerling and Craig, 1994; Kurz and Brook, 1994) have helped to increase awareness of the general aspects of *in-situ* cosmogenic isotope analysis among the geomorphological community.

The purpose of this chapter is to review of the use of *in-situ*-produced cosmogenic isotopes to explore quantitatively exposure ages and denudation histories of bedrock surfaces. The principles and assumptions behind the technique are discussed in detail as it is necessary to appreciate these issues to understand the interpretation of measured concentrations. To date, more than 12 *in-situ* cosmogenic isotopes have been detected in rocks by a variety of methods but only five of these are routinely measured and applied for geomorphic purposes (Lal, 1988). Table 2.1 shows these five commonly applied cosmogenic isotopes with their early pioneering production rate studies and some recent applications. The isotopes are: ^{3}He, ^{10}Be, ^{21}Ne, ^{26}Al and ^{36}Cl. Also shown are the appropriate target materials, production mechanisms and measurement techniques which, as will be discussed later, are relevant to their possible areas of application. ^{14}C and ^{41}Ca, also shown in Table 2.1, are in their early stages of development and are only briefly mentioned in the following review but appear to have geomorphic potential (Jull *et al.*, 1992, 1994; Fink *et al.*, 1990, 1994). The principal five isotopes will be discussed in each section but the review will concentrate on ^{10}Be, ^{26}Al and ^{21}Ne because it is these isotopes that are applied in the following three chapters.

Table 2.1: Cosmogenic isotopes commonly used and with potential for use in geomorphology with additional information relevant to their application.

Isotope	Half-life ($t_{1/2}$), a Decay constant (λ), a^{-1}	Commonly used prod. rates, at g^{-1} yr^{-1} (sea level, >60°)	Production rate references	Measurement method and measurement material	Examples of recent applications	Advantages for use in geomorphology	Disadvantages for use in geomorphology
^{3}He	stable	125 in olivine 115 in olivine 115-191 in quartz	Kurz *et al.* (1990), Cerling and Craig (1993) Brook and Kurz (1993)	MS pure quartz, olivine, pyroxene	Brook *et al.*, (1995b) Glacial history in Antarctica	High production rate, low detection limit, easy sample preparation.	Diffusion in quartz, high trapped component.
^{10}Be	1.5×10^{6} 4.6×10^{-7}	6 in SiO_2 4.74 in SiO_2	Nishiizumi *et al.* (1989a), Clark *et al.* (1995)	AMS BeO	Ritz *et al.* (1995) Fault slip rates in Mongolia	Extensive use to date, no naturally occurring ^{9}Be, good in quartz.	Difficult sample prep., atmospheric contamination.
^{26}Al	7.16×10^{5} 9.9×10^{-7}	36.8 in SiO_2 28.9 in SiO_2	As for ^{10}Be	AMS Al_2O_3	Bierman and Turner (1995) Denudation rates on inselbergs, Australia	Useful partner for ^{10}Be.	Problems with ^{27}Al content of samples, radiogenic production?
^{36}Cl	3.08×10^{5} 2.3×10^{-6}	Rock chemistry dependent; 9 in granite, 15 in basalt	Zreda *et al.* (1991), Phillips *et al.* (1996a)	AMS AgCl	Phillips *et al*, (1996b) Glacial chronology in the Sierra Nevada	No need for quartz or olivine rich samples.	Sample composition dependent production
^{21}Ne	stable	45 in Olivine, 16.8 in Plagioclase, 21 in quartz	Poreda and Cerling (1992), Neidermann *et al.* (1994).	MS pure quartz, olivine, plagioclase	Bruno *et al.* (1997) Dating of Sirius tillites in Antarctica.	Retained in quartz, large dating range, easy sample preparation	High radiogenic production, limited examples of use to date.
^{14}C	5730 1.2×10^{-6}	20 in basalt 21 in quartz	Jull *et al.* (1992, 1994) Donahue *et al.* (1990)	AMS C	Jull *et al*, (1992), measurement and comparison with other nuclides	Short half-life, able to detect erosion concealed by longer lived isotopes.	Atmospheric contamination, early stages of development.
^{41}Ca	103×10^{3} 6.7×10^{6}	-	-	AMS ?	No *in-situ* measurements available to date.	Different half-life from the others, useful range for Quaternary.	No applications so far, very low ratios.

2.2 Principles of *In-Situ* Cosmogenic Isotope Analysis

2.2.1 Production of In-Situ Cosmogenic Nuclides

Cosmogenic isotopes are produced by the interaction of cosmic ray particles with target atoms. Cosmic rays continuously bombard the Earth from all directions and consist of a range of highly energetic particles which are thought to be the generated from sources within the galaxy such as super nova explosions, cosmic strings and the sun (galactic cosmic rays (GCRs) and solar cosmic rays (SCRs) respectively). At the top of the Earth's atmosphere (~400 km altitude), the nucleons that comprise the primary cosmic ray incident beam are mainly high energy protons (positively charged elementary particles, ~85%). Also present in smaller numbers are alpha particles (~14%), electrons, and some heavier atomic nuclei composed of protons and neutrons (~1%), (Lal and Peters, 1967; Reedy *et al.,* 1983). As they enter the atmosphere, primary cosmic rays are strongly attenuated due to interactions with other particles, mainly oxygen and nitrogen nuclei, and these reactions produce a shower or 'cascade' of secondary particles (mainly protons and neutrons), some of which will have a high enough energy to interact and cause further reactions (Fig. 2.1, Reedy *et al.,* 1983). By the time the cosmic ray flux reaches the Earth's surface it is strongly diminished resulting in low *in-situ* (literally produced-*in-situ,* in a fixed target location on the Earth's surface) cosmogenic isotope production rates. It is estimated that only 0.1% of secondary particles produce cosmogenic isotopes within the mineral lattice of exposed rocks (Brown *et al.,* 1991). Although the cosmic ray flux at the Earth's surface varies both in time and space (section 2.2.5), the energy spectrum is invariant below 12 km permitting generalizations to be made about the flux at the Earth's surface (Lal and Peters, 1967).

There are three principal reactions which produce most *in-situ* cosmogenic isotopes at the Earth's surface:

a) Spallation induced by high energy nucleons. This is the most important mechanism in which the cosmogenic nuclide is either emitted by the target nucleus, or more often left behind as residue in a high energy disintegration caused by a neutron bombarding the target atom (Lal and Peters, 1967). High energy nucleons are needed for spallation because the of the high binding energies of the target atomic nuclei. Typical energies of GCRs and SCRs range from 1-100 GeV and 1-100 MeV respectively and atomic binding energy is about 8 MeV so there is ample energy available (Cerling and Craig, 1994). Spallation reactions decline exponentially with depth in the

atmosphere and inside a target; this is a critical assumption for interpretation of nuclide concentrations.

b) Thermal Neutron Activation. This can be a significant production mechanism for some isotopes, especially ^{36}Cl, and is a reaction in which a thermal neutron (a neutron in thermal equilibrium with the target matter) is captured by the nucleus of a stable nuclide resulting in a cosmogenic nuclide (Lal and Peters, 1967; Phillips *et al.,* 1986). The energy of thermal neutrons is low compared to those needed for spallation reactions. The flux of thermal neutrons is at a maximum below the Earth's surface although it is attenuated in the atmosphere (Reedy and Arnold, 1972). This fact complicates the assumption of exponential decrease in production with depth inside a target (section 2.2.2). However, thermal neutron activation is not an important production mechanism for most isotopes.

c) Negative Muon Capture. Muons are produced by primary cosmic ray interactions in the atmosphere (part of the secondary cascade) and are weaker elementary particles than neutrons. They do not directly cause reactions but can be captured by a target nucleus which may then decay to create a cosmogenic isotope (Rama and Honda, 1961). Muon capture is the least important mechanism for all isotopes at the surface but similar to thermal neutron activation, it can be significant for ^{36}Cl depending on target composition. Muons have larger attenuation coefficients than neutrons (~1500 g cm^{-2} (Middleton and Klein, 1987)), therefore muon capture can become significant in samples taken at depth or in areas with high denudation rates.

The relative importance of each production mechanism varies between isotopes and depends on the availability of target elements, i.e. the composition of the target material. Spallation reactions produce all seven isotopes important for geomorphology (Table 2.1). ^{26}Al is produced by neutron induced spallation of ^{28}Si and ^{27}Al and to a lesser extent from muon capture by ^{28}Si (Klein *et al.,* 1986; Nishiizumi *et al.,* 1986). ^{10}Be is produced by spallation of oxygen and to a lesser extent ^{28}Si (Klein *et al.,* 1986; Nishiizumi *et al.,* 1986). In olivines, Mg is an important target atom for ^{10}Be production by spallation. Below the surface of the earth, an increasingly larger proportion of *in-situ*-produced ^{26}Al is due to negative muon capture due to the longer attenuation length of muons compared to neutrons (Klein *et al.,* 1986). Muon production of ^{10}Be in near surface rocks has also been investiagted but is unlikely to be significant for all samples (Brown *et al.,* 1995b).

Quartz (SiO_2) is an attractive target material for measuring ^{26}Al and ^{10}Be given that the target chemistry is simple and the production rates are maximized. Quartz is also ideal as it can be found in diverse geomorphic settings, is resistant to weathering, has a tight crystal structure which minimizes contamination from atmospherically derived or meteoric ^{10}Be (see below) and has a low ^{27}Al content which allows measurement of ^{26}Al after as few as 10^3 a (Nishiizumi *et al.*, 1986) or even just a few hundred years (Finkel *et al.*, 1997). Quartz is by far the most commonly used target material for ^{10}Be and ^{26}Al but olivine, ice, pyroxene, diamonds and whole rock have also been tested (Seidl *et al.*, 1997; Lal *et al.*, 1987; Ivy-Ochs, 1996; Klein *et al.*, 1997).

Si is the only important target for spallation produced ^{21}Ne in quartz. Al, Na and Mg are also spallation targets for ^{21}Ne but are usually three orders of magnitude lower in relative concentration in quartz and are therefore not important (Graf *et al.*, 1991; Nishiizumi *et al.*, 1993). In olivine and pyroxene, however, ^{21}Ne can be produced by the spallation of Mg, Si and Fe and Mg, Al, Si and Ca respectively and has been studied in basalts (Marti and Craig, 1987). Mg is the dominant target for cosmogenic ^{21}Ne, producing over 85% of the total in olivine and pyroxene (Poreda and Cerling, 1992). Muon capture producing ^{21}Ne could be significant at depth but has not been fully investigated (Cerling and Craig, 1994).

The most important mechanism for the production of ^{36}Cl is spallation of ^{39}K and ^{40}Ca which produces up to 90% of all ^{36}Cl found in calcite and calcium feldspar (Phillips *et al.*, 1986; Stone *et al.*, 1996a). However thermal neutron capture by ^{35}Cl is also significant accounting for up to 20% of ^{36}Cl production in some rocks. Muon capture by ^{40}Ca becomes important at depth (Phillips *et al.*, 1986; Zreda *et al.*, 1991). Because ^{35}Cl, ^{39}K and ^{40}Ca are only minor constituents in rocks rich in SiO_2 it is usually advantageous to use ^{10}Be and ^{26}Al in these circumstances. However, ^{36}Cl can be measured in whole rock and is therefore more versatile than ^{10}Be and ^{26}Al which cannot be measured in whole rock due to high ^{27}Al contents and meteoric ^{10}Be contamination (Nishiizumi *et al.*, 1986; Klein *et al.*, 1997).

The two major production mechanisms for ^{3}He are spallation of heavy nuclei (O, Al and Si) and thermal neutron capture by ^{6}Li (Kurz, 1986a; Lal, 1987; Trull *et al.*, 1991). The relative importance of a third mechanism involving muons increases with depth inside a target (Cerling and Craig, 1994). Target materials for studies of ^{3}He are commonly pyroxene and olivine from basalts (Kurz, 1986a; Nishiizumi *et al.*, 1990). Although the production mechanisms and suitable targets point to quartz as an obvious choice, problems with post-production diffusion have reduced the potential of this particular combination (Cerling, 1990; Trull *et al.*, 1991, 1995;

Brook and Kurz, 1993; Summerfield *et al.,* 1998a), (section 2.2.3). ^{14}C is principally produced by spallation of oxygen and studies have used quartz or whole rock as target materials (Jull *et al.,* 1992). ^{41}Ca is produced by thermal neutron capture by ^{40}Ca but has not yet been investigated in terrestrial rocks (Kurz and Brook, 1994).

Non-cosmogenic sources of the same isotopes shown in Table 2.1 can represent a significant component of a measured nuclide concentration in a rock and must be distinguished from the true cosmogenic component before interpretation or else resultant exposure ages/rates will be in error. There are three possible non-cosmogenic components: trapped (sometimes called inherited but not in the geomorphic sense), radiogenic (or nucleogenic) and atmospherically derived (meteoric or garden). Contamination by atmospherically derived nuclides is not relevant for ^{3}He or ^{21}Ne as they are not transferred from air to soil or rock. For ^{26}Al there are too few suitable targets in the atmosphere but for ^{10}Be, ^{36}Cl and ^{14}C the meteoric flux can be significant. In most cases, leaching rocks with acid during initial sample preparation can remove any meteoric nuclides (section 3.3), (Kohl and Nishiizumi, 1992; Zreda *et al.,* 1991; Seidl, 1993; Ivy-Ochs, 1996).

A trapped or inherited component of stable isotopes, ^{3}He or ^{21}Ne, can arise from fluid inclusions within a target crystal lattice. Because these trapped gases usually have a distinct isotopic ratio (such as a constant atmospheric ratio) and are commonly released during sample crushing or at particular temperatures, they can be distinguished from a cosmogenic component during measurement (Craig and Poreda, 1986; Kurz, 1986a, b; Niedermann *et al.,* 1993). Radioisotopes almost always have no inherited component (Cerling and Craig, 1994).

A radiogenic component can result from the neutron flux associated with natural fission (although these neutrons do not always have enough energy) or from (α,n) or (α,p) reactions (literally reactions involving an alpha particle with either a neutron or a proton) with the alpha particles produced by U-Th decay in, or close to, the target material (e.g. ^{18}O (α,n) ^{21}Ne (Faure, 1986)). Radiogenically produced ^{26}Al can be a significant in certain cases but in surface rocks with a low U-Th content radiogenic ^{10}Be and ^{26}Al is usually negligible (Sharma and Middleton, 1989). For ^{21}Ne and ^{3}He, separation of multiple components can be accomplished successfully during mass spectrometry measurements assuming the number of components is not larger than the number of isotopes (Kurz, 1986a; Neidermann *et al.,* 1993). In general, stable isotopes are more likely to have problems associated with radiogenic production, and the older the formation age of the rock the higher the nucleogenic component will be (Cerling and Craig, 1994).

2.2.2 *Variation of Production with Depth Inside a Target*

While traversing through matter cosmic rays are attenuated by nuclear interactions and ionization losses which lead to a pronounced reduction of production with depth inside a target (Lal, 1991). The depth below the surface of a target is usually expressed in g cm^{-2} (i.e. the distance multiplied by the density of the material (ρ)) rather than simply by a length scale. This unit is used to indicate a shielding mass per unit area and to compensate for density variations; the equivalent depth is called the 'shielding depth' (Sarda *et al.*, 1993). The variation of production with shielding depth, known as the attenuation coefficient, has been shown theoretically, and for some isotopes experimentally, to follow closely the absorption mean free path of the neutron component of cosmic rays through air, although it is not formally identical (Brown *et al.*, 1992). The absorption mean free path is the distance over which rays decrease in intensity by a factor of 1/e (or a percentage reduction of ~63%). This is sometimes known as the e-folding length or skin depth because the energy of the cosmic rays is reduced significantly in only a thin surface layer. For isotopes whose principal production mechanism is neutron spallation, their reduction in production with depth inside a target can be approximated to an exponential decrease (Lal and Arnold, 1985).

Brown *et al.* (1992) have demonstrated empirically the expected theoretical exponential decrease for ^{10}Be and ^{26}Al and revealed a statistically similar attenuation coefficient for both isotopes of ~145 g cm^{-2} in quartz down a 1.1m vertical drill core (Fig. 2.3). Kurz (1986b) demonstrated that ^{3}He in three basalt cores from Hawaii decreased exponentially with depth with best fit values of the attenuation coefficient of 170±2, 165±7 and 164±3 g cm^{-2}. Sarda *et al.* (1993) showed that cosmogenic ^{21}Ne decreases exponentially with an attenuation coefficient of 165±6 g cm^{-2} in basalt following an identical path to ^{3}He (Fig. 2.3).

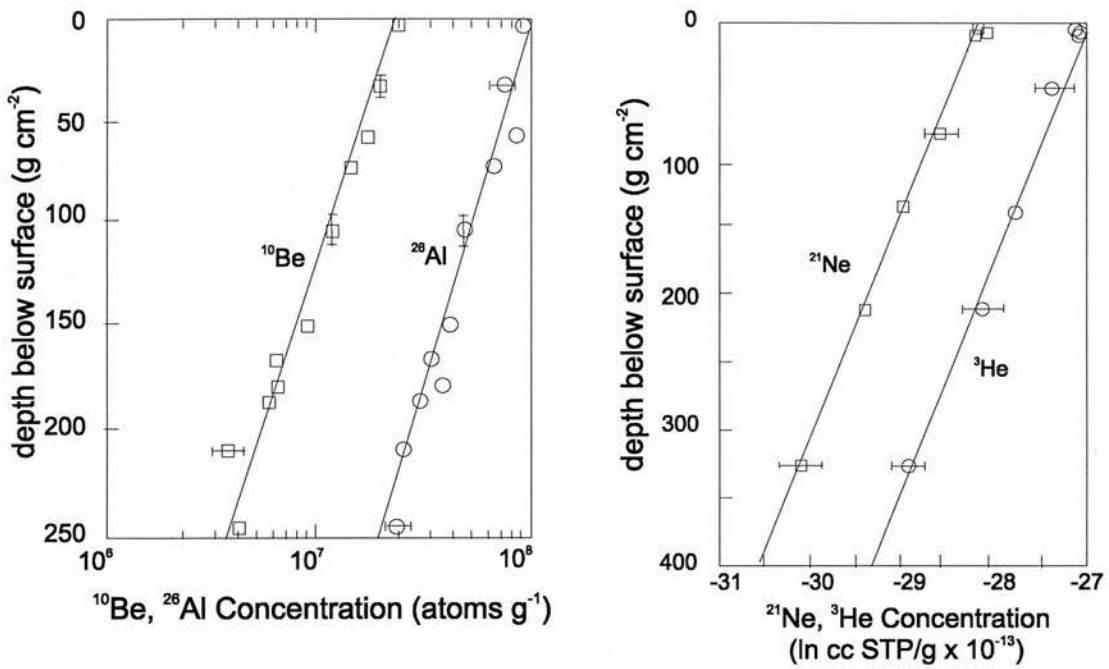

Figure 2.3: The depth dependence of ^{10}Be, ^{26}Al, ^{3}He and ^{21}Ne from empirical studies (after Brown et al., 1992 (^{10}Be and ^{26}Al) and Sarda et al., 1993 (^{21}Ne and ^{3}He)).

For isotopes produced by spallation reactions (^{10}Be, ^{26}Al, ^{3}He, ^{21}Ne and almost certainly ^{14}C) the production rate at depth in a target can be described over the first several metres in an exponential expression as follows (Lal, 1991):

$$P_X = P_O e^{-\rho x / \Lambda} \qquad [2.1]$$

where P_x = production rate at depth x in atoms g^{-1} a^{-1}, P_o = production rate at the surface in atoms g^{-1} a^{-1}, ρ = density of the rock in g cm^{-3}, x = depth in cm , Λ = attenuation coefficient in g cm^{-2}.

The integrated production rate over a certain interval is described by the following equation which is obtained by integration of equation 2.1:

$$P_{(o\ to\ x)} = P_0 \frac{\Lambda}{\rho x}\left(1 - e^{-\rho x/\Lambda}\right) \qquad [2.2]$$

where P_o, ρ, Λ, and x are defined as above and $P_{(o\ to\ x)}$ = the average production rate for the interval from the surface downward to a given depth.

Thermal neutron capture production mechanisms do not follow the same exponential attenuation path as neutron induced spallation mechanisms. Therefore, for isotopes that have a significant component produced by thermal neutron capture, such as ^{36}Cl, production at depth has to be calculated somewhat differently from the equations described above. The production of ^{36}Cl actually increases relative to the surface value up to a depth of about 45 g cm^{-2} because thermal neutrons are able to escape back out to the rock surface (for details see Fabryka-Martin (1988)).

Muons have greater attenuation lengths than neutrons, therefore at rock depths over a few meters and in areas of high denudation rates, muon capture should be evaluated for the total production rate of cosmogenic nuclides (Kurz, 1986a, b; Nishiizumi *et al.*, 1989a). Kurz (1986b) demonstrates that at depths greater than 170 g cm^{-2} reactions involving muons take over as the dominant production mechanism of ^{3}He. However, it is generally assumed that for depths <1 m in surface rocks, the contribution from muons is negligible compared to the total cosmogenic flux (Cerling and Craig, 1994).

2.2.3 Post Production Diffusion

An important assumption of the cosmogenic technique is that cosmogenic nuclides are fully retained *in situ* in the target material after production. Post-formation losses from diffusion or migration are a potential uncertainty in the method but are only significant for the stable isotopes (^{3}He and ^{21}Ne). There has been debate over the limitations of using ^{3}He (Kurz, 1986b; Cerling, 1990; Trull *et al.*, 1991; Brook and Kurz, 1993; Brook *et al.*, 1993) but it is now generally agreed that diffusion of ^{3}He is greater in quartz than in olivine (Kurz and Brook, 1994). Factors that may affect the diffusivity of ^{3}He in quartz include grain size (Kurz, 1986b; Cerling, 1990; Trull *et al.*, 1991), temperature (Trull *et al.*, 1991, 1995) and exposure age (Brook *et al.*, 1993).

In general, ^{21}Ne is more fully retained in quartz than ^{3}He and is less affected by diffusion losses over geological time scales (Graf *et al.,* 1991). Hudson *et al.* (1991) compared ^{21}Ne and ^{3}He in Antarctic quartz and found no ^{21}Ne losses relative to ^{10}Be and ^{26}Al concentrations but major ^{3}He losses. Summerfield *et al.* (1998a) found a similar trend with ^{3}He ages between 2 and 55 times lower than ^{21}Ne ages in Antarctic quartz, clearly demonstrating a fundamental problem with using cosmogenic ^{3}He in quartz (section 6.5). Although research is limited, it seems that ^{21}Ne and ^{3}He are fully retained in olivine and clinopyroxene (Marti and Craig, 1987) but small diffusion effects are a possibility (Bruno *et al.,* 1997).

2.2.4 Production Rate Determination

Knowledge of the production rates of *in-situ* cosmogenic nuclides is a prerequisite for their application in geomorphology. Rates for some isotopes have been estimated both by theoretical calculation (Masarik and Reedy, 1995) and experimental measurement (Nishiizumi *et al.,* 1989a). The generally accepted current rates for each isotope at sea level and high latitude (> 60°) are shown in Table 2.1. Significant spatial variation, and to a lesser extent temporal variation, means that for each separate area of investigation production rates must be adjusted using appropriate scaling factors to the study site (sections 2.2.5 - 2.2.7). There are still significant uncertainties, up to ±20%, in absolute rates for most isotopes and those shown in Table 2.1 are liable to change in the future with the acquisition of additional data (Gosse *et al.,* 1996). A conference entirely dedicated to the problems associated with accurate production rate determination testified to the ongoing nature of research in this area (Santa Fe Workshop Abstracts, 1996).

In an influential paper, Lal and Peters (1967) used results of cosmic ray reactions in photographic emulsions and cloud chambers at high altitude in the Earth's atmosphere to evaluate the atmospheric production rate of many isotopes. They subsequently developed curves of nuclear disintegrations in the atmosphere using energy spectra data of nucleons, enabling the measured rates to be extrapolated to all latitudes and altitudes. As will be shown later, these scaling curves, summarised and updated in polynomial form by Lal (1991), have been used in the majority of cosmogenic studies to date. The actual rates, however, have been superseded by modern empirical studies.

Theoretical calculations of production rates have been put forward by several authors. Yokoyama *et al.* (1977) used a three step cascade model and cosmic ray flux data to calculate *in-situ* rates of production for several nuclides including ^{3}He, ^{10}Be, ^{14}C, ^{26}Al, ^{36}Cl, ^{24}Na and ^{22}Na.

The model was tested using empirical measurements of ^{22}Na and ^{24}Na in aluminium plates exposed for 8 to 20 years in various structures at high altitude in the French Alps. Fair agreement was obtained between the theoretical and experimental results for high and low energy reactions indicating an overall accuracy of between ± 20% and ± 35%.

Theoretical estimates of production rates are generally inaccurate because of a lack of data on the excitation functions of nuclides and poor knowledge of the probabilities of the formation of nuclides (cross sections) in different reactions (Lal, 1991). To overcome this problem, Masarik and Reedy (1995) used a Monte Carlo model to investigate the production systematics of cosmogenic isotopes and used a series of well tested model components for the production of cosmogenic nuclides in extraterrestrial matter instead of the uncertain cross sections used in previous attempts. The model enabled them to calculate particle fluxes as a function of altitude, chemical composition and latitude and therefore calculate production rates for any isotope. Although theoretically derived rates are sometimes used (Bruno *et al.,* 1997), experimentally determined rates are more often applied.

Experimental determination of absolute production rates for any cosmogenic isotope requires a target sample of known exposure age that has been reliably dated by an alternative method such as radiocarbon dating. The sample must also have had experienced no denudation or burial since the exposure event. Ideally, one requires rock that has been buried for a long time and then suddenly exposed to cosmic rays to eliminate problems with inherited nuclides. By careful measurement of the nuclide concentration and geochemical composition of the target, the production rate can be calculated for the particular altitude and geomagnetic latitude of the sample, provided the production mechanisms are understood.

This method is exemplified by the work of Nishiizumi *et al.* (1989a) who studied the concentrations of ^{10}Be and ^{26}Al in quartz crystals from glacially polished granite in the Sierra Nevada. This work yielded estimates of the production rates of these nuclides in SiO_2 and the rates have since been used in the majority of studies (Table 2.1). By using samples from apparently fresh glacially scoured surfaces with evidence of deep erosion by the most recent episode of glaciation, they assumed that the cosmogenic nuclides present were those that had accumulated only since the last glacial retreat. Deglaciation in the area had been radiocarbon dated to a calendar age of 11 ka and this was used as the exposure age of the samples. The measured ratio of ^{26}Al to ^{10}Be was found to be in good agreement for all 12 samples with an average of 6.04 ± 0.54. This is regardless of differences in altitude, exposure and snow cover as

these factors do not affect the ratio, only the absolute rates for the individual nuclides. Total production rates due to nucleons and negative muons were found to be 6.03 and 36.8 for ^{10}Be and ^{26}Al respectively at sea level and high latitude (Nishiizumi *et al.,* 1989a). Similar rates were calculated by Brown *et al.,* (1991) for Antarctic rocks but a slightly higher rate for ^{26}Al yielded a production ratio of ~6.5. A similar production rate ratio was determined by Ivy-Ochs (1996) but the rates do not vary outside the error limits from those of Nishiizumi *et al.* (1989a). Clark *et al.* (1995) suggested significantly different rates on the basis of new radiocarbon ages for deglaciation in the Sierra Nevada and a re-evaluation of the effect of geomagnetic field changes. New radiocarbon evidence suggested deglaciation in the area was completed by at least 13 ka BP (calibrated), if not 14 ka BP (Stuvier and Reimer, 1993) which would mean the rates of Nishiizumi *et al.* (1989a) are at least 20% too high because their calibration age was too young. Clark *et al.* (1995) have suggested conservative new rates of 5.10 and 31.1 atoms g^{-1} a^{-1} for ^{10}Be and ^{26}Al respectively (sea level, >60°) but rates as low as 4.74 and 28.9 atoms g^{-1} a^{-1} are supported, although their data are preliminary. These changes which would significantly affect calculated exposure ages and denudation rates.

Studies published since Clark *et al.* (1995) have tended to retain the original rates of Nishiizumi *et al.* (1989a); however, a growing awareness of the uncertainties associated with production rates of cosmogenic isotopes means that often both rates can be accommodated within error limits if all sources of error are recognised. Recently, Nishiizumi *et al.* (1996) have tried to address the issue of ^{10}Be production by making direct measurements of production in water targets after 1-2 years exposure. Although after such a short time scale it is somewhat difficult to extrapolate the measured rates due to effects of the Earth's magnetic field over time (section 2.2.5), they found better agreement with their original rates than those of Clark *et al.* (1995) and provide a useful review ^{10}Be production rate studies.

A similar method has been used to determine production rates of cosmogenic ^{36}Cl from ^{35}Cl, ^{39}K and ^{40}Ca in young glacial moraines and lava flows (Zreda *et al.,* 1991; Phillips *et al.,* 1996). A production rate equation was solved for separate parameters corresponding to each different production mechanism. Production rates of ^{36}Cl due to spallation at sea level and high geomagnetic latitude were found to be 6020 ± 400 atoms a^{-1} mol^{-1} ^{39}K and 2940 ± 200 atoms a^{-1} mol^{-1} ^{40}Ca. The thermal neutron capture rate (^{35}Cl) was calculated to be (3.07 ± 0.42) x 10^5 neutrons (kg of rock)$^{-1}$. This corresponds to a average rate in granite of ~8 atoms g^{-1} a^{-1} (sea level, > 60° latitude, Zreda *et al.,* 1991). These values differ from previously calculated values such as those of Yokoyama *et al.* (1977) which was larger by a factor of four. This is due to

differences in scaling factors and uncertainties in the excitation functions used for the theoretical calculations. Recently, Stone *et al.* (1996a) and Evans *et al.*, (1997) have carried out further work on the production of ^{36}Cl due to spallation of ^{40}Ca and in K feldspar.

Production rates for cosmogenic ^{21}Ne have not been measured directly in samples of known age but have been estimated by determining a production ratio relative to other isotopes. The production ratio of $^{21}Ne/^{26}Al$ measured in quartz is 0.67 ± 0.11 (valid for approximately 10^4 years due to the decay of ^{26}Al), (Graf *et al.*, 1993; Neidermann *et al.*, 1994) and was found to agree well with ratios observed in extraterrestrial matter. Using the production rate of Nishiizumi *et al.* (1989a) for ^{26}Al, the ratio corresponds to a production rate for ^{21}Ne of 21 atoms g^{-1} a^{-1} in quartz at sea level and >60° latitude. This cosmogenic ^{21}Ne rate is therefore open to the same criticism from Clark *et al.* (1995) as the ^{10}Be and ^{26}Al rates. Sarda *et al.* (1993) used the production ratio of cosmogenic $^{3}He/^{21}Ne$ (3.5 ± 0.1) to estimate a production rate of 169 atoms g^{-1} a^{-1} (2330 m, 21° latitude) in basalt olivines at Réunion, this rate is strongly dependent on target composition. Recently, Bruno *et al.* (1996) used the elemental ratios from Masarik and Reedy (1995) and a rate of 45 atoms g^{-1} a^{-1} in Si (Neidermann *et al.*, 1994) to calculate a ^{21}Ne production rate from Mg, Al, Si, Ca and Fe in pyroxene and whole rock.

There have been various attempts to constrain the production rate of ^{3}He, most of which have used radiocarbon dated lava flows and samples from surfaces which retain original morphology indicative of zero denudation (Kurz, 1986a, b; Cerling, 1990; Kurz *et al.*, 1990; Cerling and Craig, 1993). Although the rates have been commonly measured in olivine, the rates are weakly dependent on composition and are broadly applicable to all silicates (Kurz *et al.*, 1990). Indeed, rates that have been determined for olivine (Cerling and Craig, 1993) have been used to determine exposure ages of Antarctic sandstone boulders (Brook *et al.*, 1995). Kurz *et al.* (1990) estimated a present day rate of 125 ± 30 atoms g^{-1} a^{-1} but determined that during the past 10,000 a this rate had varied by a factor of $\pm$ 2.3. The proposed cause of this significant variation was changes in the strength of the Earth's magnetic field although denudation and poor calibration could also have had an effect (see below). Other investigations have yielded rates that have been broadly compatible but the production rate of ^{3}He is still relatively uncertain (Brook and Kurz, 1993; Brook *et al.*, 1995b). Cerling and Craig (1993) estimated a rate of 115 atoms g^{-1} a^{-1} which has been utilised recently by a number of studies (Brook *et al.*, 1995b; Bruno *et al.*, 1997).

2.2.5 *Effects of Variation in the Earth's Magnetic Field*

The Earth's magnetic field is not constant, its force varying both spatially and temporally. Change in the field can be a result of slow secular variations or abrupt magnetic storms. Cosmogenic production rates are affected by the strength of the field because intensity of the incident cosmic ray flux is controlled by the cutoff energies (or rigidities) of the field (Lal and Peters, 1967). A cutoff energy is the lowest energy with which a cosmic ray can enter the Earth's atmosphere. Cutoff energy values vary spatially with latitude due to the configuration of the magnetic field; they are lowest at the magnetic pole and highest at the equator. Rates therefore increase from the equator to the pole and reach a maximum at about 60° remaining constant above this geomagnetic latitude. The poleward amplitude of production as a function of geomagnetic latitude has been calculated variously as 1.77 (Lal and Peters, 1967), 4.1 (Yokoyama *et al.,* 1977) and 1.5 (Staudacher and Allégre, 1991). As discussed below (section 2.2.7), the latitude scaling factors of Lal (1991) based on Lal and Peters'(1967) work are generally the most accepted.

As the strength of the magnetic field varies through time, more or less cosmic radiation is able to bombard the Earth, thereby affecting nuclide production rates. Variation of production rates through time is of concern because it has a direct affect on the applicability of measured/calculated rates and the accuracy of ages/rates determined by the technique. In general, production is inversely proportional to geomagnetic field strength (Lao *et al.,* 1992, Sarda *et al.,* 1993). As with spatial variation, temporal changes in the geomagnetic field have greatest affect at the equator and becomes less significant at high latitudes >60°. Kurz *et al.* (1990) suggested that any kind of calibration or adjustment for temporal changes in the field will only be necessary for low latitude investigations but the issue is relevant to all studies which require high levels of accuracy, for example, in dating glacier fluctuations.

Experimentally determined production rates represent integrated values for the entire exposure age of the calibrated sample, reflecting long-term averages and ignoring short-term fluctuations in the cosmic ray flux and magnetic field strength. As previously mentioned, Kurz *et al.* (1990) calculated integrated production rates for *in-situ* cosmogenic ^{3}He from radiocarbon dated lavas in Hawaii and found that rates varied considerably with age of sample. The mean ^{3}He production rate in the time period 2000 - 7000 a BP was calculated as 55 ± 15 atoms g^{-1} a^{-1} whereas the mean value for younger samples was 125 ± 30 atoms g^{-1} a^{-1}. Samples between 7000 and 10 000 a old yielded a mean of 127 ± 19 atoms g^{-1} a^{-1}. Of all the possible causes of production rate

variation, Kurz *et al.* (1990) cited the strength of the terrestrial dipole as the most important and showed that the variation of rate with age closely follows the inverse of changes in field strength, although the amplitude of production rate variation is less than the amplitude of field variation. Kurz *et al.* (1990) also demonstrated that variation in the dipole moment has a smaller effect on production at sea level than at high altitude because cosmic rays consist of higher energy particles at sea level which are not affected by the magnetic field as much as lower energy particles found at altitude which are gradually filtered out by the atmosphere.

In general, temporal changes in the Earth's magnetic field strength are more important in samples with a low cosmogenic nuclide concentration and recent exposure. The influences of changes in geomagnetic latitude are averaged out over time based on the 'time-averaged geocentric axial dipole field hypothesis' in which geomagnetic latitude can be approximated to equal geographic latitude integrated over thousands of years (R. Thompson, *pers. com.*). Therefore although it is technically correct to use a geomagnetic latitude rather than geographic latitude to locate a sample in terms of its exposure to cosmic radiation, most studies, and especially those concerned with samples exposed for 10,000 a or more, use geographic latitude as an approximation (Bierman and Turner, 1995; Brook *et al.,* 1995b).

2.2.6 Other Spatial and Temporal Shielding Effects

In a similar way to depth inside a sample, production rates decrease with increasing depth inside the atmosphere due to an increase in atmospheric shielding. A sample at 3 km elevation will have a production rate 8 to 10 times higher than a sample at sea level (Kurz *et al.,* 1990) Spatial variation in the Earth's magnetic field, as discussed above, means that the effect of altitudinal shielding is greater near the equator than near the poles. As for latitudinal effects, factors are available to account for different site elevations and are presented in section 2.2.7.

Partial shielding of a target surface from cosmic rays results in lower production rates. If there is partial shielding of a site, the proportion of the cosmic ray flux reaching the surface has to be calculated for each location individually. Commonly, this assumes that the shielding has not changed through time. Partial shielding results from two possibilities: 1) nearby topographic features that obscure part of the sample from the incident flux and 2) from angled surfaces. These effects are collectively known as complex target geometries. A sample taken from a vertical face will have experienced approximately half the production rate of a horizontal sampling surface (assuming that it only receives cosmic rays from 0° up to 90°). However, the

change in the energy of the incident flux is not uniform from 0° to 90°, in fact incident energy is minimal below 45°. Therefore, if the shielding angles are low or the surface is only tilted slightly, the corrections for partial shielding are small. The effect of shielding can be quantified by integrating the free access of cosmic radiation for the angular dependence of incident cosmic rays (Nishiizumi *et al.,* 1989a; Cerling and Craig, 1994) according to the relationship:

$$F(\theta) = \sin^{2.3}\theta \qquad [2.3]$$

which can then be compared to the case for no shielding (i.e. 2π exposure). Field data required for these calculations are the dip of the surface taken with respect to the horizontal, the azimuth angle and the profile of features blocking the cosmic rays in all horizontal directions (2π) around the sample (Nishiizumi *et al.,* 1989a). In most cases, shielding corrections of this sort are <5% but in high relief areas they may be very important.

Production rates can vary through time due intermittent shielding of the sample site by snow, volcanic ash, rock debris, soil, wind blown sand or vegetation. Episodic accumulations can be thought of as equivalent to a temporary increase in depth of the sample. The density of the overlying material is important and for snow the density is so low that a considerable thickness is required for a significant effect. It is likely that temporary burial would have more of an effect on flat lying sites than angled surfaces but this is not always the case and is particularly debated for snow cover (Nishiizumi *et al.,* 1989a; Gosse *et al.*, 1995a, b). It is important to assess the possibility and significance of temporary shielding at each new sampling site as both exposure age determinations and denudation rate estimates assume that there has been none. Use of two isotopes can help to distinguish between those samples which have had a simple exposure history with no phases of burial from those that have experienced complexity (section 2.4.4).

2.2.7 Scaling for the Effects of Latitude and Altitude

Scaling factors that enable production rates to be adjusted to any latitude and altitude on the Earth's surface have been proposed by several authors including Lal (1991). Although other models exists (e.g. Yokoyama, 1977), the scaling information from Lal (1991) is most commonly applied and has been summarised in Table 2.2. Empirical investigation into the altitudinal dependence of the production of ^{36}Cl indicated that these were the most appropriate factors of those available (Zreda *et al.,* 1991). A scaling factor (x) calculated using the indices in Table 2.2 can be used to convert any existing rate, for example 21 atoms $^{21}Ne\ g^{-1}\ SiO_2\ yr^{-1}$ at sea level and

>60°, to a specified altitude and latitude. The scaling factor formulation is based on extensive cosmic ray data on slow neutrons as an index for nuclear interaction rates as well as experimentally measured fluxes (Lal and Peters, 1967). Lal (1991) has proposed that the relative latitude-altitude variation in nuclear disintegrations in his scheme are accurate to within ±10%.

Table 2.2: Altitudinal and latitudinal scaling indices to fit the third order polynomial $x=a+b.y+c.y^2+d.y^3$, where y=altitude (km) and x is the scaling factor relative to the production rate at sea level and high latitude. (After Lal, 1991; Zreda, 1994)

Geomagnetic latitude	a	b	c	d
0	0.587	0.454	0.175	0.036
10	0.590	0.447	1.197	0.037
20	0.678	0.483	0.235	0.044
30	0.833	0.700	0.174	0.084
40	0.933	0.897	0.252	0.104
50	1.014	1.044	0.303	0.135
60-90	1	1.104	0.315	0.140

2.2.8 Summary

The principles of cosmogenic isotope analysis have been shown to be generally well constrained. The development of understanding of production mechanisms and the factors affecting production in rocks at the Earth's surface has become suitably well advanced to make the measurement of nuclide concentrations worthwhile, despite some remaining uncertainties. Accurate production rate determination is still vitally important. Theoretical studies are hampered by a lack of data on the probability that reactions will take place. The greatest problem facing experimental determination is locating suitable sites with well constrained exposure ages and simple exposure histories over geologically meaningful time scales. Current uncertainties in production rates are usually estimated at ±20% (Gosse *et al.*, 1996). Factors that effect the production rate of cosmogenic isotopes can be summarised into two categories: those for which corrections are known and those which have poorly constrained effects but are likely to be significant. Those known include variation of production with depth, with latitude and altitude and the effect of complex exposure geometries. Those unknown (or that remain without generally accepted correction factors) include the significance of variation of Earth's magnetic field, other possible changes in the incident flux and temporary shielding at the sampling site. Irrespective of these problems, the principles of the technique do allow for meaningful interpretation of measured concentrations of *in-situ*-produced cosmogenic isotopes at the Earth's surface.

2.3 Sample Preparation and Measurement of *In-Situ* Cosmogenic Isotopes

Sample preparation requirements vary according to the nuclide being measured and the composition of the target material. Nuclide separation should avoid contamination, while data are also required on the geochemical composition of the target material to assess production mechanisms and determine production rates particularly when isotopes, such as ^{36}Cl, are generated from a wide range of elements that naturally occur in varying abundances. Sample preparation for ^{21}Ne and ^{3}He requires separation of crystals of suitable minerals such as olivine, pyroxene or quartz for mass spectrometer measurement and analysis of the target composition, but is minimal compared to sample preparation requirements for ^{10}Be, ^{26}Al, ^{36}Cl and ^{14}C. Details on mineral separation and the chemical procedure for separating ^{10}Be and ^{26}Al from quartz are described Chapter 3. Details on sample preparation for ^{36}Cl and ^{14}C can be found in Ivy-Ochs (1996) and Jull *et al.*, (1992).

2.3.1 Stable Isotope Measurement Using Conventional Mass Spectrometry

Within the last 15 years, improvements in mass spectrometric techniques have made it possible to measure the small amounts of stable cosmogenic isotopes produced *in situ* in terrestrial samples, and concentrations of ^{3}He and ^{21}Ne have been successfully determined on a range of machines (Kurz, 1986a, b; Kurz *et al.*, 1990; Cerling, 1990; Graf *et al.*, 1991; Neidermann *et al.*, 1993, Brook, 1993; Seidl, 1993; Summerfield *et al.*, 1998a). Mass spectrometry makes use of the fact that isotopes of every element and many molecules have almost unique mass-to-charge ratios to measure precisely the relative abundance of isotopes of an element. The basis of mass spectrometry involves the formation of ions from a prepared sample, acceleration through an electrostatic potential, separation of the ions based on their mass-to-charge ratio and measurement of the number of ions received per second in a detector (Elmore and Phillips, 1987).

As discussed in section 2.2.1, ^{3}He and ^{21}Ne can be formed in rocks by mechanisms other than interactions with cosmic rays. Separating and measuring purely the cosmogenic component can be problematic, but by knowing the distinct isotopic ratios of different components it is possible to distinguish the cosmogenic concentration. Helium has two long-lived stable isotopes, ^{3}He and ^{4}He, and essentially two components: the inherited or trapped component, and the cosmogenic component. If the $^{3}He/^{4}He$ ratio of the inherited component is known then the amount of cosmogenic helium can be calculated because cosmogenic ^{4}He is negligible compared to the

inherited ^{4}He. Kurz (1986a) has shown that most of the cosmogenic helium is contained within the solid phases whereas the magmatic inherited component is held primarily in the melt and fluid inclusions. The majority of this inherited component can be released and its isotopic composition determined by crushing a clean sample in a vacuum. A combination of crushing and step heating can effectively separate the cosmogenic helium for measurement. Measuring cosmogenic neon is more problematic due to multiple neon components. ^{21}Ne found in surface rocks is commonly a product of cosmogenic, trapped and radiogenic origin. Because there are three components, it is usually desirable to measure three isotopes, ^{20}Ne, ^{21}Ne and ^{22}Ne (Neidermann *et al.,* 1993; Bruno *et al.,* 1997). The details of cosmogenic ^{21}Ne measurement are described in Chapter 3 with additional information in section 6.5.

2.3.2 Radioisotope Measurement Using Accelerator Mass Spectrometry

Cosmogenic radionuclides (^{10}Be, ^{14}C, ^{26}Al, ^{36}Cl) are rare compared to stable cosmogenic nuclides and are not measurable using conventional (low energy) mass spectrometry due to a lack of sensitivity and efficiency with small sample sizes and very low mass ratios (Elmore and Phillips, 1987). The long half-lives and low concentrations of most of the nuclides in question also prevent accurate measurement by decay counting which would take years to get comparable results (Finkel and Suter, 1993). Research into developing AMS to measure long-lived radioisotopes began in the late 1970s (e.g. Muller, 1977) and resulted in sufficient analytical sensitivity to measure the build up of *in-situ* cosmogenic nuclides. It is now possible to measure very low isotopic abundances of as few as 10^{5} atoms and isotopic ratios of the order of 10^{-14} (radioactive isotope/stable element), (Elmore and Phillips, 1987).

Comprehensive reviews of all aspects of AMS are provided by Finkel and Suter (1993) and Elmore and Phillips (1987) and the specifics of ^{10}Be and ^{26}Al measurement are detailed by Klein *et al.* (1982), Middleton *et al.* (1983) and Raisbeck *et al.* (1987). The following paragraphs are essentially a brief summary of the important points raised in these articles as well as a basic introduction to the principles of AMS.

Today, nearly all cosmogenic isotope measurement is carried out using tandem accelerators (the name tandem refers to a two stage acceleration design, see below) and there are approximately 24 worldwide capable of detecting rare isotopes including the facility at the Center for AMS, Lawrence Livermore National Laboratory and the Eidgenössische Technische Hochschule/Paul Scherrer Institut AMS facility (Finkel and Suter, 1993). AMS uses the same basic principles as

conventional mass spectrometry but includes an acceleration to megaelectron volt (MeV) energies. This high energy acceleration together with the analysis of negative ions allows the separation and measurement of isotopes with much lower abundance ratios than is possible with low (kiloelectron volt) energy acceleration (Elmore and Phillips, 1987).

The principal components of a typical AMS instrument are shown schematically in Figure 2.4. The samples are loaded into targets in an ion source, commonly a cesium (Cs) sputter source, which produces a negative ion beam. The beam is initially mass analysed to select the mass range of interest. The ion beam is then accelerated once to the high voltage terminal in the tandem accelerator where it passes through a foil slit or narrow gas filled canal. Here, outer electrons are stripped away and the ions become positively charged. The ion beam is then accelerated for a second time into a high energy mass spectrometer and then finally detected and counted by a range of possible methods including faraday cups or gas filled ionization chambers.

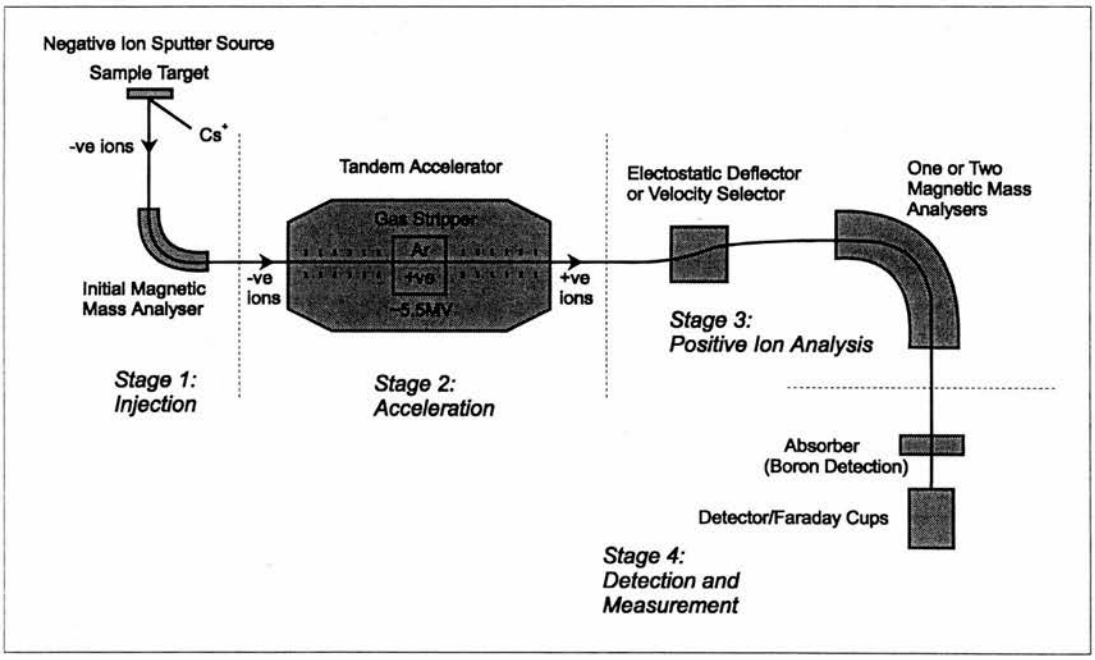

Figure 2.4: Schematic diagram of an AMS facility. See text for details (After Finkel and Suter, 1993).

Among the problems of radioisotope measurement are molecular contamination, instrumental background and interfering stable atomic isobars (Elmore and Phillips, 1987; Finkel and Suter, 1993). Interfering isobars are isotopes or molecules that have the same mass number (M) as the isotope being measured, for example ^{10}B disrupts measurement of ^{10}Be, ^{26}Mg interferes with

^{26}Al. Various techniques to deal with this can be used at different stages of analysis such as purification during sample preparation based on chemical differences of the two elements. The ion source can act as a first filter because in many cases the interfering isobars do not form stable negative ions such as ^{26}Mg and ^{36}Ar (Elmore and Phillips, 1987; Finkel and Suter, 1993). Each of the five stages described above (Fig. 2.4) can act as a filter and another example is the electron stripping stage and conversion to positive ions which can help remove molecules. High sensitivity can be maintained as problems are dealt with progressively throughout the instrument (Finkel and Suter, 1993).

To improve the precision of the isotopic ratios measured, standards (samples with a known isotopic ratio) and blanks (samples with no detectable isotopes) are run periodically for normalisation and to measure instrumental or sample preparation background. Results are often relative to these standards and therefore systematic errors (machine bias) are eliminated so long as they remain constant. Variation in systematic errors, for example those resulting from voltage drift, constitute most to the final uncertainty. The overall precision of AMS is usually in the range 3 to 10% given stable power supplies and suitable normalisation (Elmore and Phillips, 1987). Although higher accuracies are possible with conventional mass spectrometry, much lower abundance ratios can be determined using AMS. Finkel and Suter (1993) point out that uncertainties in calibration standards are not usually included in quoted errors. Measured isotopic ratios are converted to absolute nuclide concentrations in the form atoms per gram of target material. Some further details about the AMS facilities used in this project are provided in Chapter 3.

2.4. Interpretation of *in-Situ* Cosmogenic Isotope Data

The following sections describe the interpretation of measured concentrations of cosmogenic isotopes in terms of quantitative information on exposure histories of rock surfaces. It focuses on radionuclides ^{10}Be and ^{26}Al and the stable nuclide ^{21}Ne in quartz. It does not cover the interpretation of ^{36}Cl which requires special treatment due to the complex nature of its production and depth dependence (for a detailed description of ^{36}Cl interpretation see Bierman (1993) or Zreda (1994)). Literature on the interpretation of cosmogenic isotope analysis commonly refers to erosion when the broader term denudation would be more correct for it is the overall lowering of a surface which is implied rather than a specific set of processes (section 1.2). However, in order to follow convention, the term erosion will generally be used here.

2.4.1 *Accumulation of In-Situ Cosmogenic Nuclides*

The accumulation of cosmogenic radioisotopes at the Earth's surface over time can be described as follows:

$$N = \frac{P}{\lambda + \frac{\rho\varepsilon}{\Lambda}}\left[1 - e^{-\left(\lambda + \frac{\rho\varepsilon}{\Lambda}\right)t}\right] \qquad [2.4]$$

or rearranged with respect to time (t):

$$t = -\frac{1}{\lambda + \frac{\varepsilon}{\Lambda}}\ln\left[1 - \left(\lambda + \frac{\varepsilon}{\Lambda}\right)\frac{N}{P}\right] \qquad [2.5]$$

where: N = the concentration of radionuclides, atoms g SiO_2^{-1}

P = the local corrected production rate, atoms g SiO_2^{-1} a^{-1}

λ = the decay constant of the radionuclide ($\ln 2/t_{1/2}$), a^{-1}

ρ = the rock density, g cm^{-3}

ε = the erosion rate, cm a^{-1}

Λ = the cosmic ray attenuation length in target rock, g cm^{-2}

t = the length of time the surface has been exposed to cosmic radiation, a

For stable isotopes, which do not decay (i.e. no λ), this simplifies to:

$$N = \frac{P}{\frac{\rho\varepsilon}{\Lambda}}\left[1 - e^{-\left(\frac{\rho\varepsilon}{\Lambda}\right)t}\right] \qquad [2.6]$$

Equations 2.4, 2.5 and 2.6 are based on the following assumptions:

1. When the sample was exposed it contained a zero concentration of cosmogenic nuclides (i.e. when t = 0, N = 0).
2. Nuclides are quantitatively retained in the target material and have not been lost via diffusion or migration.

3. The only way nuclides are removed from the system is through radioactive decay (λ, for radionuclides only) and by erosion (ε).
4. The production rate, and therefore the cosmic ray flux and exposure geometry of the sample, is assumed to have been constant over the exposure time.
5. Production is assumed to decline exponentially with depth.
6. Erosion is assumed to be steady state, i.e. have been uniform and caused by the removal of layers of rock significantly less than the attenuation length of ~0.5.m. This is a specific definition of steady-state erosion and should not be confused with other uses of the term to describe geomorphic systems.

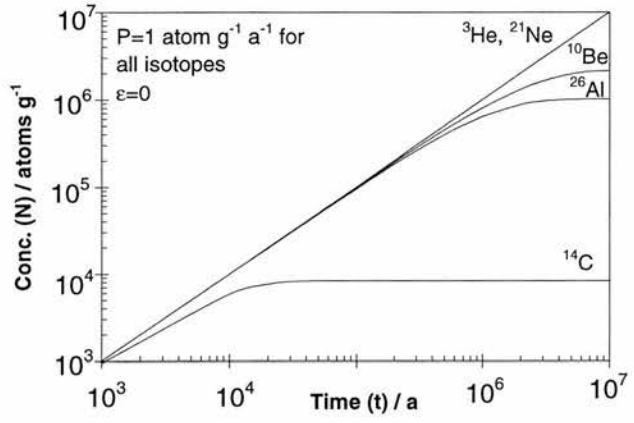

Figure 2.5: Accumulation of cosmogenic isotopes with constant unit production and no erosion. Stable isotopes accumulate linearly whereas radioisotopes accumulate to a maximum saturation concentration related to their half-life known as secular equilibrium.

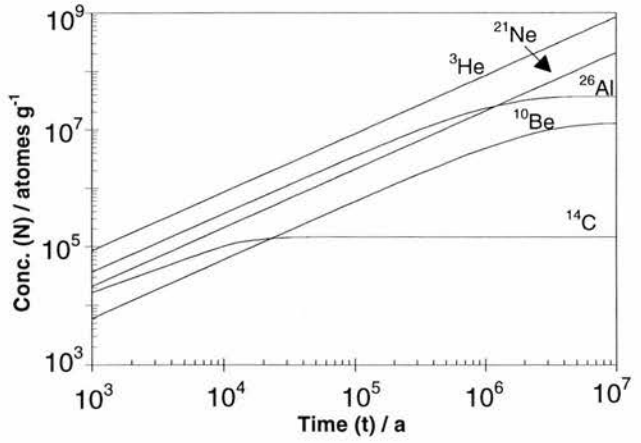

Figure 2.6: Accumulation of cosmogenic isotopes with currently accepted production rates at sea-level and >60° latitude in quartz, subject to zero erosion. Radioisotopes reach secular equilibirum after ~3-4 half-lives.

Fig. 2.5 shows how all five isotopes accumulate over time with respect to a unit production rate, decay constants as provided in Table 2.1 and the assumption of no erosion (i.e. $\varepsilon = 0$ in equations 2.4 and 2.6). After about 3-4 times the half life, radioisotopes ^{10}Be, ^{26}Al, ^{36}Cl and ^{14}C reach a saturated concentration known as secular equilibrium with respect to production and loss through decay (Honda and Arnold, 1967). This is when the build-up of nuclides has reached such a point that the number of nuclei decaying will equal the number being formed so that no further changes of concentration can occur. (It is sometimes rather confusingly referred to as a steady-state concentration.) Stable nuclides, however, like ^{21}Ne, continue to accumulate linearly. Fig. 2.6 shows how the isotopes accumulate relative to each other using the currently accepted production rates at sea level and high latitude (>60°) in quartz. ^{3}He will always have the highest concentration of any isotope given its high production rate (assuming no diffusion). Concentration ratios between the isotopes vary according to the exposure time.

2.4.2 Exposure Age Determination

Assuming zero erosion, equations 2.4 and 2.6 simplify to:

$$N = \frac{P}{\lambda}\left(1 - e^{-\lambda t}\right) \qquad [2.7]$$

or:

$$t = \frac{\ln\left(1 - \frac{N\lambda}{P}\right)}{-\lambda} \qquad [2.8]$$

For stable isotopes equation 2.7 simplifies further to:

$$N = P \times t \qquad [2.9]$$

In equations 2.7 and 2.9, N is entirely dependent on one unknown variable, that is the time of exposure (t). If this time represents an exposure event, N can give the 'exposure age' of the rock that has been revealed by the event, be it, for example, a landslide or episode of glacial erosion. The assumption that N = 0 when t = 0, is particularly important for this style of interpretation to be valid. As will be discussed later, such an assumption can be hard to verify, but, by using two or more isotopes it can be tested. If calculated ages coincide and concentration ratios reflect production ratios, then the result is more likely to represent a true age. Lal (1995) suggested that

the result be called an 'event age' rather than exposure age to make it more clear what the calculation represents.

For stable isotopes there is no theoretical time limit to the range of exposure age dating because nuclides continue to accumulate in a linear fashion indefinitely (Figs. 2.5 and 2.6). However, radionuclides can only be used for accurate exposure age dating before secular equilibrium has been reached. After secular equilibrium has been reached the calculated age will remain the same regardless of further exposure and is termed an apparent or effective age. The limit on exposure age dating using ^{10}Be, ^{26}Al, ^{14}C and ^{36}Cl is ~4 x their half-lives. For ^{10}Be and ^{26}Al the limits on exposure age dating are therefore ~ 5 Ma and ~2.5 Ma respectively. Experimental calibration of production rates (section 2.2.4) uses independently dated surfaces and interprets measured concentrations using equations 2.7 and 2.9 to solve for P rather than t. (In some cases (e.g. Kurz 1986b) independent estimates of t and ε, allow equations 2.7 and 2.9 to be used for this purpose.) It is clear that for the result to be accurate the value of t must be well constrained.

The assumption of zero erosion, and therefore the applicability of equations 2.7 and 2.9, is seldom realised in reality; in almost all environments bedrock outcrops experience some kind of alteration by weathering processes and erosion. The concept of an exposure age is therefore only truly applicable in a limited number of geomorphic scenarios and should always be regarded as a special case (sections 2.5.1 and 2.5.2). It must be remembered that all exposure ages are entirely model dependent and subject to errors associated with each limiting assumption. If the assumption of zero erosion cannot be verified, or the concentration has reached secular, equilibrium then calculated ages are minimum ages rather than true exposure ages. Exposure age equations yield the lowest amount of time that could have elapsed to accumulate the measured concentrations, therefore ages are usually termed minimum ages to allow for some undetermined margin of error. Obviously, the effect of erosion will be enhanced over time and therefore exposure ages are usually more accurate for younger events.

2.4.3 Erosion Rate Determination

The effects of erosion on both stable and radionuclide accumulation are shown in Figures 2.7 and 2.8. Erosion reduces the time that a radionuclide takes to reach secular equilibrium because it increases the amount of nuclides that are lost through time. Figure 2.7, shows that for ^{10}Be, the concentration of nuclides reaches secular equilibrium with an erosion rate of 1m Ma^{-1}, 10 Ma years earlier than with no erosion. As shown in Figure 2.8, a stable nuclide can also reach a

saturated concentration with respect to production and erosion. Comparing Figures 2.7 and 2.8 shows that for the same erosion rate, stable nuclide concentrations take longer to reach secular equilibrium than radionuclide concentrations because there are no losses through decay.

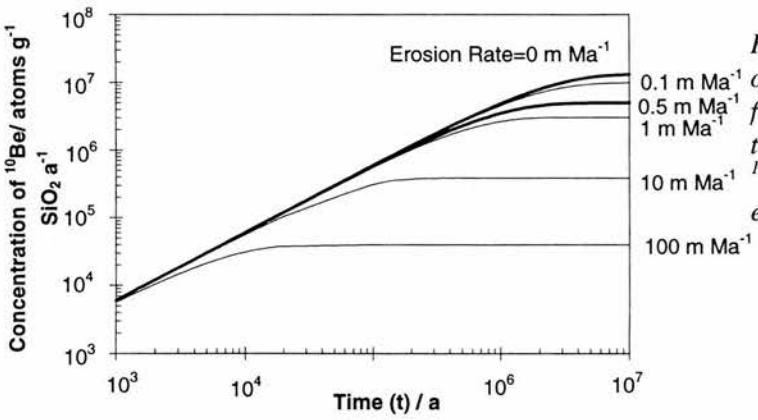

Figure 2.7: Effect of erosion on the accumulation of ^{10}Be for various rates. The higher the erosion rate the sooner ^{10}Be reaches secular equilibrium.

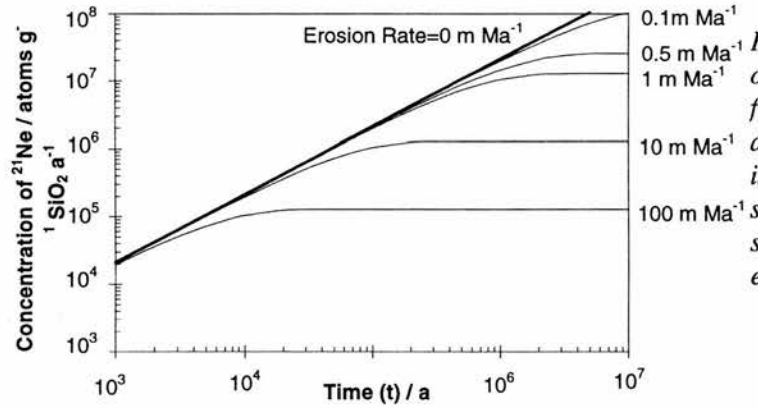

Figure 2.8: Effect of erosion on the accumulation of ^{21}Ne for various rates. Subject to a finite erosion rate stable isotopes also reach a saturation concentration subject to production and erosion.

By assuming that nuclides concentrations have reached secular equilibrium, i.e. that $t>>1/(\lambda+\rho\varepsilon/\Lambda)$ (Lal, 1995), then an erosion rate can be calculated such that:

$$N = \frac{P}{\lambda + \frac{\varepsilon\rho}{\Lambda}} \qquad [2.10]$$

or:

$$\varepsilon = \frac{\Lambda}{\rho}\left(\frac{P}{N} - \lambda\right) \qquad [2.11]$$

In general, the resultant erosion rate will be a maximum, unless one can be certain that secular equilibrium has been reached in which case the result will represent a true erosion rate. The validity of this erosion rate model can be tested using a combination of nuclides (see below). It must be emphasised that erosion rates calculated in this way are heavily model dependent and require an accurate knowledge of production rates. At low erosion rates, uncertainty in P is particularly influential. As mentioned above, stable isotopes can also reach a steady-state saturated concentration with respect to P and ε, although this is seldom recognised. It is unusual to use a stable isotope alone to determine an erosion rate because it takes such a long time for the nuclides concentration to reach saturation. However, in particular geomorphic scenarios, it is reasonable to use a stable isotope in this way (Summerfield *et al.*, 1998a).

The modelled erosion rates from equations 2.10 and 2.11 are necessarily integrated over the period of time that an isotope takes to acquire secular equilibrium with such an erosion rate. In other words, the minimum amount of time to which a modelled erosion rate applies is the time it takes for the lines in Figs. 2.7 and 2.8 to flatten out. This value is equivalent to the apparent or effective exposure age of the sample. No maximum limit on the duration of the calculated rate is imposed by the model. This is because the concentration of the isotope is assumed to be in secular equilibrium and will remain so for an infinite period of time. In reality, of course, the erosion rate and perhaps the production rate will change through time and therefore extrapolation must be based on a consideration of the variables affecting erosion rates, such as climate, that can vary through time.

2.4.4 Using the 'Erosion-Island' Graph to Determine Exposure Histories

So far two end-member interpretive models have been considered: minimum exposure ages assuming no erosion, and maximum erosion rates assuming concentrations are in secular equilibrium. In each case, it is obviously beneficial to use more than one isotope to verify the underlying assumptions. If ages and rates coincide for different isotopes the results are more likely to reflect the true exposure ages and erosion rates for the particular site. If, however, erosion is occurring but nuclide concentrations have not reached secular equilibrium, the relationship between nuclide concentrations and their ratios with other nuclides can be used to

decipher exposure histories and determine erosion rates. In addition, examination of the ratio between isotopes can determine the extent to which an exposure history may have been complex. This is because the ratio of concentrations of two nuclides in an eroding rock surface changes sensitively with erosion and the rate of erosion (Klein *et al.*, 1986; Nishiizumi *et al.*, 1989a; Lal, 1991).

A graph of the concentration of one nuclide on a log scale against its ratio with another is a smooth curve reaching an end point when both nuclides have reached saturation and the ratio becomes fixed. If one is considering ^{10}Be and ^{26}Al and plotting N_{Be} against N_{Al}/N_{Be} then the saturation ratio steadily decreases as the erosion rate decreases. A family of curves for ^{10}Be and ^{26}Al for various erosion rates plots as shown in Figure 2.9 and is sometimes known as a 'bananagram,' for obvious reasons. A central zone on the graph is defined by an upper curve for $\varepsilon = 0$, assuming that there was zero initial concentration in the sample, and the lower, saturation ratio curve. It is known as the 'steady-state erosion island' since all samples with a simple erosional history characterised by steady-state denudation will plot within the zone between these two curves (Klein *et al.*, 1986; Lal, 1991; Nishiizumi *et al.*, 1989a). (Note that Klein *et al.*, 1986 do not use a log scale for their concentration/ratio plot and therefore their diagrams do not resemble bananas but triangles.) All lines within the erosion island represent the evolution of the ratio of ^{10}Be and ^{26}Al with time for different erosion rates except the lowest (dotted) line which merely connects the final saturation ratios for all possible erosion rates. Above the $\varepsilon=0$ curve is a 'forbidden zone'. Samples that plot in this area contain a ratio potentially indicative of higher production rates in the past, possibly as a result of a period of time at a higher elevation, or an inherited component from prior exposure for one isotope, or possibly some sort of measurement error, for example insufficient removal of meteoric ^{10}Be. Samples which plot below the saturation curve will have had a complex exposure history which may have included periods of burial. During a burial phase which cuts off production totally, for example due to a thick accumulation of ice or rock debris, the ratio between the isotopes would evolve due to the influence of radioactive decay, but the evolution would follow a different trajectory on the erosion-island graph from that which it was following before burial. This would move the concentration ratio for the sample below the erosion-island. After re-exposure the memory of the burial phase would remain in the relative concentrations of isotopes in the upper rock layers until enough time has passed for denudation to expose rock from a depth greater than the zone of production - that is a depth of about 1-2 m.

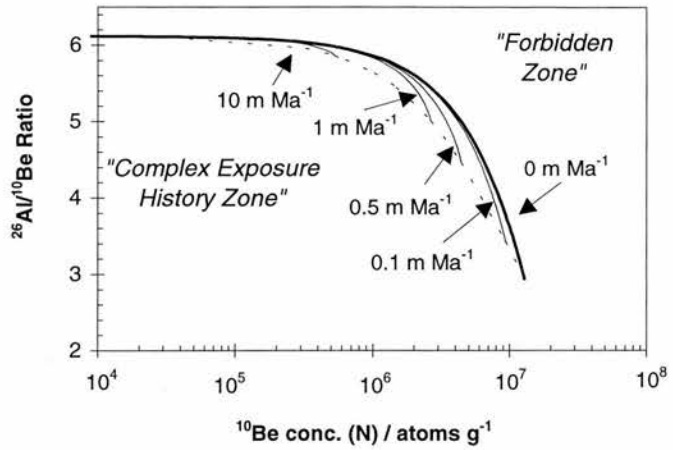

Figure: 2.9: Erosion-island graph for ^{26}Al and ^{10}Be. See text for explanation.

Samples that plot below the erosion-island could support an infinite number of burial and re-exposure scenarios - there is no single mathematical or geomorphic solution for a position in the complex exposure zone. Obviously, some likely scenarios could be proposed or excluded on the basis of the individual sampling site, but in general the actual sequence of events cannot be interpreted from the graph. In addition to phases of burial, the removal of a rock layer greater or of the order of the cosmic ray attenuation length (a 'chip' event) invalidates the steady-state assumption and results in data that would plot below the erosion-island (Lal, 1991). Small *et al.*, (1997) have recently focused on the problem of samples from surfaces characterised by episodic erosion with a series of chip events. They have shown that the steady-state model can yield rates that are both greater and smaller than the true mean rate of erosion. In addition they demonstrate that for relatively fast rates of erosion (>1 m Ma^{-1}) the conventional erosion-island is not a sufficient test because the removal of large rock fragments tends to lower the ^{10}Be concentration but will not significantly alter the $^{26}Al/^{10}Be$ ratio and therefore data can potentially move within the erosion-island but not out of it. The errors associated with episodic erosion imply that under such circumstances it is best to use an average rate from many samples, assuming that the chip events have not been synchronous at all sites (Small *et al.*, 1997).

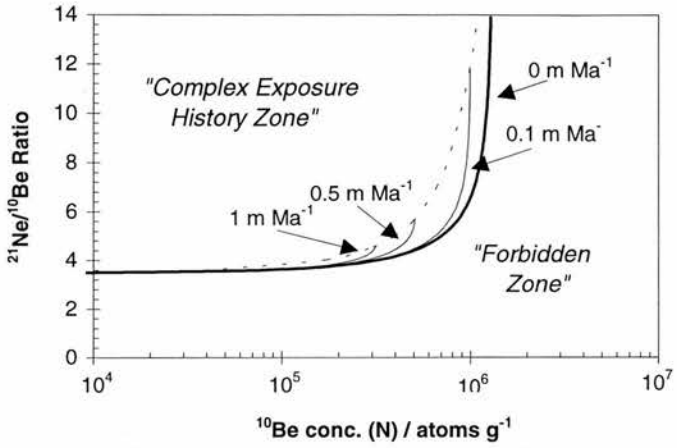

Figure 2.10: Erosion-island graph of ^{21}Ne and ^{10}Be.

Erosion rates and complex histories can also be determined using an erosion-island graph with ^{10}Be and ^{21}Ne as shown in Figure 2.10, or other combinations, e.g. ^{26}Al and ^{21}Ne (Graf *et al.*, 1991). The erosion-island is the other way up compared to the $^{10}Be/^{26}Al$ plot because ^{21}Ne has a higher production rate than ^{10}Be and does not decay. Unlike the $^{10}Be/^{26}Al$ plot, the curve for $\varepsilon=0$ never reaches a saturation ratio because ^{21}Ne is stable and accumulates in a linear, infinite fashion when the sample is not experiencing erosion (Fig. 2.8). The $^{10}Be/^{21}Ne$ erosion-island is particularly useful for revealing prior exposure because ^{21}Ne is retained by buried samples (Ivy-Ochs, 1996). Any sample plotting above the erosion island in Figure 2.10 will have more ^{21}Ne than expected for the corresponding ^{10}Be concentration and therefore must have experienced some prior exposure to cosmic rays before the most recent period of exposure. The problem of prior exposure is discussed in the following section.

2.5 Geomorphological Applications of *In-Situ* Cosmogenic Isotope Analysis

After the introduction of the cosmogenic technique in the mid-1980's, the majority of work was concerned with the systematics of production, calculation of production rates, calibration and testing of the technique using samples from independently dated sites and refinement of measurement techniques. In general, this work was aiming to prove the potential of *in-situ* cosmogenic isotope analysis to quantify exposure histories of rocks at the Earth's surface, first recognised by Davis and Schaeffer (1955). It is this work that has been reviewed in sections 2.2, 2.3 and 2.4. The use of *in-situ* cosmogenic isotope analysis to solve unanswered problems began later as confidence grew in the methodology and interest spread from geochemists and physicists to a wider group including geomorphologists and geologists. As mentioned previously, there is

still uncertainty associated with modelled erosion rates and exposure ages, not least from estimated production rates, but as these issues continue to be tackled, more and more often the technique is being applied in new areas to provide the first information of its kind, be it chronological or kinematic control of geomorphic phenomena. Some examples of recent applications are given in Table 2.1. They have been selected to show the wide range of problems that have been tackled using the five different principal isotopes. The following sections review geomorphic/geologic applications to date divided into three categories; glacial chronology, other exposure age dating applications and estimating rates of denudation.

2.5.1 Applications in Glacial Chronology

At the onset, the major benefit of *in-situ* cosmogenic isotope analysis was in providing a surface exposure dating technique that evaluated 'ages' directly rather than by association with radiocarbon dated organic material or some other stratigraphic marker. Consequently, a large majority of work has been concerned with exposure dating. Exposure dating was also a way of verifying the technique and many applications have been in areas where some chronological control already exists.

Glacially eroded environments generally provide ideal settings for cosmogenic exposure age determination with plenty of exposed, scoured bedrock surfaces representing glacial erosion with striations indicating surface preservation and minimal subsequent erosion. Glacial chronology is a crucial part of understanding Quaternary climatic change and has been a focus for cosmogenic isotope analysis since the development of the technique. A significant proportion of this work has been carried out in Antarctica where high production rates and low denudation rates in terms of global comparisons further enhance the applicability of the technique. Difficulties with more conventional radiocarbon dating have meant geomorphologists have looked for other methods to determine glacial histories (Brown *et al.*, 1991; Brook and Kurz, 1993; Brook *et al.*, 1993, 1995a, b; Ivy-Ochs *et al.*, 1995; Bruno *et al.*, 1997). However, other glaciated regions have also been subject to exposure age dating including the Swiss Alps (Ivy-Ochs *et al.*, 1996), western Norway (Brook *et al.*, *1996*), the Sierra Nevada (Nishiizumi *et al.*, 1989a; Phillips *et al.*, 1990, 1996) and the Rocky Mountains (Gosse *et al.* 1995a, b; Jackson *et al.*, 1997).

Several of the applications mentioned above (Ivy-Ochs *et al.* 1996; Gosse *et al.* 1995a, b; Phillips *et al.* 1990, 1996) have sampled boulders on moraines in order to constrain glacial histories. Exposure ages of glacial erratics have also been derived (Jackson *et al.*, 1997). However, the use

of boulders as opposed to bedrock surfaces as sampling sites is a practice that has been debated for some time, both with respect to moraines (Hallet and Putkonen, 1994) and more generally (Seidl *et al.,* 1997). The main issue involved is whether boulders in, for example, moraines or flood deposits, can accurately represent an event age or whether they necessarily reflect accumulated exposure because of their often complex emplacement history, and are therefore a poor choice of site. Hallet and Putkonen (1994) argue that there is no simple relationship between a boulder exposure age and a moraine age, rather that the boulder age reflects the competing effects of moraine erosion and boulder weathering. Also of significance is whence the boulder was eroded, whether it has been reworked by a series of glaciers, how much of its recorded exposure reflects time at source, for example on a valley side, and how much in transit, and whether or not the boulder has rolled to its present position. Some of these issues can be eliminated by careful site selection but others can have significant consequences (Brook and Kurz, 1993). However, several applications in glacial chronology using boulders on moraines have been successful (Gosse *et al.,* 1995a, b; Ivy-Ochs, 1996). Gosse *et al.* (1995b), for example, measured ^{10}Be to get an average age of the Inner Titcomb Lakes moraine, Wind River Mountains, Wyoming of 11.0 ± 0.7 a. The small error from a sample set of 10 shows that sampling moraines does not always have to be problematic. Their results lend support to a growing line of evidence of a Younger Dryas cooling event in western North America.

Not all applications in glacial chronology have used moraines or erratics. Brook *et al.* (1996) measured ^{10}Be and ^{26}Al in bedrock samples from a vertical transact on a valley side at Skåla, western Norway, to delimit the height and chronology of the Fennoscandian ice sheet. Their results indicate that summit tops in the region (>55 ka) were not overridden during the last glacial maximum, ice receded from a previously identified trimline at the time of the last glacial maximum (~ 23 ka) and that a lower trimline was formed during a standstill between 13 and 18 ka BP. Bierman *et al.* (1996) considered arctic upland bedrock surfaces on Baffin Island and using ^{10}Be and ^{26}Al have discovered that although there is complexity to the exposure history, there has been minimal erosion by either ice or subaerial processes during the late Pleistocene.

2.5.2 Applications of 'Exposure Age Dating' for Other Purposes

The major use of all *in-situ* cosmogenic isotope analysis to date has been for exposure or event age determination in a wide variety of settings for various reasons, some purely for dating (Staudacher and Allégre, 1993; Cerling *et al.,* 1994; Stone *et al.,* 1996b) and others to quantify processes (Ritz *et al.,* 1995; Bierman *et al.,* 1995; Seidl *et al.,* 1997). Late Quaternary lava flows

in well mapped volcanic complexes have been a popular choice of site to test the ^{10}Be, ^{36}Cl, ^{3}He and ^{21}Ne methods against existing chronological data. These applications have moved on from the calibration tests of Kurz *et al.* (1990) and Cerling (1990) but still largely rely on intercalibration to support their findings. Staudacher and Allégre (1993) were among the first to use ^{3}He and ^{21}Ne with existing production rates from Kurz *et al.* (1990) to date olivine from basalt volcanoes on Réunion. They successfully showed that eruption ages from K-Ar dating (62 ka) were very similar to cosmogenic exposure ages (65 ± 2 ka), indicating minimal erosion. They also provided the first direct dating of a fault by sampling the lower part of a collapsed caldera wall to 23.8 ± 2 ka. Younger basaltic rocks are not as easy to date using K-Ar or $^{40}Ar/^{39}Ar$ as older ones (<100 ka) due to a low K content and there have been attempts, when these techniques have failed or been inconclusive, to use cosmogenic isotope analysis to validate chronologies. Zreda *et al.* (1993) used ^{36}Cl on samples from the Lathrop Wells volcanic center in southern Nevada with adjusted production rates from Zreda *et al.* (1991). Their results ranged from 73 to 93 ka with a mean age for the eruption of 84 ± 8.1 ka. Variable and higher dates from $^{40}Ar/^{39}Ar$ analysis suggest that erosion might have affected the ^{36}Cl results but this is unlikely due to the consistency of the cosmogenic data and the possibility could be easily eliminated with further depth profile analysis (Zreda *et al.*, 1993). Their results do not support an existing hypothesis of multiple eruptions of the volcano, but neither do they preclude it. Laughlin *et al.* (1994) used ^{3}He to date young basalts from the Zuni-Bandera volcanic field, New Mexico. Their results fall into three main age ranges with average values of 3, 11 and 57 ka. The low ages compare very well with radiocarbon dates on charcoal found below the flows supporting the use the production rate of Cerling (1990) when adjusted for recalibration of the ^{14}C time scale. They also propose that ^{3}He analysis on olivine can serve as a useful monitor for excess ^{40}Ar which is one cause of problems with dating young basalts. Shepard *et al.* (1995) use ^{10}Be and ^{36}Cl to date basalt flows from the Lunar Crater volcanic field in Nevada. On one flow they obtained similar ^{10}Be and ^{36}Cl ages with an average of 38.1 ± 9.7 ka, but which is an order of magnitude lower than the K-Ar age. A pristine morphology and unweathered olivine suggest an excess Ar problem in this flow.

Cerling *et al.* (1994) dated the Big Lost River flood on the Snake River Plain, Idaho using cosmogenic ^{3}He and ^{21}Ne in eroded basalt boulders and scoured bedrock. They measured two ages between 19 and 22 ka and two much older ages which they attributed to an inherited, pro-flood component. They proposed a 20.5 ± 1.9 ka age for the flood that coincided with other estimates for floods in the same area. This work clearly highlights the importance of eliminating the possibility of a inherited component in samples, especially in applications where there is no

prior age control. Trull *et al.* (1995) measured ^{10}Be and ^{3}He in beach ridges to investigate Pleistocene lake levels in Death Valley but experienced problems with diffusion of ^{3}He (section 2.2.3) and inconclusive ^{10}Be ages. Prior exposure in beach material is the likely cause of poor results (Trull *et al.* 1995), again emphasising the difficulties of using non bedrock samples.

Dating of morphological features displaced along active faults is conventionally problematic and there have been at least four recent attempts to use cosmogenic isotope analysis to overcome this problem and evaluate slip rates and earthquake recurrence intervals. Ritz *et al.* (1995) used minimum ^{10}Be ages from gneiss boulders on misaligned alluvial surfaces on the Bogd Fault System, Gobi-Altai, Mongolia and measured a horizontal slip rate of ~1.2 mm a^{-1} in one area and a vertical rate of movement of ~1.1 mm a^{-1}. These rates are significantly lower than rates estimated by correlation of humid periods of alluvium deposition and the new data indicated a recurrence interval of ~5 ka for large earthquakes. Bierman *et al.* (1995) used a similar method with ^{10}Be and ^{26}Al measurements in quartz from offset debris flow fans in Owens Valley, California. They calculated an earthquake recurrence interval of 5- 8 ka but were unable to reveal the temporal relation between fan and moraine deposition in the region due to a small number of samples. Finkel *et al.* (1997) assessed active tectonics in the Tibetan Plateau using ^{10}Be and ^{26}Al and determined a slip rate of ~12 mm a^{-1} for the Kunlun fault which matches inferred rates for other segments of the same fault. An interesting point about this study is that Finkel *et al.* (1997) were able to constrain very low exposure ages of <1-2 ka because of the high production rates prevailing at their high elevation sites.

An innovative application of cosmogenic surface exposure dating has been to understand desert pavement evolution (Well *et al.* 1995; Shepard *et al.* 1995; Anderson and Wells, 1997). Alternative hypotheses exist for the formation of desert pavements, including wind deflation or winnowing by fluvial action of fine particles leaving a coarse lag, migration of clasts up through the soil column or deposition of windblown sediments between the clasts which are therefore maintained on an accretionary mantle. Wells *et al.* (1995) used ^{3}He in the Mojave Desert, California, to date pavement clasts and adjacent uneroded basalt flows and found concordant exposure ages between all samples. They concluded that clasts must have remained at the surface since the emplacement of underlying flows and therefore reflect the accretionary model of evolution by deposition of windblown dust rather than models in which clasts concentrate at the surface randomly through time. Shepard *et al.* (1995) have also supported this hypothesis using a similar sampling strategy in the Lunar Crater volcanic field, Nevada.

Cosmogenic isotope analysis and exposure age determination has been used in a variety of studies to address problems in fluvial geomorphology, in particular incision rates and profile evolution (Molnar *et al.* 1994; Seidl 1993; Seidl *et al.* 1997; Burbank *et al.* 1996; Repka *et al.*, 1997). Molnar *et al.* (1994) measured ^{10}Be in cobbles from river terraces to determine channel abandonment times in the Tien Shan, China. Their results suggest that the lowest terrace from one river was formed after deep incision (~150 m) during, or just before, the last global deglaciation, ~20 - 13 ka BP. This conclusion is at odds with previously accepted chronologies for the region (Molnar *et al.*, 1994). Burbank *et al.* (1996) used a similar method, but more extensively, with ^{10}Be and ^{26}Al in bedrock samples from pristine, uneroded strath terraces above a section of the Indus river, in the Nanga Parbat region of the Himalayas. Ages ranged from 4 to 68 ka with strath elevations from 65 to 410 m above the present river. By assuming that the interval of strath formation was short in comparison to the time since abandonment, they calculated mean bedrock incision rates of ~2-12 mm a^{-1}, representing some of the highest sustained bedrock incision rates ever recorded. In a particularly successful application of cosmogenic isotopes analysis, Burbank *et al.* (1996) go on to examine the relationship of their incision rates with uplift rates and slope evolution for the Nanga Parbat region, concluding that hillslope denudation in the region is ultimately controlled by rock strength. Recent work on the incision of the Fremont River, Utah, has been carried out by Repka *et al.*, 1997) by evaluating ^{10}Be and ^{26}Al concentrations in sediment on terraces. Although they were able to assign ages to three terraces, in general, work in river sediments is problematic and liable to large errors compared to the studies using bedrock samples outlined above.

Seidl (1993) and Seidl *et al.* (1997) used all five commonly used isotopes in olivine (the only study to date to do this) to test the potential of cosmogenic isotope analysis to elucidate the role of knickpoint propagation in longitudinal river profile evolution. Calculated ages of samples from Kaulaula Valley on Kauai, Hawaii, show considerable inconsistency between isotopes which could reflect analytical problems, loss of stable isotopes or prior exposure of sampled boulders, although this seems unlikely (Seidl *et al.*, 1997). Overall, the data are consistent with a model of knickpoint propagation up stream with migration rates on the order of 1 mm a^{-1}.

2.5.3 Applications to Estimate Rates of Denudation

Although there has been an emphasis on exposure age determination in applications carried out to date, there have been some successful attempts to evaluate rates of denudation. Such studies have used a variety of approaches: some have utilised independent dating methods, particularly

K-Ar ages of lava flows, to estimate denudation rates based on the discrepancy between apparent cosmogenic exposure ages and the real exposure age of sample sites (Sarda *et al.*, 1993), others have used depth profile analysis to estimate rates (Strack *et al.*, 1994), some have interpreted the concentration of cosmogenic isotopes in sediment for spatially averaged rates (Granger *et al.*, 1996; Bierman and Steig, 1996), others have used the decay and inheritence of radioisotopes in both alluvium and bedrock to monitor river incision and glacial erosion (Granger *et al.*, 1997; Briner and Swanson, 1998), and a few have used the method outlined in sections 2.4.3 and 2.4.4. A collection of denudation rates derived from *in-situ* cosmogenic isotope analysis in bedrock surfaces using the steady-state erosion model presented in section 2.4.3 is shown in Table 2.3.

Table 2.3: Denudation rates calculated from *in-situ* cosmogenic isotope analysis

Author(s) and Year	Location	Isotope / Rock Type	Rate, m Ma^{-1}
Nishiizumi *et al.* (1993)	Himalayas	^{10}Be and ^{26}Al, granodiorite	[a]14 [a]56
as above	Grand Teton, Wyoming	^{10}Be and ^{26}Al, granodiorite	[a]48
as above	Mt. Evans, Colorado	^{10}Be and ^{26}Al, granite	[a]8
Bierman and Turner (1995)	Eyre Peninsula, Australia	^{10}Be and ^{26}Al, granite	0.7
Nishiizumi *et al.* (1991)	Antarctica	^{10}Be and ^{26}Al, mainly granite	<1
Small *et al.* (1997)	Western USA	^{10}Be and ^{26}Al, gneiss and granite	2-19
Brown *et al.* (1995a)	Luquillo Forest, Puerto Rico	^{10}Be, quartz-diorite	[a]25
Albrecht *et al.* (1993)	Pajarito Plateau, New Mexico	^{10}Be and ^{26}Al, tuff	1-10
Stone *et al.* (1994)	North and South Australia	^{36}Cl, limestone	4.5-184
Bierman (1993)	Southern USA	^{10}Be and ^{26}Al, granite	7-12
Kurz *et al.* (1990)	Hawaii	^{3}He, basalt	7-11

[a] rate from a single measurement only.

The studies of denudation rates shown in Table 2.3 demonstrate the clear potential of cosmogenic isotope analysis to derive denudation rates. The rates have been measured for various environments and geomorphic settings and consequently show considerable variation. However, the rates are all for bedrock surfaces, principally those that contain quartz, and therefore the range of rates is relatively small compared to the full range of denudation rates operating at the

Earth's surface, for example, on unconsolidated material or softer lithological units that do not contain suitable minerals for analysis.

Some of the denudation rate values shown in Table 2.3 represent single measurements only. Because the data are site specific, the true meaning of such rates is difficult to constrain because there is no knowledge of the spatial variation of denudation across the site. In order to produce more reliable data, a larger number of samples spread over an area are needed. As the technique develops and analytical techniques become more routine, it should be easier (and cheaper) to process samples and therefore to assess spatial variation across sampling areas. One approach could be to combine the use of *in-situ* cosmogenic isotope analysis in bedrock outcrops with analysis of *in-situ* cosmogenic isotopes in fluvial sediments and compare the data for a defined catchment area. Brown *et al.*, (1995a) advocated such a methodology and carried out a 'proof of method' application in a small well studied drainage basin in Puerto Rico. Although the results were satisfactory, the interpretation of sediment data are subject to a large number of assumptions, for example regarding sediment storage, which would be difficult to assess in other more complex drainage basins.

Apart from problems associated with spatial extrapolation, other potential uncertainties exist. Analytical and production rates errors will hopefully decrease with continuing research but the greatest problem is likely to continue to be with choice of sampling site and the extent to which the limiting assumptions of the interpretive model are fulfilled at that site. This is equally true of exposure age determination and any other model using to interpret cosmogenic isotope concentrations. As Bierman (1994) emphasises, it not enough simply to understand the assumptions of a model - they must also be valid. In many of the studies shown in Table 2.3 the geomorphic setting of specific sampling sites is only briefly described but this information, coupled with the use of multiple isotopes, are probably the key requirements to assess the accuracy of denudation rate data in the future.

2.6 Conclusions

Analysis of cosmogenic isotopes produced *in situ* in terrestrial rocks at the Earth's surface is a valuable new technique that can yield geomorphic information on the exposure histories of surface samples over time scales up to several million years. Measured concentrations of cosmogenic nuclides can be interpreted in terms of either an exposure age that relates to a specific exposure event, or in terms of a denudation rate assuming that the isotopes have reached

secular equilibrium. To date, five isotopes, ^{3}He, ^{10}Be, ^{21}Ne, ^{26}Al and ^{36}Cl, are routinely measured and being applied in a growing number of geomorphological applications every year. Scaling factors exist for calibration of measured or theoretically estimated production rates to all latitudes and altitudes and are accurate to within ±10%. Despite an overall uncertainty in production rates of ±20%, the technique offers the chance to place quantitative constraints on rates of bedrock denudation in geomorphic settings and over time scales that have hitherto been unobtainable. The interpretive models for exposure ages and denudation rates require careful field sampling (section 3.2) and a full appreciation of the assumptions on which they are based. Use of two or more isotopes is often a convenient way to check the validity of such assumptions.

Chapter 3:

Field and Analytical Techniques

3.1 Introduction

A full account of the field and analytical techniques employed during the preparation of this thesis for cosmogenic isotope analysis of *in-situ*-produced cosmogenic ^{10}Be, ^{26}Al and ^{21}Ne in quartz are presented in this chapter. Cosmogenic isotope analysis has three practical components: field sampling, sample preparation and measurement. Field sampling is isotope independent and a basic report that applies to ^{10}Be and ^{26}Al as well as ^{21}Ne is presented in section 3.2. However, sampling is ultimately dependent on the particular nature of the problem under investigation and on the geomorphic intricacies of each individual site. Therefore, only general comments regarding the collection of samples have been given here and sampling details are provided in sections 4.6, 5.5 and 6.4. Sample preparation and measurement are largely isotope-specific, although for ^{10}Be and ^{26}Al they are linked. The analysis of ^{10}Be and ^{26}Al as a pair is considered separately in section 3.3 from analysis of ^{21}Ne in section 3.4. Sample preparation of ^{10}Be and ^{26}Al, particularly the extraction of ^{10}Be and ^{26}Al from quartz, is not yet a routine procedure due to the developing nature of the cosmogenic technique. Comparison of existing descriptions of chemical procedures (Seidl, 1993; Brook, 1993; Ivy-Ochs, 1996) reveals significant variation and therefore a detailed description of the methods employed in this thesis has been provided. Measurement of ^{10}Be and ^{26}Al by accelerator mass spectrometry (AMS) is well documented (Klein *et al.*, 1982; Middleton *et al.*, 1983; Elmore and Phillips, 1987; Finkel and Suter, 1993) and the basis of the measurement technique has been described in section 2.3. Some further details of AMS measurement, most of which are specific to the AMS facilities used in this thesis are provided in section 3.3.3.2. Sample preparation for ^{21}Ne analysis is described in section 3.4.1. Although somewhat simpler than for ^{10}Be and ^{26}Al, measurement and interpretation can be more problematic due to multiple neon components (section 2.2.1). Measurement of ^{21}Ne by conventional mass spectrometry is also well documented (Neidermann *et al.*, 1993, 1994; Bruno *et al.*, 1997; Summerfield *et al.*, 1998a) but a practical overview is provided in section 3.4.2.

3.2 Field Techniques

The importance of good sample selection for cosmogenic isotope analysis cannot be over-emphasised. The information obtained from the technique is site specific and thus sample selection is critical to the success of a project. The most important question to ask during sampling is whether or not the sample will elucidate the geomorphic event or process under investigation. An adequate geomorphological understanding of the field situation is absolutely necessary to obtain meaningful results. Sampling strategy and the number of samples collected depends primarily on the complexity of the problem and the geomorphic setting of the sites, but also on analytical restrictions.

In total, over 100 samples were collected in central Namibia and the Transantarctic Mountains, Antarctica from bedrock exposures in order to quantify denudation rates. Samples were selected that appeared to have had a simple denudation and exposure history in well constrained geomorphic settings. Sites were selected so that the information obtained would be as representative as possible of a wider area. Overhangs and sites that could have been persistently covered by soil, snow, sand or falling debris were avoided. Although it is possible to apply the technique to boulders and sediments, the exposure history of these sites can be hard to constrain and denudation rate estimates would be consequently hard to interpret. Bedrock samples were chosen because, in most cases, the problem of a possible inherited cosmogenic component is avoided and they are most likely to have been undergoing continuous denudation over prolonged periods of time (see section 2.5.1 for further discussion). Lithologies were chosen that contained a significant proportion quartz for ^{10}Be, ^{26}Al and ^{21}Ne analysis (granite and quartzite), and quartz veins were exploited where possible. Samples were taken using a hammer and chisel from the top 20 mm in order to maximise the concentration of nuclides. Sample size depended on rock type and the suspected denudation rate of the site (i.e. the expected concentration of cosmogenic nuclides in the sample) but 2 kg was usually more than sufficient.

In order to interpret measured cosmogenic isotope concentrations in rock surfaces in terms of meaningful denudation rates a number of field data about each site were required. Table 3.1 lists the data and information that was recorded at every site in the field as well as the rationale for its collection and the equipment used. The majority of field data were required to scale production rates for each isotope to the individual sites which is an integral part of interpreting isotope concentrations. The exposure geometry of the site was recorded by measuring the angle to the nearest horizon at 15° intervals surrounding the sample in order to estimate the proportion of

incident cosmic radiation that reached the sample (Appendix A). Detailed notes about the geomorphic context of the sites were recorded at all scales as well as a full photographic record to aid interpretation.

Table 3.1: Field data recorded at each sampling location.

Data/Information	Units	Rationale	Equipment
Altitude	metres (m)	Production Rate Scaling	Altimeter/Topographic Maps
Position (Lat. & Long.)	degrees (°)	Production Rate Scaling	GPS/Topographic Maps
Exposure Geometry	degrees (°)	Production Rate Scaling	Compass/Abney Level/ Radial Graph Paper
Dip and Orientation of Sample Surface	degrees (°)	Production Rate Scaling	Compass/Amney Level
Sample Thickness	millimetres (mm)	Production Rate Scaling	Tape Measure
Lithology, Mineralogy	type, % composition	Production Rate/Analysis	Hand Lens/Field Identification Guide
Sample Mass	kilograms (kg)	Field Logistics/Analysis	Spring Balance/Estimate
Temporary Shielding?	-	Production Rate Adjustment	Visual Assessment
Human/Animal Interference?	-	Production Rate Adjustment	Visual Assessment
Estimated Exposure Age/Erosion Rate	a / m Ma^{-1}	Amount of Pure Quartz Required	Relative Assessment Based on Site Context
Geomorphic Context	-	Interpretation of Data	Visual Assessment (also tape measure, aerial photos etc.)
Photographs	-	Interpretation and Recording	Camera

3.3 Analytical Techniques for ^{10}Be and ^{26}Al

3.3.1 Quartz Separation

^{10}Be and ^{26}Al analysis requires 15 - 50 g of clean mono-minerallic quartz. Kohl and Nishiizumi (1992) presented a technique developed especially for the preparation of quartz for cosmogenic isotope analysis and it has several advantages over the more conventional heavy liquid separation or other methods (e.g. Syres, 1968). For ^{10}Be and ^{26}Al analysis it is important not only to separate effectively feldspars and clays from the quartz but also to eliminate meteoric ^{10}Be present on the surface of quartz crystals, both of these requirements are met by the Kohl and Nishiizumi (1992) technique. The method also produces quartz with a low, inherent aluminium

concentration which is crucial to the measurement of low $^{26}Al/^{27}Al$ ratios. The method for quartz separation used in this project was very similar to that described by Kohl and Nishiizumi (1992) with slight modifications.

3.3.1.1 Initial preparation

Samples were sawn into suitable sized pieces for a jaw crusher set with the crushing plates as close together as possible. Samples were crushed and hand sieved and the 250-500 μm sized fraction selected. This size fraction usually eliminated composite mineral grains. Rock chips >500 μm were crushed and sieved again. If further size reduction was necessary, the sample was ground in a tungsten carbide tema for 10 seconds. Approximately 300 g of crushed sample were required to yield sufficient quartz for analysis. It was important to minimise cross contamination between samples by carefully cleaning the crushing equipment and sieves between each sample and only working with one sample at a time. Crushed samples were rinsed thoroughly with ultra-pure water (MilliQ Plus, 18 MΩ) to remove fine material and then dried overnight in open beakers in an oven at <70 °C.

Samples were magnetically separated three or four times, in a Franz separator, in order to remove mafic minerals. During this process the sample was fed through a magnetic field via a vibrating chute. Magnetic material was selectively attracted to one side, dividing the sample into two fractions which were collected separately. Typical settings of the magnetic separator and the yields from each run for the four major lithologies sampled are shown in Table 3.2. Contamination was avoided by brushing and vacuum cleaning the separator between samples. The amount of sample that needed to be processed depended on the magnetic component; ~100 g of non-magnetic material (principally quartz and feldspar) were commonly required.

Table 3.2: Typical settings and average yields of magnetic separation for Namibian and Antarctic samples.

Rock Type	Mag.Sep. Setting* Nº 1/° & A	Magnetic content as % of total	Mag.Sep. Setting Nº 2/° & A	Magnetic content as % of total	Mag.Sep Setting Nº 3/° & A	Magnetic content as % of total	Total magnetic content as %
Gamsberg Granite	30, 15, 0.5	7	25, 10, 1	16	20, 4, 1.25 (x2)	5	28
Gamsberg Quartzite	20, 15, 0.5	2	20, 10, 1.25	5	15, 3, 1.25	2	<9
Donkerhuk Granite	30, 15, 0.5	14	25, 10, 1	25	20, 4, 1.25 (x2)	5	44
Beacon/Arena Sandstone	20, 15, 0.5	~1	20, 10, 1.25	3	15, 3, 1.25	<1	<5

* Slope angle of chute (°), tilt angle of the chute (°), current to the magnet (A).

3.3.1.2 Chemical separation of quartz

7.5 g aliquots of non-magnetic sample material were added to screw-top, polypropylene beakers with 1 litre of 1% HF and 1% HNO_3 solution. Quartz is very unreactive with dilute acids and is dissolved more slowly than feldspar in HF, especially when combined with HNO_3 (Potts, 1987). Therefore, leaching the sample in a weak HF and HNO_3 solution selectively isolated quartz from feldspar and other more easily dissolved constituents such as clay. To prevent saturation of the solution immediately surrounding the sample grains the beakers were placed in an ultrasound bath to provide constant agitation. A shaker table would have had a similar effect. The solution was changed after successive 24 hour periods and the total leaching time was 96 hours. When the solution was changed, the sample was rinsed in ultra-pure water to remove fine and dissolved material, a very small and variable proportion of quartz grains was also lost during rinsing. After the final leach, the samples were thoroughly rinsed with ultra-pure water and dried in open beakers in a flow bench. The amount of material that needed to be processed for each sample varied slightly depending on the proportion of feldspar present. Yields at successive stages in the leaching process for a typical Namibian granite and quartzite sample are shown in Figure 3.1. There was a large initial drop in sample weight after the first leach as the majority of feldspars were dissolved quickly. During leach steps 2, 3 and 4, the surface of the quartz grains are slowly etched and the decline in mass is more gradual.

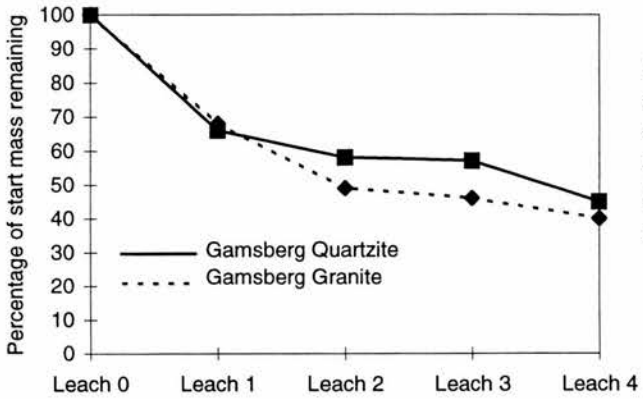

Figure 3.1 Sample weight remaining after four successive chemical leaches shown as a percentage of the start mass of 7.5 g for a typical Namibian granite (5B/95) and quartzite (8A/95) sample during the chemical isolation of quartz.

The purity of the quartz separates was initially tested under an optical microscope but it was often difficult to distinguish between quartz and feldspar. A more rigorous test was to measure the total Al content of the quartz. The separation procedure was designed to produce quartz with a low, stable Al content, that is the inherent Al content of the quartz. Al has been shown to be homogeneously distributed throughout quartz grains and commonly varies between 15 and 400 ppm (Kohl and Nishiizumi, 1992). Any undissolved feldspar would significantly increase the amount of Al present in a sample. Figure 3.2 shows the results of Al content determination using graphite furnace atomic absorption spectrometry (GFAAS) for a typical Namibian granite and quartzite sample at successive stages in the quartz separation procedure. 0.1g aliquots of samples at each leach step were dissolved in HF and HNO_3 and diluted to an estimated concentration of ~100 ppb for measurement. The results (Fig. 3.2) show that the Al content stabilised satisfactorily only after at least three leach steps. The results are in accordance with those obtained by Kohl and Nishiizuni (1992) and similar results to those shown in Figure 3.2 were obtained for other Namibian samples and Antarctic quartzites. The Al content values in the final leach steps gave a good indication of the purity of the separate but could not be used as an accurate measure of the Al content of the sample to convert $^{26}Al/^{27}Al$ ratios into absolute concentrations. This is because there is always slight inhomogenity in the distribution of Al among the whole 15-50 g sample. An apparent rise in the Al content in sample 1A/95ii between leach steps 3 and 4 can be explained by inhomogenity between the 0.1 g aliquots of the sample.

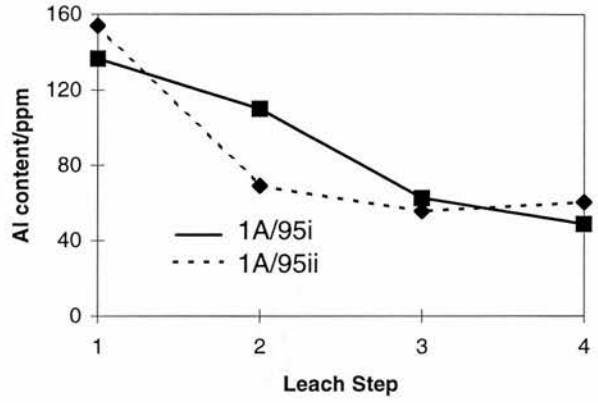

Figure 3.2a: Al content in two aliquots of a typical Namibian granite (1/95) sample after four successive leach steps during the chemical isolation of quartz.

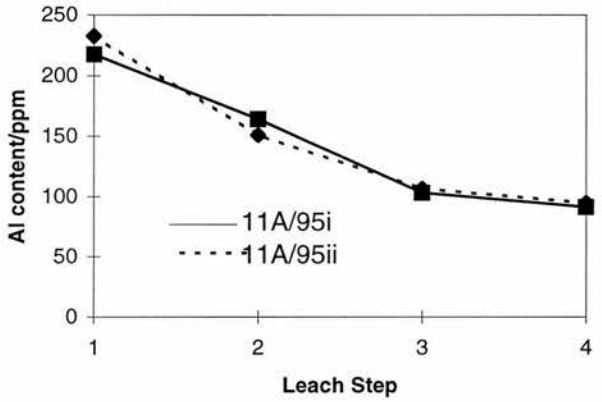

Figure 3.2b: Al content in two aliquots of a typical Namibian quartzite (11/95) sample after four successive leach steps during the chemical isolation of quartz.

The separation procedure not only dissolved unwanted feldspar but also etched the surface of the quartz grains. This eliminates meteoric ^{10}Be which is absorbed into the surface of mineral grains from precipitation. Including the meteoric ^{10}Be component would have lead to excess cosmogenic ^{10}Be and inaccurate denudation rate estimates. Kohl and Nishiizumi (1992) have shown that ^{10}Be content in bulk samples can be up to 300 times higher than the ^{10}Be content of pure quartz after 10,000 years of exposure to precipitation, but ^{10}Be contents level off (measured relative to ^{26}Al) after one or two leaching steps have removed the meteoric component. Ivy-Ochs (1996) has highlighted the difficulty of effectively removing meteoric ^{10}Be from pyroxene because although ^{10}Be content is seen to level off after a few leaching steps, this by itself does not prove that all meteoric ^{10}Be has been removed. Measured relative to ^{3}He and ^{21}Ne, an excess ^{10}Be component in old pyroxene can still be detected. The reason for the difference between quartz and pyroxene is the strong resistance of quartz to weathering and therefore limited number of sites (cracks and pits on the crystal surface) to which meteoric ^{10}Be can adhere. In contrast, pyroxene weathers more extensively enabling meteoric ^{10}Be to penetrate much further into the crystal lattice, therefore reducing the effectiveness of surface etching. A similar problem has

been encountered measuring ^{10}Be in olivine (Seidl, 1993). It seems that the problem becomes more significant with increasing exposure age of the sample as minerals become more weathered.

3.3.2 Be and Al Extraction from Pure Quartz

Sample size, i.e. the mass of quartz used for extraction, depended on the suspected ^{10}Be and ^{26}Al content of the sample. Samples exposed for long periods of time with low denudation rates have a higher concentration than more quickly eroding rocks. Therefore less quartz was used from the Antarctic samples than the Namibian samples as denudation rates in Antarctica were expected to be lower. Sample sizes ranged from ~15 g to ~50 g (Appendix A). AMS can detect anything in excess of 10^6 cosmogenic atoms provided $^{10}Be/^{9}Be$ and $^{26}Al/^{27}Al$ ratios are one to two orders of magnitude greater than the machine background blank (commonly ~10^{-14}). There is no naturally occurring ^{9}Be in quartz therefore samples were spiked in order to create a Be isotopic ratio. 0.5 mg of Be carrier was added to the Namibian and Antarctic samples (section 3.3.2.1). ^{27}Al naturally occurs in quartz, therefore no carrier was needed but the Al content had to be accurately measured using GFAAS (section 3.3.3.1).

Figure 3.3 shows the final sequence of procedures used in the separation of Be and Al from pure quartz. The protocol was based on that used at Lawrence Livermore National Laboratory (LLNL) but evolved over the course of the sample preparation period. The major steps in the protocol are the dissolution of quartz thereby putting Be and Al into solution, several purification steps to remove major interfering elements Fe, Mg and Ca, a cation exchange column to separate Be and Al and finally precipitation of Be and Al from solution. In total, 31 samples were successfully prepared for analysis in 5 batches (Appendix A).

One or two process blanks were run alongside each batch of samples subject to exactly the same chemical procedure to monitor the possibility that Be or Al had been introduced during the sample preparation. Blanks were made from the same ^{9}Be standard solution used to spike the samples and from a similar ^{27}Al standard. Procedural blank ratios were always two or three orders of magnitude less than the samples ratios, on the order of 10^{-14} and were used to make minor corrections to the sample data. Blank ratios from each AMS run are included in sections 4.6, 5.5 and 6.4.

Boron (^{10}B) is a potentially serious contaminant because it is an interfering isobar with ^{10}Be in AMS measurement. As such it had to be kept to a minimum during the sample preparation

procedure. The main sources of ^{10}B are dust and tap water (Ivy-Ochs, 1996). By working in a clean air environment as much as possible (flow bench or clean lab) and rinsing all labware in ultra-pure water several times before use, ^{10}B contamination was limited. Perchloric acid fuming at ~200 °C was used to help eliminate boron as it is volatile at high temperatures. Borosilicate glass can also give rise to B contamination but all chemical procedures for the extraction of Be and Al were carried out in teflon labware and reagents were stored in plastic bottles. AMS measurement of ^{10}Be can give an indication of the number of counts in the measurement process that are due to ^{10}B contamination. Samples prepared at LDEO were contaminated by up to 2% while all other samples were free of ^{10}B contamination. Blank samples yielded spurious counts due to boron in the AMS of up to 20% of the total ^{10}Be. However, this is merely a reflection of the very small (background) ^{10}Be component of the process blanks and not that the blanks were subject to more boron input than the samples.

3.3.2.1 Quartz dissolution

The pure quartz was weighed into labelled, 180 ml, Savillex PFA teflon beakers. The samples were spiked with 0.5 ml of ^{9}Be carrier (BDH Spectrosol Be Standard Solution 1000 ppm) using a precisely calibrated Finnpipette. A 1:1 mixture of conc. HF (48%) and 1:1 HNO_3 (69% conc.) was added to the beakers in order to digest the quartz. The beakers were heated on a hot plate in a fume cupboard, without lids, at ~100°C until all the quartz had dissolved. During this process, silicon is dissolved and removed as volatile silicon tetrafluoride (SiF_4). HF is the only acid that will readily dissolve silicate material, but used on its own it is not always totally efficient because some salts and elements do not have a high enough solubility to stay in solution in fluoride form (Potts, 1987). It is therefore common to use an accompanying acid, in this case HNO_3. Dissolution was a lengthy process; 35g of quartz took approximately seven days and ~200 ml of acid to dissolve. The beakers were 'swirled' occasionally and were sometimes placed in an ultrasound bath to speed up dissolution by clearing the surface of the grains and exposing fresh quartz to acid attack.

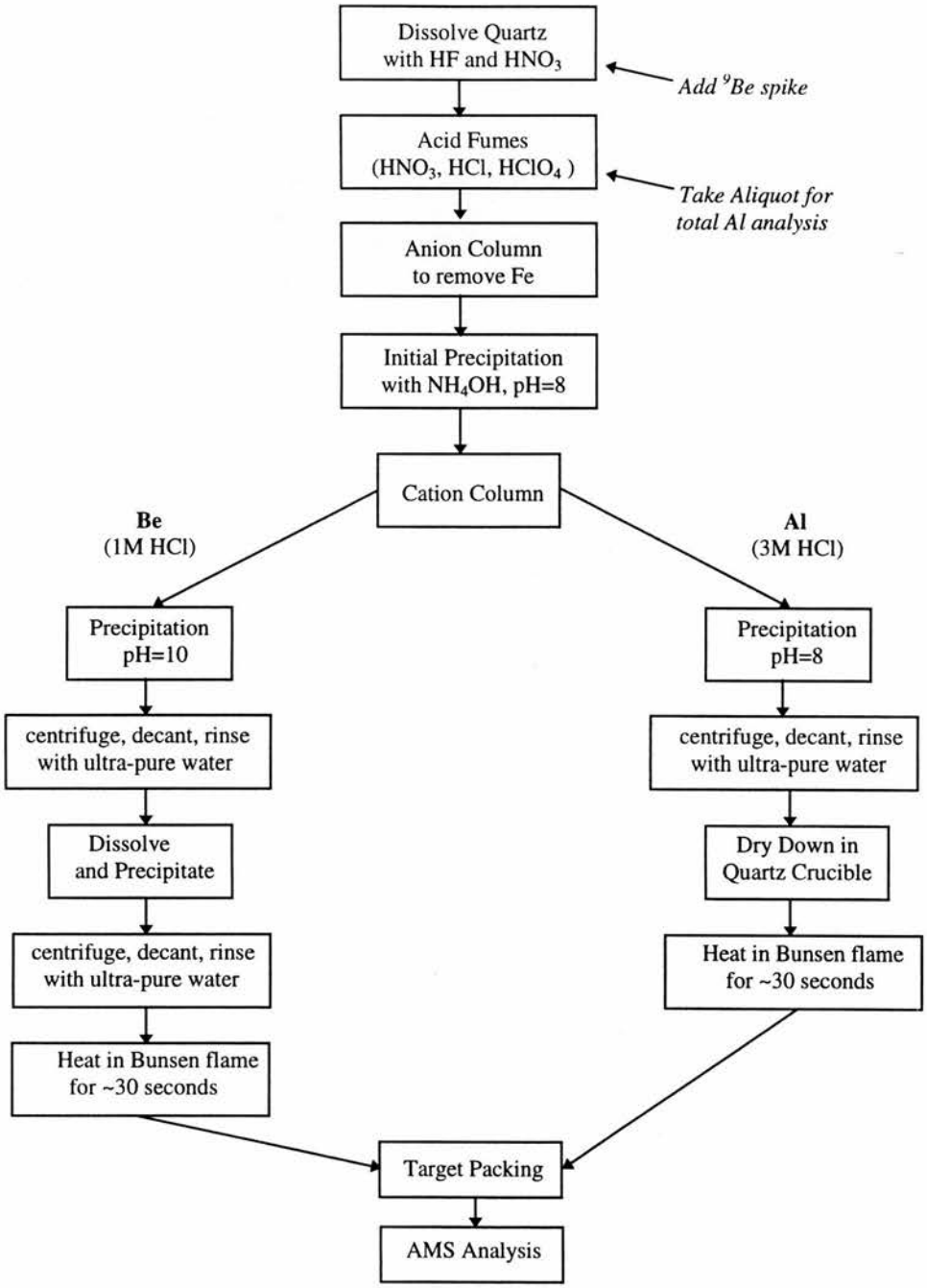

Figure 3.3: Flow chart showing the final sequence of principal chemical procedures used to extract ^{10}Be and ^{26}Al from pure quartz (after Ivy-Ochs, 1996).

After dissolution, the sample was fumed to dryness three times with ~5 mls conc. HNO_3 and three times with ~5 mls conc. HCl. It was then fumed three times with a similar amount of perchloric acid ($HClO_4$). $HClO_4$ helps to eliminate any remaining unwanted fluorides and traces of HF. Residual HF and fluorides can interfere with GFAAS measurement of Al and upset column chemistries by overloading the columns. At first, approximately the same amount of $HClO_4$ was used as HF to dissolve the sample but this was reduced to three smaller fumes. $HClO_4$ is a dangerous acid and strong oxidiser that can easily explode when heated. The work was carried out in a fume cupboard with wash down facilities behind an explosion proof screen. If, after the suggested amount of $HClO_4$ had been fumed, the sample still contained fluorides (visible as fibrous, opaque precipitates) then more $HClO_4$ was used. The step was repeated until the sample was fully dissolved when gently heated in HCl. The HF/$HClO_4$ evaporation scheme fails to dissolve certain resistant minerals such as zircon. Small, rounded, dark specks, possibly zircons, could be seen in the final cake or solution after $HClO_4$ fuming. The specks were removed by carefully avoiding them when the sample was transferred from the teflon beaker during the next step or, if unavoidable, they were filtered out in the top of the anion column later on.

After the $HClO_4$ fume, an aliquot for measurement of the total Al content of the quartz was taken. It is very important to have an accurate measurement of the total Al content of the sample because absolute concentrations of cosmogenic ^{26}Al are determined from this measurement, the measured $^{26}Al/^{27}Al$ ratio and the weight of quartz dissolved. Once the sample had been dissolved and homogenised with the Be carrier, it was assumed that the isotopic ratios were fixed and that no mass fractionation occurred throughout the remaining chemical procedures. Thus, failure to achieve 100% yield to the end of the protocol did not affect the ratio that was measured by AMS but it is critically important to maintain total yield and work quantitatively up to the taking of the aliquot. The samples were dissolved in ~3 ml conc. HCl and made up to 100 ml in a volumetric flask with ultra-pure water. The teflon beaker was rinsed several times to get complete transfer of the sample to the flask and a 5 ml fraction was taken for analysis. For the first two batches of samples aliquots were taken from a more concentrated solution by weight but the volume method described above proved to be easier and was subsequently used. The sample solutions were transferred from the flasks into clean teflon beakers and heated to dryness. $AlCl_3$ is volatile at 183°C, therefore it was important to keep the hotplate at 100°C or less during this heating step. The samples were brought up in <5 ml of 9M HCl in preparation for the anion exchange column.

3.3.2.2 Anion exchange column

The principal purpose of the anion exchange column was to remove iron (Fe). Fe can interfere with the separation efficiency of the cation column by overloading it. The majority of samples were bright yellow in ~5 ml 9M HCl thus indicating a high iron content. Bio-rad 20 ml PFA columns with AG 1-X8 anion resin, analytical grade, chloride form, 100 - 200 dry mesh size were used. The resin was cleaned in ultra-pure water before use and expanded to a water equilibrated state which was used to fix the column volume. When packing the column, it was important to get an even resin bed with no air pockets to ensure even flow. In an ion exchange procedure, the sample ions replace the counterions in the resin, which have the same charge, and can then be eluted selectively by using a pH gradient of acid strength. In an anion column, the gradient is from high to low. The columns were conditioned using three column volumes of 9M HCl. The sample solution (~5 ml) was loaded on to the column using a disposable pipette and allowed to run through before any acid was added. A column calibration curve is shown in Figure 3.4 for a sample made from Be and Al standard solutions. As such, the influence of other elements, including Fe, that may be present in a real sample solution were unknown but do not appear to have had any consequences. Be and Al were eluted into a clean teflon beaker using two column volumes of 9M HCl, then four column volumes of 0.5M HCl were used to elute Fe. Fe could be seen clearly coming off the column as the resin gradually returned to pale yellow from a darker yellow. Unwanted fractions were stored in polypropylene bottles for future reference and the sample was dried down at ~100°C.

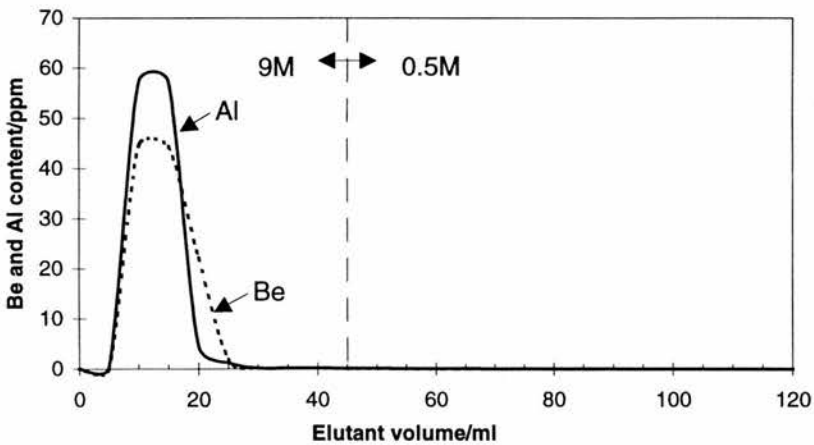

Figure 3.4: Anion column calibration curve. Be and Al measurements performed using ICPMS. Yield = 100% for Al and >90% for Be. Negative Al values were an artefact of ICPMS measurement and probably reflect zero readings.

3.3.2.3 Cleaning steps

The most important changes made to the protocol over the sample preparation period were to the cleaning steps carried out between the anion and cation columns. Essentially, all major procedures between the initial sample dissolution and Be and Al separation on the cation column were cleaning steps for the elimination of elements other than Be and Al. The procedures should not have altered the resultant ratio but would have affected how pure the samples were which influenced how well they ran on the AMS and the extent of measurement uncertainty. The original protocol included an acetylacetone extraction with an acid back-extraction and acid fumes as described below.

The purpose of the acetylacetone extraction (or organic extraction) and subsequent HCl extraction and fuming steps was to remove Mg and Ca. These two elements can interfere with AMS measurement and can overload the cation exchange column due to their higher affinity with the cation resin compared to Be and Al. The dried cake from the anion column was dissolved in ~5 ml of conc. HCl, ultra-pure water and ammonium hydroxide (NH_4OH, NH_3 aq.). The pH was adjusted to 7 using small amounts of NH_4OH and conc. HCl. The sample solution was transferred to a separatory funnel and a volume of acetylacetone equal to half that of the sample solution was added. The solution was mixed by shaking vigorously for 5 minutes, during which time it turned a milky white colour. It was very important to vent the funnel periodically to release gas. Chloroform ($CHCl_3$) was added in two stages with shaking and venting between each stage. When left to stand, the solution separated into an upper aqueous and a lower organic phase. Poor separations were improved by further shaking. The organic phase (containing the dissolved Al and Be) was transferred to a second separatory funnel and a further acid back-extraction was performed with HCl. A volume of 6M HCl equal to three quarters the volume of the total $CHCl_3$ was added and the sample shaken vigorously again. The upper aqueous phase containing the Be and Al was transferred into a clean teflon beaker. This was dried down and then cleaned by fuming with small quantities of (~5 ml) HNO_3 and $HClO_4$.

The acetylacetone extraction is particularly important when extracting Be and Al from olivine which has a high Mg component. For quartz, this extraction is not so necessary as Mg and Ca is not present in such large amounts. It is good practice to clean the samples of as many potential contaminants as possible but the separation is not always straightforward. The samples prepared at LDEO (Batch 1, see Appendix A) were all subject to an acetylacetone extraction without any problems but with the second batch of samples (50-57/95, Batch 3) good separation was

problematic. Very small resultant amounts of BeO and Al_2O_3 may have been a result of the poor separation and the protocol was subsequently reviewed. Unfortunately, it was not possible to check the waste fractions of the acetylacetone extraction for 'lost' Be and Al because of the sensitivity of GFAAS and ICPMS to organic compounds.

An alternative procedure of an initial hydroxide precipitation of Be and Al was incorporated into the final sample preparation protocol after the anion column (Fig. 3.3). The sample was brought up in ~2 ml of conc. HCl and transferred to a 15 ml centrifuge tube. The beaker was rinsed with ~5 ml of ultra-pure water. $Be(OH)_2$ and $Al(OH)_3$ were precipitated with NH_4OH. NH_4OH was added until the precipitate could be seen and the pH carefully adjusted to 8 at which both Be and Al formed solid precipitates (Ochs and Ivy-Ochs, 1997). After thorough mixing, the samples were left overnight in order to fully precipitate. The samples were centrifuged for 15 minutes at 3000 rpm and the waste solution was decanted. During this procedure, Mg and Ca and B were mostly held in the waste solution rather than forming a precipitate, assuming that a pH of 8 is maintained throughout the precipitation (Ochs and Ivy-Ochs, 1997). The precipitate (~1 ml of white gel) was redissolved with a few drops of conc. HCl and brought up to ~ 5 ml with ultra-pure water.

3.3.2.4 Cation exchange column

The purpose of the cation exchange column was to separate Be and Al from each another. The cation column works on a similar principle to the anion column. In this instance, Bio-Rad AW-50W X8 resin was used in similar 20 ml columns. The columns were conditioned with ten column volumes of 6M HCl and three volumes of ultra-pure water. Al may not separate from Be effectively unless the samples are loaded onto the column in <1M HCl. Cation column calibration curves are shown in Figure 3.5a and 3.5b. Standard calibration samples were run with two different strengths of acid to remove Al over 15 column volumes. The two calibration runs clearly show that the higher the acid strength to take off Al the quicker Al comes off the column. On the basis of the calibration runs the following protocol was adopted: First, Be was eluted with 1M HCl. Be was found in column volumes 4-12 therefore column volumes 3-13 of 1M HCl were collected in a clean teflon beaker and volumes 1, 2 and 14, 15 were set aside in bottles. Any remaining Mg and Ca would most likely have been in column volumes 1 and 2 and excluding these fractions helped to purify the samples. Al was taken off with 3M HCl in column volumes 16-19. The wanted fractions were dried down in clean teflon beakers ready for the final stages of sample preparation.

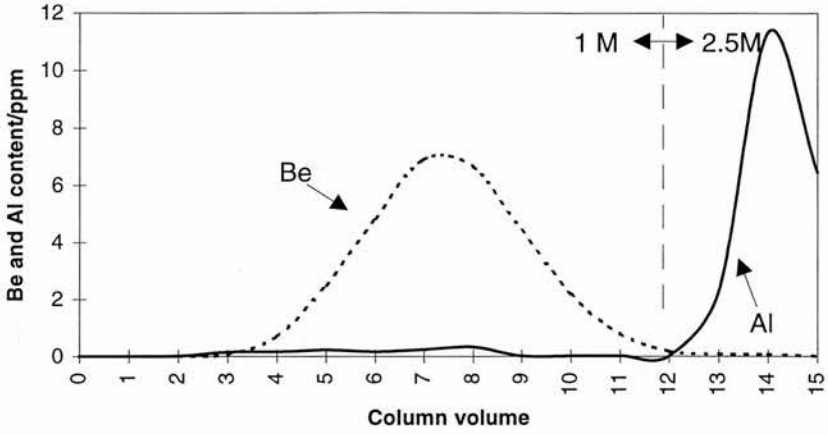

Figure 3.5a Cation column calibration curve for the separation of Be and Al using 1M and 2.5M HCl. Measurements performed by ICPMS, yields = 100% for Be, 80% for Al. Negative Al values were an artefact of ICPMS measurement and probably reflect zero readings.

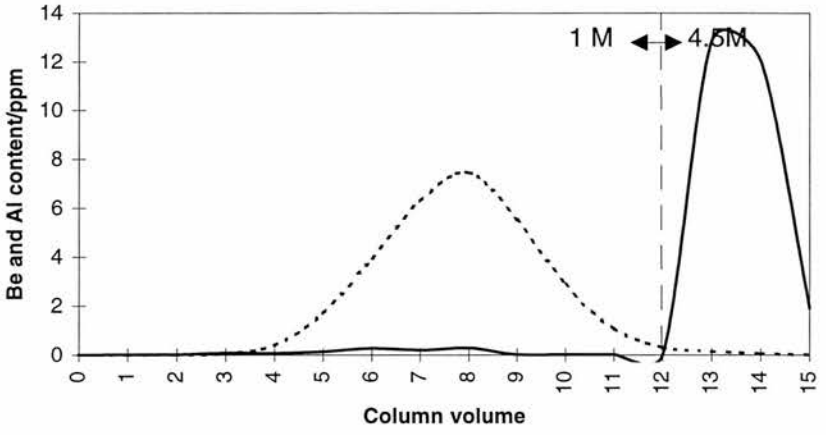

Figure 3.5b Cation column calibration curve for the separation of Be and Al using 1M and 4.5M HCl. Measurements performed by ICPMS, yields = 100% for Be, 90% for Al. Negative Al values were an artefact of ICPMS measurement and probably reflect zero readings.

3.3.2.5 Be and Al precipitation and oxidation

Be and Al were precipitated separately in a similar way to the initial precipitation described in section 3.3.2.3. The samples were brought up in approximately 3mls of 1:1 HNO_3 and transferred to a 15 ml centrifuge tube. Be $(OH)_2$ and Al $(OH)_3$ were precipitated with NH_4OH at pH 10 and 8 respectively (Ochs and Ivy-Ochs, 1997). The samples were left overnight to fully precipitate and were then centrifuged for 15 mins at 3000 rpm and the waste solution pipetted from the precipitate. The $Be(OH)_2$ was redissolved with acid and then reprecipitated with NH_4OH. Finally, both the Be and Al precipitates were rinsed with ultra-pure water one or more times. In these final stages, rinsing, stirring and shaking the Be precipitate helps B go back into the bulk solution (Finkel and Suter, 1993). To encourage B dissolution, the Be fraction was reprecipitated and rinsed more thoroughly than the Al fraction.

The whitish, gelatinous hydroxides were transferred from the centrifuge tubes to hand blown quartz vials in a drop of ultra-pure water using a disposable pipette. The samples were dried overnight in the quartz vials in a custom designed block heater at 40°C. Avoiding cross contamination at this stage was critical and clean gloves were used to handle each sample. In order to fully oxidise the samples to BeO and Al_2O_3 ready for AMS analysis, the vials were held using tweezers in a hot Bunsen flame for ~30 seconds until the sample glowed red. The final product of the sample preparation procedure consisted of a few off-white flakes of pure BeO and Al_2O_3 in the base of the quartz vials.

3.3.3 Measurement

There were two measurement stages in the analysis of ^{10}Be and ^{26}Al. Total ^{27}Al of 5 ml sample aliquots taken after the $HClO_4$ fume were measured by inductively coupled plasma mass spectrometry (ICPMS) and graphite furnace atomic absorption spectrometry (GFAAS). As previously mentioned this value is required to convert final measured $^{26}Al/^{27}Al$ ratios to absolute concentrations and accuracy is paramount. The second measurement procedure is accelerator mass spectrometry (AMS) of the isotopic content of BeO and Al_2O_3.

3.3.3.1 ICPMS and GFAAS measurement

A combination of ICPMS (Fisons VG PlasmaQuad at SURRC and also at XRAL Laboratories) and GFAAS (Spectra AA at the Department of Geology and Geophysics, Edinburgh) was used to measure the total Al content of the samples in aliquots taken after the perchloric fume as well as column calibrations and checks of the quartz separates (Appendix A, Figs. 3.2 - 3.5). Comparison tests between the two machines gave very similar results but neither was ideal for all the applications. Doubly coupled plasma mass spectrometry (DCPMS) was also used to measure the Al aliquots of one batch of samples (Appendix A).

ICPMS has the advantage of multi-element analysis so that Be and Al can be measured at the same time in one sample and was therefore used for column calibration measurement. However, Al contamination from the ICPMS automatic sampler particular to the SURRC machine meant that each sample had to be manually introduced and even after taking this precaution there was still a high and variable Al blank signal. Therefore, ICPMS could not be used to determine Al content in samples aliquots at the level of accuracy required. Also, Be is the best internal standard for measuring Al on the ICPMS but because the samples contained Be, ^{125}In was used

instead which is not ideal because of the large mass difference between Al and In (M. McCartney, *pers. com.*). At XRAL Laboratories, which were used to measure one set of Al aliquots for samples in Chapter 4, no problems were reported. An overview of ICPMS is provided by Potts (1987).

GFAAS proved more suitable for accurate Al analysis but Be measurements by GFAAS were not possible because the Edinburgh instrument was not equipped with a Be lamp (see Potts (1987) for details). To ensure that measurements of total Al content were not subject to matrix effects or drift over the course of the GFAAS run a method of three standard additions was used. The standard additions technique involves dividing every sample into separate aliquots and adding increasing quantities of a standard Al solution to set up a calibration curve for each sample individually. One addition should be of a blank sample. A graph was constructed of the concentration of standard added versus the analytical signal, in this case atomic absorption. When the graph was extrapolated back to the x-axis, the point of intersection gave the (negative) concentration of Al present in the sample (Fig. 3.6). Uncertainty in the total Al measurements was better than 5% .

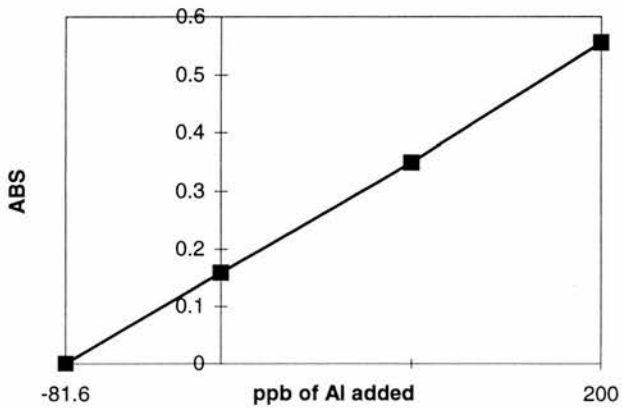

Figure 3.6: Standard additions calibration plot for sample 16A reproduced from the original GFAAS data sheet. The Al concentrations of the three standard additions were 0, 100 and 200 ppb. The Al concentration of the diluted sample was 81.6 ppb which converted to 29.28 ppm in the quartz separate. (ABS = GFAAS absorption units).

3.3.3.2 AMS target packing and measurement of ^{10}Be and ^{26}Al

The majority of samples were packed into targets and measured at the Center for Accelerator Mass Spectrometry at Lawrence Livermore National Laboratory (LLNL). Some samples were packed and measured at the Eidgenössische Technische Hochschule/Paul Scherrer Institut (ETH) AMS facility in Zurich (Appendix A). ^{10}Be is a potentially harmful substance and targets were always prepared inside a bench top fume hood or equivalent to prevent inhalation. Target packing is machine specific as each AMS commonly has a different sample feeder system and

ions source set up. At ETH, the sample material was thoroughly mixed with copper powder (~4:1 ratio of copper to sample) inside the quartz vial before being transferred to the target. Targets consisted of copper disks, 20mm in diameter, with a precisely drilled 1.5 mm hole that was filled with the sample mixture. The targets were pressed to secure the sample material in place. Contamination was avoided by cleaning all packing equipment (tweezers, spoons etc.) in dilute HCl and ultra-pure water and by spraying with clean air to eliminate dust. At LLNL samples were packed in a similar way but were mixed with silver powder inside the quartz vial before being transferred a bullet shaped target housing (M. Seidl, *pers. com.*).

The targets were loaded into the ion source of the AMS. At both LLNL and ETH a Cs sputter negative ion source was used to produce a beam of BeO^- molecules or Al^- ions. The basic details of AMS measurement have been provided in section 2.3.2. Typical negative ion currents at ETH are 0.5-1.0μA and 0.1-0.2μA for Be and Al respectively (Synal *et al.*, 1997). At LLNL beam currents are typically 4μA and 1μA respectively (Roberts *et al.*, 1997). Background ratios for ^{10}Be are 1×10^{-14} at LLNL and $< 10^{-14}$ at ETH. For Al, background ratios are 2×10^{-15} at LLNL and 5×10^{-14} at ETH (Roberts *et al.*, 1997; Synal *et al.*, 1997). An initial mass analyser selects the isotope to form the beam that enters the accelerator (Fig. 2.4). For 90% of the time at ETH this was the less abundant cosmogenic isotope (^{10}Be or ^{26}Al). Interference from ^{10}Be was monitored at both LLNL and ETH in an absorber cell directly infront of ^{10}Be detector. Isotopic ratios were determined from the beam current, the number of counts in the detectors and the detection time and normalised to standard samples. For further details on AMS measurement at LLNL and ETH see Roberts *et al.* (1997), Davis *et al.*, (1990), Southon *et al.*, (1990), Synal *et al.* (1997) and references therein.

3.4. Sample Preparation and Measurement of ^{21}Ne

3.4.1 Sample Preparation

Analysis of ^{21}Ne in quartz does not require such high quality mineral separates as ^{10}Be and ^{26}Al and chips from vein quartz, or large hand picked crystals can be analysed successfully (F. Stuart, *pers. com.*). However, as pure separates had already been made, clean quartz was used for ^{21}Ne in this thesis. Nucleogenic $^{18}O(\alpha,n)^{21}Ne$ reactions are initiated by U- and Th-derived alpha (α) particles and contribute to the number of Ne components that have to be separated in order to measure the cosmogenic ^{21}Ne component (section 2.2.1). Pure quartz contains no α-particle sources but they can recoil with a range of 10-40 μm into quartz crystals from adjacent minerals

or inclusions such as zircons. The etching process of the separation procedure removes ~15 μm from the surface of quartz grains and therefore effectively removes a large proportion of implanted α-particles and reduces the measured nucleogenic component. It has been suggested that the separation technique increases the chance of diffusion and therefore loss of ^{3}He or ^{21}Ne due to low temperature release of both noble gases (Neidermann *et al.*, 1993). But temperatures during sample preparation do not exceed 100°C, and it is probable that cosmogenic gas release, particularly of ^{21}Ne, does not occur at or below this temperature (Neidermann *et al.*, 1993). It is therefore preferable to use high quality quartz separates when they are available for ^{21}Ne analysis. Traces of HF on the quartz grains can interfere with MS measurement of ^{21}Ne ($H^{19}F^{+} \approx {}^{20}Ne$, Neidermann *et al.*, 1993) and therefore the separates were be thoroughly rinsed before use.

3.4.2 Mass spectrometry of ^{21}Ne

Approximately 250 mg of quartz were needed for measurement of cosmogenic ^{21}Ne (Summerfield *et al.*, 1998a). Any remaining dark grains in the quartz separates, which could have been due to the presence of zircon inclusions, were removed by hand picking. Samples with known masses were wrapped in aluminium foil and loaded into the extraction system of the mass spectrometer and evacuated to $<10^{-8}$ torr over 48 hours prior to analysis. All the Ne measurements were made on a VG 5400 noble gas mass spectrometer at the Vrije Universiteit in Amsterdam by F. Stuart and T. Dunai (Appendix A). This mass spectrometer has an ion source with a modified Nier-type geometry and is equipped with an axial electron multiplier to detect low concentrations and an off-axis Faraday cup for when less sensitivity is required (for more details see Summerfield *et al.* (1998a)). Noble gases (He, Ne, Ar, Kr and Xe) were initially extracted from the quartz by heating the samples for 15 minutes to 1400°C in a double vacuum resistance furnace with a tungsten heating element and a molybdenum crucible. The extracted mixed gas was purified on two Ti-getters (at 250°C and 800°C) and a SAES-getter at room temperature. Ar, Kr and Xe were separated from Ne and He by successive absorption onto two charcoal traps cooled with liquid nitrogen. Ne was then absorbed onto a charcoal trap called a cryogenic finger at 45K (-228°C). Whilst the Ne was held on the finger, He was analysed in the residual gas in the mass spectrometer. He was measured because ^{4}He concentrations are required to determine the radiogenic component of ^{21}Ne but it is also interesting to compare ^{3}He concentrations with cosmogenic ^{21}Ne as a test for the diffusivity of He in quartz (section 6.5). Ne was released from the finger at 100K (-173°C) and the isotopic composition analysed in the mass spectrometer. It took over 3 hours for each sample to be analysed for He and Ne.

Noble gas abundances were determined by peak comparison with known amounts of gas. ^{3}He-enriched geothermal gas ($^{3}He/^{4}He = 14.3 \pm 0.1$ Ra, where Ra is the atmospheric ratio of 1.39×10^{-6}) was used for the He calibrations. The He elemental and isotopic abundances in the geothermal standard were determined by repeated cross-calibration with 0.25 cc STP air. Neon calibrations were made on 95.2 ± 0.5 µcc STP air. $^{40}Ar^{2+}$ and $^{44}CO_2^{2+}$ can interfere with the measurement of ^{20}Ne and ^{22}Ne respectively which would lead to inaccurate ^{21}Ne determination. However, corrections were made on the basis of $^{40}Ar^{2+}/^{40}Ar^{+}$ and CO_2^{2+}/CO^{2+} ratios determined at the start of the run that were assumed to be held constant. The abundances of H_2 and $H_2{}^{18}O$ were routinely measured (these can also interfere with ^{20}Ne measurement) but displayed no significant variation throughout analysis. (For further details on interference monitoring see Neidermann *et al.* (1993)). Concentrations of cosmogenic ^{21}Ne were determined from the measured ^{21}Ne value by correcting for a nucleogenic component determined from the concentration of ^{4}He and accounting for an atmospheric component (for further details see sections 2.3.2 and 6.5).

Chapter 4:

In-Situ Cosmogenic Isotope Analysis Applied to the Problem of Escarpment Retreat: ^{10}Be and ^{26}Al Data from the Gamsberg, Central Namibia

---

4.1 Introduction

The break-up of the southern supercontinent Gondwana was a highly significant tectonic event in terms of landscape evolution at the macroscale and created many new passive continental margins (Summerfield, 1991a). Passive margin morphology takes many forms, but it is often characterised by a major seaward facing escarpment (known as a great escarpment) flanking a marginal upwarp and separating a variably dissected coastal plain from a higher elevation interior plateau (Figs. 4.1 and 4.2; King, 1962; Ollier, 1985; Gilchrist and Summerfield, 1994; Seidl *et al.,* 1996). Large-scale escarpments on passive margins are, therefore, highly significant landforms and their geomorphic evolution is a critical component of understanding margin development. Central to many conceptual and quantitative models of passive margin evolution is the notion that the escarpment has retreated to its present position since initiation near the major rift fault at continental break-up (Ollier, 1985; Gilchrist and Summerfield, 1990).

Over the past decade it has been increasingly appreciated that there is an important link between tectonic mechanisms and surface processes acting on passive margins (Beaumont *et al.,* 1998) but a growing problem facing landscape modelling of passive margins is a lack of empirical constraints about the way escarpments evolve. In this chapter, concentrations of cosmogenic ^{10}Be and ^{26}Al have been used to quantify the pattern and rate of denudation for part of the Great Escarpment of southern Africa at the Gamsberg, a flat-topped residual, in central Namibia. This provides the first direct measurements of escarpment retreat over the past ~10^5-10^6 a for the region.

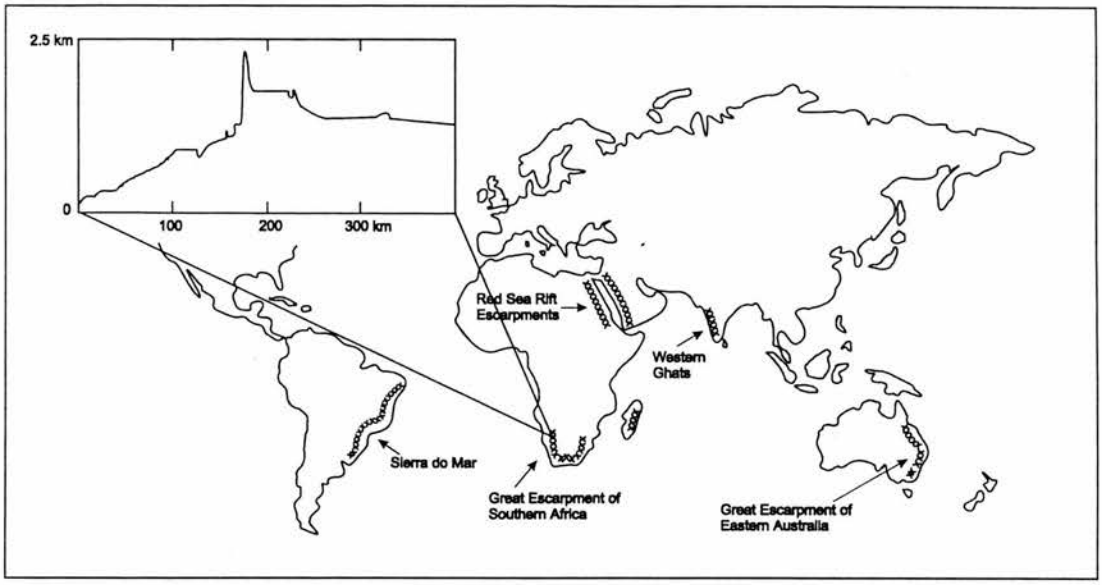

Figure 4.1: The location of great escarpments on passive margins. The insert shows a topographic profile across the south-west African margin at approximately 23°S (after Summerfield, 1991a; Kooi and Beaumont, 1994).

The escarpment in central Namibia on the south-west African passive margin was selected as the field site for several reasons:

1. The macroscale topography is characteristic of several other passive margins (Figs. 4.1 and 4.2).
2. Theoretical and quantitative models of margin development have been applied specifically to this margin and provide a useful research framework (Gilchrist and Summerfield, 1990; Gilchrist *et al.,* 1994b).
3. There are some existing empirical constraints on long-term denudation of the margin from analysis of the onshore and offshore sedimentary record (Ward *et al.,* 1983; Rust and Summerfield, 1990; Gilchrist *et al.,* 1994b) and apatite fission track thermochronolgy (Brown *et al.,* 1990, 1994, 1998) with which to compare cosmogenic isotope analysis data.
4. An arid climate means that the escarpment is largely free of vegetation or soil cover along most of its length and much of it comprises exposed bedrock slopes. Bedrock exposures are necessary for sampling for cosmogenic isotope analysis and a dominance of exposed bedrock makes the data more representative of the escarpment as a whole.

The Gamsberg was chosen as the specific study site because it is one of the clearest and morphologically most simple expressions of the escarpment along the south-west African margin. Comprising exposed quartz arenite and granite, it is suitable for sampling for *in-situ* cosmogenic ^{10}Be and ^{26}Al.

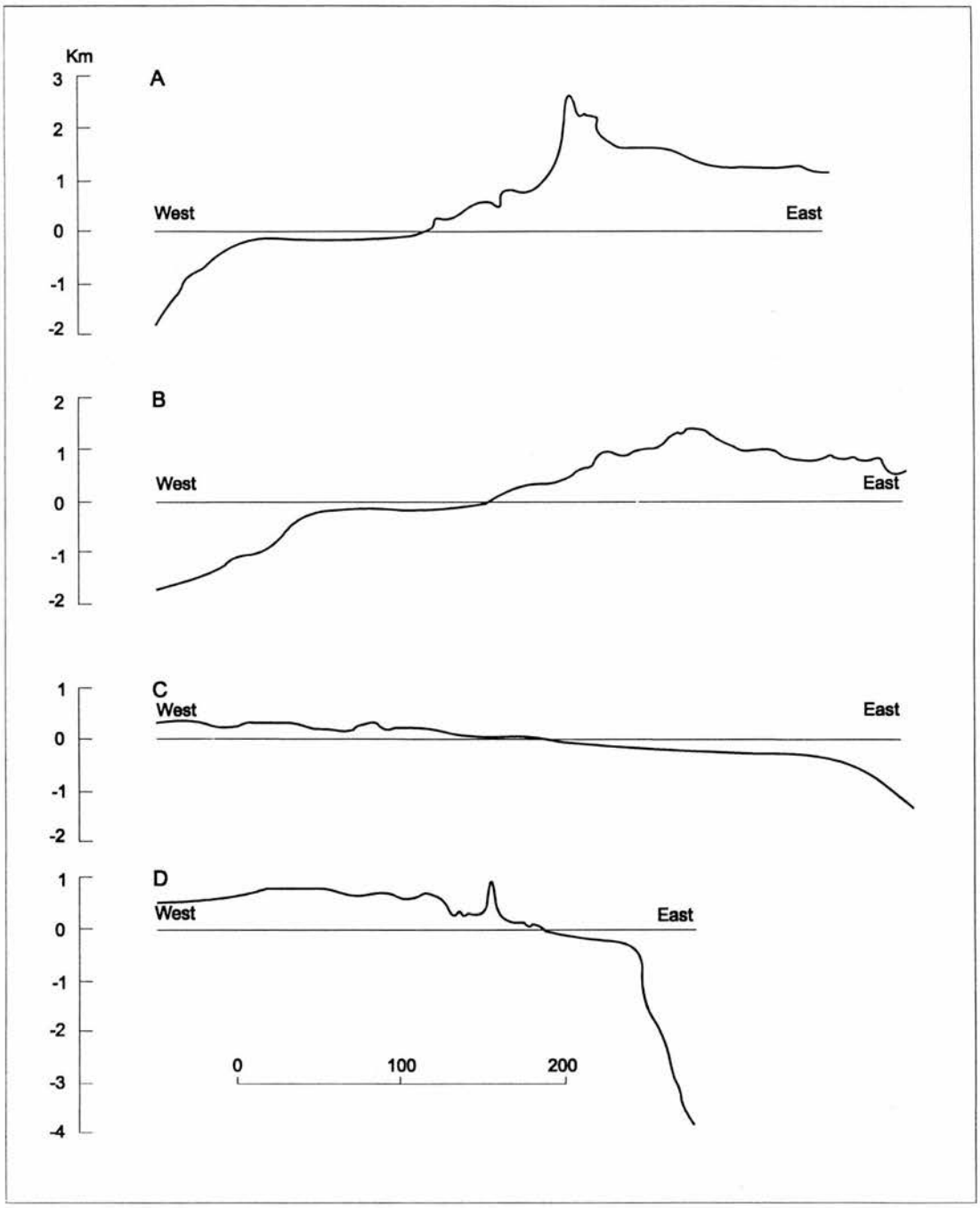

Figure 4.2: Topographic profiles across passive margins showing a distinction between high and low elevation margins. A: High elevation Arabian margin of the Red Sea at latitude 10°N; B: High elevation south-west African margin at latitude 27°S; C: Conjugate low-elevation eastern South American margin at latitude 33°S; D: eastern Australian margin showing high elevation at 30°S. Profile irregularities are due primarily to major margin-parallel drainage incision. (After Gilchrist and Summerfield, 1994, profiles constructed from 1:1M Operational Navigation Charts and 1:10M General Bathymetric Chart of the Oceans).

This chapter begins with a description of the morphology of the south-west African margin, with an emphasis on the Namibian section, and how the morphology relates to the regional drainage network and geology. This is followed by a review of theoretical and quantitative models of passive margin development which present a possible sequence of morphological development. Current understanding of the morphotectonic evolution of the Great Escarpment in Namibia is then reviewed followed by a brief synthesis of the current uncertainties and limitations. A detailed picture of the Gamsberg and its physical setting is provided in section 4.6 with sampling site details and strategy given in section 4.7. Cosmogenic data are presented and interpreted in section 4.8. The implications of these data are then discussed in relation to a denudation chronology for Namibia as well as in the broader context of passive margin evolution and it is for this reason that a relatively large amount of background material on these subjects has been included.

4.2 Morphology and Geology of the South-West African Margin

It is often assumed that the macrogeomorphology around the edge of the whole of southern Africa, including the south-west margin, is generally consistent with the overall form of high elevation passive margins shown in Figure 4.2. A large-scale, seaward facing escarpment separating an inland plateau from a coastal plain extending from Angola in the west to the Limpopo trough in the east has been identified by many authors and is known as the Great Escarpment of southern Africa (Fig. 4.1), (Rogers, 1920; Jessen, 1943; Wellington, 1955; Ollier and Marker, 1985). Wellington (1955) provided an excellent morphological and geological description of the Great Escarpment (Barnard, 1997), and pointed out that, although the escarpment is extensive and can be roughly traced around the edge of a central southern African plateau, there is considerable variation along its length probably reflecting variation in rock types and structures, drainage, and possibly climate. The escarpment is clearly defined along the eastern edge of southern Africa, particularly in the Drakensberg, but in the south the escarpment is usually defined inland of the high elevation Cape Fold Belt region coincident with the southern edge of out cropping Mid Jurassic dolerite sills (Brown *et al.*, 1998). The presence of the Cape Fold Belt seaward of the escarpment implies that the southern section of the escarpment probably has had a more complex history than other sections. Given also that the break-up events responsible for the south-east and south-west margins were of significantly different styles (Summerfield, 1996b) it seems somewhat misleading to continue the practice of referring to a unified landform. In this chapter, the term Great Escarpment will be used but will apply to the south-western margin in the eastern Cape region of South Africa, Namibia and southern Angola only.

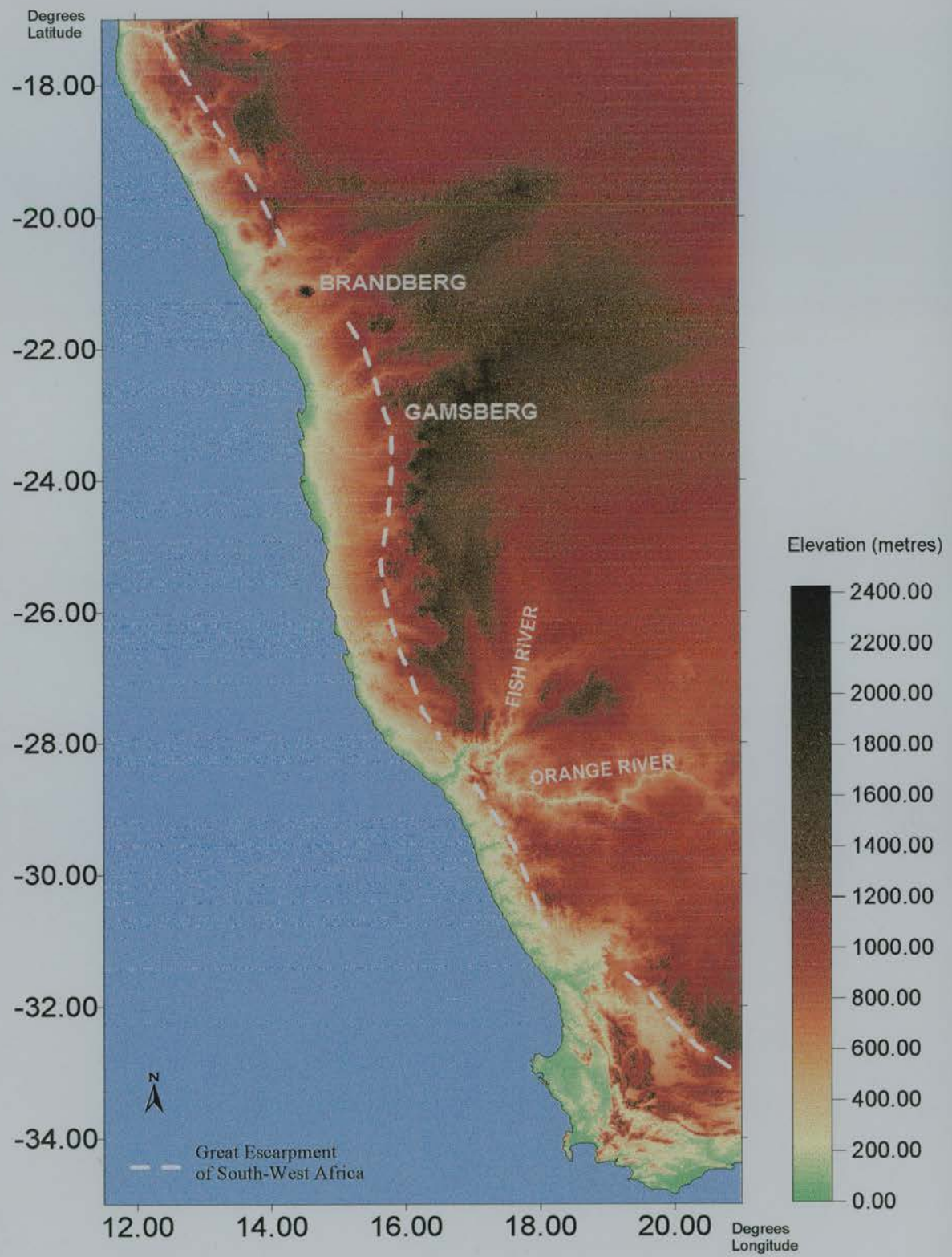

Figure 4.3: Morphology of the south-west African margin from a 1km resolution digital elevation model. The location of the Great Escarpment and major morphological features are shown (constructed from US Geological Survey 1 km topogrphic data).

In Figure 4.3, there is clearly discernible inland plateau (red/black) and coastal plain (green/yellow) along the south-west African margin. Land below 1000 m appears to be confined to a coastal zone less than 200 km wide except in the Orange River Valley where the river has incised into the plateau which dips gently into the Kalahari Basin in the centre of the sub-continent. A generally accepted location of the Great Escarpment based on the topography of the periphery of the highland areas collectively known as the south-west African Highlands is marked on Figure 4.3. This is broadly coincident with a line of maximum elevation (Ollier and Marker, 1985). It also marks the zone of maximum local relief (Gilchrist *et al.*, 1994b). In Figures 4.1 and 4.2. 'typical' large-scale topographic profiles across the Namibian margin demonstrate the classic shape identified on other high elevation passive margins but when considered in detail, as Wellington (1955) pointed out, the morphology of the margin varies considerably along its length and there are several 'gaps' in the escarpment (Fig. 4.3).

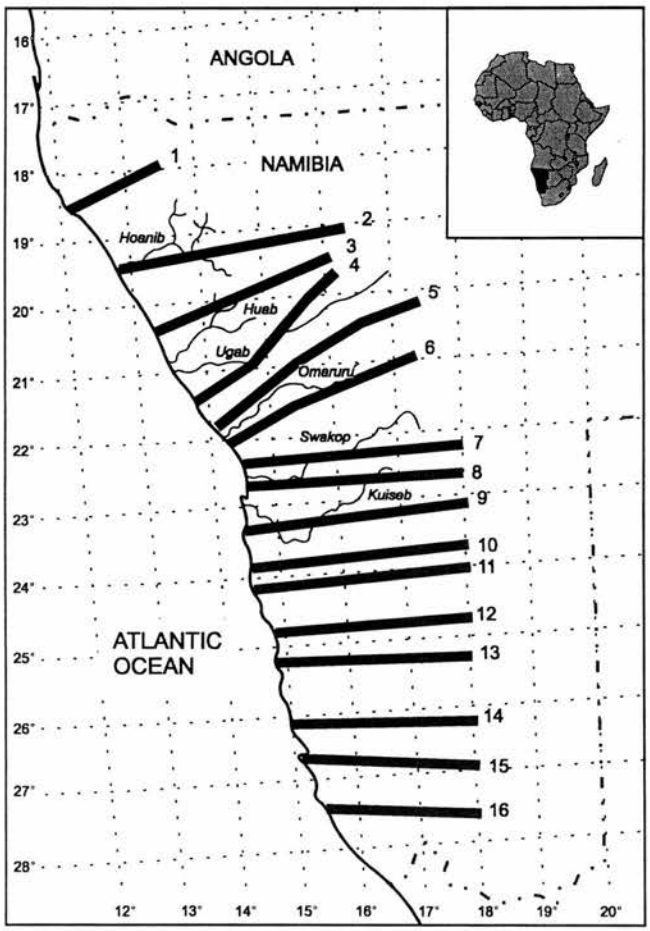

Figure 4.4a: Location of 16 topographic profiles across Namibia shown in Figures 4.4b and c (After Hüser, 1989)

Figure 4.4a shows the locations of 16 profiles constructed from 1:250 000 topographic maps across the south-west African margin between latitudes 18° to 28° in Namibia (Hüser, 1989). The profiles are displayed in figures 4.4b and c and demonstrate that 'typical' margin morphology is depicted in profiles 7 - 12 only. In profiles 1-3 and 13-16, the coastal plain, escarpment and inland plateau are poorly defined. In profiles 4-6 an escarpment is missing, and the coastal plain rises directly to the plateau interrupted by the Brandberg igneous complex and Erongo granite intrusions (~135 Ma old). This area has been termed the 'Randstufenlücke', literally 'gap in the escarpment', and is the longest break in the escarpment on the south-western margin (Spönemann and Brunotte, 1989).

At a simplified, regional level, the geology of south west Africa can be divided into seven principal sections (Fig. 4.5). Along most of its length the escarpment is underlain by crystalline basement rocks older than the Mesozoic Karoo sedimentary/volcanic sequence which covers the majority of the rest of southern Africa. South of the Orange river, the escarpment is formed across metamorphic rocks of the Namaqua complex (>1000 Ma old) and the coastal plain is covered to a certain extent by recent Cenozoic sediments. North of the Orange River valley, the escarpment is underlain by gently dipping sedimentary strata of the Precambrian Nama Group which covers crystalline basement and helps to create a clear escarpment edge in this region. Further north Nama rocks merge with the metamorphic and igneous rocks of the Pan-African (~500 Ma old) Damara metamorphic belt. In this central region and throughout the Damara area basement granites are exposed in many locations. The inland plateau region in southern Namibia has been dissected by the Fish River, a major tributary to the Orange (Figs. 4.3 and 4.4b). The Khomas Hochland is a high elevation mass comprising mica schists of the Damara orogen and marks the northern part of the central, well defined section of the escarpment (Figs. 4.3 and 4.5). The gap in the escarpment north of this may reflect a higher erodibilty of some NE-SW trending Damaran units (Spönemann and Brunotte, 1989).

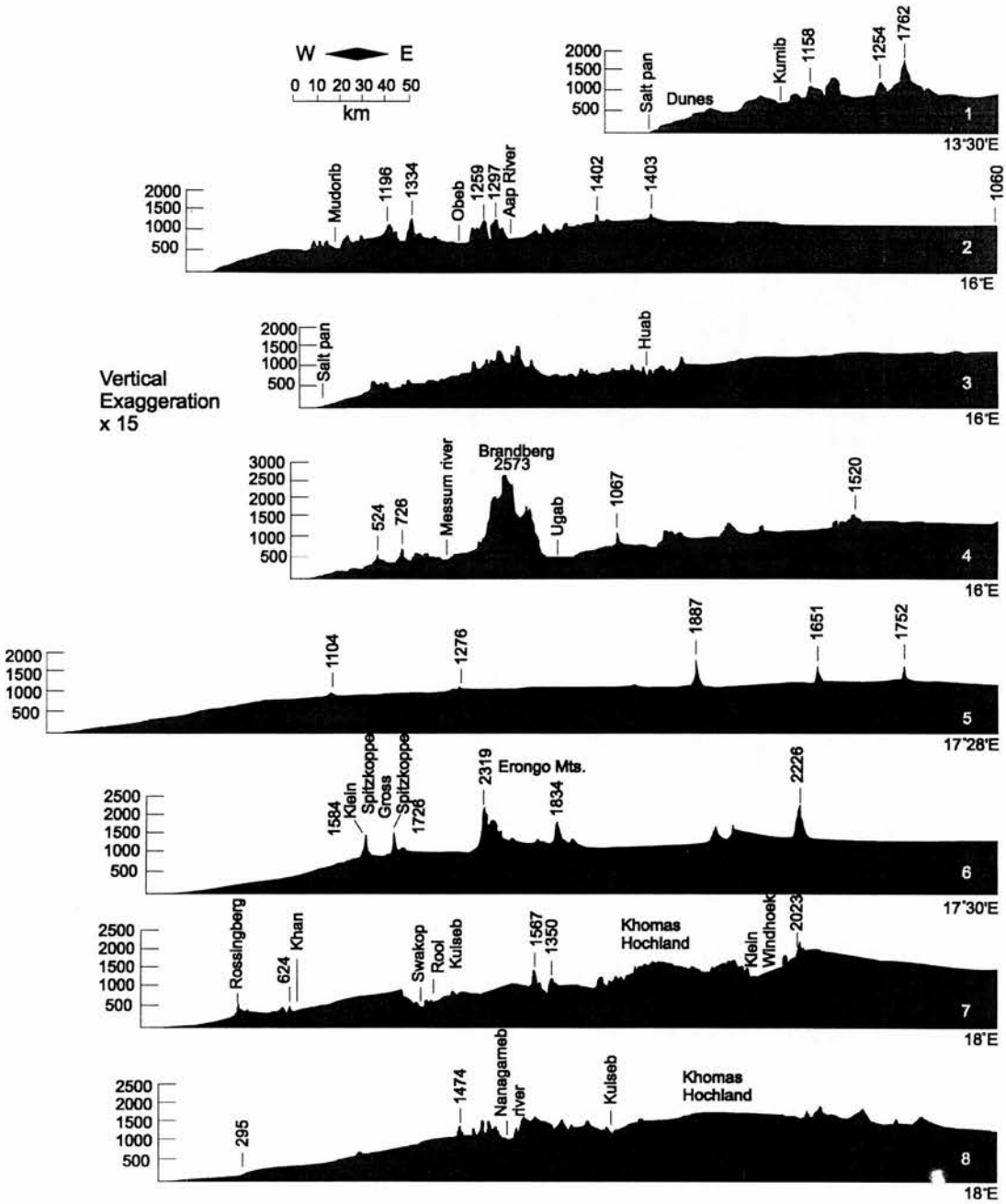

Figure 4.4b: Topographic profiles 1-8 across the northern half of Namibia (after Hüser, 1989)

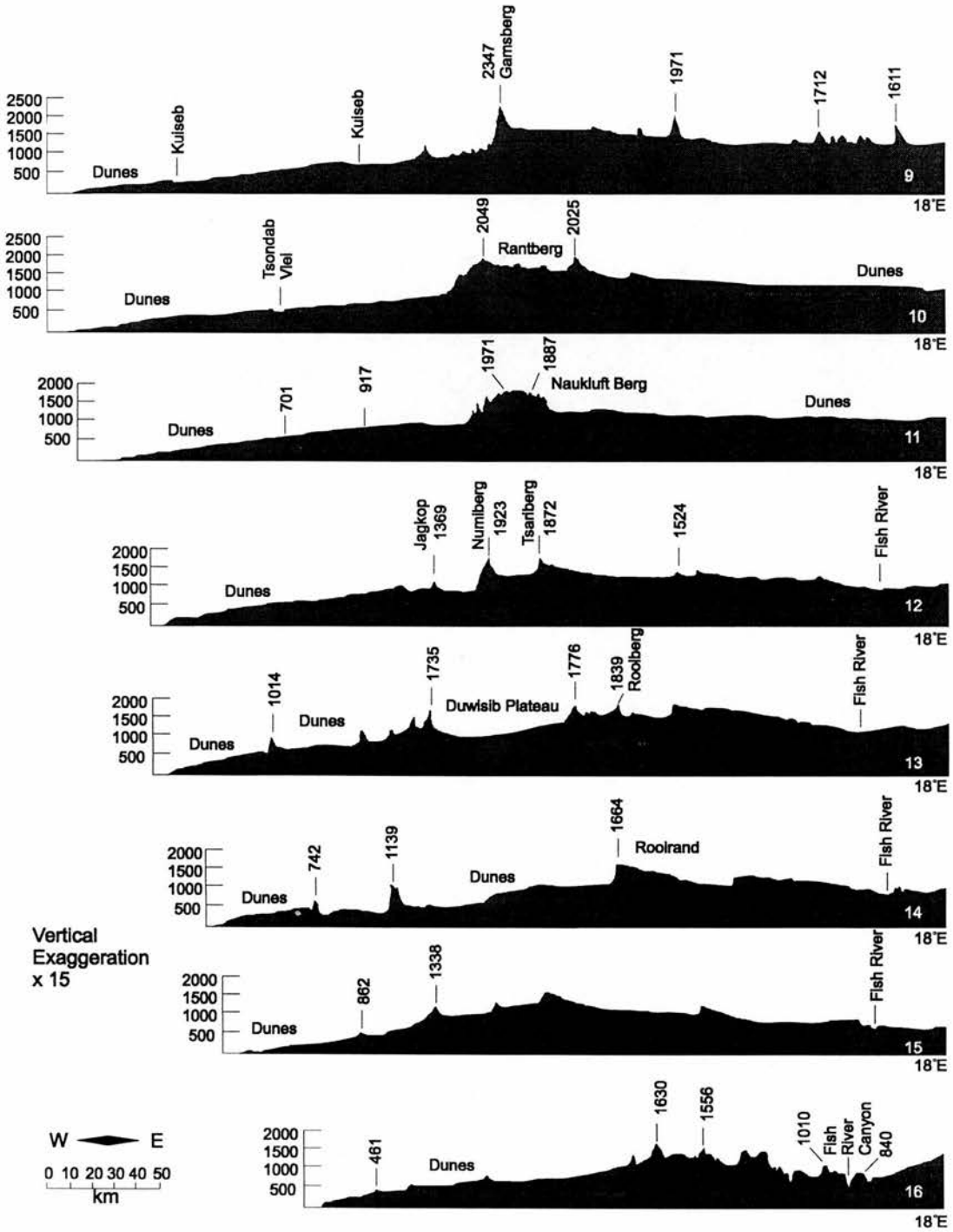

Figure 4.4c: Topographic profiles 9-16 across the southern half of Namibia (after Hüser, 1989)

In northern Namibia and southern Angola the escarpment becomes clearer and cuts across the Etendeka lava province. The lava province is similar to the Paraná basalt province on the originally congruent margin in Brazil and was formed at the same time as continental break-up (Turner *et al.*, 1984). Inland of the escarpment, Kalahari sediments cover a large area becoming progressively thicker towards the east. Below the escarpment, Namib Group Sediments, most significantly the main Namib Sand Sea from ~27° to 23° S, cover large areas of the plain that is principally cut across Damara and equivalent age rocks. Remnants of Permian Dwyka formation crop out in exhumed palaeovalleys in northern Namibia (Martin, 1953, 1981). These are glacial deposits around which can be found striated bedrock and indicate that in places in the northern Namib at least, the coastal foreland represents an exhumed Permo-Carboniferous landscape (Visser, 1987).

Drainage of passive margins is often characterised by a dual drainage pattern reflecting the morphological contrasts between the landscape exterior and interior to the marginal upwarp/escarpment (De Swardt and Bennet, 1974). Along the south-west margin, small, westward flowing, essentially linear catchments drain the front of the escarpment and the coastal plain. Larger, more dendritic catchments drain the interior and connect to the sea through breaches in the marginal upwarp, provided in this case by the Orange River (Figs. 4.3 and 4.5). In central Namibia, the escarpment is broadly coincident with the drainage divide and a dual drainage pattern is evident (Ollier and Marker, 1985; Gilchrist *et al.*, 1994b). It is apparent that some of the breaks in a clearly defined escarpment are coincident with the location of rivers and that where there is a close agreement between the location of the drainage divide and the escarpment, a landscape step is most clearly defined. The implications that this drainage pattern may have on the evolution of the landscape are discussed in 4.4.3.

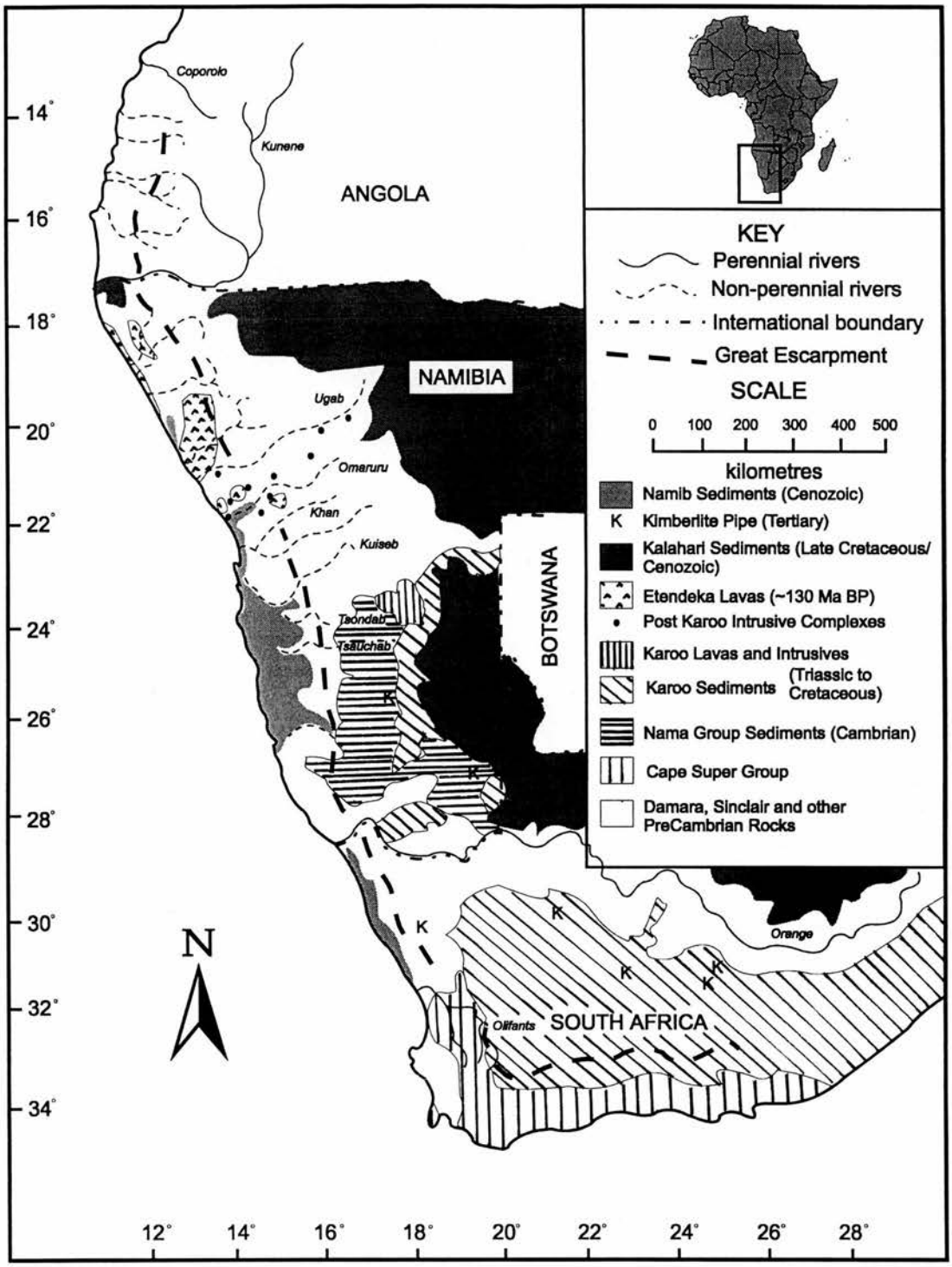

Figure 4.5: Map showing the location of major rivers and simplified surficial geology in relation to the Great Escarpment of south-west Africa. No data are shown for Botswana or Angola. (After Wellington, 1955; Ollier and Marker, 1985; Gilchrist et al., 1994b; and 1:1 000 000 geological maps of the Namibian Geological Survey.)

Figure 4.6: View south from the summit of the Gamsberg on the Great Escarpment in central Namibia. Note the dissection of the landscape infront of the escarpment but the clear step from the elevation of the coastal plain (~1000m) across the escarpment zone on to the plateau (~1500-2000 m).

Figure 4.7: View from the summit of the escarpment at Spreetshoogte (Rantberge) in central Namibia looking west out over the coastal plain.

4.3 Models of Passive Margin Evolution

4.3.1 Classical Ideas About Margin Evolution

Macroscale models of long-term landscape evolution were the focus of geomorphic thought throughout the first half of the Twentieth Century and were governed to a large extent by the cyclic approach of W. M. Davis (1899). In the simplest scenario, Davis (1899) envisaged large-scale downwearing of the landscape in response to a single tectonic uplift event. The progress of an evolutionary cycle of a landscape could be determined from an analysis of the landform assemblage evident. The ultimate end product was a low elevation landscape surface with minimal relief known as a peneplain. Davis did acknowledge other climatic and tectonic scenarios (e.g. Davis, 1905) and explained flat surfaces or peneplain remnants at high elevations by allowing for a series of tectonic or 'rejuvenation' events that would create a polycyclic landscape. The timing and extent of endogenic (tectonic) processes therefore could be 'read' in the landscape by filtering out the exogenic (surface processes) component with reference to a general landscape evolution model. This approach forms the basis of classical landscape analysis.

With respect to passive margins, L. C. King (1951, 1962, 1983) has been perhaps the most influential advocate of such a methodology (Twidale, 1992). However, King's general model differed from Davis's in that he envisaged landscapes responding to changes in base level through slope retreat and backwearing rather than downwearing. King thought that surface uplift or some other factor producing a drop in base level along a continental margin would initiate large-scale parallel retreat of a seaward facing scarp and growth of a pediment towards the continental interior, a process King termed 'pediplanation'. The ultimate end product of the model was similar to a peneplain but King used the term pediplain to indicate the underlying difference between the two models. Episodic rejuvenation would initiate several landscape cycles and produce a stepped margin topography consisting of a series of relatively flat planation (or erosion) surfaces separated by steep escarpments (Fig. 4.8). Planation surfaces were viewed as stable landscape elements being gradually consumed by scarp retreat only and not by downwearing. Surfaces could therefore be assigned ages relating to their formation at sea level or to a minimum age thereby recording a chronology of endogenic events and landscape development (Fig. 4.8). Remnants of ancient landscapes (>100 Ma old) were thought to be preserved at the highest elevations. King (1962) formulated his model based on the landscapes of southern Africa but proposed that planation surfaces across other continents could also be identified and correlated to produce a coherent global history of landscape development.

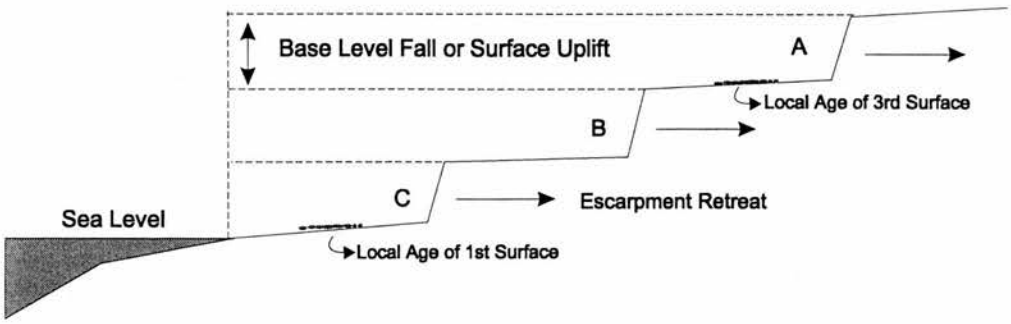

Figure 4.8: Schematic representation of King's idealised model of landscape evolution. Sea level fall or surface uplift of the entire landmass initiates a new landscape cycle (A), characterised by escarpment retreat towards the continental interior. Subsequent episodes of base level fall initiate further cycles of landscape evolution (B and C). King proposed that minimum ages of erosion surfaces could be assigned by the age of local deposits on their surface and therefore surfaces of regional or even continental extent relating to a single period of surface uplift could be identified despite later alteration or dissection by rivers. (After Summerfield, 1991a)

The classical approach to landscape analysis was not accepted universally and has been criticised for a number of reasons. Wellington (1955) was one of the earliest critics of King's work in southern Africa and questioned the preservation of landscape remnants for millions of years. A major criticism of the classical approach was that it lacked a coherent tectonic framework (Summerfield, 1985). Although in early studies this can be attributed to lack of knowledge, in more recent times (King, 1983; Partridge and Maud, 1987), it is arguably a result of reluctance to acknowledge and incorporate the wider range of inter-disciplinary information now available for passive margins (Gilchrist and Summerfield, 1994). The difficulties of integrating classical theories with contemporary tectonic thought led to new approaches in some areas (e.g. Young, 1983; Bishop, 1988). But King's ideas have retained prominence in southern Africa; there have been recent attempts to update King's framework of a series of dated erosion surfaces on the basis of new information, principally for the south-east margin of Africa (Partridge and Maud, 1987, 1988; Birkenhauer, 1991). A new conceptual model based on a revised notion from King (1962) for the downwarping of the coastal region of continental margins has recently been proposed (Ollier and Pain, 1997). Further criticisms of the classical approach have proposed that some surface remnants ascribed cyclic significance are in fact caused merely by resistant lithological layers (De Swardt and Bennet, 1974). Also, inconsistencies have been identified in the association of unconformities in the offshore sedimentary record with a chronology of onshore denudation and the gross assumptions of this method have been challenged (Summerfield, 1985). King (1955), Pugh (1955) and Partridge and Maud (1987) all proposed that an isostatic response to a threshold of escarpment retreat could explain apparent periods of discrete pulsed uplift identified on passive margins. Gilchrist and Summerfield (1991) demonstrated that rather than

explaining the existence of raised landsurfaces, their concept was a misinterpretation of the original work by Gunn (1949) concerning flexural isostasy. Lack of suitable dating control and vague extrapolations of landsurfaces based on the similarity of elevations of preserved remnants over large regions have also been highlighted as problems of the classical approach.

While the true significance of the landsurfaces and denudation chronologies proposed by King and others after him remain unclear, ideas about passive margin evolution have moved away from classical landscape analysis and have focused on margin tectonics and the influence that these may have on the evolution of the landscape (Gilchrist and Summerfield, 1994)

4.3.2 Tectonic Models of Continental Rifting

Ideas about continental drift developed throughout the first half of the Twentieth Century into a coherent theory of plate tectonics in the late 1960s. Plate tectonics provided a new framework in which to study continental evolution and cemented a link between continental rifts, extensional basins and passive continental margins. The principal focus of early research was to explain the formation and subsidence of sedimentary basins (e.g. McKenzie, 1978) but these early models could not adequately explain the associated uplift of rift flanks and therefore were of little use in explaining landscape evolution. More recently, however, explanations of observed uplift patterns and large-scale topographic features have also been sought and are recognised as fundamental to models of margin development (see Allen and Allen, 1990 for review). Tectonic models of rifting are often divided into two categories; 'passive' and 'active' (Allen and Allen, 1990; Summerfield and Gilchrist, 1994; van der Beek, 1995). Active rifting requires an initial thermal anomaly, possibly from the impingement of a thermal plume on the base of the lithosphere, which causes convective thinning, domal uplift and ultimately crustal extension. During a model of passive rifting, tensional stresses in continental lithosphere cause initial thinning and subsequent passive upwelling of hot asthenospheric material beneath the rift. In both models, thermal events, thinning of the crust and lithosphere, and uplift are all closely related and it is therefore hard to discriminate between driving mechanisms and resultant processes (Allen and Allen, 1990). Passive margins appear to exhibit aspects of both these styles of rifting therefore one can question whether a twofold distinction is still valid (van der Beek, 1995). However, concern over the timing of uplift relative to rifting has focused attention on the geomorphic history of passive margins (Steckler and Omar, 1994; Gilchrist and Summerfield, 1994).

Several reasons have been proposed to explain uplift patterns and account for elevated topography on newly rifted margins. Several of these invoke thermal mechanisms. Mantle

convection under rift flanks produced by extension and thermal erosion of the lithosphere is capable of producing uplift of around 1000m and has been suggested as an important component of Red Sea rift flank uplift (Steckler, 1985; Buck, 1986). However, this uplift mechanism fails to account for prolonged uplift as thermal influences will decrease as the lithosphere cools (thermal time constant of the lithosphere = ~ 60 Ma) and the thermal effects are limited to the immediate vicinity of the rift and so cannot account for margin upwarps which maybe located more than 100 km from the rift hinge. Subaerial erosion of thermally uplifted rift flanks after thermal processes have decreased will mean that in some models, the margin will eventually subside below sea level which is clearly not the case (Weissel and Karner, 1989). Also, Bouguer gravity anomalies do not indicate the presence of large amounts of hot, low density material directly under rift flanks but instead suggest that the lithosphere retains finite rigidity and that rift flanks are mechanically supported by upward flexure.

An alternative model of continental rifting concentrates on the flexural isostatic response of the lithosphere to mechanical unloading during lithospheric extension. Weissel and Karner (1989) present two kinematic models and their results are a good approximate fit to oceanic and continental rifts including the Rhine Graben. They conclude that the uplift of rift flanks can be explained as the flexural isostatic rebound of the lithosphere following its mechanical unloading during extension provided the lithosphere retains finite mechanical strength or flexural rigidity even though it is extended. The uplifted topography forms at the time and as a direct consequence of rifting, but once created remains a permanent deformation of the lithosphere unlike the in thermal models described above. Thermal effects will also occur but they will subside through time and have limited effect. Uplift of several kilometres can be generated by this model but as for the thermal mechanisms described above, the axis of uplift is located at the rift hinge and would not propagate inland and therefore it does not explain old marginal upwarps which are located hundreds of kilometres inland of the hinge line. Also, sediment accumulation and loading in the rift will significantly reduce the amplitude of residual surface uplift (Gilchrist and Summerfield, 1990, 1994).

It is generally agreed that the continental lithosphere is compositionally layered and that rheological differences occur between the quartz-rich crust and olivine-rich mantle (Weissel and Karner, 1989). This implies that different things will happen at different depths and that the uniform stretching model of McKenzie (1978), for example, is too simple. Royden and Keen (1980) investigated depth dependent stretching of the lithosphere and found this could generate up to 1.5 km of uplift. Braun and Beaumont (1989) used a dynamic approach to model the response of a rheologically layered lithosphere to extensional necking. If a strong, resistant layer

is placed deep enough, it will focus the level of necking to produce dynamically supported upwardly flexed rift flanks. The problem with these seemingly attractive models is that the rheology of the lithosphere is poorly constrained and this makes it hard to assess the importance of the uplift mechanism. However, in the model of Weissel and Karner (1989), similar patterns of uplift are produced for both oceanic and continental lithosphere, suggesting that rheological differences are not a dominant factor in the response of the lithosphere to extension. Braun and The dynamic approach of Beaumont and Beaumont (1989), however, does reveal possible mechanisms for surface uplift which are not included in kinematic models.

White and McKenzie (1989) proposed a model of continental rifting whereby partial melting of the asthenosphere occurs as the lithosphere actively thins due to decompression and the melted material, which is hot (~1300°C) and less dense, wells up passively beneath the rift (i.e. the classic passive rifting scenario). When rifting sites coincide with hot spots or mantle plumes, (unlike some other researchers they do not believe hot spots actively control the location of rifts) a large-scale (approx. 1000 - 2000 km across) uplifted dome of hotter than average asthenosphere is present under the rift and at continental break up large-scale magmatism occurs with extensive extrusive and intrusive igneous activity. Underplating, that is accretion of material within, or on, the underside of the thinned continental crust occurs, thereby promoting prolonged mechanical uplift of the rift flanks. They give examples from around the world showing that indeed the highest elevated passive margins are characterised by rift related volcanism at hot spots.

Asymmetric models of margin evolution have also been proposed (Lister *et al.,* 1986; Etheridge *et al.,* 1989) whereby an upper plate margin lies adjacent to a lower plate that consist of faulted upper plate remnants. In this model considerable amount of uplift of the upper plate can be caused by the rise of the mantle geotherm and although this is largely a temporary thermal effect, the model also provides for underplating of the upper plate as proposed by White and McKenzie (1989). A simple model of asymmetric rifting is useful for explaining asymmetry in the morphology of conjugate margins such as is found between the topography and shelf morphology of South Atlantic margins (but see also Davidson, 1997).

Of the tectonic models described above, the magmatic underplating model (White and McKenzie, 1989) and the flexural response model (Weissel and Karner, 1989) appear to best describe the uplifted topographic features of continental rifts. However, they are not without their problems and criticism; Gilchrist and Summerfield (1990) point out that the amplitude of the rift flank surface uplift will be reduced by sedimentation in the rift in the flexural model of Weissel and Karner (1989) and the domal uplifts created by underplating are broad topographic swells of

significantly greater wavelength than those characteristic of mature rifted margins. Also, although the rift mechanisms may produce uplift at the hinge line marking the boundary between rifted and unrifted continental lithosphere, the axis of the marginal upwarp is now on average 100km inland from this axis on many old margins and is therefore not adequately explained.

4.3.3 Morphotectonic and Surface Process Models of Margin Evolution

The models of rift evolution described above have generally assumed that subaerial denudation on the rifted margin plays no significant role in the generation of surface uplift. But the substantial amounts of offshore sediments located in rift basins suggest that the loading and unloading effects of rift related denudation may be significant. Gilchrist and Summerfield (1990, 1994) proposed a quantitative/conceptual model whereby marginal upwarps on mature continental margins are maintained if the lithosphere responds flexurally to differential unloading both inland and seaward of a retreating escarpment. This model imposes considerable conceptual constraints on the way the topography must have evolved but it is independent of the mechanism of rifting provided there is initial high elevation at the rift margin due to any unspecified cause. They envisage the simple dual terrain model with two distinct denudational systems as proposed by De Swardt and Bennet (1974). The coastal catchment consists of short, high energy rivers draining the rift flank or marginal upwarp graded to the new, oceanic base level separated from the interior catchment which is largely unaffected by the new base level and erodes at a lower rate. This kind of system has been proposed for several margins based on differential depths of denudation in coastal and interior catchment systems suggested by apatite fission track analysis (Red Sea margin - Bohannon *et al.* (1989), southeast Australia - Moore *et al.* (1986)). The coastal catchment area is assumed to increase linearly over time with the retreat of the escarpment from zero at rifting to a maximum value set by the present day situation on old margins. The differential unloading from this system creates a flexural isostatic response which increases elevation of the marginal upwarp by up to 600m. The model of Gilchrist and Summerfield (1990) exemplifies the recent revelation that denudation and rearrangement of mass at the Earth's surface exerts a first order control on large-scale patterns of tectonics and isostatic uplift, a notion largely missing from topographic studies in the past (Tucker and Slingerland, 1994).

Quantitative surface process models have been developed to examine escarpment evolution in more detail and are useful to further test the feasibility of ideas on sequences of morphological development, such as that proposed by Gilchrist and Summerfield (1990). Kooi and Beaumont (1994) used a surface processes model to investigate factors that might control escarpment

evolution and retreat on rifted margins. The two basic elements of their model are diffusive hillslope transport (short-range transport) and fluvial transport (long-range transport). By adjusting the relative efficiency of these two processes, they can investigate through the reaction of their model the influence of climate and lithology on escarpment morphology. Their principal conclusions are that antecedent topography and the location of the drainage divide are first order controls. For retreat to occur and a high elevation escarpment to be maintained, the top of the escarpment must coincide with the drainage divide. If they are far apart, then the escarpment will decline to a low angle feature without much retreat. Flexural isostasy helps to preserve the escarpment by continuous backtilting which maintains a marginal upwarp and sustains the location of the drainage divide. Escarpments are favoured by arid model conditions with low substrate detachability (i.e. high bed rock exposure with low erodibility). While trying to assess the applicability of their model results, they complain about the lack of knowledge concerning model parameter values in natural systems. Due to a lack of empirical constraints on the rates of processes operating in escarpment systems under different conditions, the model parameters are often arbitrary values unsupported by geomorphic reality. In general, their model does provide useful insight into the possible central role of drainage divide location for escarpment development. However, the basic premises of their model, for example the poor preservation of escarpments when the drainage divide is located further inland, are not found on all margins (Bishop and Goldrick, 1998). Tucker and Slingerland (1994) also used a landscape evolution model to define the necessary and sufficient conditions for long term, long distance escarpment retreat. They find that headward propagation of steep bedrock channels assisted by (and contributing to) flexural isostatic uplift, provides a viable driving mechanism, albeit idealised, for prolonged escarpment retreat.

Beaumont *et al.* (1998) have proposed that the future progress of passive margin modelling depends on the successful integration of tectonic models with surface process models, i.e. a coupled approach including feedback mechanisms. It is important to ensure integration of geomorphic, geological and geophysical studies of passive margins because although some models may be 'tweaked' to give attractive looking planforms and appear to operate over sensible time frames their usefulness can be questioned if sufficient empirical constraints are lacking. Essentially, the value of modelling so far has been in assessing what the important controls on long-term landscape development might be. They are useful in answering questions of a 'what if' type and provide insights into possible pathways of landscape development rather than representing 'real' landscapes (Merritts and Ellis, 1994; Bishop, 1998).

4.4 Morphotectonic Evolution of the Great Escarpment of Namibia

Current understanding of the morphotectonic evolution of south-west Africa has been pieced together from several different empirical and theoretical approaches. With the emphasis placed on denudation and the evolution of the Great Escarpment in Namibia, the information is reviewed below divided into four categories: ideas from a classical approach; insight from the use of stratigraphic information both onshore and offshore; thermochronological evidence, specifically from apatite fission track analysis; and the implications of quantitative modelling techniques.

4.4.1 Early and Classical Ideas

Early Twentieth Century, predominantly German, research into the large-scale landscape features of southern Africa focused on the spectacular and most prominent features of the landscape such as the Drakensberg escarpment on the south-east margin. Reviews of the history and development of ideas in the German literature and later work are provided by Bremmer (1985), Partridge and Maud (1987, 1988) and Birkenhauer (1991). Rogers (1920) was one of the first scholars (after Penck (1908)) to recognise that the previously described escarpment feature on the south-east margin of Africa was a denudational landform unrelated to faulting and that a near continuous escarpment could be recognised around the whole of South Africa to which he gave the name Great Escarpment. In southern Angola and Namibia, Jaeger (1930) identified a similar feature ('Randstüfe' meaning marginal scarp) and seeing that it was developed across folded rock over long distances inferred that it was related to uplift, tilting and erosion as had previously been suggested for the Drakensberg by Penck (1908) and Rogers (1920). Jessen (1943) introduced the term 'Randschwellen' (meaning marginal rise) for the upwarp of the escarpment based on his interpretation of the continental margin in Angola. Jessen's (1943) ideas of 'Randschwellung' (meaning marginal uplift) and his associated identification of five main erosion surfaces in Angola and northern Namibia is one of the earliest examples of the classical approach to unravelling landscape histories in southern Africa, and certainly the most detailed for the south-west margin.

After Jessen (1943), the majority of classical constructions on southern Africa have focused on the south-east margin (King, 1948, 1951, 1962, 1983; Partridge and Maud, 1987, 1988). In Namibia there have been only a few focused attempts to build up a classical chronology of landscape cycles. However, it is clear that King (1962) thought that many of the surfaces identified for the south-east could be extrapolated across the continent to Namibia. Other studies,

such as those of Hüser (1989) and Spönemann and Brunotte (1989), have been largely descriptive and have included only limited development of King's ideas for the region. The problems with the classical approach have been reported in section 4.3.1. In Namibia, the situation regarding the lack of geochronological data is more pronounced than for other areas and this may have inhibited further correlation of landsurfaces.

4.4.2 Stratigraphic Evidence of the Tectonic and Denudational History of Namibia

On the basis of seismic mapping of the sedimentary sequence on the continental shelf of Namibia, it has been inferred that the onset of continental rifting occurred in the mid-late Jurassic (160-145 Ma BP) (Tankard *et al.*, 1982; Gerrard and Smith, 1982). This was followed by a second rift phase at 130-120 Ma BP coincident with the initiation of sea floor spreading (Maslanyj *et al.*, 1992; Light *et al.*, 1993). The inferred timing of rifting is broadly coincident with $^{40}Ar/^{39}Ar$ dating of preserved Etendeka flood basalts in northern Namibia which has most recently suggested an age ~131 Ma BP for eruption and progressive rifting from south to north (Turner *et al.*, 1994; Renne *et al.*, 1996). There is a large difference in the volume of preserved lava in the Etendeka volcanic province in northern Namibia and the associated Paranà flood basalt region on the opposite margin in Brazil (1.2×10^6 km^3 vs. 1.5×10^4 km^3; White and McKenzie, 1989; Gallagher and Hawkesworth, 1994). This probably reflects asymmetry in the volume of basalt extruded on to each margin at the time of rifting rather than in extent of post-rift denudation. This hypothesis is based on similar apatite fission-track analysis estimates of denudation for both the Namibian and Brazilian margin (see below) and has been explained by migration of the mantle plume associated with flood basalt production combined with asymmetry in the style of rifting (Gallagher and Hawkesworth, 1994; Brown *et al.*,1998). From this it can be inferred that the initiation of hypothetical large-scale escarpment retreat could begin only after ~130 Ma BP.

Further examples of analysis of syn- and post-rift sediments on the continental shelf of Namibia are limited despite its areal extent (>100 km wide, Bremner (1981), Gerrard and Smith (1982)). The spatial and temporal pattern of rift-related and post-rift sedimentation are important because they record the timing and extent of denudation (unloading) onshore and loading of the continental shelf which control isostatic flexure and tectonic evolution of the margin (Gilchrist and Summerfield, 1994). The Namibian offshore continental area can be divided into four small basins, collectively known as the Cape Basin. From the Falkland-Agulhas fracture zone ridge northwards these are the Orange, Luderitz, Walvis and Namibe Basins, the latter occurring north of the Walvis Ridge and having more in common with the narrower Angolan Shelf (Light *et al.*,

1993). The distribution of >7 km thick Cretaceous-Cenozoic sediments in the Orange Basin has been used to infer changes of the course of the Orange River during this time period and an overall reduction in sediment supply from the Late Cretaceous to the Neogene (Dingle and Hendey, 1984). Further investigation into sediment isopach data coupled with borehole analysis from the Orange and Walvis Basins indicated four stages of sedimentation. The timing of these phases was originally based on age constraints from Emery and Uchupi's (1984) work in the North/Equatorial Atlantic. However, a slightly revised timing for sedimentation periods identified by Rust and Summerfield (1990) has been proposed on the basis of Gerrard and Smith's (1982) chronology for the South Atlantic (K. Gallagher, *pers. com.*). The phases are as follows: relatively low amounts of sedimentation from the rift onset in the late Jurassic to the drift onset unconformity at ~132 Ma BP, a second phase of thicker sedimentation to the mid Cretaceous, the third phases of maximum depths of sedimentation to base Tertiary and a final stage of reduced depths of sedimentation up to the present (Rust and Summerfield, 1990). The total sediment accumulation is equivalent to a mean, minimum post-rifting denudation depth of 1.8 km for the total westward draining catchment area, including the whole Orange-Vaal drainage system (mean denudation rate of 11.8 m Ma^{-1} (Rust and Summerfield, 1990)).

A major problem with assessing sediment volume data in relation to onshore denudation is an inherent lack of control on the temporal and spatial variations of the source area of the sediment (section 1.3). Although the Walvis Ridge and Falkland-Agulhas fracture zone ridge form effective barriers to sediment within the Cape Basin, it is still not possible to distinguish changes in the overall rates of erosion in the source drainage basins from changes in source basin area. Rust and Summerfield (1990) attempted to assess continental denudation rates from offshore data in more detail assuming general models of drainage evolution in which drainage area increases from relatively small catchments draining a marginal upwarp to larger westward flowing rivers and the eventual breaching of a retreating escarpment by a dominant internal river, in this case the Orange at ~85 Ma BP. Average erosion rates decline as the catchment expands after breaching of the marginal upwarp. Calculated average rates were 16-32 m Ma^{-1} for their third period and 7.1-8.7 m Ma^{-1} for the fourth. (NB. The change in ages for the boundaries recently proposed does not affect these values just their relative timing.)

Examination of the onshore stratigraphic record is one way that can help clarify the meaning of offshore deposits. The earliest known sedimentary deposits in Namibia are the Giraul Conglomerates in northern Namibia and the Pomona Beds in south. The Giraul Conglomerates are thought to represent a phase of terrestrial sedimentation ~105 Ma BP of coarse alluvial-fan deposits, 200 m thick, reportedly derived from a young escarpment (Ward *et al.*, 1983). The

surface of the fluvially deposited Pomona Beds appears to represent an eroded landsurface that has been correlated with the bedrock platform of the coastal plain in central Namibia. In central Namibia this is known as the Namib Unconformity Surface and has been dated, on the basis of correlation with the Pomona Beds, as late Cretaceous (Ward *et al.*, 1983; Ollier, 1978). As previously mentioned, in places in the north it is thought to represent an exhumed Permo-Carboniferous landscape on the basis of remnants of Dwyka formation in exhumed palaeovalleys (Martin 1953; 1981; Visser 1987). From this information it can be inferred that that the coastal plain, up to an unconstrained width, was a fixed feature of the margin by at least the late Cretaceous.

The most important deposit in central Namibia in terms of the denudational history of the escarpment is arguably the Tsondab Sandstone Formation. Similar arenites have also been found near the Orange River and in south-west Angola, and as a group they form the oldest deposits found on most of the coastal plain. The Tsondab consists of fossilised sand dune systems, carbonated layers and some fluvially bedded units. The sediments are thought to have been blown in from the continental shelf during marine transgressions (Ward, 1987), or consist of fluvial sediments from the east derived from sandstones such as those that cap the Gamsberg, assuming it once had a more extensive cover (Besler and Marker, 1979; Besler and Pfeiffer, 1993; Besler 1996). Exposed remnants of the Tsondab preserved in the Kuiseb/Gaub drainage basin and further south cropping out along the eastern edge of the present day sand sea border the escarpment to within 3-30 km of its base (Ward, 1987; Besler, 1996). Recent identification of six types of giant bird eggs, similar to ostrich eggs, fossilised *in situ* at numerous localities has led to the best biostratigraphic dating of the Tsondab and southern arenites to date (Pickford and Dauphin, 1993; Senut *et al.*, 1994; Pickford *et al.*, 1995; Senut and Pickford, 1995). Dating by association with rodents teeth, that can be correlated with geochronologically constrained sites in East Africa, indicates that the eggs found in the Tsondab span a period from the Pliocene (>2 Ma BP) to the Middle Miocene (>13 Ma BP) (Senut and Pickford, 1995). Although the lower units of the Tsondab are thought to have a much older maximum age of ~55 Ma BP (lower Eocene) (Ward, 1987), the youngest age limit is now constrained and the position of eggs in the Tsondab relative to the escarpment can provide constraints on escarpment retreat rates. Sites at Elim and the Diep River between the Tsondab and Tsauchab rivers, approximately 20 km east of the base of the escarpment in central Namibia, both contain the oldest found eggs of the *Namornis oshanai* species that have been ascribed a middle Miocene, (>13 Ma BP), as well as younger eggs (Pickford *et al.*, 1995; Senut and Pickford, 1995). This implies that the average maximum rate of escarpment retreat is <1.5 km Ma^{-1} over the past 13 Ma. Further work of this type may be able to provide more constraints on the movement of the escarpment.

The relationship between morphology and surficial geology has been used in other locations in south-west Africa to provide gross estimates of denudation over known time scales (Gilchrist *et al.*, 1994b; Gilchrist, 1995). Kimberlite intrusions located inland of the Great Escarpment in southern Namibia (Fig. 4.5) retain their original crater infill implying insignificant denudation since their intrusion at the beginning of the Tertiary (Janse, 1975; Gilchrist *et al.*, 1994b). Subvolcanic igneous intrusion complexes in northern/central Namibia, ~135 Ma old, form large inselbergs on the coastal plain, for example the Brandberg and Messum complexes, suggesting more than 1.5 km of denudation must have occur around them (Eales *et al.*, 1984; Gilchrist *et al.*, 1994b). It has also been inferred that >1 km of denudation must have occurred at the coast since rifting given the landward dip of Karoo beds further inland and the fact that these must have at one time covered the region joined to equivalent rocks now in Brazil. Incorporating evidence for exhumation of Permian glacial valleys in the north and the relationship of Etendeka lavas to Dwyka sediments near the escarpment as well as evidence for minor denudation in the Kalahari Basin (Thomas and Shaw, 1990), Gilchrist *et al.* (1994b) inferred a consistent chronology of denudation for the margin. First, that most of the region, except the Kalahari Basin, has been significantly denuded (~0.5-3.5 km) since rifting and that the coastal plain has been more denuded than the interior highlands. Secondly, that the majority of this denudation was accomplished prior to the beginning of the Cenozoic, after which time, denudation has been minimal.

4.4.3 Thermochronological Evidence

Although a 'stratigraphic' approach to constraining the denudation chronology of south west Africa has yielded useful results, the dominance of denudation on passive margins means that there is an overall lack of reliable, datable and regional stratigraphic markers. Several of the examples described above provided only localised or poorly constrained, integrated rates over long periods of time. An alternative approach that can provide improved temporal and spatial detail on a regional scale is apatite fission track thermochronology. The number of fission tracks (damage lines in the crystal lattice from the spontaneous fission of ^{238}U) in apatite crystals and their track length distribution from surface samples can yield a cooling history for the sample through the upper 3-4 km of the crust (see Brown *et al.*, 1994 for review). By making certain assumptions and using thermal modelling to derive cooling histories (Gallagher, 1995), fission track data can be translated into a depth of denudation and the timing of that denudation at each sampling location.

An extensive regional sampling strategy in south west Africa including profiles across the escarpment in Namibia has indicated substantial crustal cooling for the entire margin (Brown, 1991, 1992; Brown *et al.*, 1990, 1994, 1998). Inferred syn- and post-rift denudation contour maps for south west Africa are shown in Figure 4.9. Several features of the data are apparent: First, the margin was subject to moderate to low amounts of syn-rift denudation (< ~1 km) but the post-rift contour map clearly shows large amounts of denudation for the entire area since 118 Ma BP (~3-5 km). Secondly, total depths of denudation since rifting are greatest for the coastal area and decrease inland towards the continental interior and are therefore consistent with the first conclusion of Gilchrist *et al.* (1994b). However, the significant depths of denudation recorded east of the escarpment are contrary to classical interpretations of the landscape which assume the interior plateau contains extensive preserved uplifted remnants of a landsurface dating back to the early Tertiary (Partridge and Maud, 1987) or possibly even the Jurassic (King, 1962). The data cannot be adequately explained by any landscape model that implies downwarping of the coastal plain rather than large-scale denudation in front of the escarpment, as recently proposed in the model of Ollier and Pain (1997). A third aspect of the data is that denudation is not uniform through time and the majority of denudation had occurred prior to the beginning of the Tertiary. An accelerated phase of crustal cooling from ~80-60 Ma in the late Cretaceous inferred for many sites is interpreted as recording a period of rapid denudation associated with the early development and uplift of the margin (Brown *et al.*, 1990). The timing of denudation inferred from fission track data has been broadly correlated with offshore basin borehole data from Rust and Summerfield (1990) (Brown *et al.*, 1990). The data are therefore also consistent with the second conclusion of Gilchrist *et al.* (1994b) and with other stratigraphic evidence which imply low rates over the Tertiary (Ward *et al.*, 1983). A fourth feature of the fission track data is that the timing and magnitude of denudation vary geographically, in particular along the strike of the margin. Significant variation in the spatial distribution of denudation provides further argument against classical theories which assume cycles of erosion affect large areas simultaneously. Brown (1992) suggests that reactivation of pre-existing crustal structures in response to reorganisation of ocean basins during the break-up of Gondwana in conjunction with climatic and lithological factors could explain the timing and pattern of the observed phases of denudation.

Figure 4.9 (Overleaf): Syn-rift (158-118 Ma BP - map A) and post-rift (118-0 Ma BP - map B) denudation contour maps for south-west Africa based on the interpretation of apatite fission track analysis. Black dots show the location of samples. The scale for denudation thickness is the same for both maps (from Brown et al., 1998).

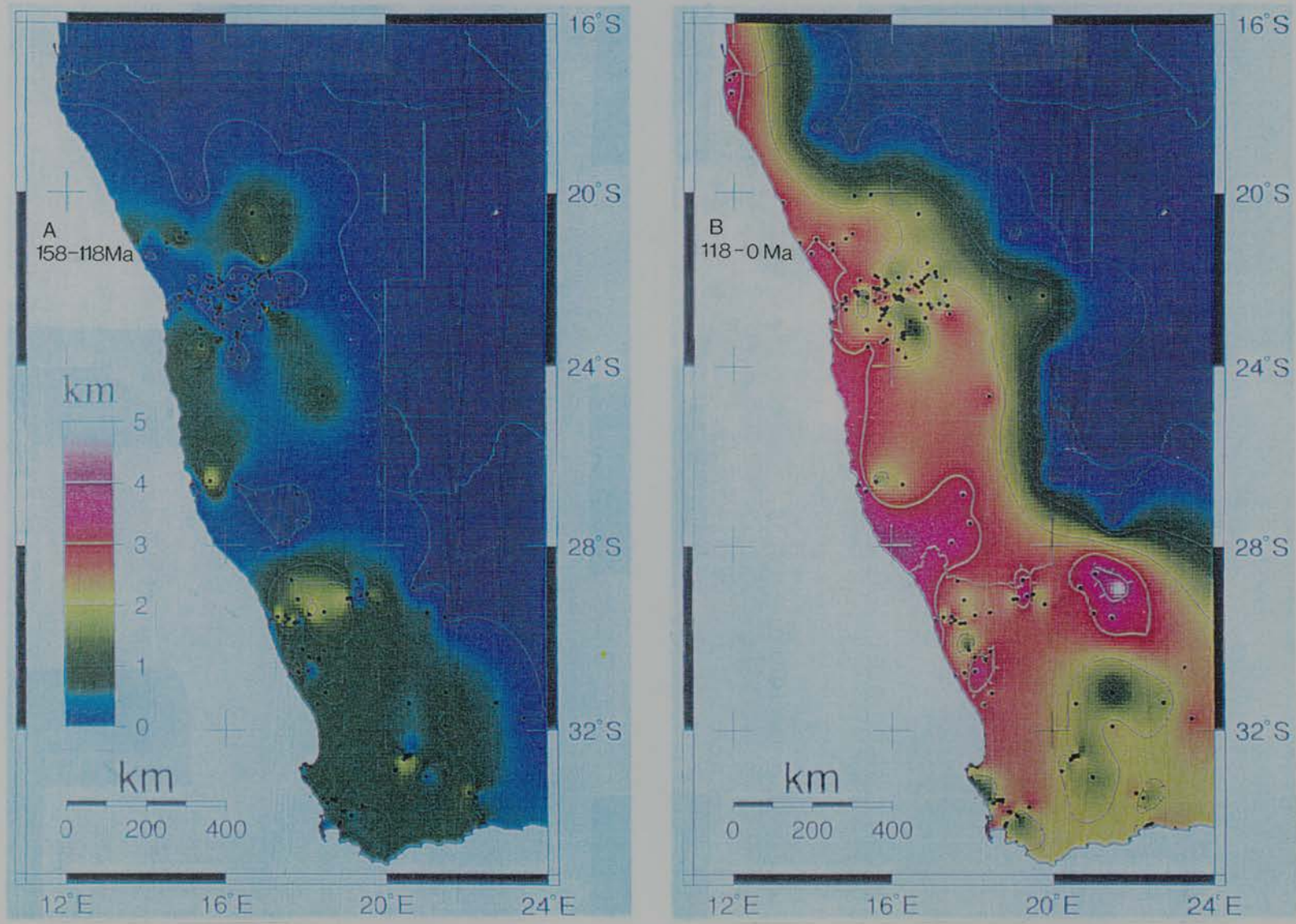
A
158–118Ma
km
5
4
3
2
1
0
km
0 200 400
16°S
20°S
24°S
28°S
32°S
12°E
16°E
20°E
24°E
B
118–0 Ma
km
0 200 400
16°S
20°S
24°S
28°S
32°S
12°E
16°E
20°E
24°E

4.4.4: Morphotectonic and Surface Process Models for South-West Africa

The conceptual isostatic model of Gilchrist and Summerfield (1990) can explain the persistence of marginal upwarps on old passive margins provided that landscape development proceeds by escarpment retreat with a dual drainage system and that the lithosphere responds flexurally (section 4.3.3). Application of the model constrained by the present day topography of the south-west African margin, and some offshore and fission track evidence, demonstrated >600 m of surface uplift assuming a constant retreat rate of a 1 km high escarpment of 667 m Ma^{-1} since rifting. The model assumed an initial high elevation of ~1 km at the time of rifting. The implications of the presence of a mantle plume in the South Atlantic (White and McKenzie, 1989) and the fact that the region was then near the centre of a large continent (Summerfield, 1991a) suggest that this is not unreasonable.

Using the basic model from Kooi and Beaumont (1994), Gilchrist *et al.*, (1994b) presented four numerical surface process models to simulate how an escarpment may have been created within the broader context of the large-scale stratigraphic observations outlined above. They showed that the landscape of south-west Africa could have evolved in one of four styles depending on the influence of climate, the presence of resistant lithological layers, inherited drainage patterns and the timing of integration of an internal drainage system to a common base level but that escarpment retreat could only have been maintained in certain model runs. They determined that escarpment retreat is dependent on the drainage divide being consistent with the marginal upwarp and that its retreat will be slowed as soon as the interior catchments of their dual drainage system attain sea level as base level. The escarpment in effect becomes pinned as the topography on either side of the escarpment becomes similar. In central Namibia, the incision of the Fish River may be contributing to escarpment pinning (Fig. 4.3). If the drainage divide had started near it present position, then within the confines of their model an escarpment formed at the coast would have been denuded and then reformed at the drainage divide after large-scale downwearing of the coastal plain and bedrock river incision. Resistant lithological layers are necessary for a clearly defined scarp. The value of this model is in highlighting the significance of drainage divide control on escarpment evolution and in suggesting that escarpment evolution in Namibia has had second order controls from lithology and climate.

4.5 Existing Approaches: Summary and Limitations

The implications of the different types of investigation into the morphotectonic history of the Namibian margin reviewed above have been summarised in Table 4.1. Also included is the general statement, initially proposed by King (1983), that escarpments retreat at a rate on the order of 1-2 km Ma^{-1} if they are assumed to have retreated uniformly from an initial position at the rift edge. This rate, for want of other better constrained data, is often cited as the actual rate of Great Escarpment retreat and used in passive margin development studies (e.g. Selby, 1993; Ollier and Pain, 1997).

Table 4.1: Evidence for denudation of the south-west African passive margin

Author(s) and Year(s) of Study	Nature of Investigation	Principal Conclusions	Implications for Denudation/Escarpment Retreat.
Ward et al. (1983)	Interpretation of the sedimentary succession in the coastal plain of Namibia	Coastal plain formed by late Cretaceous, old sediments abut escarpment.	Large amounts of denudation after rifting in coastal zone, slow rates during Tertiary
Pickford and Senut (1995), Senut et al. (1994)	Biostratigraphy of Tsondab Sandstone based on giant bird egg fossils	Stratigraphic units identified and ascribed ages from <2 Ma to >13 Ma	Little denudation and rates of <<1.5 km Ma^{-1} for escarpment retreat since Miocene
Gilchrist et al. (1994b)	Interpretation of dated kimberlite pipe stratigraphy on Nama plateau	Original crater infill of lacustrine sediment retained	Minimal denudation (<100m) of southern plateau since early Tertiary
as above	Measurement of relief surrounding dated igneous intrusive complexes	Up to 2 km difference between peak elevations and surrounding surfaces	Rates of denudation on coastal plain of 7 to >14 m Ma^{-1} since rifting
as above	Extrapolations of Karoo sediments across coastal plain	Denudation of >1km in exterior catchment, increasing towards coast	Denudation on coastal plain of 5 to >18 m Ma^{-1} since Karoo deposition, >180 Ma BP
as above	Interpretation of Etendeka lava remnants in relation to Dwyka deposits	>500 m of denudation in front of escarpment in northern Namibia	Denudation of northern coastal plain of 4 to >17 m Ma^{-1} since Etendeka extrusion
Thomas and Shaw (1990)	Analysis of Kalahari sediments	Prolonged sedimentation within Kalahari, some humid phases.	Low rates of denudation in continental interior since continental rifting
Rust and Summerfield (1990)	Offshore sediment volumes from isopach and borehole data	4 phases of sedimentation and rates based on assumed landscape evolution model	16-32 m Ma^{-1} post rifting and 7.1-8.7 m Ma^{-1} post Tertiary for exterior drainage area
Brown et al. (1990, 1998)	Apatite fission track analysis	Ages increase and mean track length decreases with elevation towards interior	Low syn-rift but high (3-5 km) post rift denudation. Max. at coast, decreases inland. Pulse in Late Cretaceous.
King (1983) and many others	General statement about margin development	Escarpments retreat from initial position over period since rifting	Assuming uniform retreat, escarpment retreat = ~1-2 km Ma^{-1}
Inferences and parameters of surface process models:			
Gilchrist and Summerfield (1990)	Conceptual/quantitative isostatic model	Flexural uplift maintains marginal upwarp assuming escarpment retreat	Uniform retreat rate of 667 m Ma^{-1} yields >600 m uplift
Gilchrist et al., (1994b)	Surface process model to investigate climate, lithology, initial topography and drainage	Drainage divide location and drainage configuration are important controls on SW Africa topographic evolution	Escarpment retreat only occurs under some model configurations, uniform retreat is special case.

The information reviewed above from a range of different approaches does provide an overall insight into denudation of the margin over long-periods of time. Many of these independent techniques, such as fission track thermochronology and analysis of the stratigraphic record both onshore and offshore, produce inferences about denudation at the macroscale that are broadly compatible (Table 4.1). The limitations of the individual approaches have been discussed in sections 4.4.1 to 4.4.4, but the data are also limited in a more general sense. Because of the regional spatial scale at which the most of the data are applicable, there is little constraint on the morphological development of the margin. This poor spatial resolution means that the existing data are of little use in deciphering the evolution of specific landscape components, particularly the central feature, the escarpment. Coupled with the large spatial scale of most of the techniques outlined above, the denudation rate data are commonly integrated over very long periods of time. Inferences on the timing and rate of denudation events from apatite fission track data for example can only be resolved to periods of $>10^7$ a (Summerfield, 1996a). The data provided in Table 4.1 provide little detail about what has been happening in more recent geological time.

For a full appreciation of the development of the Namibian margin data on intermediate time scales, finer spatial and temporal data on morphological evolution and denudation is needed. Without it, existing data provide a poor basis on which to evaluate quantitative models of margin development. For although such models commonly use a resolution of 1 km grid squares, this is finer than can be resolved from the much of the data shown in Table 4.1. Behaviour of specific landscape components such as escarpments is still poorly understood but is nonetheless demanded by conceptual and quantitative models of landscape evolution. As discussed in Chapter 1, *in-situ* cosmogenic isotope analysis has potential for refining the resolution of data on rates of denudation and styles of morphological development in passive margin settings. Analysis of cosmogenic ^{10}Be and ^{26}Al in quartz at the Gamsberg on the Great Escarpment in central Namibia has been used to address this issue and provide a direct assessment of escarpment behaviour over the past 10^5-10^6 a.

4.6 The Gamsberg

4.6.1 Morphological and Geological Setting

The Gamsberg (23° 20' S, 16° 12' E) is an impressive flat topped feature (Fig. 4.10). It consists of a uniform quartz arenite caprock with a cliff edge overlying basement granite, which gives it a conspicuous table-top shape. At 2347m high it is second only to the Brandberg in elevation in Namibia (Fig. 4.3). It is situated directly on the escarpment, on the eastern edge of the Khomas Hochland, and is the highest point along its length (Fig. 4.3). The Klein Gamsberg (2326m) approximately 2 km to the north-east is a similar but smaller feature (Figs. 4.10 and 4.11). The Gamsberg is an elongate mountain aligned NNE to SSW (Fig. 4.11). The western side forms a very distinctive edge to the escarpment and the caprock cliff edge and underlying granite ridges fall off sharply over a distance of ~ 1 km to an elevation of ~1300 m. Beyond this there is a slightly more gradual decline through the highly dissected upper reaches of the Gaub and Kuiseb rivers to the edge of the coastal plain at ~ 1000 m elevation. This whole area is highly dissected and the seaward edge of the Gamsberg consists of steep (~30°) bedrock ridges separated by chasms up to 200 m deep. These create a headland/embayment planform to the caprock edge visible in Figure 4.11. The ridges appear to be influenced by a steeply dipping foliated structure in the basement granite and large sheet faces are exposed on the northern side of them. The eastern side of the mountain has a more gradual topography sloping down to the inland plateau surface about 450 m below. This side is also characterised by ridges but they are less steep and less sharply defined.

The quartz arenite caprock on the Gamsberg (commonly known as Gamsberg Quartzite) covers an area of approximately 3 km^2 while on the Klein Gamsberg it is only a few thousand m^2. The highest point is on the south-western most part of the caprock and there is a very gradual (<1°) slope towards the north. The Gamsberg surface is remarkably smooth and local surface relief is everywhere <1m. The surface is patchily covered by cap rock debris which increases in size towards the edges. In the central region, ~15 m away from the edge, the surface is partially covered by sand, silt and quartz pebbles. There is some limited grass and shrub cover. The edge of the caprock and the cliff face are well defined and sharp on the western side. Here, there is no overall gradient towards the edge and the quartzite caprock forms ~25 m high, near-vertical cliffs (Fig. 4.12), although the top of these cliffs are slightly rounded. The contact of the quartz arenite and the underlying basement is visible along most the western edge and forms a sharp break in slope. There are no signs that the caprock is being actively undercut except for one small (~ 5 m wide), inaccessible cave. There is also no evidence that the caprock is retreating faster then the

granite ridges as there are no horizontal upper sections of the granite ridges. In places, the slope below the caprock is covered in quartzite talus with angular rock fragments up to 1 m across. Talus accumulates in the gullies between ridges. On the eastern side, the caprock is much more degraded and forms a stepped, gradual transition from the surface to the underlying granite (Fig. 4.13). The rock contact is not visible because it is usually covered by talus and vegetation. The caprock forms a continuous scarp but occasional gullies ~ 1-2 m wide have incised and broken up the smooth edge. During storm events water from the surface is channelled down these gullies (T. Neckle, *pers. com.*).

Figure 4.10: The Gamsberg. View from the coastal plain towards the east. Klein Gamsberg is visible to the left in the background.

There are several denudational processes that appear to be operating at the Gamsberg. On the granite ridges, granular disintegration and sheeting from <5 mm up to 1 m thick is occurring. Sheeting is more evident on the western side and appears to take advantage of large, exposed foliated structures in the granite. On the eastern side vegetation is more prolific and large sheets of rock are rare. The quartzite cap rock appears to be retreating as well as downwearing by a combination of processes. Cracking and mass movement in the form of slumping and rock falls

seem to be occurring around the edge of the caprock. Three large cracks, ~15 m long were observed 1-3m from the edge in three separate locations on the western and south-east edges. Blocks of smaller dimensions that had slumped and broken away from the main caprock were evident at 6 locations. Quartzite talus trails below the caprock suggest that rock falls of various dimensions occur all around the caprock. The caprock face and edge of the summit surface have been broken up *in situ* into angular blocks. These range in size from < 0.1 m to ~ 0.7 m in diameter. Salt weathering, pressure release mechanisms, the influence of bedding within the quartzite and even frost shattering could all enhance this process. Small-scale removal of thin quartzite slivers is occurring on fresh quartzite as well as the weathering out of gypsum crystals to produce a pitted effect on the surface of some boulders (Wittig, 1976).

Geological maps of the Gamsberg region are not available at a scale larger than 1:1,000 000 but the geology of the region has been described in detail by Schalk (1983). The Gamsberg consists of a residual protrusion of a large, medium-grained, red granite intrusion, approximately 1100 Ma old, unconformably capped by a layer of red-brown quartz arenite of aeolian origin. A smaller outcrop of the quartz arenite caps Klein Gamsberg but there are no other examples of the same rock. Other, even older (>1800 Ma) basement rocks in the region include a succession of quartzites, conglomerates, slate and basic lavas that are exposed in the highly dissected upper portion of the Gaub drainage basin to the south and south west of the Gamsberg. Micaschist, gneiss, marble, granite and quartzite of the Damara Sequence (~600 Ma BP) is currently exposed, showing signs of extensive denudation, over most of central and northern Namibia and it surrounds the Gamsberg Granite region to the west, north and east. The Damara Orogen is part of the Pan-African network of ancient orogenic belts and the area directly to the north of the Gamsberg represents a triple junction of two branches of the Damara and the southern Gariep orogen (Miller, 1983). Foliation of the Gamsberg Granite lies parallel and appears to be related to the main south-west trending structure of the Damara Orogen. The quartz arenite caprock on the Gamsberg (Gamsberg Quartzite) is the youngest unit in the region except for surfical Cenozoic deposits which are largely confined to the coastal plain below the escarpment and on the plateau much further inland to the east.

Figure 4.11: (Overleaf.) Aerial photo of the Gamsberg showing the locations of sampling sites. The contrast in the morphology of the eastern and western sides, and the relative position of Klein Gamsberg can also be seen.

N
KLEIN
G
14
15
GAMSBERG
1204

Figure 4.12: The western (seaward) side of the Gamsberg showing the remarkably smooth summit surface, clearly defined caprock cliff face and talus accumulations on the underlying granite slopes. The dissected, steeply dipping metamorphic rocks of the Damara Orogen are visible to the north in the background.

Figure 4.13: View north of Klein Gamsberg from the eastern (inland) edge of the Gamsberg. Note the highly degraded nature of the caprock cliff edge on this side compared to Fig. 4.12.

The Gamsberg Quartzite caprock is ~25 m thick. It consists of fine, well sorted and rounded, highly compact quartz grains with a little feldspar and chert (de Waal, 1966). Secondary silification is evident and has no doubt contributed to its evident strength. A basal red-brown, ~1 m thick section of the quartzite includes small clasts of the underlying bedrock (Schalk, 1983). The overlying quartzite is paler and show cross bedding indicative of aeolian deposition by a westerly wind (Schalk, 1983). Near the top the quartzite becomes coarser grained and fluvial cross bedding and asymmetric ripple marks are developed (de Waal, 1966). In places there is evidence for an upper layer of red-brown quartzite (Schalk, 1983).

There are three types of fissures (up to 10 cm wide) developed in the granite and quartzite which are all run in a N-S direction (Wittig, 1976); those which have formed solely in the granite and are filled with granite debris, those which have formed in the granite and are filled with basal red quartzite and those which have formed through the granite and overlying red and pale quartzites and were filled with red-brown quartzite from above. Wittig (1976) suggests that the most likely cause of these fissures is severe earthquakes resulting from crustal extension during continental rifting in the Cretaceous.

The age of the Gamsberg Quartzite is uncertain mainly because no fossils have been found in it on which to base a correlation. Although unimportant for denudation rates estimated from the build up of cosmogenic isotopes over a few million years, the stratigraphic significance of the Gamsberg Quartzite is very important in terms of the timing and extent of sedimentation and denudation in the escarpment region just prior to and during margin formation. Debate has surrounded two very different classifications. Realising the influence of horizontal strata in the formation of the Gamsberg, Dixey (1938) was the first to suggest that the caprock could be either of Nama (Cambrian) or Karroo (Carboniferous to Triassic) age, both of which exhibit flat lying or shallowly dipping sedimentary units elsewhere in southern Africa. Du Toit (1954) suggested that the Gamsberg caprock was in fact made of the hard basal Kuibis formation of the Nama System which lies unconformably on older crystalline basement rocks throughout south and central Namibia. The Kuibis Quartzites are siliceous and often cross bedded, weathering buff or brown, though typically bluish when fresh (Du Toit, 1954). Presumably following du Toit's (1954) description, Wellington (1955) also reported on the Gamsberg as an impressive 'tafelkop' feature where a basal fragment of the Nama system unconformably overlies granite. De Waal (1966) thought that this interpretation was incorrect mainly because the Gamsberg Quartzite was obviously of aeolian origin whereas the Kuibis beds were, "ill-sorted, psephitic quartzites, definitely deposited by water" (de Waal, 1966, p. 196). Sandstones and quartzites of aeolian origin and of upper Karroo, Triassic/early Jurassic age are relatively common throughout

southern Africa. The Clarens Sandstone Formation (formally Cave Sandstone) in South Africa, the Etjo Sandstone Formation in northern Namibia, the Kaokoveld Sandstone also in northern Namibia and sandstone cappings near Keetmanshoop (south-central Namibia) are all lithologically similar indicating a period of extensive aridity and dune development throughout the upper Triassic to the lower Cretaceous (Gevers, 1937; Martin, 1982). Aeolian sandstone units of a similar age have also been found in the Paraná Basin of South America which was immediately adjacent to Namibia prior to continental rifting. The Gamsberg Quartzite is now generally stratigraphically classified as Etjo Sandstone (de Waal, 1966, Martin, 1982; Schalk, 1983; Miller and Schalk, 1980: South West Africa Geology Map, 1:1,000,000) but some uncertainty remains (Wittig, 1976; R. Brown, *pers. com.*).

Apatite fission track evidence from granite samples in the Gamsberg/Gaub area indicate depths of denudation in the late Cretaceous of 2.5-3.5 km (Brown, 1992). A basal Nama quartzite is much further down the stratigraphic column than an upper Karroo sandstone and although thickness vary enormously and a full depositional sequence is not necessarily deposited everywhere, it is easier to explain the large depths of denudation indicated by fission track analysis if the caprock is older. If the caprock is young, then the large depths of denudation have to be explained by removal of Etendeka lavas, the only significant lithological unit that is younger than the latest Karoo unit. However, lavas this thick would be exceptional and there is no other evidence for lava having covered this area.

4.6.2 Present and Past Climates

The Great Escarpment of Namibia is at the western edge of a transitional zone between two contrasting climatic regimes of aridity to the west and humidity/summer rainfall in the east (Gevers, 1936; Lancaster *et al.,* 1984, Stokes *et al.,* 1997). To the west of the Gamsberg, on the coastal plain, is the central Namib Desert. There is a steep climatic gradient over a distance of ~150-200 km from hyper-aridity along the coast to arid/semi-arid conditions at the foot of the escarpment (section 5.2.3; Lancaster *et al.*, 1984). Winds in the coastal plain are predominantly from the west and there is very limited rainfall. A climatic gradient continues up and over the escarpment into a summer rainfall region over central and eastern southern Africa. East winds from the Indian Ocean create much wetter conditions over south-eastern Africa and the effects of these winds are occasionally felt as far west as the Gamsberg. Mean annual rainfall in the vicinity of the Gamsberg is ~150 mm a^{-1}, although this value is subject to high annual fluctuations depending on the extent of the influence of east winds (Gevers, 1936; Lancaster *et al.,* 1984). Although cold over the plateau these winds are warm by the time they reach the

coastal plain. Mean annual temperature in the central-eastern region of the coastal plain at Ganab is ~21°C with only a small mean annual range (Lancaster *et al.,* 1984). Temperature fluctuates more on the plateau than on the coastal plain, and although data are lacking, the interior uplands can get "excessively hot" (Gevers, 1936, p. 63). Temperatures on the escarpment and plateau are generally cold at night, often dropping below zero from April to October when frost is a common occurrence (Gevers, 1936). Snow is rare but the interior uplands of central Namibia, including the Gamsberg, have received snow at least once in the last five years.

There is little information on past climates for the escarpment region of Namibia. However, a large body of evidence has been collected about palaeoenvironments in the coastal plain (section 5.2.4) and more limited data area available for the Kalahari Basin. Evidence for fluctuating periods of fluvial deposition and erosion throughout the Quaternary have been collected for several westward flowing drainage basins including the Kuiseb and Gaub which drain the Gamsberg area of the escarpment (Ward *et al.,* 1983). Although the depositional environments of these are now generally considered to reflect prolonged aridity in the coastal plain, the story for the escarpment and interior highlands is less clear (Lancaster, 1984a; Ward, 1987; Wilkinson, 1990). Inferred increases in discharge for westward flowing rivers draining the escarpment and interior highlands indicate that rainfall has fluctuated in these highland regions. The timing and extent of climatic fluctuations, however, are poorly constrained. During glacial periods, it is generally considered that aridity was at a peak and desert systems commonly expanded. In the south-western Kalahari, it has recently been shown that dune activity has been more sustained than in the north-eastern region since the last interglacial but evidence for more humid conditions and reduced dune activity has been found for three periods close to the end of, or post, the last mid glacial at 22-16 ka, 6-10 ka and ~2 ka BP for an area inland of the Great Escarpment in southern Namibia (Stokes *et al.,* 1997). It has been inferred that increases in moisture in the western portion of the Kalahari are a function of changes in the summer rainfall gradient across central and eastern southern Africa which are in turn related to sea-surface temperature in the south eastern Atlantic ocean. Therefore it is likely that the climate at the Gamsberg has fluctuated to some extent over the Quaternary period.

4.7 Sampling Strategy and Sites

Samples were collected from the Gamsberg in order to assess denudation rates of the three principal topographic elements, namely the quartz arenite caprock summit, the caprock cliff face and the granite ridges extending from the base of the caprock. Samples were selected that were thought to be as representative as possible of these three elements. Characterising the rate of denudation on each of the three elements provides an overall insight and quantification of the rate of evolution of the Gamsberg that should also apply to the very similar adjacent, Klein Gamsberg. An understanding of the rate of evolution of the Gamsberg should also be able to place constraints on the rate of retreat of the Great Escarpment in central Namibia over a period of at least ~10^5 a. This should be particularly true of the rate of denudation on the granite ridges of which similar features can be found in many other locations along the Great Escarpment in central Namibia, assuming that the caprock does not significantly retard retreat of the underlying ridges.

38 samples were collected from the Gamsberg in two field seasons. 14 of these, two from the first season and 12 from the second, were analysed for cosmogenic ^{10}Be and ^{26}Al. The division of analysed samples between the three topographic elements was as follows: three (10/95, 12/95 and 14/94) from the Gamsberg summit surface, five (# 7/95, 8/95, 9/95, 11/95 and 15/94) from the caprock cliff face and six (# 1-6/95) from two separate granite ridges (ridge profiles 1 and 2). The locations and names/numbers of the samples and sites are shown in Figure 4.11 and in Figure 4.14 schematically in cross section. Sample and field data have been provided in Table 4.2.

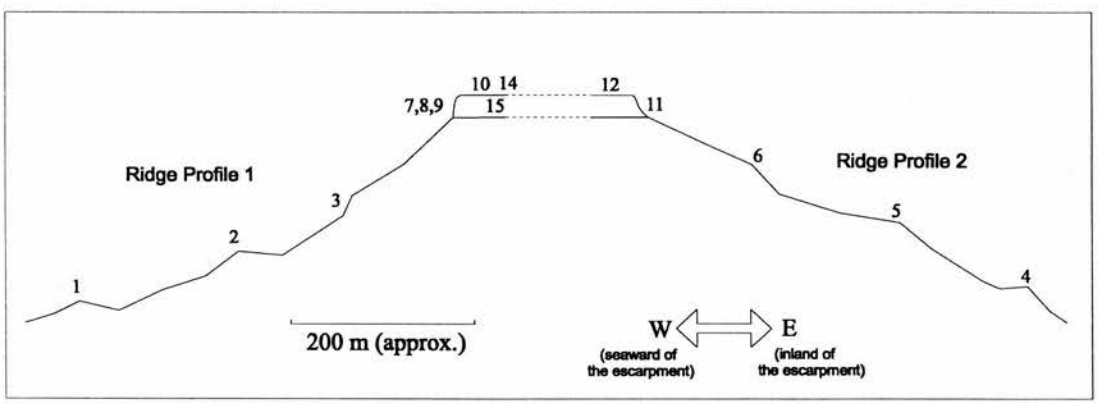

Figure 4.14: Schematic cross section of the Gamsberg showing the location of analysed samples.

All samples were collected in keeping with the overall field methodology described in section 3.2. Every sample was from a bedrock exposure with an apparently simple exposure history and was no more than 20 mm thick. Samples 1/95, 2/95 and 3/95 were taken in a profile along the top of a granite ridge extending from the south west point of the Gamsberg (ridge profile 1, Figure 4.14 and 4.15). Sample 1/95 was taken from a site at the end of the sampling profile, 217 m below the top of the caprock and ~500 m horizontal distance away from it. The sample was from a large, gently sloping, bedrock outcrop on a 'ridge peak'. Sample 2/95 was from a similar setting, ~200 m from sample site 1. Sample 3/95 was taken from a quartz vein exposed on the front of a ~10 m high, sloping step on the ridge about 150 m horizontal distance from the caprock cliff. Above sampling site 3/95 the ridge slope was covered by patches of talus evidently from the caprock cliff and although there were some bedrock granite exposures, it seemed likely that these may have been prone to temporary burial by rock debris. There were no significant talus accumulations below site 3/95. Therefore sample 3/95 was the closest sample to the caprock selected for analysis along ridge profile 1.

Samples 4/95, 5/95 and 6/95 were also collected along the top of a granite ridge extending from the caprock summit but from the north-eastern side of the Gamsberg (ridge profile 2). This ridge was more extensively covered by talus, debris and vegetation than ridge profile 1 but there were numerous bedrock exposures. All samples were taken from the top of small peaks along the length of the ridge. Sample 4/95 was ~ 465 m horizontal distance from the caprock face and ~220 m below it (Fig. 4.16). Sample 5 was ~ 150 m up the ridge (horizontal distance) from sample 4 and 215 m from sample 6. Sample 6 was ~85 m below the caprock cliff where talus accumulations were insignificant

All caprock cliff face samples were taken from the bottom 2-5 m section of exposed caprock except sample 15/95 which was sampled from ~1.5 m below the top of the cliff. All samples were from surfaces with slopes ranging from 65° to 88° (Table 4.2). Samples 7/95 and 8/95 were collected from the south-western side of the Gamsberg where the caprock cliff is most clearly defined (Fig. 4.18). They were taken from large, relatively smooth, quartzite faces. Sample 9 was taken from the front of an apparently slumped section of the caprock at the top of ridge profile 1. The slumped section was ~20 m wide and appeared to have become detached and fallen in one piece approximately 5 m with very slight upward rotation. This upward rotation would not have altered the exposure geometry of the site significantly The contact between the caprock proper and the slumped section was difficult to distinguish and obscured by quartzite debris up to 0.7 mm in diameter. The front of the slumped section did not appear different from the intact caprock face to the left or right of it but provided a better sampling surface. Sample

15/94 was taken from the northern side, almost directly below sample 14/94. Sample 11/95 was from the eastern side and was located at the top of ridge profile 2. Here the caprock face was much more degraded than at sampling sites 7-9 or 14. Along the eastern side further suitable sampling locations were difficult to find and no more samples were analysed from this side of the Gamsberg.

Samples 14/94, 10/95 and 12/95 were all taken from the flat summit surface of the Gamsberg at the locations shown in Figure 4.11. Sample 14/04 was taken ~ 10 m in from the edge on the northern side of the Gamsberg. Sample 10/95 was taken ~ 5 m from the edge above ridge profile 1 (Fig. 4.18). Sample 12/95 was taken from ~3 m from the edge on the south-western side of the mountain. Summit samples were taken from relatively near the edge because suitable bedrock exposures could not be found nearer the centre. However, there was no apparent reason why the overall rate of bedrock lowering would vary significantly across the flat summit surface

Figure 4.15: View of ridge profile 1 from the summit of the Gamsberg looking south. The orange band on the horizon in the background is the northern limit of the main Namib Sand Sea. In the foreground foliation of the granite can be seen as well as talus accumulations on the upper portion of the granite slope extending from the base of the quartz arenite caprock.

Figure 4.16: View looking south from a typical sampling site on ridge profile 2 on the north-western side of the Gamsberg. Background view is the same as in Figure 4.15. Note the more extensive vegetation and debris cover on this side of the mountain.

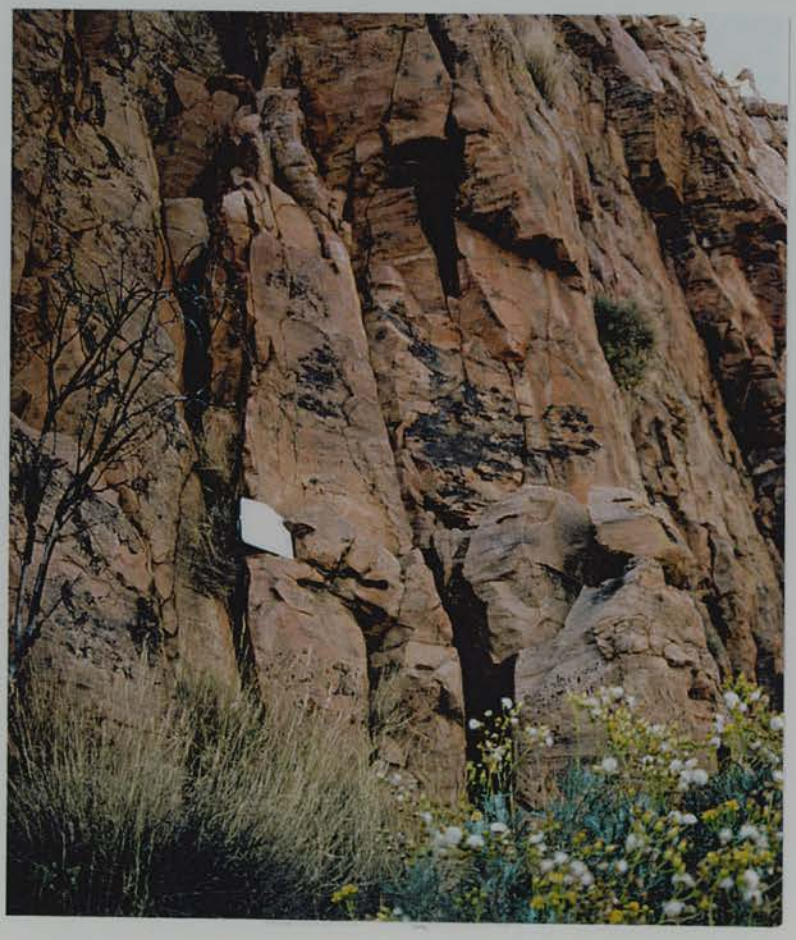

Figure 4.17: Sample 8/95 on the caprock face on the south-western side of the Gamsberg.

Table 4.2: Sample and field data for Namibian Gamsberg samples.

Sample Number	Location Long. & Lat.	Altitude (m)	Lithology	Surface Slope (°)	*Exposure Geometry
Ridge Profile 1					
1/95	16° 12' 35" 23° 20' 56"	2130	Gamsberg Granite	37°	partial shielding
2/95	16° 12' 40" 23° 21' 01"	2183	Gamsberg Granite	47°	partial shielding
3/95	16° 12' 42" 23° 21' 02"	2246	Quartz Vein	33°	partial shielding
Ridge Profile 2					
4/95	16° 12' 12" 23° 20' 52"	2119	Gamsberg Granite	0°	partial shielding
5/95	16° 14' 13" 23° 20' 49"	2191	Gamsberg Granite	0°	partial shielding
6/95	16° 14' 10" 23° 20' 40"	2293	Gamsberg Granite	0°	partial shielding
Caprock Cliff Face					
15/94	16° 14' - 23° 20' -	2327	Gamsberg Quartzite	80°	partial shielding
7/95	16° 12' 52" 23° 20' 58"	2318	Gamsberg Quartzite	88°	partial shielding
8/95	16° 12' 53" 23° 21' 01"	2321	Gamsberg Quartzite	65°	partial shielding
9/95	16° 12' 49" 23° 21' 04	2325	Gamsberg Quartzite	70°	partial shielding
11/95	16° 14' 10" 23° 20' 38"	2330	Gamsberg Quartzite	80°	partial shielding
Gamsberg Summit					
14/94	16° 14' - 23° 20' -	2343	Gamsberg Quartzite	0°	full exposure
10/95	16° 12' 52" 23° 21' 02"	2346	Gamsberg Quartzite	0°	full exposure
12/95	16° 13' 26" 23° 20' 57"	2339	Gamsberg Quartzite	0°	full exposure

*For full exposure geometry see Appendix A.

Figure 4.18: Sample 10/95 in situ on the summit of the Gamsberg. Note the pitted and uneven nature of bedrock exposed on the summit and the degraded top edge of the caprock cliff.

4.8 Analysis, Results and Interpretation

Samples 14/94 and 15/94 were prepared for ^{10}Be analysis at Lamont-Doherty Earth Observatory of Columbia University under the supervision of M. Seidl. The remaining 12 samples were prepared at the University of Edinburgh in two laboratory batches for ^{10}Be and ^{26}Al analysis (Batches 3 and 5: Appendix A). All the samples were prepared according to the final methodology described in Chapter 3 except samples 14/94 and 15/94 which were subject to a similar chemical protocol involving an additional acetylacetone extraction but no initial precipitation (section 3.3.2). Total ^{27}Al measurements on sample aliquots were performed by doubly coupled plasma mass spectrometry (DCPMS) for Batch 3 (2/95, 3/95, 6/95, 8/95, 10/95 and 11/95) and by inductively coupled plasma mass spectrometry (ICPMS) for Batch 5 (1/95, 4/95, 5/95, 7/95, 9/95, 10R/95 and 12/95). All ^{10}Be/^{9}Be and ^{26}Al/^{27}Al ratios were measured by accelerator mass spectrometry (AMS) at the Center for Accelerator Mass Spectrometry, Lawrence Livermore National Laboratory (LLNL).

Corrected production rates for each sampling site at the Gamsberg are shown in Table 4.3. Basic production rates of 6 (^{10}Be) and 36.8 (^{27}Al) atoms g^{-1} SiO_2 a^{-1} for sea level and high latitude (>60°) from Nishiizumi *et al.* (1989a) were used. There have been recent attempts to refine these estimates (e.g. Clark *et al.*, 1995; Nishiizumi *et al.*, 1996) but the original values have been retained because recent applications have continued to use them and there appears to be no consensus as yet for a shift by researchers in the cosmogenic field. Production rates were initially scaled for the effects of altitude and latitude according to the nuclear disintegration rates of Lal (1991) (section 2.2.7). Production rates were also corrected for the effects of the dip of the sampled surface and topographic shielding based on the exposure geometry of the site collected in the field (section 2.2.6; Appendix A). The steep surface angles of the cliff face samples mean, in many cases, there is a significant reduction in the production rate. It was assumed that the exposure geometry of the site has not changed and that the geographic latitude has equalled the average geomagnetic latitude of the site integrated over the accumulation time of the cosmogenic isotopes in the samples (Brown *et al.*, 1991; Bierman and Turner, 1995). A 20% error has been included in the final production rate estimates and propagated through denudation rate calculations to account for current levels of uncertainty (Gosse *et al.*, 1996).

Table 4.3: Production rates of ^{10}Be and ^{26}Al for Gamsberg sampling sites corrected for the effects of topographic shielding and dip of sampled surface, (atoms g^{-1} SiO_2 a^{-1})

Sample Number	Scaled Production Rate		Correction Factor for Partial Shielding	Corrected Production Rate Including 20% Error	
	^{10}Be	^{26}Al		^{10}Be	^{26}Al
Ridge Profile 1					
1/95	19.03	115.34	0.981	18.67 ± 3.7	113.15 ± 22.6
2/95	19.67	119.23	0.946	18.61 ± 3.7	112.79 ± 22.6
3/95	20.44	123.90	0.951	19.44 ± 3.9	117.83 ± 23.6
Ridge Profile 2					
4/95	18.89	114.54	0.985	18.61 ± 3.7	112.86 ± 22.6
5/95	19.77	119.82	0.998	19.73 ± 3.9	119.58 ± 23.9
6/95	21.06	127.63	0.995	20.96 ± 4.2	127.00 ± 25.4
Caprock Cliff Face					
15/94	21.51	130.31	0.601	12.93 ± 2.6	78.32 ± 15.7
7/95	21.39	129.60	0.578	12.36 ± 2.5	74.90 ± 14.9
8/95	21.43	129.84	0.826	17.70 ± 3.5	107.25 ± 21.5
9/95	21.48	130.15	0.836	17.96 ± 3.6	108.85 ± 21.8
11/95	21.57	130.71	0.766	16.52 ± 3.3	100.13 ± 20
Gamsberg Summit					
14/94	21.72	131.59	1	21.72 ± 4.3	131.84 ± 26.3
10/95	21.76	131.84	1	21.76 ± 4.4	131.84 ± 26.4
12/95	21.66	131.27	1	21.66 ± 4.3	131.27 ± 26.3

Sample masses, results of DCPMS and ICPMS analysis of the total ^{27}Al content of sample aliquots, as well as AMS isotopic ratios and calculated ^{10}Be and ^{26}Al concentrations are shown in Table 4.4. Total Al content was lowest in the quartz vein sample (3/95) and in general was <100 ppm for granite samples and >100 ppm for quartz arenite samples. Sample 8/95 had an unusually high Al content of 322.57 ± 16.1 ppm which may have been caused by some residual feldspar in the quartz separate. Isotopic ratios have been corrected for background from process blanks and normalised to standard samples prepared at LLNL (KNSTD3770, $^{10}Be/^{9}Be = 3.77 \times 10^{-12}$ and KNST5000, $^{26}Al/^{27}Al = 5.00 \times 10^{-12}$). A correction for the $2\pm1 \times 10^{-14}$ ratio of the Be carrier solution used in making the LLNL standards was also applied. The process blank ratios were $7.57 \times 10^{-15} \pm 2.0 \times 10^{-15}$ and $1.33 \times 10^{-14} \pm 3.4 \times 10^{-15}$ for Be in laboratory batches 3 and 5 respectively. For Al in batches 3 and 5 they were $1.43 \times 10^{-14} \pm 5.5 \times 10^{-15}$ and $6.9 \times 10^{-15} \pm 6.9 \times 10^{-15}$ respectively. Spurious counts due to boron contamination were all <1% except for the blank samples which were 28% and 15% in batches 3 and 5 respectively. Errors in Table 4.4. have all been quoted at 1σ and include machine measurement error for Al concentrations (5%) and AMS ratios (~3%) and both these uncertainties have been quadratically propagated in the calculations of the concentrations (N) of cosmogenic ^{26}Al. Similarly, ^{10}Be concentrations include AMS error and a 2% uncertainty in the amount of ^{9}Be carrier added. The reproducibility of measured concentrations of cosmogenic nuclides for sampling site 10 from the samples 10/95 and 10R/95 which were run in separate laboratory batches is excellent for ^{10}Be (within 2 %) and within 1σ error limits for ^{26}Al. Although reproducibility is an important component of the uncertainty of the results, an error value has not been included in the subsequent calculations because only one sample was duplicated and other sources of error, for example in the production rate, are large. Typical reproducibility of other data sets (e.g. Ivy-Ochs, 1996) is ~4-8%.

Table 4.4. ^{10}Be and ^{26}Al isotopic data for Gamsberg samples.

Sample Number	Sample Mass (g)	Al content (ppm)	Background Corrected $^{10}Be/^{9}Be$ AMS Ratio	Background Corrected $^{26}Al/^{27}Al$ AMS Ratio	^{10}Be Concentration (N) (10^6 at. g^{-1} SiO_2)	^{26}Al Concentration (N) (10^6 at. g^{-1} SiO_2)
Ridge Profile 1						
1/95	42.0575	73.49 ± 3.7	$1.65 \times 10^{-12} \pm 3.3 \times 10^{-14}$	$5.15 \times 10^{-12} \pm 1.5 \times 10^{-13}$	1.46 ± 0.04	8.43 ± 0.49
2/95	45.02106	71.82 ± 3.6	$8.4 \times 10^{-13} \pm 2.2 \times 10^{-14}$	$2.21.x 10^{-12} \pm 8.4 \times 10^{-14}$	0.61 ± 0.02	3.52 ± 0.22
3/95	45.00417	32.64 ± 1.6	$1.45 \times 10^{-12} \pm 4.0 \times 10^{-14}$	$9.0 \times 10^{-12} \pm 2.4 \times 10^{-13}$	1.10 ± 0.04	6.53 ± 0.37
Ridge Profile 2						
4/95	42.34074	83.28 ± 4.2	$4.63 \times 10^{-12} \pm 9.7 \times 10^{-14}$	$1.25 \times 10^{-11} \pm 3.8 \times 10^{-13}$	4.01 ± 0.12	23.19 ± 1.36
5/95	41.43633	65.22 ± 3.3	$2.42 \times 10^{-12} \pm 4.9 \times 10^{-14}$	$8.58 \times 10^{-12} \pm 2.6 \times 10^{-13}$	2.14 ± 0.06	12.46 ± 0.73
6/95	44.59402	80.74 ± 4.0	$3.29 \times 10^{-12} \pm 6.8 \times 10^{-14}$	$7.86 \times 10^{-12} \pm 2.10 \times 10^{-13}$	2.51 ± 0.07	14.10 ± 0.80
Caprock Cliff Face						
15/94	50.02	-	$1.75 \times 10^{-12} \pm 4.5 \times 10^{-14}$	-	1.17 ± 0.04	-
7/95	32.13122	108.60 ± 5.4	$5.1 \times 10^{-14} \pm 5.7 \times 10^{-15}$	$1.53 \times 10^{-12} \pm 1.9 \times 10^{-14}$	0.06 ± 0.007	0.37 ± 0.05
8/95	35.00454	322.57 ± 16.1	$1.26 \times 10^{-12} \pm 4.30 \times 10^{-14}$	$1.0 \times 10^{-12} \pm 3.2 \times 10^{-14}$	1.22 ± 0.05	7.18 ± 0.43
9/95	38.99972	148.7 ± 7.4	$1.29 \times 10^{-12} \pm 2.8 \times 10^{-14}$	$2.23 \times 10^{-12} \pm 7 \times 10^{-14}$	1.26 ± 0.04	7.39 ± 0.44
11/95	35.03961	146.42 ± 7.3	$5.57 \times 10^{-13} \pm 2.10 \times 10^{-14}$	$9.27 \times 10^{-13} \pm 3.10 \times 10^{-14}$	0.54 ± 0.02	3.02 ± 0.18
Gamsberg Summit						
14/94	50. 03	-	$2.53 \times 10^{-11} \pm 4.7 \times 10^{-13}$	-	16.88 ± 0.46	-
10/95	30.01181	163.82 ± 8.2	$1.69 \times 10^{-11} \pm 5.70 \times 10^{-13}$	$2.51 \times 10^{-11} \pm 6.8 \times 10^{-13}$	19.13 ± 0.75	91.34 ± 5.20
10R/95	14.96368	173.26 ± 8.7	$8.03 \times 10^{-12} \pm 2.6 \times 10^{-13}$	$2.18 \times 10^{-11} \pm 7.10 \times 10^{-14}$	19.40 ± 0.74	83.88 ± 4.20
12/95	25.91193	95.83 ± 4.8	$1.3 \times 10^{-14} \pm 3.4 \times 10^{-15}$	$3.5 \times 10^{-11} \pm 6.5 \times 10^{-13}$	16.14 ± 0.43	74.79 ± 3.99

Denudation rates for the Gamsberg samples were calculated using the steady-state erosion model of Lal (1991). Rates have been calculated based on the measured concentrations of cosmogenic ^{10}Be and ^{26}Al assuming secular equilibrium had been reached by both isotopes and that denudation processes operating at every site were steady-state according to the specific definition inherent to the cosmogenic technique (section 2.4.3) whereby:

$$\varepsilon = \frac{\Lambda}{\rho}\left(\frac{P}{N} - \lambda\right) \qquad [4.1]$$

where N is the concentration of the cosmogenic isotope (atoms g^{-1} SiO_2), P is the production rate (atoms g^{-1} SiO_2 a^{-1}), λ is the decay constant of the radionuclide (a^{-1}), Λ is the cosmic ray attenuation coefficient in quartz (150 g cm^{-2}), ρ is the rock density (2.7 g cm^{-3}) and ε is the steady-state denudation rate (cm a^{-1}) (Lal, 1991; Brown *et al.*, 1992). Calculated denudation rates are shown in Table 4.5 and in Fig. 4.19. Errors include 2 σ uncertainty on N, as well as ±20 % on P. The data are shown on an erosion-island graph in Fig. 4.20 (excluding samples 14/94 and 15/94 in which only ^{10}Be concentrations was measured). The erosion-island graph acts as a test for the two assumptions inherent in equation 4.1, namely, that the isotopes have reached secular equilibrium and that they have been subject to steady-state erosion with no phases of burial (section 2.4.4). Interpretation of the data is presented below.

Table 4.5. Denudation rate estimates for Gamsberg samples.

Sample Number	$^{26}Al/^{10}Be$	^{10}Be Denudation Rate (ε) (m Ma^{-1})	^{26}Al Denudation Rate (ε) (m Ma^{-1})
Ridge Profile 1			
1/95	5.78 ± 0.74	6.86 ± 1.43	6.90 ± 1.59
2/95	5.79 ± 0.83	16.76 ± 3.54	17.27 ± 4.08
3/95	5.95 ± 0.74	9.59 ± 2.02	9.49 ± 2.18
Ridge Profile 2			
4/95	5.79 ± 0.76	2.32 ± 0.48	2.15 ± 0.50
5/95	5.8. ± 0.76	4.85 ± 1.01	4.78 ± 1.11
6/95	5.63 ± 0.71	4.39 ± 0.91	4.46 ± 1.03
Caprock Cliff Face			
15/94	-	5.89 ± 1.24	-
7/95	6.39 ± 2.24	118.18 ± 35.78	111.73 ± 37.30
8/95	5.68 ± 0.83	7.77 ± 1.67	7.76 ± 1.80
9/95	5.86 ± 0.77	7.65 ± 1.60	7.63 ± 1.77
11/95	5.59 ± 0.82	16.74 ± 3.64	17.90 ± 4.18
Gamsberg Summit			
14/94	-	0.45 ± 0.09	-
10/95	4.77 ± 0.66	0.38 ± 0.08	0.32 ± 0.07
10R/95	4.32 ± 0.54	0.37 ± 0.08	0.26 ± 0.06
12/95	4.63 ± 0.55	0.49 ± 0.10	0.42 ± 0.10

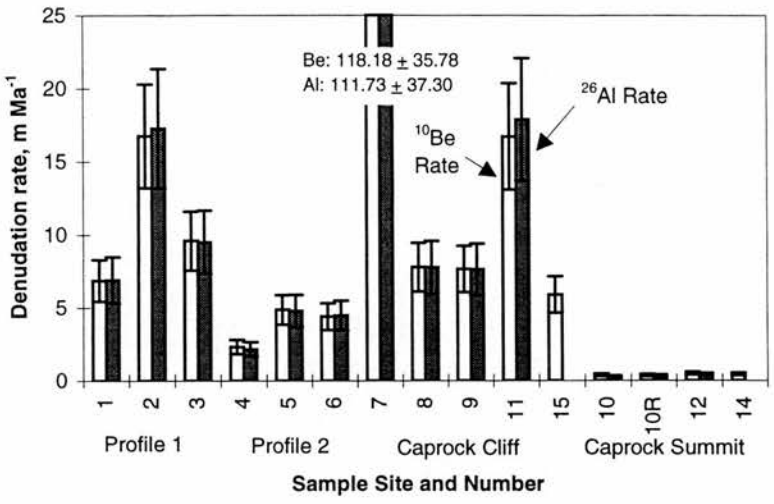

Figure 4.19: ^{10}Be and ^{26}Al denudation rates for Gamsberg samples. 2 σ error bars are shown.

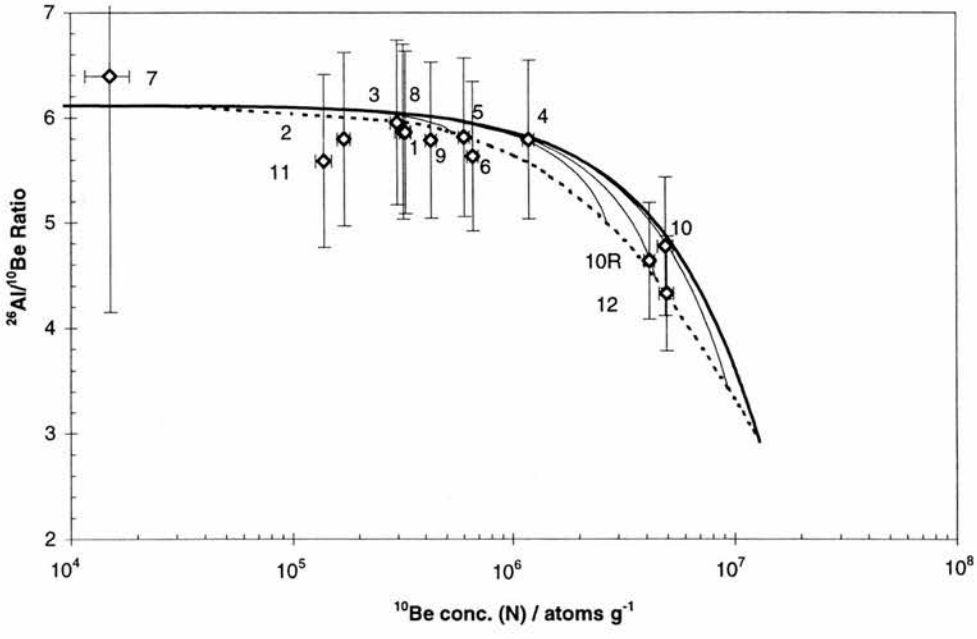

Figure 4.20: Erosion-island plot of $^{26}Al/^{10}Be$ against ^{10}Be for the Gamsberg samples. ^{10}Be concentrations have been adjusted to sea level and high latitude (>60°). Error bars include 2σ uncertainty in the concentrations of ^{26}Al and ^{10}Be. Samples that plot within the island support a model of simple, steady-state denudation; samples that plot on the dotted, lower limit of the erosion island are in secular equilibrium and samples plotting below the island indicate that the sampling site has been subject to some complexity in the exposure history. Samples that plot above the island contain "forbidden" ratios relative to ^{10}Be concentration and indicate possible analytical error or elevation changes for the sample (for further details see section 2.4.4).

The denudation rates shown in Table 4.5 and Figure 4.19 have been calculated assuming that both ^{10}Be and ^{26}Al have reached secular equilibrium (equation 4.1). Overall, the rates calculated from ^{10}Be and ^{26}Al concentrations in each sample show remarkable consistency. Within error, the locations of all the samples on the erosion-island graph support the assumption of secular equilibrium by plotting on the saturation concentration (dotted) line (Fig. 4.20). However, because the error bars are large, it could equally be true that the samples all plot within the erosion-island, thereby supporting steady-state denudation but suggesting that not enough time has passed for the samples to become saturated ($t<1/(\lambda+\rho\varepsilon/\Lambda)$ (Lal, 1991). Assuming this scenario, all the rates shown in Table 4.5 should be considered maxima. If the data are considered to plot below the saturation line, it is feasible that the samples have been subject to some complexity in their exposure history, possibly from phases of burial or detachment of rock layers of a thickness greater than the cosmic ray attenuation length of ~0.5 m (Small *et al.*, 1997). (Cosmic ray attenuation length = attenuation coefficient (150 g cm^{-2}) multiplied by the density of the rock (2.7 g cm^{-3})). If it is inferred that any of the samples plot on the zero erosion line (upper thick line of the erosion-island) the concentrations of ^{10}Be and ^{26}Al should be modelled in terms of an exposure event age rather than a denudation rate (section 2.4.2). The geomorphic setting and field observations of processes at each site can be used to distinguish between these possibilities and to assess the true significance of the calculated rates.

The data appear to fall into three distinct groups. The most obvious distinction, clearly visible in Figs 4.19 and 4.20, is between samples 10/95, (10R/95), 12/95 and 14/94 from the summit of the Gamsberg and all the other samples. Calculated rates for the summit are all <1 m Ma^{-1} and range from 0.26 ± 0.06 m Ma^{-1} (10R/95, ^{26}Al) to 0.49 ± 0.1 m Ma^{-1} (12/95, ^{10}Be). The bedrock surfaces from which the samples were taken (Fig. 4.18) showed evidence of weathering in the form of pitting, flaking and cracking and there is no evidence to suggest that these site have not been subject to denudation. The paired data for samples 10/95, 10R/95 and 12/95 all support the model of steady-state denudation (equation 4.1), and also could be interpreted as supporting the saturation concentration assumption of the model if they are assumed to plot on the dotted line in Fig. 4.20. Given the difficulty in proposing a geomorphic mechanism for complex exposure either in the form of burial or detachment of thick rock layers, it is reasonable to interpret the data from the summit as providing good estimates of the rate of summit denudation. The minimum amount of time that the isotopes take to become saturated subject to the calculated rates is >1 Ma for the Be rates and ~900 ka for the Al rates (section 2.4.3). On this basis, it is proposed that the summit of the Gamsberg has been lowering at an average rate of ~0.4 m Ma^{-1} for at least the last 1 Ma.

The second group of samples includes all the caprock cliff and ridge profile samples, excluding sample 7/95. These plot in a central cluster in Fig. 4.20. Although there appears to be little distinction between the average magnitude of the modelled rates calculated for the profiles and for the caprock cliff samples (Fig. 4.19), interpretation of the data will be dealt with separately because of the significant difference between the style and exposure geometry of the sampling sites (Table 4.2). Modelled rates for samples 1-3/95 on ridge profile 1 are generally higher than for samples 4-6/95 on ridge profile 2. An average rate for ridge profile 1 from both ^{10}Be and ^{26}Al for the three samples is 11.15 ± 2.6, whereas an average for ridge profile 2 is 3.83 ± 1. Although an explanation based on the relatively higher relief of the western side compared to the eastern side of the Gamsberg could potentially be offered, it is more likely to be a simple function of surface slope (Table 4.2). Whereas the lower rates for ridge profile 2 were all collected from horizontal surfaces (Fig. 4.16), samples from ridge profile 1 were all taken from angled surfaces. The highest ridge rates, from sample 2/95 (17.27 ± 1.59 m Ma^{-1}, ^{26}Al and 16.76 ± 3.54 m Ma^{-1}, ^{10}Be), are from the steepest angled surface of 47°.

For the granite ridge samples at the Gamsberg the denudational processes in the immediate vicinity of the sites appeared to involve only the detachment of rock layers <0.5 m thick. Also, the samples were, in general, taken from ridge peaks unlikely to have been covered by slope debris. Therefore it would seem reasonable to interpret the data for the ridges as supporting the assumptions of steady-state denudation and possibly secular equilibrium. However, bedrock exposures on the ridges are, in places, eroding through the detachment of granite slabs up to 1 m thick. These slabs appear to form rounded boulders which then either break up *in situ* or move down slope through the influence of gravity and maybe surface wash events. Given this style of denudation, it is possible that samples from the ridges have experienced some complexity in their exposure history, the evidence for which would have since been removed. Small *et al.* (1997) demonstrated that in the central section of the ^{26}Al/^{10}Be erosion-island plot, it can be difficult to distinguish between a model of complexity or simple exposure because the influence on the ratio of the nuclides would be small and tend to shift data to the left along the x-axis rather than below the erosion-island. Under these circumstances an average rate from a number of spatially distinct samples is likely to provide the best estimate of the true rate of denudation (Small *et al.*, 1997). For the granite ridges at the Gamsberg, an average rate of denudational lowering is ~7.5 m Ma^{-1}. On the basis of the time the isotopes take to attain secular equilibrium with this rate, the rate is assumed to have been active for at least 70 ka.

4.8.1 The Steady-State Denudation Model and Steeply Angled Surfaces.

The steady-state denudation model of Lal (1991) assumes that the sampled surface is horizontal and yields a modelled rate of vertical lowering. This is an important assumption because of the angular dependence of the incident flux of cosmic rays (section 2.2.6). Where tilted or angled surfaces are sampled, model parameters must be corrected for the effect this has on the incident flux. The energy of rays coming in vertically is much higher than rays hitting a sample from low angles. The energy of rays below angles of ~45° is almost insignificant compared to the incident flux from 45° to 90°. Therefore, surface production rate corrections are minimal for angled surfaces up to ~45° but once this angle is exceeded, correction become much more significant. This is evident if one compares the surface angle of samples (Table 4.2) and the exposure geometry corrections provided in Table 4.3. In addition to surface production, the depth dependence of cosmic rays is also a function of the angle of the assumed profile and is parameterised in Lal's model (Λ). The attenuation of cosmogenic nuclide production with depth normal to a surface is not the same for steeply dipping surfaces as it is for horizontal surfaces. To date, all empirically measured profiles in terrestrial rocks have been in vertical drill cores and the resultant reduction in production in depth has been closely linked to the absorption mean free path of neutrons in air (section 2.2.2). Because of the insensitivity of the cosmic ray flux below angles of ~45°, an attenuation length of 150 g cm^{-2} is generally applicable to samples on relatively gently dipping surfaces. The denudation model of Lal (1991), which assumes a horizontal surface and vertical depth dependence, can therefore be applied in most cases without severe limitations. However, as angles of sampled surfaces tend towards 90°, it would appear that the erosion model becomes less applicable because the assumption regarding depth dependence becomes more tenuous. To date, only exposure age estimates (as opposed to erosion rates) have been published for steeply dipping surfaces but this is not problematic since surface production rates can be adequately adjusted and exposure age determination does not make assumptions about production at depth (since it assumes zero denudation - section 2.4.2). Presently there are no publications which address the issue of angular dependence of attenuation or explain (or model) the relationship between the concentration of *in-situ* cosmogenic isotopes and denudation rates on steeply angled surfaces. In these situations the applicability of the existing denudation model appears questionable.

It is outside the scope of this thesis to consider the denudation model further. It is sufficient to appreciate that the model may not apply to steep surfaces (>45°) and that a limitation of the

cosmogenic technique in terms of modelling denudation in real geomorphic situations has been identified. Obviously, future work must address the applicability of the denudation model for cosmogenic isotope analysis to realise its full potential. At the time of writing, research on this issue was in progress but had not yet been published (J. Stone, *pers. com.*). From this discussion, it is apparent that the denudation rates calculated for the caprock cliff samples (Table 4.5) are likely to be in error and should be treated with caution. If is assumed that attenuation lengths are shorter on steeply angled surfaces then, using the current model (equation 4.1), the calculated denudation rates would also be reduced. As soon as new information becomes available, the concentrations will be able to provide useful estimates of the retreat of the caprock cliff face. It should be noted, however, that, as with the existing model, detachment of rock layers thicker than the attenuation length would invalidate any model that assumes steady-state denudation. This style of denudation on steep slopes, including those at the Gamsberg, is common, and should be addressed by any future modelling attempts.

At this stage, it is not possible to ascertain the relationship between the true rate of caprock cliff retreat and the rates for these sites shown in Table 4.5. However, given that there now exist reliable estimates of denudation for the caprock summit and the granite ridges some speculations can be made. If the profile of the Gamsberg remains constant through time, a caprock retreat rate can be calculated from an average horizontal retreat of the granite ridges. Moon and Selby (1983) proposed that through time, the form of slopes at four locations on the Great Escarpment, including the Gamsberg, adjusts to the mass strength of the rock and therefore parallel retreat only occurs where the overall mass strength is uniform. Although mass strength does vary within lithological units as a function of joint spacing, the overall simplicity of the stratigraphy at the Gamsberg suggests that an assumption of profile maintenance through time is reasonable. Furthermore, the overall similarity of the form of the Klein Gamsberg and the Gamsberg (Figs. 4.10 and 4.13) supports the assumption of an overall preservation of form through time. Assuming an average slope angle of ridge profile 1 of 35° and an average vertical lowering rate of the ridge of 10 m Ma^{-1}, then the horizontal retreat rate can be calculated using simple trigonometry and is ~15 m Ma^{-1}. If similar assumptions are made for ridge profile 2 with an average angle of 30° and a lowering rate of 4 m Ma^{-1}, the horizontal retreat rate is ~7 m Ma^{-1}. Interestingly, these values are not that different from those calculated here using the model of Lal (1991) (excluding sample 7/95).

Sample 7/95 suggests a very high denudation rate for one location along the western edge of the Gamsberg caprock. However, given the broad agreement between the concentrations of other

caprock samples and a style of denudation that may involve the detachment of thick blocks, it is likely that sample 7/95 reflects a recent exposure and that the isotopes have not yet reached secular equilibrium. This is supported by a $^{10}Be/^{26}Al$ value close to the production ratio of 6.1 which implies no erosion (Table 4.5, Fig. 4.20). Exposure ages for this site are 4.69 ka (^{10}Be) and 4.96 ka (^{26}Al). (The high error values for this sample reflect the low abundance of cosmogenic nuclides in the sample.)

4.9 Discussion

4.9.1 Denudation of the Gamsberg

Analysis of *in-situ* cosmogenic isotopes ^{10}Be and ^{26}Al at the Gamsberg has yielded modelled maximum rates of ~0.4 m Ma^{-1} for summit lowering and an average modelled rate of denudation for two granite ridges of ~7.5 m Ma^{-1}. These rates are necessarily integrated at least over the past 1 Ma and 70 ka respectively. Due to the similarity of all the granite ridges forming the flanking slopes of the Gamsberg, both in terms of form and evident active processes, average rates of denudation calculated for the two ridges are likely to be representative of all the ridges as a whole. Interpretation of concentrations of cosmogenic isotopes on the third morphological element of the Gamsberg, the caprock cliff face, has been precluded by the poor suitability of the steady-state erosion model for steeply angled surfaces. However, by implication, caprock cliff retreat is thought to be similar to granite ridge retreat, on the order of ~10 m Ma^{-1}, assuming maintenance of a constant slope profile over the caprock and down the granite ridges through time. These results represent the first direct assessment of denudation in the escarpment zone for any section of the Great Escarpment in Namibia over a time period of $\leq 10^6$ a.

The future of the Gamsberg and Klein Gamsberg can be predicted if assumptions are made about the continuation of the denudation rates measured here. If the rate of summit downwearing (~0.4 m Ma^{-1}) and the estimated rate of overall slope retreat (~10 m Ma^{-1}) were to characterise the future, the caprock on the Klein Gamsberg would disappear in ~10 Ma but would still be ~15-20 m thick in its final stages. The Gamsberg would retain its caprock for >25 Ma and, as the quartzite is slightly thicker than that which caps the Klein Gamsberg at present, it would also be ~20 m thick at the end. However, if the retreat of the caprock is linked to the area of the summit, for example by the amount of surface wash available to each cliff section, the rate of retreat would decrease through time as the area becomes proportionally smaller compared to the length of the cliff face. This would increase the length of time which the caprocks ultimately survive

but demands a greater understanding of the controls on cliff face retreat to be fully assessed. Although the rate of summit denudation is low, it is active and it is therefore wrong to assume that surfaces, however flat or smooth, can be preserved unmodified. Whether or not the ratio of backwearing to downwearing estimated here to be 25:1 is characteristic of other surfaces remains to be seen. However, models of landscape evolution which do presume that downwearing is negligible over long periods of time (e.g. King, 1962, 1983) need to be reconsidered.

4.9.2 Extrapolation of Denudation Rates from Cosmogenic Isotope Analysis

In order to assess the implications of the calculated denudation rates and inferred rate of escarpment retreat at the Gamsberg for evolution of the Great Escarpment in Namibia, it is necessary to assess the validity of regional extrapolation of the Gamsberg results. Denudation rates modelled from cosmogenic isotope concentrations are site-specific and depend on the geomorphic setting of the sampling site. It is therefore necessary to consider the extent to which the geomorphic settings of the Gamsberg sites are replicated elsewhere. Distributed along the length of the escarpment in Namibia, many other locations are characterised by outcrops of crystalline, often granite, basement rocks. For example, granite of the Sinclair Sequence in the southern-central part of Namibia and granites of the Damara Sequence throughout northern Namibia comprise sections of the escarpment (Fig. 4.5). In southern Namibia, horizontally bedded sedimentary units of the Nama system (e.g. Kuibis quartzites) overlie crystalline basement that forms ridges and together create an edge to the escarpment that is broadly similar to the situation at the Gamsberg (Brown *et al.,* 1998). Although the Gamsberg is an outstanding morphological feature of the Great Escarpment, similar geology and a consistent topographic configuration in places, as well as similar climatic conditions characterise central and southern Namibia. This suggests that denudation rates and slope retreat rates at the Gamsberg are typical of other areas of the escarpment, thereby permitting some degree of spatial extrapolation.

The extent to which the caprock at the Gamsberg influences denudation of the granite ridges is obviously important to consider for extrapolation of the data to other granite ridges which do not have caprocks. In general, the relationship between caprocks and their underlying substrates is poorly understood. The evolution of rock slopes as a whole is a complex subject of diverse opinions (Selby, 1993; Oberlander, 1997) and it is not possible to resort to accepted models. However, surrounding the Gamsberg there are some residual granite hills and it is reasonable to assume that these were once covered by the quartz arenite unit. Two of these are clearly visible in Figure 4.13 and have retained the same overall slope profile as the Gamsberg and Klein

Gamsberg. It can therefore be inferred that the presence of the caprock at the Gamsberg does not have a significant effect on the style of granite ridge denudation, and possibly the overall rate of denudation. The data derived from cosmogenic isotope analysis may therefore be more widely applicable, in the vicinity of the Gamsberg at least. In addition, given the preservation of the Gamsberg as an elevated feature, it is reasonable to assume that downwearing rates at other locations have not been significantly lower or else other locations along the escarpment would also be characterised by high elevation residuals. Because the escarpment is, in general, evenly spaced at a distance from the coast any significant differential between rates along the escarpment cannot have been sustained because the Gamsberg would stand out from the escarpment edge which would have retreated further inland. It is therefore reasonable to assume that significantly higher retreat rates cannot have characterised other sections of the escarpment region.

As previously mentioned, the calculated rate of retreat is necessarily integrated over the past ~70 ka. This period of time encompasses Quaternary climatic oscillations that have characterised most of the Earth and resulted in fluctuation of the rate of denudational processes which, by implication, may have affected the rate of escarpment retreat. The question is to what extent these global climatic fluctuations will have affected the rate of retreat of the Great Escarpment, specifically at the Gamsberg. Climate in the vicinity of the Gamsberg is likely to have fluctuated (section 4.6.2) but the magnitude of fluctuation does not appear to have been sufficient to affect the steady-state (as defined for cosmogenic isotope analysis) nature of the denudational processes acting at the sites, both for the ridges and the summit samples (Fig. 4.20; section 4.8). Therefore the calculated rates may well characterise the average denudation rate during the late Quaternary over the past 1 Ma at least and possibly over the entire Quaternary period.

4.9.3 Implications for Escarpment Evolution in Namibia

Whatever the exact representativeness of the rate of escarpment retreat calculated at the Gamsberg for the rest of the margin, the average rate of ~10 m Ma^{-1} is two orders of magnitude less than the commonly assumed rate for retreat of Great Escarpments of ~1 km Ma^{-1}. High rates of this kind are based on the assumption of uniform retreat of an escarpment since initiation at continental break-up. A rate of this magnitude for the retreat of Great Escarpments has been recently cited and advocated by many authors (e.g. King, 1983; Selby, 1993; Seidl *et al.,* 1996; Ollier and Pain, 1997) and the assumption of uniform retreat is often used as a basic model component for passive margin evolution (Gilchrist and Summerfield, 1990). Assuming that

large-scale escarpment retreat has occurred, it is clearly incorrect to assume an average retreat rate for the Escarpment at the Gamsberg in central Namibia, and probably for much of south-west Africa. If other areas of the escarpment had been retreating at an average rate of 1 km Ma^{-1} and the Gamsberg was atypical, by now it would have become an isolated outlier rather than remaining an integral part of the scarp front.

The available evidence for the denudational history of south-west Africa (section 4.5) suggests significantly higher rates of denudation soon after continental break-up and is compatible with the low rate of denudation in the Escarpment zone calculated from cosmogenic isotope analysis for the more recent past. The collected data, in particular from apatite fission track analysis, suggest that such low rates may have characterised the south-west margin since early Tertiary times. By implication, escarpment retreat would have been much faster during the late Cretaceous, assuming retreat from the rift zone. If the calculated present rate of escarpment retreat at the Gamsberg is thought to have characterised the past 60 Ma, then <100 m of retreat would have occurred in this time. Thus said, large-scale retreat from an initial position coincident with the major rift boundary fault across the coastal plain to within 100 m of its present position would require an average escarpment retreat rate of ~5 km Ma^{-1} over 30 Ma. Although rates of scarp retreat of this magnitude, from 0.5-6.7 km Ma^{-1}, have been determined for the Colorado plateau (Schmit 1987, 1989), such high rates appear critically dependent on specific hydro-geological conditions that produce widespread and aggressive ground water sapping. Such conditions do not occur in central Namibia and have probably never applied to the south-west margin, which means that the operation of such high rates of escarpment retreat is unlikely. Also, it should be noted that the basis for determining such high rates has been criticised (Oberlander, 1997).

Two fundamental questions raised by the discussion so far include 1) what has determined the apparent switch in rate of denudation (and by inference retreat of the escarpment) from high to low since rifting, and 2) has large-scale escarpment retreat from the coast really happened? The cosmogenic isotope data for the Gamsberg alone cannot provide answers but in light of this new empirical data some speculations can be made.

The arid climate of the central Namib Desert has been remarkably stable during much of the Cenozoic and is discussed in detail in section 5.2.4 (Ward *et al.,* 1983; Ward, 1987; Lancaster 1984a, b; Wilkinson, 1990). It could be argued that the apparent decline in rates of denudation and escarpment retreat reflect a progressive change in climate from the beginning of the

Cenozoic and that an arid climate at the Gamsberg is controlling the magnitude of present-day rates. However, climate alone is not generally considered to enforce such dramatic changes in denudational regimes. Preliminary cosmogenic isotope data from the Drakensberg (south eastern margin of Africa) on a basalt ridge extending from the escarpment, which currently experiences sub humid/humid climatic conditions, suggest a denudation rate on the order of ~30 m Ma^{-1} (A. Fleming, *pers. com.*). It seems that even a considerable alteration in climate could not be the sole reason for the apparent decline in denudation rates since rifting.

Surface process models, as described in sections 4.3.3 and 4.4.4, have been useful in deciphering the principal controlling factors of topographic margin evolution and escarpment retreat and confirm that climatic regime is of secondary importance. Gilchrist *et al.* (1994b), Kooi and Beaumont (1994) and Tucker and Slingerland (1994) all demonstrated that the first order controls on margin development are drainage divide location related to antecedent (pre-rift) topography, and the timing of integration of internally drained catchments. In the models, large-scale retreat of a clearly defined escarpment depends on the escarpment crest coinciding with a migrating drainage divide. The models also suggest that escarpments and drainage divides can become pinned and retreat can slow once the topography inland of the escarpment becomes similar to that in front of it. This is dependent on the timing of integration of the internal drainage rivers with a common base level (sea level) (see Kooi and Beaumont, 1994, fig. 2). These model inferences provide a potential mechanism for the inferred rapid escarpment retreat soon after rifting and a slowing of retreat later on the south west African margin. In support of this, the Orange River is though to provide the key link between external and internal catchments by breaching the marginal upwarp, dated somewhat speculatively at ~85 Ma BP (Rust and Summerfield, 1990). Though the topography of the south west margin does not show as much dissection and low relief landward of the current escarpment as is depicted by Kooi and Beaumont's models, despite some incision by the Fish River (Fig. 4.3).

Along the south-west African margin the difference in the distance of the drainage divide and the escarpment form the coast varies from between 0 and 280 km (Ollier and Marker, 1985). Although the cosmogenic data cannot provide insight into possible divide migration and provide data on the relatively recent past only, they do emphasise the question of whether large-scale escarpment retreated from the coast has actually occurred in Namibia. Tucker and Slingerland (1994) proposed that headward migration of bedrock channelled river systems is an important mechanism for the retreat of drainage divides and escarpments, but Bishop (1995) has argued that in reality, drainage head retreat may not be as significant as is commonly cited in the

literature. Quantitative modelling has shown that if a drainage divide is located inland at the time of rifting, large-scale rapid denudation takes place soon after rifting and a coastal escarpment is denuded but then reformed at the inland location of the divide (Kooi and Beaumont, 1994; Gilchrist *et al.*, 1994b). If a combination of interior catchment denudation, isostatic uplift/tilting, climate and lithology were then to maintain the escarpment in roughly the same position, then the collected data from south-west Africa including the cosmogenic isotope data would broadly support such a scenario.

In general, neither of the evolutionary models described above can be accepted or rejected on the basis of cosmogenic isotope data from one location along the Great Escarpment of Namibia, but the provision of new empirical data offers scope for further integration of modelling and field based studies. Admittedly, quantitative models have needed simplified parameters but as empirical constraints on actual rates of denudation and escarpment retreat over various time scales become available, basic assumptions and models should be replaced.

4.10 Conclusions

Denudation rates at the Gamsberg, a flat topped residual on the Great Escarpment of south-west Africa in central Namibia, based on analysis of *in-situ* cosmogenic ^{10}Be and ^{26}Al in quartz, range from 0.26 ± 0.06 to 0.49 ± 0.1 m Ma^{-1} for the summit and 2.15 ± 0.5 to 17.27 ± 4.08 m Ma^{-1} for two granite ridges. Interpretation of these data yield a rate of escarpment retreat of the order of 10 m Ma^{-1} for at least the past 1 Ma and possibly for the entire Quaternary period. An average rate of ~10 m Ma^{-1} is likely to be representative of the rest of the escarpment in Namibia given the overall similarity of lithology, climate and morphology at other locations as well as the consistent present-day distance between the escarpment and the coast along its length. To improve the accuracy of both spatial and temporal extrapolations of the data, further work is required. Ideally this would involve similar cosmogenic isotope studies at several new locations along the Great Escarpment, both in other locations that exhibit caprocks and perhaps more importantly, those that do not.

A rate of ~10 m Ma^{-1} for the recent geological past is compatible with existing data from other approaches, such as fission track thermochronology, that indicate large amounts of denudation for the margin soon after rifting but lower amounts and, by implication, lower rates of escarpment retreat throughout the Cenozoic. However, a rate of 10 m Ma^{-1} is two orders of magnitude lower than commonly assumed rates of retreat for Great Escarpments and implies that

some existing models, for south-west Africa at least, should be rejected. Further work on other margins would be able to determine the extent to which this is true elsewhere. *In-situ* cosmogenic isotope analysis yields data on escarpment behaviour on an intermediate time scale between short-term process studies and long-term data from other existing techniques. Coupled with data from techniques which have a longer-term perspective, *in-situ* cosmogenic isotope analysis can provide the much needed empirical constraints for quantitative models of passive margin evolution.

Chapter 5:

In-Situ-Produced Cosmogenic ^{10}Be and ^{26}Al Denudation Rate Estimates for Bornhardts in the Central Namib Desert, Namibia

---

5.1 Introduction

Bornhardts are prominent and defining landforms of tropical landscapes and southern Africa is usually considered their type locality (Thomas, 1994). Controversy about their evolution is well documented, but in central Namibia extensive work has indicated that their origin is largely a result of structural control (Selby, 1977a, b, 1982a, b). The aim of this chapter is not to test theories of bornhardt evolution but rather to quantify how fast they are denuded and to consider the implications this has for the style of mass wasting of bornhardts in the Namib and what significance this has, if any, for the weathering processes operating. Denudation rate estimates from analysis of cosmogenic ^{10}Be and ^{26}Al in quartz for three bornhardts in the central Namib Desert are presented.

Bornhardts in the coastal plain of Namibia were specifically chosen for two reasons. First, the coastal plain is a key topographic component of the south-west African passive continental margin. As such, knowledge of its geomorphic evolution is needed to constrain models of margin development in much the same way as the evolution of the escarpment was used in Chapter 4. Characterising denudation rates on two of the key elements of the south-west-African margin is preferable to one and should lead to a more complete, quantitative understanding of the way the landscape has evolved. Secondly, the central Namib Desert (Fig. 5.1) exhibits a diversity of attributes required to assess long-term denudation rates in an arid environment using cosmogenic isotope analysis. These include an unusually stable climatic history, a well mapped geology and numerous exposed bedrock features in simple geomorphic settings. A well-constrained climatic history is critical if integrated rates from cosmogenic isotope analysis are to represent real rates of denudation and allow for possible extrapolation over time. In addition to these reasons, there are existing data on denudation rates from other techniques such as fission track thermochronology which are useful for comparative purposes (Brown *et al.*, 1990, 1998).

Cosmogenic data should help to create a more detailed denudation chronology by providing complimentary information at a scale which has hitherto been unobtainable as well as providing an insight into the evolution of a classic tropical landform.

Rounded granite inselbergs, commonly known as bornhardts, particularly in the description of African landscapes, were selected as sampling sites for several reasons. First, they are abundant on the coastal plain in the central Namib suggesting that rates of denudation on a small number of bornhardts may be representative of a larger number of features, thereby allowing some spatial extrapolation (Fig. 5.2). Secondly, they all share a relatively simple morphology. Thirdly, they have extensive, smooth, bare, bedrock surfaces which appear to have had a simple exposure history making them ideal as sampling locations for cosmogenic isotope analysis. Fourthly, they have a broader significance for the mode and rate of landscape evolution across south-west Africa due to their strategic location on the coastal plain between the escarpment and the coast. There are no other sites on the coastal plain that would be as suitable for cosmogenic isotope analysis, the other major landscape element being pediments. Although pediments are mainly made of bedrock, they are predominantly covered by a thin layer of sediment and are likely to have experienced a complex exposure history due to periods of burial by thicker and thinner layers of wind-blown sand or fluvial debris in the past. Lastly, a majority of the bornhardts are of a suitable quartz bearing rock type for ^{10}Be and ^{26}Al analysis.

Bornhardts were defined by Willis (1934) as a particular type of inselberg. Inselberg is a general term for any large, isolated, residual hill which usually rises abruptly above a gently sloping eroded plain. Willis (1934) considered bornhardts as 'true inselbergs', defining their distinguishing characteristics as, "bare surfaces, dome-like summits, precipitous sides becoming steeper towards the base, an absence of talus, alluvial cones or soil, a close adjustment of form to internal structure" (Willis, 1934, p. 124). Bornhardts are sometimes known simply as 'granite inselbergs' because their defining characteristics are usually only found in granitoid, massive rocks. It should follow then that all bornhardts can be considered as inselbergs but that not all inselbergs are bornhardts. However, such is the debate and controversy over the origins and development of bornhardts and inselbergs that even this seemingly simple classification does not always hold true. Some consider that the specific properties of granite influence the evolution of bornhardts to such an extent that they cannot be used to understand other types of non-granite inselbergs such as buttes that normally consist of horizontally bedded sedimentary rocks (Thomas, 1994).

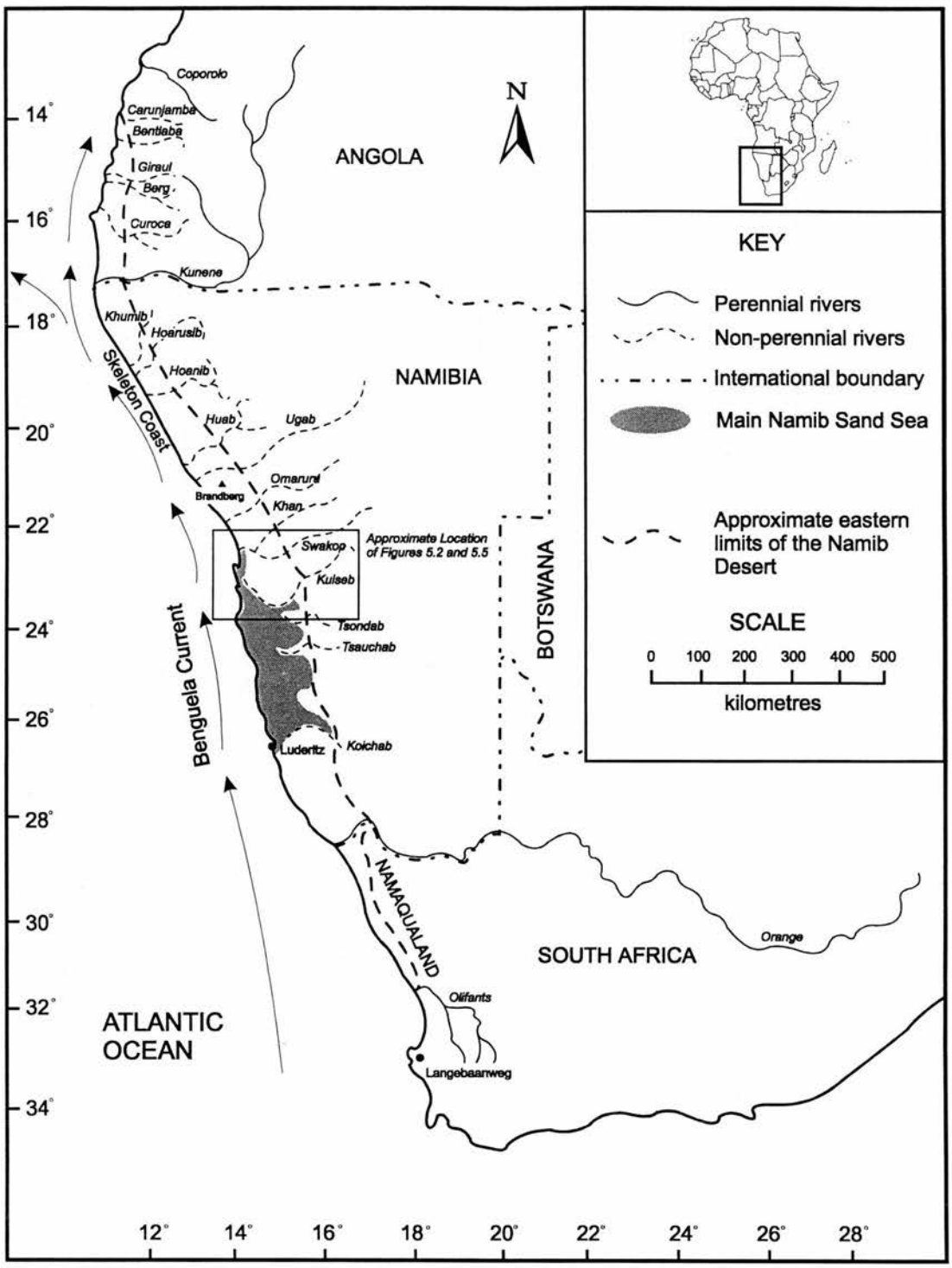

Figure 5.1: Map of south-west Africa showing the location and extent of the Namib Desert and other features mentioned in the text (after Ward et al., 1983).

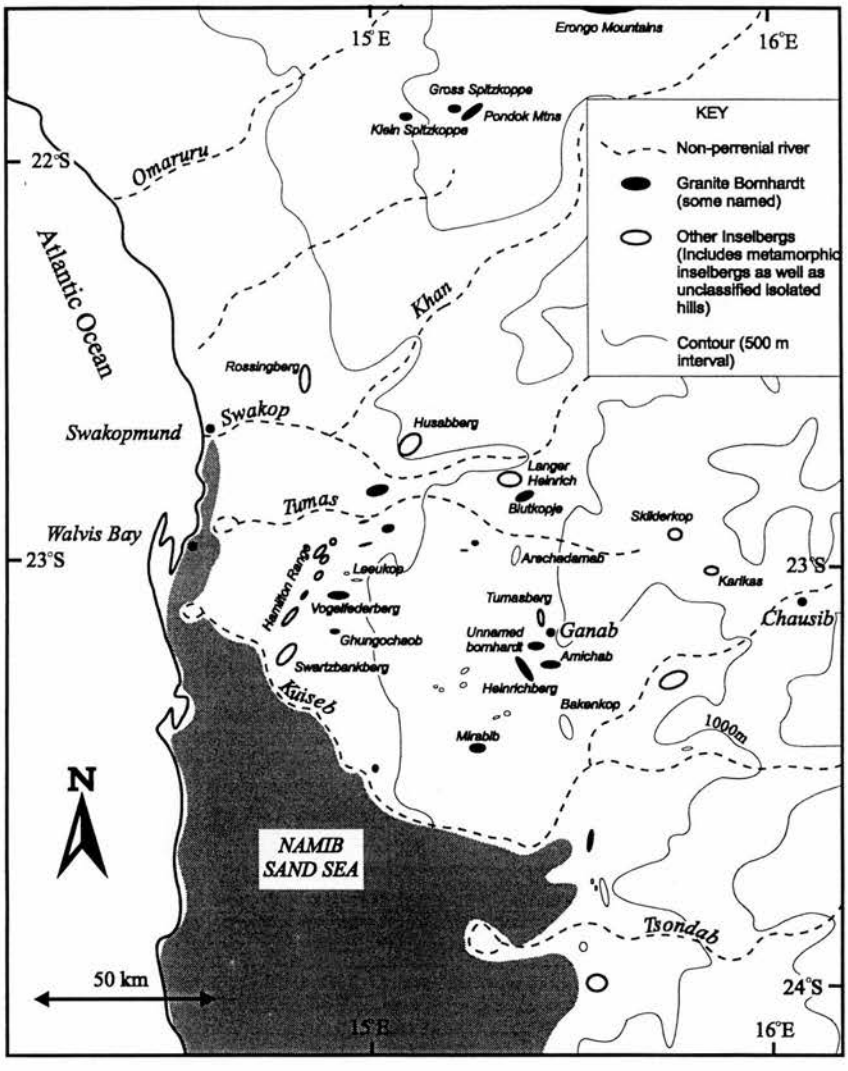

Figure 5.2: The location of some granite bornhardts and other inselbergs in the central Namib Desert (locations from 1:250 000 Topographic Maps and after Selby, 1977a, 1982 a, b; Ollier, 1978).

5.2 Physical Setting

5.2.1 Morphotectonic Development of the Coastal Plain

The morphotectonic development of south-western Africa has been described in detail in Chapter 4 (sections 4.2 and 4.4); of importance here is the formation of the coastal plain, a major component of passive margin topography. Prior to rifting (~130 Ma BP), the elevation of the landsurface would have been above sea level when the present-day coastal plain of Namibia was near the centre of Gondwana. Actual elevation data do not exist, but estimates of the amount of post rifting denudation seaward of the escarpment indicate that a thickness of up to 5 km of crust

has been removed with a large pulse of erosion soon after continental break-up in the late Cretaceous (Brown *et al.*, 1990). The cause of this pulse of denudation is likely to have been rapid incision by rivers in response to a sudden drop in base level to the newly created ocean cutting through the old, elevated continental surface (Summerfield, 1996b). Evidence for magmatic underplating of the margin lends some support to the notion of high elevation prior to break-up (White and McKenzie, 1989). There are many different views on how the topography of newly rifted margins develops involving isostatic, thermal, tectonic and geomorphic mechanisms (section 4.3). Central to many arguments is the notion of escarpment retreat, the focus of Chapter 4. Regardless of the details of the model applied to Namibia, the coastal plain is clearly a result of large-scale denudation triggered by the rifting event. It is probable that the coastal plain of central Namibia had been formed, and was close to its present width, by the early Cenozoic, ~60 Ma BP (section 4.4.2).

5.2.2 Morphology and Geology of the Central Namib

The Namib desert extends over 2,000 km from the Olifants river (South Africa) in the south to the Carunjamba river (Angola) in the north (Fig. 5.1; Ward *et al.*, 1983). It covers a coastal strip of land mostly less than 200 km wide. Along its length, there are a variety of arid environments including dune fields, gravel plains, predominantly ephemeral river channels, salt flats and pans, low hill ranges and inselbergs. The central Namib is usually defined as the hyper-arid to arid (<150 mm per year) area roughly in the middle stretching from the Ugab River and the Brandberg in the north to the Kuiseb River in the south (Fig. 5.1). For the purpose of discussion in section 5.2.4, the Tsondab drainage basin east of the main Namib Sand Sea has also been included in the area defined as the central Namib. The central Namib is distinguishable from the main Namib Sand Sea lying to the south of the Kuiseb (sometimes referred to as the Dune Namib) and the Skeleton Coast and Kaokoveld of the northern Namib. The central Namib desert is ~150 km wide, located on the gently sloping coastal platform that rises with an average regional slope of ~0.5° from the coast to an elevation of ~1000 m at the base of the escarpment.

The coastal platform in the central Namib has been cut across basement rocks comprising Precambrian metamorphic rocks of the Damara system as well as some pre-Damara rocks (e.g. Gamsberg Granite) and later Jurassic intrusions of granite and dolerite (section 4.2.1). The Damara is an ancient orogenic belt, part of the network of Pan-African orogenic belts that surround and dissect Africa (see Miller (1983) and references therein). There are four main groups of the Damara Sequence, dating from ~800 to 540 Ma BP. In the central Namib, outcrops

are mainly of the Nosib and Swakop Groups; the Otavie and Mulden, and Nama Groups are confined to the north and south respectively. The principal rock types of the Damara orogen cropping out in the central Namib are mica schist, granite gneiss, quartzite and marble. Granite intrusions of Donkerhuk age (500-560 Ma BP) as well as dolerite dykes of Karoo age (late Mesozoic) crop out throughout the central Namib. There are no remnants of any Karoo sedimentary units in the central Namib. The bevelled surface of the old rocks is known as the Namib Unconformity Surface (NUS) and is generally assumed to have been in place by the end of the Cretaceous. Alteration during the Cenozoic has meant that in some places under the main Namib Sand Sea this unconformity surface is highly uneven, but the NUS shows no evidence of chemical alteration and in general it forms a smooth, albeit polygenetic, stratigraphic baseline throughout the study area.

The NUS is overlain by a relatively thin and patchy veneer of Cenozoic sediments. Collectively known as the Namib Group, they including sandstones, calcretes, conglomerates and gravels (Ward, 1987). Many discrete Tertiary and Quaternary Formations have been recognised. The oldest deposit of the Namib Group in the central Namib region is the 40-200 m thick Tsondab Sandstone Formation, the lowest unit of which sits unconformably on the NUS. It consists principally of fossilised dune deposits and covers an area from Luderitz in the south to just north of the Kuiseb River, although similar arenite deposits have been found both further north and south (section 4.4.2). It is the most areally extensive formation and is covered by carbonate-cemented and calcified conglomerates especially in the western portion of the Kuiseb drainage basin below the escarpment. The main Namib Sand Sea to the south of the study area rests directly on Tsondab Sandstone which may have been an important sediment source for the younger, smaller dune field (Besler, 1996). In the central Namib, younger sediments are distributed more locally, mainly preserved as terrace and flood deposit remnants in river valleys.

The morphology of the central Namib comprises extensive, relatively flat (<2°) plains of limited relief interspersed with incised river valleys and isolated mountain ranges (Fig. 5.3). Gevers (1936) provides an excellent early description. Desert plains are the most areally extensive morphological element. These comprise coalesced pediments which extend from the foot of the escarpment and from the base of inselbergs into river valleys and towards the sea. True pediments are made of bedrock but the term has been used more generally to describe any low gradient, low relief slope. Bedrock pediments are thought to be formed by slope and scarp retreat under a semi-arid climate but there is a continuing debate as to their true origin and climatic significance (Oberlander, 1974, 1997; Moss, 1977). Pediments in the central Namib are

generally cut across bedrock (principally Damaran mica schists and granite) and are covered by a thin layer of silt, sand, quartz pebbles and granite grus (Selby, 1977a). The cover is commonly in the form of a desert pavement where the surface is armoured by stones (~10 mm diameter) with finer material beneath. The lack of relief and uniform nature of these pavements over many thousands of square kilometres in the central and northern Namib is remarkable. In places, the pediment surface is underlain by calcrete of variable thickness up to ~20 m. Where relief on the NUS is greatest, calcrete deposits are thickest. Near present day river valleys, calcrete thickness and sediment cover become progressively thicker (rock pediments extend into detrital pediments), but planed off bedrock often crops out at the surface; smooth granite is clearly visible near Gobabeb and around Vogelfederberg.

Drainage in the central Namib consists of five major westward flowing non-perennial rivers: the Ugab, Omaruru, Khan, Swakop and Kuiseb (Fig. 5.1). The convergence of the Swakop, Khan and Kuiseb in the vicinity of Walvis Bay reflects a fundamental control on location by ancient structures of the north-east trending Damara Orogen. There is some evidence for rearrangement of drainage courses from elongate, sediment-filled depressions in the NUS that may represent palaeochannels (Wilkinson, 1990). In the study area, between the Swakop and Kuiseb rivers, there is a highly ephemeral river, the Tumas, as well as tributaries of the major channels. The long profiles of rivers in the Namib are convex rather than concave due to a pronounced reduction in discharge downstream as a result of high evaporation rates. All of the rivers display evidence of past changes in base level and have deeply incised canyoned sections with dissected valley sides ('gramadullas') apparently representing a synchronous period of incision at the end of the Tertiary (Rust and Wieneke, 1980; Ward, 1987). The Kuiseb acts as the northern barrier to the main Namib Sand Sea (Fig. 5.4) and has a particularly impressive canyoned section where the river has incised up to 150 m into mica schists of the Damara Orogen to the east of the Sand Sea below the escarpment.

Figure 5.3: View of a typical, pavement-covered, low-relief desert plain in the central Namib near the Swakop River. Note the presence of inselbergs on the horizon.

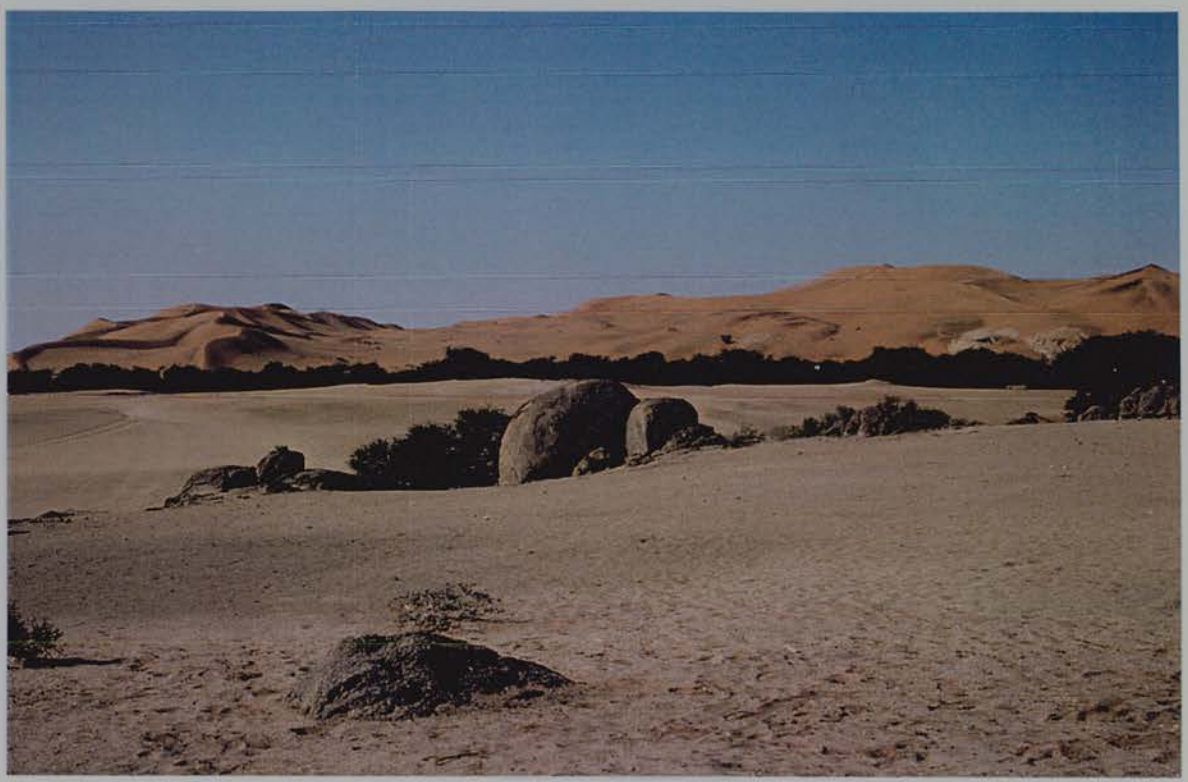

Figure 5.4: View looking south-west of the northern limit of the main Namib Sand Sea near Gobabeb. The thick line of vegetation marks the "linear oasis" of the ephemeral Kuiseb River which acts as a barrier to the >200 m high advancing orange coloured dunes in the background. Granite boulders in the foreground rest on planated granite covered by a layer of debris.

5.2.3 *Present-Day Climatic Conditions*

The present-day climate of central Namibia is thought to be controlled by the cold Benguela oceanic current flowing northwards along its coast and the associated upwelling of cold water, and the relative positions and strengths of the persistent South Atlantic and southern African continental high pressure zones (Tyson, 1986). The strong and relatively stable anticyclone over the South Atlantic, which is centred just off the Namibian coast, causes subsiding and diverging winds to have an aridifying effect over south-western Africa. The annual latitudinal range of this system is ~4°, with an average position at ~30°S (van Zinderen Bakker, 1975). The drying effect is intensified during most of the year by the neighbouring southern African anticyclone. Cold water (10-14°C) from a depth of several hundred metres wells up along the coast of Namibia due in part to the upwelling of the Benguela current and in part due to offshore SE Trade Winds. The upwelling contributes to aridity along the coast of Namibia by causing stabilisation of the coastal air mass, suppression of convection clouds and consequent rainfall, and a downward flux of sensible heat (Flohn, 1984). The combined effects of these large-scale forces produce a narrow arid coastal tract along the length of south-west Africa with a steep precipitation and temperature gradient with distance from the coast. The present-day climate changes from a winter rainfall/arid zone in the south to a hyper-arid zone in the central Namib to a summer rainfall/arid zone in the north and east.

Detailed description of the climate of the central Namib desert is provided by Lancaster *et al.* (1984) based on observations from ten meteorological stations over a five year period from 1976 to 1981. The stations were distributed in an area from Swakopmund (20 m elevation) in the north-west to Narabeb (400 m elevation) in the south to Ganab (1000m elevation) in the east, an area of ~17,000 km^2. The coastal belt is classified as extremely arid (Meigs, 1966) but there is a very large, almost six-fold, increase in rainfall from the coast to the foot of the escarpment, a trend that continues up the escarpment and over the plateau (Lancaster *et al.*, 1984). Typical mean annual rainfall at the coast is <20 mm rising to ~100 mm at Ganab (Fig. 5.2). During the study period, variability from year to year was high and a period of seven years without effective rainfall has been recorded at Gobabeb between 1969 and 1976. In the vicinity of the escarpment typical precipitation values rise to 150-200 mm a^{-1} (Jacobson *et al.*, 1995). Areas immediately at the foot of the escarpment, in the east of the coastal plain are affected by storms moving westward over the escarpment but due to a strong temperature inversion over the coastal plain the effect of these storms is rarely felt further west.

Coastal fog is a distinctive feature of the Namib and results from moist oceanic air flowing inland over cold offshore waters (Lancaster *et al.*, 1984; Olivier, 1992). Its importance for the flora and fauna of the Namib is well documented (Seely, 1978) but it is also probable that it plays a major role in creating suitable conditions for weathering processes to occur such as salt weathering (Goudie *et al.*, 1997), solutional weathering (Sweeting and Lancaster, 1982), and hydration. Fog penetrates inland for at least 100 km (Lancaster *et al.*, 1984; Olivier, 1992) and can, occasionally, reach the foot of the escarpment. Fog precipitation is far more regular and in places much greater than mean annual rainfall. For example, at Vogelfederberg mean annual rainfall from 1976-1981 was 21.45 mm whereas the mean annual fog precipitation over the same four year period was 183.48 mm (Lancaster *et al.*, 1984). Fog precipitation occurs most frequently at the coast but the amount of fog-water precipitation appears to increase from the coast to a maximum at 35-60 km inland and then decreases further inland (Lancaster *et al.*, 1984). This trend has been related to increasing elevation from the coast but could also be an artefact due to lack of data coverage. Maximum amounts of fog water precipitation per day per month have been recorded in June or July throughout the coastal plain (Lancaster *et al.*, 1984).

Temperatures in the central Namib are fairly cool and equable throughout the year. Mean annual temperatures range from 15.5 °C at the coast (Pelican Point near Walvis Bay) to 21.5 at Ganab, the furthest inland station (Lancaster *et al.*, 1984). The mean annual amplitude of temperature is least at the coast at 5.5 °C and most at Vogelfederberg at 16.4 °C. Minimum temperatures below 0 °C occur only once on average per year. Extreme maximum temperatures over 40 °C occur at all inland stations in March or April but not generally for more than one or two days. Diurnal temperature changes in the Namib are usually only 8 °C (Schulze and McGee, 1978). Mean annual humidity is highest at the coast (87%) and lowest inland (37% at Ganab; Lancaster *et al.*, 1984). The pattern of humidity variation across the coastal plain reflects temperature variation at each station but with greater amplitude; the annual variation is least at the coast (9%) and most at Vogelfederberg (59%; Lancaster *et al.*, 1984). Dominant seasonal winds from three directions are common at weather stations in the central Namib (Lancaster *et al.*, 1984). From September to November dominant winds are usually from the south-west when the South Atlantic anticyclone is at its strongest and heating effects on land are greatest. From December to February dominant winds are from the north-west and in March to August the strongest winds are from the north-east and east. Highest velocities (up to 60 km h^{-1}) are associated with warm 'berg' winter winds which blow from the plateau down onto the coastal plain, and occasionally cause dust storms (Lancaster *et al.*, 1984; Wilkinson, 1990).

5.2.4 Climatic and Palaeoenvironmental History

The climatic and associated environmental history of the Central Namib has been a source of debate since Koch (1961) first suggested that arid conditions had prevailed in the region for many millions of years, an idea based on the highly adapted nature of the Namib fauna (Vogel *et al.*, 1981, Ward *et al.*, 1983). Koch (1961) thought that the richness and endemism of native species, in particular the tenebrionid beetle, required a long and undisturbed evolutionary period with prevailing arid conditions. Recognising the importance for aridity of the cold Benguela current, which at the time was thought to have been initiated 70 to 80 Ma BP, Koch (1961) ascribed a late Cretaceous age to the origin of the Namib Desert. Since then, several authors have used a variety of palaeoenvironmental indicators in an attempt to evaluate climatic conditions over a range of time periods for south-western Africa (van Zinderen Bakker, 1975, 1984a, b; Tankard and Rogers, 1978; Ward *et al.*, 1983; Lancaster, 1984a, b; Wilkinson, 1990). Some very different conclusions have been drawn from the various lines of evidence and the main themes of the debate are outlined below.

5.2.4.1 Pre-Quaternary climatic history

The fragmentation of Gondwanaland during the Cretaceous was not only an important event in terms of the landscape evolution of south-western Africa but it also had profound implications for the climate (Tyson, 1986). The opening of the South Atlantic permitted the initiation of the high pressure cells which control the climatic system today. The development of a circumpolar current and the closing-off of the circum-equatorial current dramatically altered the climate of the southern hemisphere and intensified latitudinal zonation of the oceans. The development of a cold Southern Ocean was necessary for the initiation of cold upwelling water off the coast of Namibia. Van Zinderen Bakker (1975) ascribed an early Oligocene age (~35 Ma BP) to the aridifying effects of the cold water and upwelling associated with the Benguela current after Shackleton and Kennet (1975) concluded that it was at this time that the deep water temperatures of the Southern Ocean and South Atlantic became as low as they are today. Supported by some geological and geomorphic evidence, van Zinderen Bakker (1975) proposed an early Oligocene age for the Namib Desert. More recent ideas about circulation in the southern Hemisphere have been used to infer a more youthful age for the initiation of arid conditions in the Namib. It is now generally assumed that the modern day Benguela current and upwelling system was not in place until the late Miocene, 25 Ma after the early Oligocene cooling of bottom waters and that arid conditions in the Namib could therefore not have been initiated until this time (~10-12 Ma

BP) (Seisser, 1978, 1980; Tankard and Rogers, 1978). Despite the cold Southern Ocean, full development of the Antarctic convergence by late Miocene times and opening of the Drake Passage ~25 Ma BP was thought necessary for the current intensity of upwelling to occur and desiccation of the Namib to begin.

Prior to the late Miocene, fluctuations in climate during the Tertiary are a common element of several studies involving marine and terrestrial evidence from south-west Africa, most of which have supported a youthful age for the Namib Desert. Palaeobotanical data led Tankard and Rogers (1978) to infer an arid/summer rainfall climate regime for the Oligocene, but significant climatic fluctuations to much wetter conditions throughout the Miocene and Pliocene. They proposed a Pliocene/early Quaternary age for the most recent onset of persistent arid conditions in the Namib consistent with initiation of a strong Benguela system. Coetzee (1980) also used a palaeobotanical approach and supported a relatively young age for the current Namib Desert at the end of the Miocene. The pollen and fossil evidence cited by both Tankard and Rogers (1978) and Coetzee (1980) was principally from the Langebaanweg region and the Namaqualand coast in the southern Cape. Macrofaunal remains from the central Namib thought to be Pliocene in age have been used to support a youthful age for the onset of arid conditions (Tankard and Rogers (1978), Dingle *et al.* (1983) and references therein).

5.2.4.2 Quaternary climatic history

The extent of Quaternary fluctuations in the climate of the central Namib is debated. It had previously been assumed that glacial periods in the Pleistocene resulted in intensification of arid conditions in the Namib and some northward shifting of the boundaries of the arid zone along the south west African coast (van Zinderen Bakker, 1975, 1984a; Tankard and Rogers, 1978). A latitudinally contracted, but significantly wider, central arid core was thought to be preserved at glacial maxima but shifted approximately 5° further north. Associated with the core was intensification of arid conditions in the northern Kalahari and expansion of dune systems into Angola and the Congo (van Zinderen Bakker, 1975). Rust and Vogel (1988) studied fluvial features in the northern Namib and rejected the notion of a fully arid core throughout the Quaternary. In one of few studies in the northern desert area, Rust and Vogel (1988) proposed a model of at least three significant climatic oscillations from arid/semi-arid conditions to more humid during the late Quaternary. Conversely, Selby *et al.*(1979) argued for prolonged arid conditions throughout the past 240 ka based on $^{234}U/^{230}Th$ dated lake deposits in the central Namib. The survival of the lake deposits on the ground surface precluded significantly wetter

periods and indicated that any northward propagation of arid conditions was an expansion rather than a shift of the arid zone. A great many other studies have been concerned with the detail of identification and dating of wetter periods or pluvials throughout the Quaternary principally from fluvial geomorphic features and there is large body of radiocarbon dated evidence from Namib river basins to support numerous inferred climatic fluctuations to a variety of extents (Vogel, 1982; Vogel and Visser, 1981; Rust and Wieneke, 1980; Heine and Geyth, 1984; Rust *et al.*, 1984 (review paper); Eitel and Zöller, 1996). Holocene fluctuations in climate have largely been inferred from the archaeological record in rock shelters (Sandelowsky, 1977). Three distinct, moister periods have been identified but the extent of changes in rainfall is uncertain.

5.2.4.3 Sedimentary evidence for past climates

Investigation into the sedimentary succession of the central Namib has led to a revaluation of most of the palaeoclimatic reconstructions outlined above and a strong case put forward for persistent and long-lived aridity throughout the Quaternary and pre-Quaternary times (Ward *et al.*, 1983, Lancaster, 1984a, b; Ward, 1984, 1987; Wilkinson, 1990). Studies that support significant climatic fluctuation have been criticised on several grounds. Firstly, the palaeobotanical work of Tankard and Rogers (1978) and Coetzee (1980) has been criticised for excessive spatial extrapolation. Their evidence from the southern Cape is unlikely to be a good indication of conditions in the central Namib given the discontinuous nature of the Benguela current and the large distance, ~1000 km, between the regions (Wilkinson, 1990). More generally, the Namib should probably not be considered as a single desert given that the major characteristics of the present day climate change from south to north and that such differences have probably also characterised the past (Ward *et al.*, 1983). Secondly, Ward *et al.*, (1983) and Ward (1987) have suggested caution with existing interpretations of faunal and floral evidence from the Namib and stress the important implications of a steep climatic gradient over the narrow desert tract. The present day hyper-arid coastal environment is often home to many large mammals, fossils of which have in the past perhaps incorrectly been used to infer a coastal savannah grassland environment (Tankard and Rogers, 1978). A range of animals including leopards, elephants and baboons can be found living in seemingly inhospitable areas of the Kuiseb Valley and the northern Namib but their presence is undoubtedly due to much more mesic conditions near by in the escarpment area and groundwater flow sustaining year-round vegetation in the major river valleys (Fig. 5.4). Strong, easterly berg winds blow from areas with substantially more rainfall than the central Namib and it has been shown that pollen from these areas has been carried and incorporated into modern fluvial sediments potentially providing an

unrepresentative assemblage of modern conditions (Ward *et al.,* 1983). This problem was also identified by van Zinderen Bakker (1984b) in one of the only pollen studies carried out in the central Namib area. Pollen in silt layers from Sossus Vlei at the end of the Tsauchab River dating from ~19 ka (calibrated) BP was dominated by indicators of arid conditions such as Chenopadiaceae. Mountain species were thought to have been brought from the upper portions of the catchment and although the silts themselves indicate more water in the catchment, the presence of interbedded dune sands and arid pollen species were interpreted as indicating an overall arid climate from the glacial maximum to the present.

A critically important assumption underlying the interpretation of fluvial deposits and events discussed above is that, in broad terms, river incision represents a wet climate and aggradation represents a dry climate. This rather basic approach is most likely a gross simplification particularly in sub-tropical arid and semi-arid areas (Helgren, 1979; Thomas, 1994). Stream mechanisms are more likely to be controlled by load quantities, sediment storage and to what extent energy is expended on moving sediment, or is directed towards incision. Rivers are therefore more likely to exhibit a 'complex response' to external climatic events (Schumm, 1979). As a result, an incision event cannot be unequivocally attributed to an increase in discharge because it could also reflect a change in the distribution of available energy (Lancaster, 1984a). In addition, the fact that many of the rivers which flow across the central and northern Namib begin outside the arid zone suggests that evidence for increased water availability may not be indicative of local conditions in the coastal desert but rather in the escarpment and interior highlands which experience much more rainfall.

The main conclusions of Ward *et al.,* (1983), Lancaster, (1984a) Ward, (1983), Ward, (1987) and Wilkinson, (1990) are summarised in Table 5.1. Their findings reflect detailed investigations of the depositional environments of the Cenozoic Namib Group preserved in the central Namib drainage basins of the Kuiseb, Tumas and Tsondab rivers. The sedimentary succession appears to yield a more consistent, correlative and relevant record than most of the work previously outlined because local environmental conditions can be distinguished from discharge events which may not reflect the local environment. Correlation between drainage basins is sometimes problematic due to the paucity of reliable dates, variation in catchment characteristics and morphology. For example, the Kuiseb is a much more extensive catchment than the Tumas or Tsondab and is influenced by rainfall events further inland. A large proportion of the Tsondab load is solutional due to limestone exposed in it source area in the Naukluft Mountains. The Kuiseb has a confined valley cut into Damara Schist whereas the other two rivers drain more

openly over Tsondab Sandstone. Wilkinson (1990) proposes that depositional sequences are of more use than geomorphological features such as inselbergs and pediments because uncertainties over their climatic significance are usually less marked.

Prior to the Tertiary there is little sedimentary evidence in the central Namib. In the southern Namib, the Pomona beds are indicative of a fluvial environment under increasingly arid conditions and have been used to date formation of the NUS to the late Cretaceous (Ward *et al.*, 1983). Tertiary and Quaternary sediments that lie on top of the NUS in the central Namib indicate eight or more periods of variable fluvial activity in the three catchments, but the depositional environments indicated are all arid to semi-arid. Fluctuations in rainfall appear to be limited to the highland parts of catchments. Evidence for an extensive, early to mid/late Tertiary sand sea from the Tsondab and Tumas Sandstone units is the most striking evidence of Tertiary aridity and suggests that a direct correlation does not necessarily exist between Namib climate and the existence, intensity and position of the zone of Benguela Current upwelling (Ward *et al.*, 1983; Wilkinson, 1990). This may explain the variability in the ages ascribed to the onset of aridity by previous workers who invoked upwelling as the principal driving mechanism (van Zinderen Bakker, 1976; Tankard and Rogers, 1978; Coetzee, 1980). Preserved calcrete caprocks on the Tsondab Sandstone dating back to the end of the Miocene indicate that the climate has not been much more humid since this time because these crusts would have been dissolved (Yaalon and Ward, 1982). The extent of inferred more humid conditions at the end of the Miocene for the central Namib depends on the climatic parameters assumed for calcrete formation. Today calcrete can be found in areas with a mean annual precipitation up to 600 mm, but other duricrusts such as gypcrete that are also be found in the central Namib depend on much lower mean annual precipitation of <200 mm (Watson, 1988; Goudie, 1983). Quaternary aridity throughout glacial and interglacial periods is confirmed for the Namib Desert but it is likely that changes did occur further east outside the Namib in the escarpment and plateau regions.

In summary, the overall trend of palaeoclimates in the central Namib appears to have been no more humid than semi-arid throughout the Quaternary and possibly over most of the Tertiary. This does not imply that all evidence for fluctuation is wrong, although some has been clearly questioned, but that the magnitude of climatic changes has not been great enough to cause significant variation in the overall trend. For a large proportion of the Cenozoic, climatic conditions were hyper-arid to arid and environmental conditions were similar to today. Despite a vigorous debate, it is the local sedimentary evidence of Ward (1987), Wilkinson (1990) and others that seems to be most pertinent to this study of denudation rates and landscape change in

the central Namib. Prolonged aridity in the Namib makes it one of the most consistently arid locations on the Earth. A conclusion of overall long-term aridity is important in the context of potential temporal extrapolation of denudation rates inferred from cosmogenic isotope analysis. In the central Namib, denudation rates from analysis of *in-situ* ^{10}Be and ^{26}Al, which may be integrated over a period of up to ~3 Ma depending on the actual rate, can be considered to be representative of a much longer time period assuming that the climate has not fluctuated significantly.

Table 5.1 (overleaf): Summary of the sedimentary succession in the Kuiseb, Tumas and Tsondab drainage basins and the palaeoenvironmental implications for the central Namib during the Cenozoic. (Sources: Kuiseb: Ward, 1984, 1987; Tumas: Wilkinson, 1990; Tsondab: Lancaster, 1984b; Other Areas: Ward *et al.*, 1983; Lancaster, 1984a; Dingle *et al.*, 1983)

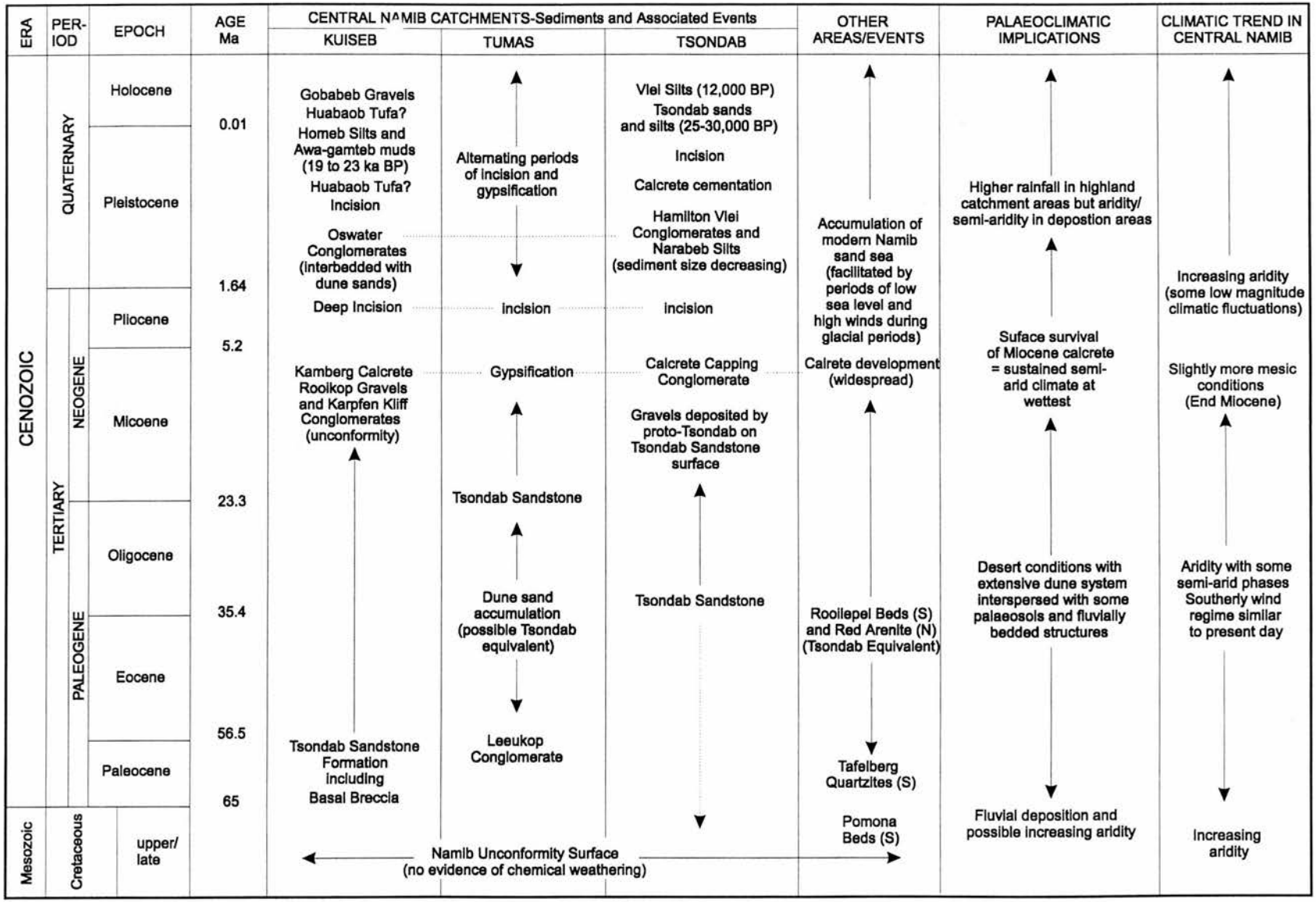
ERA
PERIOD
EPOCH
AGE Ma
CENTRAL NAMIB CATCHMENTS-Sediments and Associated Events
KUISEB
TUMAS
TSONDAB
OTHER AREAS/EVENTS
PALAEOCLIMATIC IMPLICATIONS
CLIMATIC TREND IN CENTRAL NAMIB
CENOZOIC
QUATERNARY
TERTIARY
NEOGENE
PALEOGENE
Holocene
Pleistocene
Pliocene
Miocene
Oligocene
Eocene
Paleocene
0.01
1.64
5.2
23.3
35.4
56.5
65
Gobabeb Gravels
Huabaob Tufa?
Homeb Silts and Awa-gamteb muds (19 to 23 ka BP)
Huabaob Tufa?
Incision
Oswater Conglomerates (interbedded with dune sands)
Deep Incision
Kamberg Calcrete Rooikop Gravels and Karpfen Kliff Conglomerates (unconformity)
Tsondab Sandstone Formation including Basal Breccia
Alternating periods of incision and gypsification
incision
Gypsification
Tsondab Sandstone
Dune sand accumulation (possible Tsondab equivalent)
Leeukop Conglomerate
Vlei Silts (12,000 BP)
Tsondab sands and silts (25-30,000 BP)
Incision
Calcrete cementation
Hamilton Vlei Conglomerates and Narabeb Silts (sediment size decreasing)
incision
Calcrete Capping Conglomerate
Gravels deposited by proto-Tsondab on Tsondab Sandstone surface
Tsondab Sandstone
Accumulation of modern Namib sand sea (facilitated by periods of low sea level and high winds during glacial periods)
Calrete development (widespread)
Rooilepel Beds (S) and Red Arenite (N) (Tsondab Equivalent)
Tafelberg Quartzites (S)
Pomona Beds (S)
Higher rainfall in highland catchment areas but aridity/ semi-aridity in depostion areas
Suface survival of Miocene calcrete = sustained semi-arid climate at wettest
Desert conditions with extensive dune system interspersed with some palaeosols and fluvially bedded structures
Fluvial deposition and possible increasing aridity
Increasing aridity (some low magnitude climatic fluctuations)
Slightly more mesic conditions (End Miocene)
Aridity with some semi-arid phases Southerly wind regime similar to present day
Increasing aridity
Mesozoic
Cretaceous
upper/ late
Namib Unconformity Surface
(no evidence of chemical weathering)

5.3 Bornhardts of the Namib Desert

The coastal plain of Namibia is dotted with inselbergs of various size and morphology ranging from elongate ridges of metamorphic rocks such as those that make up the Hamilton Range, to the classic bare rounded monolithic bornhardts like Vogelfederberg (Figs. 5.2 and 5.7). Large bornhardts, averaging 100 m high, are distributed across the coastal plain. They are the most prominent geomorphic features of the central Namib landscape and have attracted significant attention (King, 1975; Selby, 1977a, b, 1982a, b; Ollier, 1978; Twidale, 1988). They are predominantly formed in granite with some mica-schist components. Throughout the coastal plain smaller granite outcrops rise above the surface in various shapes. Field observations confirm Selby's (1977a) report of planated granite around Gobabeb as well as small koppies and tors of rounded boulders at many other locations (Fig. 5.4). The escarpment in the central Namib does not have a continuous scarp front and in places it is dissected into long protruding spurs. Where these have become isolated from the escarpment they form large inselbergs, or 'escarpment outliers' as they are sometimes known. The spurs and outliers are predominantly composed of schist but granite is exposed in places protruding above the surrounding metamorphic rocks displaying bornhardts characteristics (Selby 1977a). This was observed in the field near Chausib (Fig. 5.2). Selby (1977a) has reported that the height of inselbergs and bornhardts declines with distance from the escarpment front. Although large bornhardts do not occur near to the coast, a gradient was not obvious in the field and large bornhardts of similar size were observed in a zone 40 to 100 km from the coast during fieldwork.

Field observations and reports in the literature indicate that all granite bornhardts in the central Namib conform to Willis's (1934) description and have predominantly bare surfaces, one or more dome-like summits, steep sides and an overall absence of talus or soil cover. Geomorphic processes acting on the exposed bedrock surfaces include granular disintegration, small-scale laminar flaking, larger scale spalling of thick sheets and tafoni weathering (section 5.3.1). There is no evidence for any significant regolith accumulation around the base of inselbergs and they rise abruptly from pediments which have a gradient of 2°-6° (Selby 1977a, 1982a). The lack of talus or debris on the extensive bare rock slopes indicates that bornhardts are weathering limited landforms. Some of the larger granite inselbergs are delineated by major joints and the topographic boundary may also coincide with a geological boundary such as the edge of a granite intrusion (Selby 1977a; Ollier, 1978). However, others, such as Vogelfederberg, appear unrelated to geological boundaries as smooth granite of similar composition forms a bedrock pediment stretching away from the feature.

The bornhardts in the central Namib can be divided into two lithological groups (Selby, 1982b). The larger southern group includes the majority of bornhardts in the central Namib including all those sampled for this study. These features are composed predominantly of Donkerhuk granite of Namibian (late Precambrian) age. This is pale pink to grey porphyritic biotite granite which contains large phenocrysts of orthoclase and microline feldspar. The approximate composition of the rock is: quartz (20%), plagioclase (45%), orthoclase (22%) and mica (13%) (Selby 1977b). The northern group is smaller, containing Gross and Klein Spitzkoppe and its adjacent ridge the Pondok Mountains (Fig. 5.2). These are formed of Erongo Granite of Cretaceous age which was intruded into Old Granite of the Damara Sequence of late Precambrian age during the break-up of Gondwana (Selby, 1982b).

5.3.1 Weathering and Mass Wasting of Bornhardts in the Central Namib

A number of common physical weathering processes have been observed on the inselbergs of the central Namib (Goudie, 1972; Selby, 1977a, b, 1982a; Ollier, 1978). Granular disintegration and small-scale flaking appear to be the most prevalent small-scale processes on inselberg surfaces and affect all exposed rock types including gneiss, schist, sandstone and marble as well as granite (Ollier, 1978). The relative importance of these small-scale processes appears to be related to grain size with granular disintegration occurring preferentially on coarser-grained rocks (Selby, 1982a). Weathering pits up to 8 m long and 1 m deep observed on some Erongo Granite bornhardts in the Namib have been attributed in part to granular disintegration and laminar sheeting (Goudie and Migón, 1997). Tafoni-like weathering forms can be seen on the base slopes of some bornhardts and on the undersides of overhangs. Tafoni are weathering hollows that can occur in a variety of sizes. Clusters of small tafoni produce a honeycomb effect, but single hollows that range from a few centimetres deep on boulders to large individual caves and arches several meters high were also observed. Tafoni appear to be best developed in granite. Thin flakes and grus observable in tafoni hollows indicate that small-scale laminar sheeting and granular disintegration may be important in maintaining the weathering forms but their origin is uncertain. Salt weathering, case hardening and chemical action may all contribute (Goudie, 1972; Ollier, 1978). The sheltered conditions inside tafoni are likely to promote moisture and salt accumulation and tafoni weathering appears to exploit joints (Cooke *et al.*, 1993). A problem is deciphering the precise cause of the small-scale physical processes described above in that, unlike chemical weathering, they leave no unique indicators of their action. Comparison of small-scale laminar sheeting and granular disintegration in humid and arid environments has

shown that they are more active under dry conditions suggesting that chemical alteration of rock surfaces reduces the effectiveness of them (Selby, 1977b). Because small-scale sheeting is so prolific on granite, Selby (1977b) proposed than inherent properties of the rock may be an important contributing factor. Salts may also play an important role (Goudie *et al.,* 1997), (see below).

Exfoliated sheets of rock commonly ~0.5 m, but up to 2 m thick, are evident on most granite bornhardts in the central Namib. They spall off parallel to the rock surface and break up into boulders *in situ* or are removed from the slope surface by gradual gravity sliding or sudden rock falls. Part of a sheet that has slipped down the flank of Mirabib is visible in Figure 5.8. Exfoliation weathering, in which sheets of rock spall off, was traditionally attributed to thermally controlled expansion and contraction of the outer surface of rocks (insolation) but this has now largely been discredited as a major cause and is unlikely given that diurnal and annual temperature ranges in the Namib are small compared to other deserts or experimental test conditions (Goudie, 1972). Large-scale sheeting of the kind observable in the Namib is thought to be caused by pressure related volumetric changes due to unloading along pre-existing (primary) tectonically positioned joints or secondary unloading structures (Selby, 1977b and 1982a). Smaller-scale sheeting and disintegration of sheets is probably enhanced by hydration (Selby, 1977b).

The importance of salt weathering in desert environments is the subject of debate (see Doornkamp and Ibrahim (1990) and references therein). Controversy arose over the significance of experimental tests which were often criticised for not replicating real conditions in terms of the salts commonly found in deserts, realistic temperature and precipitation regimes and rock size and type (McGreevy and Smith, 1982; Smith and McGreevy, 1983). However, it is well established that salt weathering can promote rock break-up in three different physical ways; growth, hydration and thermal expansion of salt crystals (Goudie and Viles, 1997). Crystallisation of salts out of solution in cracks and pores produces high internal pressures pushing apart rock particles. Thermal expansion of salt crystals can have a similar effect if rock minerals expand less than the salt crystals. This has been shown to be the case for halite (NaCl) and granite (Cooke and Smalley, 1968). Hydration of salts increases their volume and can also increase pressure in rock pores. Salt crystallisation and hydration are commonly held to be most pervasive in deserts (Goudie, 1974; Cooke *et al.,* 1993). The main products of salt weathering are granular disintegration, flaking, blistering, swelling and cracking of rock surfaces and breakdown of sand into silt (Goudie *et al.,* 1979; Goudie, 1989). Tafoni weathering is also

thought to be indicative of salt attack (Bradley *et al.*, 1978) and may contribute to weathering pit formation (Goudie and Migón, 1997).

Conditions in the Namib are ideal for salt weathering given the high evaporation rates and high temperatures (Lancaster *et al.*, 1984), abundant exposed susceptible rock, high availability of salts due to proximity to the sea as well as extensive gypsum and other saline crusts and salt pans further inland (Gevers and Westhysen, 1931; Goudie, 1972; Watson, 1988). Fogs in the Namib have a high sulphate component which has been shown to be an effective agent of weathering in the form of sodium sulphate or magnesium sulphate (Goudie, 1972; Goudie *et al.*, 1997). Weathering products commonly attributed to salts (grus, rock flakes) are abundant and salt weathering has been cited as a major process. However, there are few empirical studies that have proved the association between salt and weathering in the Namib. One exception is the work of Goudie *et al.* (1997) who measured high rates of limestone block disintegration, due to halite crystallisation, over a two year period near the coast on a desert pavement surface. Goudie *et al.* (1997) suggest that salt weathering, specifically crystallisation induced by frequent wetting and drying cycles, is likely to be a major cause of rock break down and factor in the creation of subdued relief in the central Namib.

Small-scale solutional weathering features (rillenkaren) are visible on marble and limestone (Sweeting and Lancaster, 1982) but other chemical weathering in the Namib is minimal (Goudie, 1972). Varnish or case hardening on rock surfaces can involve slight chemical alteration of a micro-layer and is thought in part to be the result of biogenic processes. Orange/brown staining of granite is common on weathered exposed rock due to the release of ferric hydroxides from biotites but small-scale weathering products in the Namib show virtually no sign of any other chemical decomposition (Selby, 1977b). Spheroidal weathering is similar to flaking but the buried and exposed part of a rock is weathered around a corestone. It is indicative of chemical weathering but this process is conspicuously absent in the Namib supporting the view there is little active chemical weathering (Ollier, 1978). No other signs of past or present deep chemical weathering action or development of weathering mantles has been found anywhere in the central Namib despite extensive investigation (Selby, 1977a, 1982a, b).

Physical weathering processes account for almost all rock disintegration on bornhardts in the central Namib with the most important processes being granular disintegration, small-scale flaking, and spallation of rock sheets on inselbergs. The causes of these processes are uncertain but it seems likely that salt, rock tension and structural controls each play an important role.

Weathering appears to be active on all rock exposures regardless of lithology but there is no evidence for weathering action below the surface either active now or in the past. Weathering action is at its greatest along lines of rock weakness, in cracks and exposed joints.

5.4 Theories of Bornhardt Evolution

The origin and evolution of bornhardts remains a hotly debated subject. Thomas (1978, 1994) provides useful general reviews of the study of inselbergs and points out that in much of the literature, investigation has been restricted to landforms of crystalline rocks, most commonly granites and gneisses. In many cases, this has meant bornhardts in the strict sense. Opposing views of bornhardt development differ most fundamentally with respect to the importance of climate and climatic change. There is also significant debate as to the importance of structure, lithology and topographical setting. There are two principal theories which could explain the evolution of bornhardts in the Namib.

The first theory involves a two stage process of development whereby differential weathering of bedrock takes place initially under a deep weathering profile which is subsequently stripped following climatic change to reveal a landscape dotted with inselbergs. Linton (1955) was the first to suggest such a style of evolution in his classic paper on tor formation. He proposed that subsurface weathering processes preferentially exploited rocks with a closely spaced joint pattern. Inselbergs were masses of residual rock with a less dense joint pattern which had been less susceptible to subsurface weathering than the surrounding closely jointed planated rock. This hypothesis is closely linked to that of Büdel (1982) involving double planation surfaces and climatic controls and has been widely advocated in recent years (Cooke *et al.,* 1993). It is now generally thought chemical subsurface weathering penetrates existing joint systems exploiting weaker rock, but leaves resistant rock cores which are eventually exposed as high standing inselbergs when the overlying regolith is eroded away. The chemical weathering hypothesis was developed principally because inselbergs were associated with savannah landscapes rather than arid environments where they were assumed to be palaeoforms indicative of more humid conditions with more precipitation and deeper weathering profiles in the past. Flared slopes on some Australian inselberg have been explained as marking former levels of the weathering front in successive stages of bornhardt development through several climate cycles (Twidale and Bourne, 1975).

The debate over bornhardt formation has been mostly between the deep weathering hypothesis outlined above and an alternative view proposed by King (1948, 1966 and 1975). King's hypothesis (1948) differed most fundamentally in that he rejected any notion of subsurface weathering and excavation but advocated inselberg formation by subaerial, physical weathering processes in a landscape model of scarp retreat and backwearing under no specific climatic regime. King (1966) thought that the excavation hypothesis could not explain bornhardt covered landscapes in southern Africa because weathering mantles in excess of 20-30 m were rare but bornhardts up to 500 m high were common. This has been countered by the idea of multiple phases of chemical weathering and stripping and a great age for most bornhardts (Thomas, 1994) but there is little sign of chemical attack on many bornhardts in southern Africa. The excavation hypothesis depends on a model of vertical (Davisian) downwearing of the landscape which King (1962) rejected in favour of his own model of pediplanation and parallel slope retreat. Bornhardts and inselbergs surrounded by pediments were explained as the end products of a landscape cycle, simply as interfluve remnants which had been worn back sufficiently to leave residual resistant bedrock domes. King's (1948) model has since been supported by other workers, most notably Selby (1977a).

A third and more *ad hoc* hypothesis of selective mantle planation has also been proposed for inselbergs that correspond to geological boundaries (Ollier, 1978). Ollier (1978) thought that weathering-mantle controlled planation would reduce the level of a plain but the more durable rocks would be left as high standing residuals and rocks with low fissility such as granite would project as bornhardts. Selby (1982a) pointed out that this hypothesis was originally proposed by Mabutt (1966) and relies on compartmentation of deep weathering in the past to determine the main outlines of hills that are subsequently formed. It does not therefore differ substantially from the first hypothesis, but the notion of lithological resistance in influencing bornhardt location is useful and relevant in most theories of bornhardt evolution.

The deep weathering and excavation hypothesis of inselberg evolution was so widely accepted by geomorphologists that it almost became a geomorphological law (Selby, 1977a; Thomas, 1978). However, Selby (1977a) regarded one law for such a diverse set of landforms as too restrictive and used the concept of convergence or equifinality to propose that more than one set of processes could lead the formation of similar bornhardt features. Selby (1977a, 1982 a, b) carried out detailed examinations of inselbergs in the central Namib to test his theory and there now exists little controversy over the formation of bornhardts in the field area. Selby (1977a) rejected a hypothesis of deep weathering for bornhardts in the Namib for two reasons. Firstly,

there is a complete absence of chemically weathered regolith in the central Namib and no evidence of deep weathering has been found despite extensive field observations, mining and drilling for mining exploration (Selby, 1977a; Ward, 1987; Wilkinson, 1990). In other environments where weathering mantles are thought to have characterised inselberg evolution but where they are no longer buried or partially covered, there is often evidence for an old regolith cover in topographic hollows or river valleys (Twidale, 1976; Thomas, 1994). Also, the bornhardts show no signs of being chemically altered. Secondly, several lines of evidence suggest that the climate of the central Namib has been semi to hyper-arid for at least the last 10 Ma and possibly throughout most of the Tertiary (section 5.2.4). Deep chemical weathering does not occur under arid conditions and therefore a physical model of bornhardt formation was favoured for those found in the central Namib (Selby, 1977a, 1982b).

Selby (1982b) proposed that the overall form and location for the large majority of bornhardts in the central Namib was structurally determined (Selby, 1982b). There appeared to be some support for King's (1948, 1966, 1975) hypothesis of scarp retreat because rounded granite features could be seen in protruding spurs of the escarpment but there was no doubt that the overall form was structurally controlled (Selby 1977a, 1982b). Also, bornhardts in Namibia do not exhibit an obvious zonal distribution related to the current drainage network and therefore do not support King's (1948) idea that they are remnant interfluves, although drainage patterns may have changed. The domed form of bornhardts was attributed in part to the original form of the granite as it was intruded into Damaran mica schist and in part to large-scale sheeting along unloading structures parallel to the surface which preserved the original form (Selby, 1982b). Bornhardts were thought to be gradually exposed as surface physical weathering processes stripped surrounding schist, their locations determined by the position of discrete granite intrusions. Unequivocal evidence for this has been found for one unnamed granite dome near Amichab and Heinrichberg (Fig. 5.2) where schist conformably overlies partially exposed granite. The development of sheeting structures is also visible which will perpetuate the domed shape when the outer layers of schist are ultimately removed. It is likely that other domed granite bornhardts, although not displaying the same evidence, have also formed in this way. In general, Selby (1982b) thought that bornhardts exist because of high initial rock mass strength. This is gradually reduced by the development of orthogonal joints and the slope profile is adjusted so that the slope angle is in strength equilibrium with the new rock strength and the domed shape is lost as the bornhardt is progressively eroded. All non-granite inselbergs displayed slopes in equilibrium with their rock mass strength (Selby, 1982a). The complex multi-domed form of

some bornhardts can be explained by the intersection of orthogonal joints and non-parallel sheeting structures (Selby, 1982b).

Although the origin of bornhardts in the central Namib can now be better understood in terms of structural influences due to the detailed work of Selby (1977a, 1982b), some questions remain unanswered. For example, do the boundaries of all granite bornhardts coincide with geological or structural boundaries? Smooth granite bedrock is visible around the base of Vogelfederberg, implying that this is not true in at least one case and calls into question what controls the location of bornhardts. However, it is possible that the edges of granite intrusions are now some distance from the bornhardt because pedimentation combined with slope retreat or sheet spallation have reduced the areal extent of the inselberg (Büdel, 1982). Another uncertainty is how long these features have been in existence, although they are commonly thought of as old features, and how long they are likely to survive as upstanding features in a landscape of limited relief. Cosmogenic isotope analysis of granite bornhardts is capable of providing key insights into these issues by constraining long-term rates of denudation, their potential survival times and their mode of morphological evolution.

5.5 Sampling Sites and Strategy

Samples for cosmogenic isotope analysis were collected from three bornhardts within the Central Namib. The three sampling locations were Blutkopje, Vogelfederberg and Mirabib (Fig. 5.5). They were selected for a number of reasons. Most importantly because they are similar to, and therefore should be representative of, a large number of bornhardts and also to some extent the smaller-scale tor-like features and rock outcrops that occur throughout the central Namib. The sampling locations are spatially distinct being distributed about 50 km from each other in a zone 40-80 km from the coast, mid-way between the coast and the foot of the escarpment. They are similar in size but show some morphological differences. They all consist of Donkerhuk granite which is suitable for cosmogenic sampling. The following sections describe the location and morphology of the three bornhardts in detail. The overall sampling strategy is described in 5.5.4.

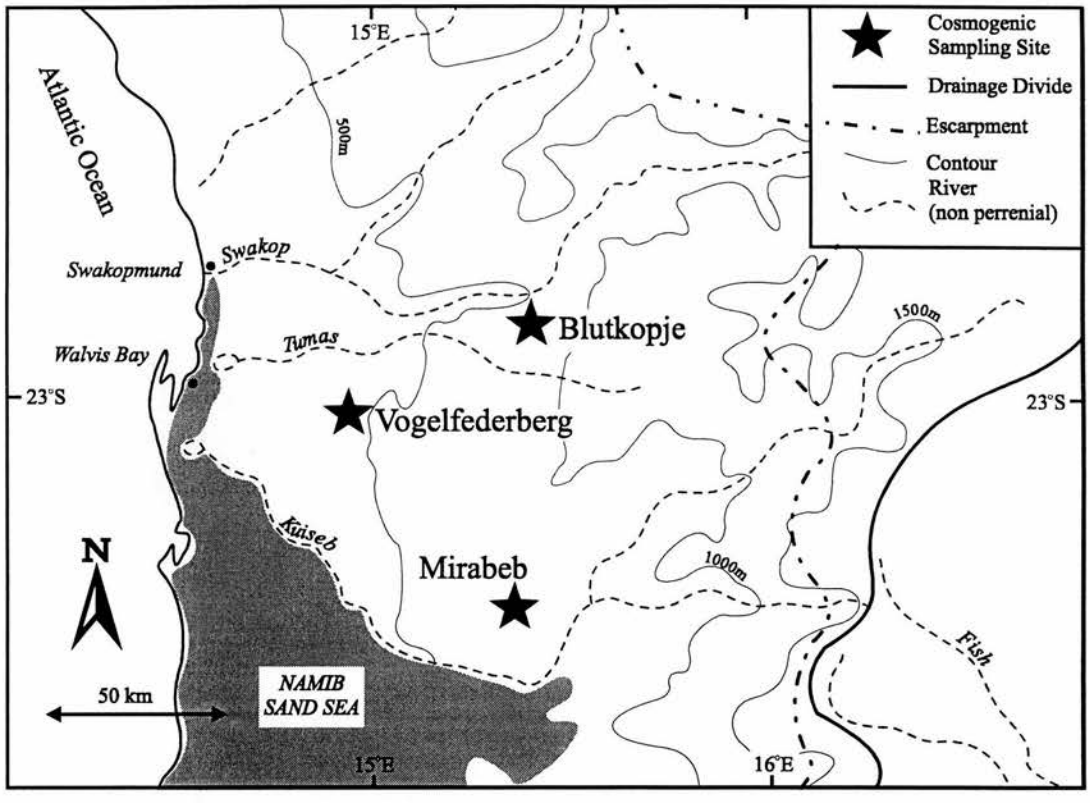

Figure 5.5: Map of the central Namib Desert showing the location of the three sampled bornhardts: Blutkopje, Vogelfederberg and Mirabib.

5.5.1 Blutkopje

Blutkopje, also known as Bloedkoppie, is located between the Swakop and Tumas rivers in the northern Namib-Naukluft park, central Namibia, situated at 22° 50' S and 15° 22' E (Fig. 5.5). It lies in the headwaters of the Gawib river, a 20 km long tributary of the Swakop, near to the local divide between the Tumas and Swakop catchments. It is 87 km inland from the coast and ~60 km west of the main escarpment. To the south of Blutkopje, the smooth, low-angled, gravel, desert plain, characteristic of this area, stretches 91 km to the Kuiseb canyon, interrupted only by ephemeral westward flowing tributaries of the Tumas and Kuiseb rivers. To the west, the Schieferberge, a 5 km^2 area of relief, is the only feature between Blutkopje and the coast across relatively smooth, 0.5° sloping, desert plains. 10 km to the north-west, Blutkopje is overshadowed by the Langer Heinrichberge, a large, 1152 m high mica schist inselberg immediately south of the Swakop river. Eastwards of the bornhardt, the desert plain rises gradually (<1° slope) over a distance of 60 km to the foot of the Khomas Hochland.

Figure 5.6: Blutkopje. Sampling locations are indicated.

Blutkopje is morphologically the most complex of the three sampled bornhardts. Figure 5.6 shows that its overall domed shape is divided into five ridges that decrease in size from east to west over a distance of ~500 m. The eastern end of the bornhardt has very steep sides whereas the western end has a gradual slope of 13°. The true summit of the bornhardt is the top of the eastern most ridge and was recorded in the field as 857 m. Altimeter readings at the base of the feature, revealed a maximum height above the surrounding pediment surface of 117 m. Between the ridges there is some debris accumulation that supports a little vegetation, but a large majority of the surface is remarkably smooth and exposed. Small-scale relief over the feature is varied and seems to be linked to the processes acting on the surface. There is micro-relief due to small-scale laminar sheeting of up to 100 mm thick. There are larger-scale sheets that appear to have spalled off and be disintegrating *in situ* that create relief of up to 2 m. Channel-like features 0.1 to 5 m deep and wide forming quasi-dendritic patterns show evidence for fluvial incision processes. The ridges themselves that are divided by chasms up to 30 m deep that could also be the result of fluvial incision processes taking advantage of large-scale jointing or veins of weakness. There are several boulders that have been isolated on pedestals, in particular on the

highest ridge there is one such isolated boulder 3.2 m in diameter. Around the base of the bornhardt there is variable debris accumulation and evidence of tafoni weathering. The bornhardt consists of grey to pink biotite granite crossed by small quartz veins and veins of larger crystal size, both of which appear relatively resistant to denudation and form small ridges (<0.5 m high) over the surface.

5.5.2 Vogelfederberg

Vogelfederberg is located 32 km to the southeast of Blutkopje, at 23° 03' S and 14° 59' E. It is situated 58 km from the present-day coastline and ~110 km from the main escarpment. It lies on the divide between the Tumas and Kuiseb river catchments. The landscape around the bornhardt is a large, extremely low relief desert plain. To the east, the plain rises gradually with a gradient of <1° towards the foot of the escarpment in the vicinity of the Gamsberg. For 50 km to the north, south and west, the only relief other than the barely perceptible broad undulations from the ephemeral river systems, are similar inselbergs, for example Chungochoab 20 km south, Swartbankberg 35 km south-west, Hamiltonberg 10 km west as well as numerous other smaller, unnamed inselberg and tor-like features (Fig. 5.2).

Vogelfederberg is a classic example of a rounded dark grey biotite granite bornhardt and is morphologically simpler than Blutkopje. It is actually composed of two similar sized distinct domes separated by ~ 40 m of highly denuded rock that has been planed off to within two meters of the level of the surrounding plain. Vogelfederberg can therefore be considered as two bornhardts, both are simple half egg-shapes and one is slightly higher than the other. The higher dome has steeper sides and is ~ 80 m high. It has a smooth profile that tapers more gradually to the west than east. The second dome (Fig. 5.7) is broader and flatter and slightly more complex with some boulders and debris on its flanks. Erosional processes have cut horizontally in to the northern flank and created an overhang 30 m long and ~7 m high. There is evidence of tafoni weathering under the overhang as well as near the base of the feature on the southern side. Both domes have clearly developed channel features with a quasi-dendritic planform, from <1 m to >5 m deep, down their flanks. There is some very limited debris accumulation within the channel features. There is little evidence for large-scale sheeting as was seen at Blutkopje, and overall small-scale sheeting appears to be less prolific here than at Blutkopje. The main weathering process appears to be granular disintegration.

Figure 5.7 (overleaf): Photo montage of Vogelfederberg. Sampling locations are indicated.

16A
16B

5.5.3 Mirabib

Mirabib, alternatively called Mirabeb, Hirabib or Anachankiab, is situated 70 km almost directly south of Blutkopje and 58 km south east of Vogelfederberg at 23° 27' S and 15° 21' E. It is 92 km inland from the coast and ~90 km from the main escarpment. It lies within the Kuiseb river catchment 26 km from the main river channel at Homeb. The surrounding landscape is very similar to that which surrounds all the isolated bornhardts of the area; a low relief desert plain with a shallow gradient (<2°) from the foot of the escarpment and its outliers to the coast. It comprises large areas of desert pavement, exposed, flat, granite bedrock, other low relief bedrock features, areas of sand and loose debris cover, dry river channels of limited incision and virtually no vegetation cover. Mirabib is the closest sampling site to the extensive Namib Sand Sea which presently terminates at the Kuiseb. There are no other named inselbergs within a 25 km radius.

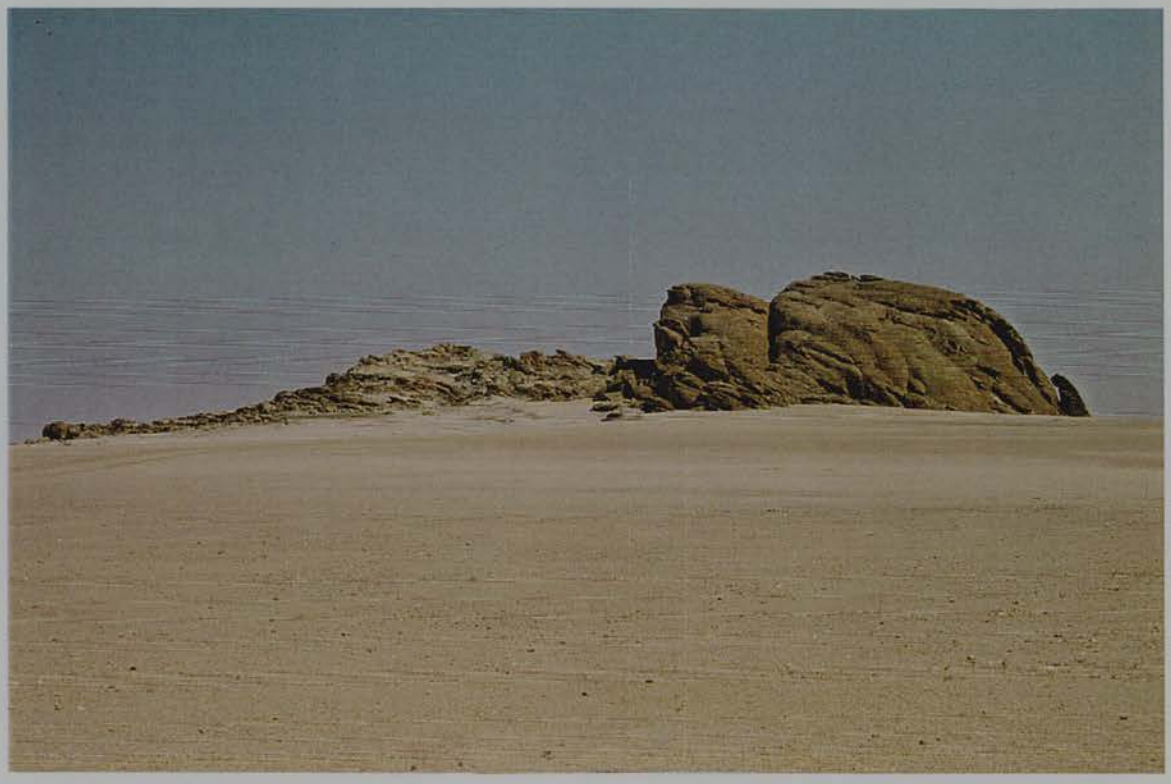

Figure 5.8: Mirabib. View looking west.

Mirabib is a complex feature but has two principal domed summits separated by a deep but very narrow gorge/joint-like fissure (Fig 5.8). The higher dome is the furthest west portion of the bornhardt and has a very steep side with tafoni weathering on an undercut (Fig. 5.9). It is ~100 m high (Selby 1982b) but the true summit of the bornhardt was inaccessible preventing an altimeter reading in the field. The rounded bornhardt section of Mirabib is made of massive Donkerhuk granite and has very steep sides (>80°). There is evidence for spalled sheets and blocks up to 3 m thick lying around the base of the domes as well as a partially detached sheet on the lower dome. Approximately half of the basal area of Mirabib consists of highly weathered gneiss and schistose granite separated from the domed part by a pegmatite dyke. The more denuded part is only ~40 m above the surrounding pediment and has more talus than the domed part. This creates a tail-like feature when viewed from west to east (Selby, 1982b).

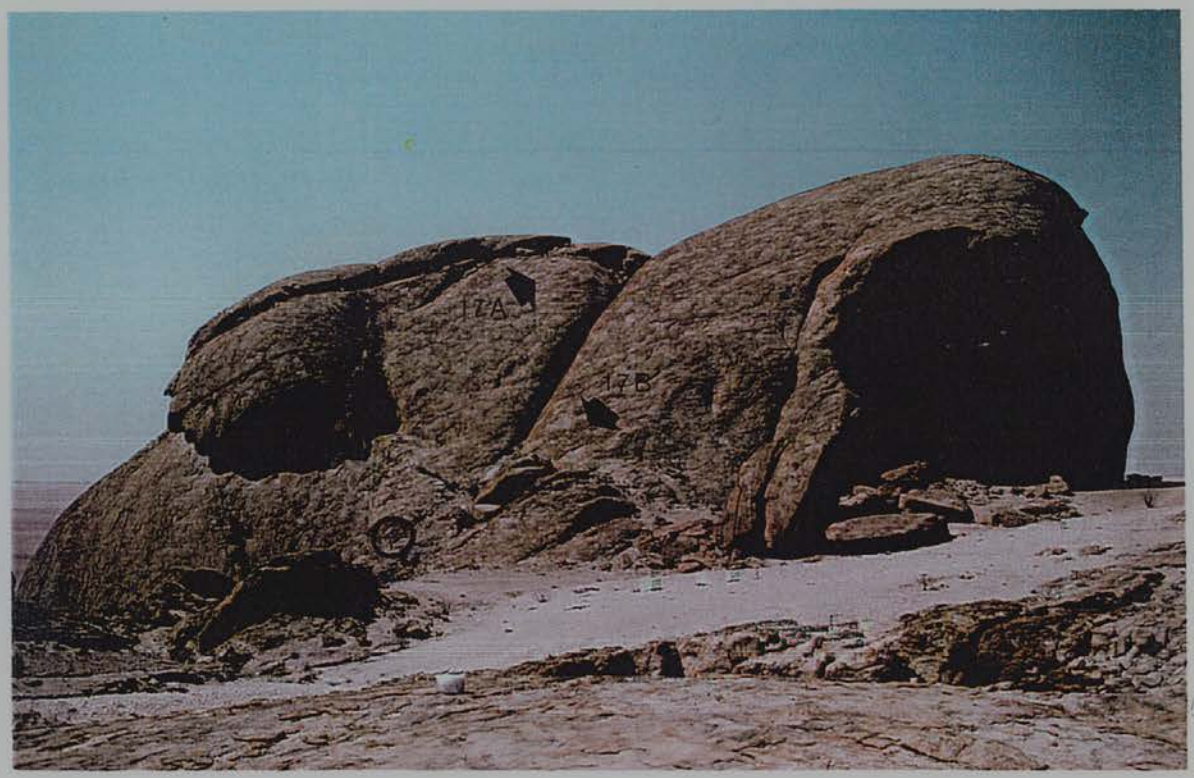

Figure 5.9: Mirabib. View looking east, sampling locations are indicated. (Figure circled for scale.)

5.5.4 *Sampling Strategy*

Several samples were collected from each bornhardt using similar sampling criteria to those described in section 3.2. Lack of vegetation and significant debris accumulation meant that large areas were suitable. Small-scale laminar sheeting facilitated collection of thin surface samples (Fig. 5.10). Two samples from each location were chosen for analysis. All six samples were surface bedrock less than 30 mm thick. At Blutkopje, two of the ridge summits were sampled (Fig. 5.6). Similarly at Vogelfederberg, samples were collected from crests on the summit of the lower dome (Fig. 5.7). All four of these samples had full exposure geometry and were collected from flat surfaces (Table 5.2). At Mirabib, one summit sample was taken from the lower dome and one sample was taken from the steeply dipping flank of the second dome, 6 m above the surrounding ground surface (Fig. 5.9). Both these samples were taken from dipped surfaces with partial topographic shielding (Table 5.2).

Samples were collected in this way for several reasons. Firstly, sampling ridge summits of three distinct bornhardts would provide directly comparable denudation rate data to monitor spatial variability. Secondly, by collecting two samples at Blutkopje and Vogelfederberg, variability across an individual bornhardt upper surface could be assessed. Thirdly, collection of one summit and one flank sample at Mirabib would yield additional information on bornhardt evolution and the relative importance of denudation over an entire feature. Because the bornhardts are similar in size and lithology, these factors can be eliminated as reasons for any variation found in the data.

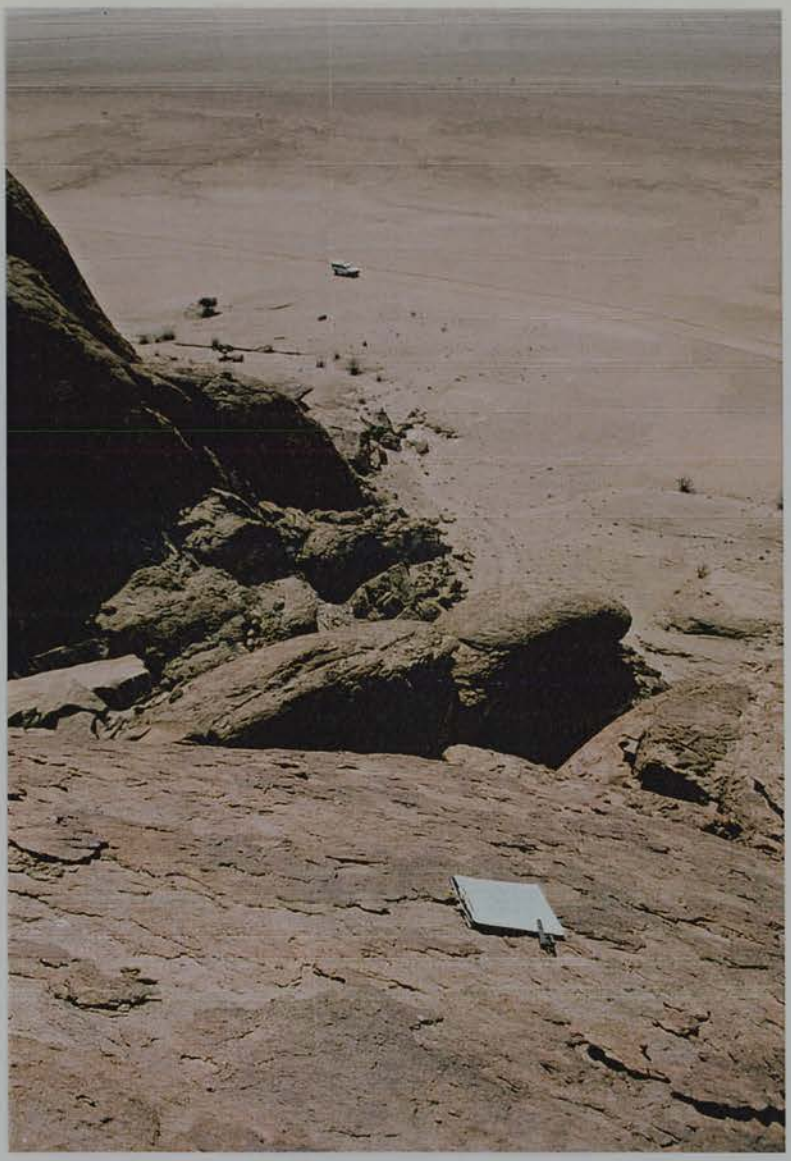

Figure 5.10: Close of sample 17A in situ on the surface of Mirabib. (Vehicle in background for scale)

Table 5.2: Sample and field data for Namibian bornhardt samples.

Sample Number	Sample Site	Location Long. & Lat.	Altitude (m)	Lithology	Surface Slope (°)	*Exposure Geometry
15A	Blutkopje	15° 22' 58"E 22° 50' 36"S	849	grey to pink granite	0	full exposure
15B	Blutkopje	15° 22' 56"E 22° 50' 33"S	846	as above	0	full exposure
16A	Vogelfederberg	14° 59' 12"E 23° 03' 22"S	531	dark grey biotite granite	0	full exposure
16B	Vogelfederberg	14° 59' 12"E 23° 03' 23"S	520	as above	0	full exposure
17A	Mirabib	15° 21' 35"E 23° 27' 08"S	785	grey to pink biotite granite	28	partial shielding
17B	Mirabib	15° 21' 27"E 23° 27' 04"S	750	as above	55	partial shielding

*For full exposure geometry see Appendix A.

5.6 Analysis, Results and Interpretation

Samples were prepared according to the final methodology described in Chapter 3 (Fig. 3.3). Total Al measurements were performed by graphite furnace atomic absorption spectrometry (GFAAS) at the Department of Geology and Geophysics, University of Edinburgh. $^{10}Be/^{9}Be$ and $^{26}Al/^{27}Al$ ratios were measured by AMS at the Center for Accelerator Mass Spectrometry, Lawrence Livermore National Laboratory.

Corrected production rates for the bornhardt sites are shown in Table 5.3 and were subsequently used throughout in data interpretation. The basic production rates in quartz of 6 (^{10}Be) and 36.8 (^{26}Al) atoms g^{-1} a^{-1} for sea level and high latitude (>60°) from Nishiizumi *et al.* (1989a) were used. Although there have been recent attempts to refine these production rates (e.g. Nishiizumi *et al.*, 1996) the original estimates have been retained for comparative purposes. Production rates were corrected for the effects of latitude and altitude according to the polynomial from Lal 1991 (section 2.2.7). Production rates were also corrected, where necessary, for the dip of the sampled surface and the effects of topographic shielding based on the angular dependence of cosmic radiation (section 2.2.6; Nishiizumi *et al.*, 1989a; Cerling and Craig, 1994). Exposure geometry shielding correction factors for samples 17A and 17B are shown in Table 5.3. It was assumed that the present-day geographic latitude of the samples equals the average geomagnetic latitude of the sampling sites, integrated over their full exposure time (section 2.2.5). No other corrections on the production rates were made but a 20% error was included in the final rates used to calculate denudation rates in order to compensate for present levels of uncertainty (Gosse *et al.*, 1996).

Table 5.3: ^{10}Be and ^{26}Al production rates for bornhardt samples corrected for the effect of topographic shielding and the dip of the sampled surface.

Sample Number	Scaled Production Rate		Correction Factor for Partial Shielding	Corrected Production Rate Including 20% Error	
	^{10}Be	^{26}Al		^{10}Be	^{26}Al
15A	7.8	47.53	1	7.8 ± 1.5	47.53 ± 9.5
15B	7.8	47.42	1	7.8 ± 1.6	47.42 ± 9.5
16A	6.4	38.76	1	6.4 ± 1.3	38.76 ± 7.5
16B	6.3	38.46	1	6.3 ± 1.3	38.46 ± 7.7
17A	7.6	46.48	0.988	7.5 ± 1.4	45.92 ± 8.8
17B	7.4	45.33	0.936	6.9 ± 1.3	42.42 ± 8.0

The results of GFAAS analysis of the total ^{27}Al content on sample aliquots are shown in Table 5.4. The method of standard additions was used to improve the accuracy of the data; 3 additions were used (section 3.4.6). The first addition was of a blank solution, the second was 100 ppb and the third was 200 ppb. All the samples had very similar ^{27}Al contents; this similarity supports the assumption that Al was retained quantitatively during sample dissolution and initial fuming (section 3.3.2.1). An overall ±5% uncertainty was included in the total ^{27}Al concentration and subsequent calculations.

Table 5.4: GFAAS results of total Al measurement for bornhardt samples.

Sample Number	Mass of Quartz/g	GFAAS results/ppb	Total Al in sample/mg	Al content of SiO_2/ppm
15A	29.44153	88.1	0.90	30.52 ± 1.5
15B	30.10317	92.4	0.94	31.31 ± 1.6
16A	28.42626	81.6	0.83	29.28 ± 1.5
16B	25.35027	71.64	0.73	28.83 ± 1.4
17A	25.75000	90.133	0.91	35.70 ± 1.8
17B	21.02916	73.54	0.75	35.67 ± 1.8

* Samples were dissolved in 100 ml of weak acid and diluted by a factor of 9.8×10^{-3}.

Isotopic ratios and denudation rates for the six bornhardt samples are shown in Table 5.5. Denudation rates were calculated assuming secular equilibrium had been reached and that denudation was steady-state such that (Lal, 1991):

$$\varepsilon = \frac{\Lambda}{\rho}\left(\frac{P}{N} - \lambda\right) \qquad [5.1]$$

where N is the concentration of the cosmogenic isotope (atoms g^{-1} SiO_2), P is the production rate (atoms g^{-1} SiO_2 a^{-1}), λ is the decay constant of the radionuclide (a^{-1}), Λ is the cosmic ray attenuation coefficient in quartz (150 g cm^{-2}), ρ is the rock density (2.7 g cm^{-3}) and ε is the maximum steady-state erosion (denudation) rate (cm a^{-1}) (Lal, 1991, Brown *et al.*, 1992). The isotopic ratios have been background corrected from process blank measurements and have also been normalised to standard samples prepared at LLNL (LLNLSTD 100000, $^{10}Be/^{9}Be=1.00 \times 10^{-11}$; KNSTD 5000, $^{26}Al/^{27}Al=5.00 \times 10^{-12}$). The process blank ratios were $7.2 \times 10^{-15} \pm 1.2 \times 10^{-15}$ for Be and $1.165 \times 10^{-14} \pm 8.3 \times 10^{-15}$ for Al. There were no spurious counts due to boron for any of the samples but the process blank was subject to a 19% boron correction. Measurement error on the AMS ratios is quoted at 1σ in Table 5.5 as this is the convention when reporting cosmogenic isotope data. The errors are low, ranging from less than 2.5 to ~ 4%.

Uncertainty in the nuclide concentration (N) and $^{26}Al/^{10}Be$ ratio is quoted at 2 σ and include 5% on the total ^{27}Al concentrations (95% confidence limit). Propagated error in the denudation rates includes the error on N as well as a 20% error in the production rate values used. The data are displayed in a bar graph in Figure 5.10 and on an erosion-island graph (Lal, 1991) in Figure 5.11 (in both cases plotted with 2σ error bars).

Table 5.5: ^{10}Be and ^{26}Al cosmogenic isotope data and denudation rates for Namibian bornhardt samples.

Sample Site and Number	Background Corrected $^{10}Be/^{9}Be$, $^{26}Al/^{27}Al$ AMS Ratio	^{10}Be Concentration (N) (10^6 at. g^{-1} SiO2)	^{26}Al Concentration (N) (10^6 at. g^{-1} SiO2)	$^{26}Al/^{10}Be$	^{10}Be ε m Ma^{-1}	^{26}Al ε m Ma^{-1}
Blutkopje						
15A	$6.41 \times 10^{-13} \pm 1.6 \times 10^{-14}$ $4.88 \times 10^{-12} \pm 1.9 \times 10^{-13}$	0.73 ± 0.3	3.32 ± 0.3	4.55 ± 0.5	5.71 ± 1.2	7.43 ± 1.6
15B	$1.41 \times 10^{-12} \pm 3.4 \times 10^{-14}$ $9.15 \times 10^{-12} \pm 2.3 \times 10^{-13}$	1.56 ± 0.07	6.36 ± 0.6	4.07 ± 0.5	2.51 ± 0.5	3.60 ± 0.8
Vogelfederberg						
16A	$5.75 \times ^{-13} \pm 2.1 \times 10^{-14}$ $4.57 \times 10^{-12} \pm 1.5 \times 10^{-13}$	0.68 ± 0.04	2.98 ± 0.3	4.40 ± 0.6	4.96 ± 1.1	6.69 ± 1.5
16B	$4.92 \times 10^{-13} \pm 1.2 \times 10^{-14}$ $5.57 \times 10^{-12} \pm 3.4 \times 10^{-13}$	0.65 ± 0.03	3.57 ± 0.4	5.51 ± 0.6	5.14 ± 1.1	5.45 ± 1.2
Mirabib						
17A (summit)	$1.01 \times 10^{-12} \pm 2.4 \times 10^{-14}$ $8.94 \times 10^{-12} \pm 3.2 \times 10^{-13}$	1.32 ± 0.06	7.09 ± 0.7	$5\ 37 \pm 0.6$	2.89 ± 0.6	3.06 ± 0.7
17B (flank)	$4.00 \times 10^{-13} \pm 1.2 \times 10^{-14}$ $4.23 \times 10^{-12} \pm 1.6 \times 10^{-13}$	0.64 ± 0.03	3.36 ± 0.03	5.28 ± 0.3	5.78 ± 1.2	6.48 ± 1.4

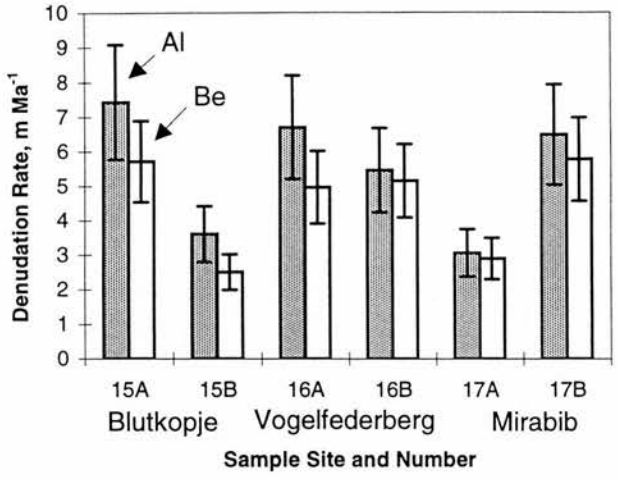

Figure 5.11: ^{10}Be and ^{26}Al denudation rates for bornhardt samples. 2σ error bars are shown.

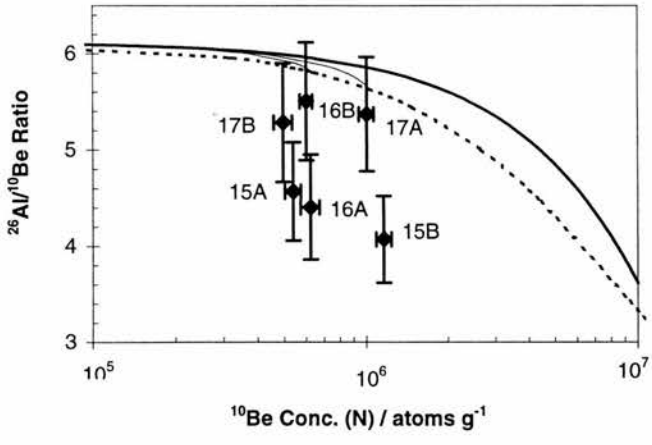

Figure 5.12: Erosion-island graph of $^{26}Al/^{10}Be$ against ^{10}Be. Concentrations have been normalised to sea level and high latitude. Curves within the erosion-island represent lines of 3 m Ma^{-1} (upper) and 5 m Ma^{-1} (lower). Data that plot below the erosion-island indicate a complex exposure history.

The denudation rates calculated from ^{10}Be and ^{26}Al concentrations overlap within error for all samples (Table 5.5, Fig. 5.11). The overall variation between samples is relatively small; the lowest measured rate is 2.51 ± 0.5 m Ma^{-1} from the summit of Blutkopje (15B, Be) whereas the highest rate, also from the summit of Blutkopje (15A, Al), is 7.43 ± 1.6 m Ma^{-1} and is therefore within the same order of magnitude. There appears to be no discernible trends in the data that could relate to spatial or lithological differences between the three bornhardts. Two of the summit samples (16B and 17A) show a very close agreement between denudation rates based on ^{10}Be and ^{26}Al and plot sufficiently close to the erosion island (Fig. 5.12) to suggest that they have been subject to a simple denudation history and uniform denudational processes. Sample 16B from the summit of Vogelfederberg yielded steady-state denudation rates of 5.14 ± 1.1 m Ma^{-1} (Be) and 5.45 ± 1.2 m Ma^{-1} (Al), whereas 17A indicates denudation rates for the summit of Mirabib of 2.8 ± 0.6 m Ma^{-1} (Be) and 3.06 ± 0.7 m Ma^{-1} (Al). Although these samples could be

interpreted as supporting saturation of the nuclides (by plotting on the lower limit of the erosion-island), this cannot be unequivocally tested as the error bars are large, these rates should therefore be considered as maxima. Sample 17B from the flank of Mirabib shows some evidence for a simple denudation history from its position on the erosion island plot; however, it is more likely that this sample has experienced some complexity in its exposure history in the form of temporary burial or removal of a layer of rock greater than the attenuation length (Lal 1991, Small *et al.,* 1997). The impact that steeply angled surfaces may have on the applicability of the steady-state erosion model (Lal, 1991) have been discussed in section 4.7.1 and it is possible that the relatively high surface angle of site 17B (55°) will introduce further error. However, the error in calculated rates is <10% for angles up to 45°, and given that the rates include an error of ~20%, this extra source of error may not be significant. Calculated rates at this site range from 5.78 ± 1.2 m Ma^{-1} (Be) to 6.48 ± 1.4 m Ma^{-1} (Al).

The data for the other three sites (15A, 15B and 16A) plot well below the erosion island and must therefore have experienced complex exposure histories (2.4.4). Reasons for their apparently complex history are discussed below in section 5.7.1 but it should be noted here that although rates of this kind have usually been classified as maximum rates always higher than the 'true' rate, it is possible that they are lower than the actual rate if operating erosional processes have not been uniform and steady (Lal 1991, Small *et al.,* 1997). Under these circumstances, rates calculated assuming secular equilibrium and steady-state denudation may be >20% different from the true rate and an average rate from different samples and isotopes is likely to be the best approximation (Small *et al.,* 1997). We infer ^{10}Be and ^{27}Al average rates of denudation for the summit of Blutkopje of ~5 m Ma^{-1}, while a second sample from Vogelfederberg yields a denudation rate of ~6 m Ma^{-1}. In order to satisfy the assumption of prolonged denudation and secular equilibrium inherent in equation 5.1, these rates are necessarily integrated over the past 3-6 x 10^5 a (section 2.4.3).

5.7 Discussion

5.7.1 Implications for Bornhardt Denudation in the Central Namib

The denudation rates measured for the three bornhardts show a remarkable consistency suggesting that the results may be broadly typical of rates of granite inselberg denudation in this environment. Irrespective of the evidence for complex exposure in some of our samples (Fig. 5.12), there is similarity in the concentrations of ^{10}Be and ^{26}Al in all of them suggesting that they

may have had broadly similar residence times in the upper layers of the three bornhardts. Figure 5.2 demonstrates the large number of inselbergs, many of them granite, that are distributed throughout the coastal plain. Whether or not the data are truly representative would obviously require more extensive sampling, however, the sites investigated here span an east-west distance of ~50 km and a north-south distance of ~80 km with no spatial trend in the data indicating that a rate of approximately 2 to 8 m Ma^{-1} is representative of similar sized granite features in the immediate vicinity at least.

The two samples (16B and 17A) that plot within the erosion-island support a simple model of uniform, steady-state denudation with continuous removal of thin rock layers and indicate that at least one of the assumptions of equation 5.1 is satisfied, whereas, the other samples indicate a more complex history over the past 3-6 x 10^5 a. There is no unique solution, mathematical or geomorphic, for a position below the erosion-island and any number of combinations of burial and exposure could produce the same location on the graph (Lal, 1991). However, there appear to be three possible explanations that could reasonably explain the data: burial by the development of a deep weathering mantle, burial by dunes from the Namib erg to the south (Fig. 5.5), burial and/or non-uniform denudation related to local processes of inselberg mass wasting.

The development, and subsequent etching, of a thick weathering mantle is clearly a component of inselberg evolution in some environments (section 5.4; Selby, 1977b; Thomas, 1994). However, it appears inapplicable in this case for two reasons. First, no such regolith has been recorded in the central Namib despite field observations, extensive drilling and excavation for mining exploration (Selby, 1977a, 1982a, b). Secondly, there has been a persistent arid climate since at least the late Miocene (section 5.2.4). Formation of weathering mantles implies chemical action at a weathering front but chemical weathering is dependent on humid conditions. The climate of central Namibia has not been significantly more humid than semi-arid for at least 10 Ma therefore the formation of a weathering mantle cannot explain the observed complexity in the data, especially given the considerable height of ~100 m of the samples above the surrounding plain.

The northern limit of the Namib erg, which contains dunes up to 300 m high, is presently demarcated by the Kuiseb River and is located only 25 km south of Mirabib, the most southerly sampled bornhardt (Figs. 5.4 and 5.5). The annual resultant drift directions of the northern part of the erg are to the north or north-east and although the maximum rate of advance into the Kuiseb River is mostly well below 1 m a^{-1}, higher rates have been recorded (Lancaster, 1989).

Partial or complete burial of bornhardts intermittently by sand in the central Namib in the past is therefore a possibility, particularly if wind regimes were strengthened during glacial episodes and the erg was more mobile. At present, however, there are no significant sand accumulations near any of the sampled bornhardts, or within the study area as a whole, and dune encroachment seems an unlikely explanation of exposure complexity for two reasons. Firstly, sand movement across the Kuiseb River Valley and into the study area is hard to account for. Although flow is highly ephemeral, the power of the Kuiseb River to hold back encroaching dunes in the recent past is apparent and occasional strong northerly berg winds help to restrain the dunes. The north-west directional trend of the lower section of the Kuiseb river from Hudaob to the coast may indicate a gradual northward forcing of the river by the dune field during the Quaternary (Marker, 1977) but the Kuiseb is thought to have the formed a successful northern boundary to sand from the Namib erg since at least early Pleistocene times (Ward, 1984, 1987). An exception to this is the 5 km wide coastal dune field between Walvis Bay and Swakopmund which represents a break through on behalf of mobile dunes in the Kuiseb delta/mouth area. Brain and Brain (1977) examined vertebrate fossils in owl pellets and concluded there was no evidence for a northward shift of dunes in the vicinity of Mirabib during the Holocene. The second reason comes from the cosmogenic data itself. A lack of unequivocal evidence of burial from the ^{10}Be and ^{26}Al data for both the flank and summit of Mirabib suggests that sand has not covered the bornhardt despite Mirabib being the closest to the northern edge of the sand sea and therefore the most vulnerable inselberg to dune encroachment of those studied. Contrasting complex and simple exposure histories recorded for samples collected just a few meters apart on the summit of Vogelfederberg (15A and 15B) also suggests that sand has not covered the bornhardt and therefore could not have produced complexity in the exposure history.

The close proximity of buried and continuously exposed samples argues for an explanation of complex exposure related to the mode of inselberg degradation. Field observations of our sampled bornhardts and other granite inselbergs in the central Namib revealed two scales of weathering and mass movement. At the small scale, there is granular disintegration and displacement of thin (<50 mm thick) laminar sheets. At the larger scale, <2 m thick sheets or blocks spall off; these appear to break up *in situ* and are then removed by either rock falls on steep slopes or by gradual creep and disintegration at lower gradients (Selby, 1982a, b). Where slow lateral movement of blocks and sheets occurs, exposed bedrock surfaces would be temporarily shielded from cosmic radiation. Toppling and gradual movement of pedestal boulders, which is clearly evident on Blutkopje, could also temporarily shield parts of bornhardt surfaces. During burial, ^{26}Al would decay faster than ^{10}Be leading to a drop of the isotope ratio

and therefore the evidence for complex exposure on the erosion-island plot (Fig. 5.12). Disintegration of blocks and sheets *in situ* into grus and finer material that may then become mobile debris across the bornhardt surface could also provide temporary shielding of a sampled surface. Debris of this kind is ultimately removed by wind or surface wash. Evidence for surface wash is in the form of quasi-dendritic gully systems up to 5 m deep that are visible on all three sampled bornhardts. Given the rarity of significant surface wash events in the Namib (section 5.5.1), the presence of these incised gullies lend qualitative support for stability of bornhardt surfaces and slow rates of denudation.

It has recently been shown explicitly by Small *et al.* (1997) how non-uniform erosional processes can affect cosmogenic isotope data and the position of samples plotted on an erosion-island graph. In their analysis they demonstrated that a position below the erosion island may reflect removal of a thick layer or layers of rock compared to the smaller scale continuous removal necessary for the sample to plot within the island (section 2.4.4). During such an event, ^{10}Be concentrations would drop in the newly exposed surface sample but the $^{26}Al/^{10}Be$ ratio would not drop significantly provided that denudation rates are fast (> 1m Ma^{-1}) and the removed rock layer is a similar order of magnitude to Λ/ρ (~0.5 m). Lal (1991) proposed that if a single 'chip event' disrupted a steady-state denudational process then the measured denudation rate would always be higher than or equal to the true continuous rate. Hence it is common for cosmogenic denudation rates to be considered maxima with respect to the steady-state denudation assumption. However, Small *et al.* (1997) have shown that if chipping events are more frequent then a measured rate may be lower than the true rate. Under such circumstances, as previously mentioned, error on a single measurement can be high (>20%), but the mean value of several samples is likely to give a more accurate representation of the true denudation rate so long as the chipping events are not synchronous for all samples (Small *et al.*, 1997).

Given that we have field evidence for potential burial as well as large 'chip' events from three different bornhardts it seems likely that complexity in our samples is from a combination of both mechanisms. What then is the true rate of granite inselberg denudation in the central Namib? Because a large uncertainty (±20%) in production rates has already been included in the rate estimates, there is overall close agreement between the data, and burial and sheeting both appear to be important, an average rate seems the most appropriate. The average of all the denudation rates is 4.98 ± 1 m Ma^{-1}, excluding the flank sample at Mirabib the average summit lowering rate is 4.74 ± 0.9 m Ma^{-1}.

The difference between rates for the flank and summit sample from Mirabib is approximately a factor of two with rates ranging from ~6 m Ma^{-1} on the flank to ~3 m Ma^{-1} on the summit. Although the rate for the flank should be treated with come caution and equally diverse rates have been measured on the summit of Blutkopje, a similar differential between summit and flank samples was also found by Bierman and Turner (1995) who investigated rates on denudation on Australian granite inselbergs using cosmogenic ^{10}Be and ^{26}Al. Based on the relative difference between the flank and summit samples, some tentative inferences can be made. The data from Mirabib support a model of preferential backwearing of bornhardt slopes compared to downwearing of inselberg summits. Through time, the height to width ratio of the bornhardt should therefore increase before the bornhardt is finally denuded. Higher rates of denudation, as might be expected, are associated with higher slope gradients. Preferential backwearing in landform evolution is integral to the hypothesis of landscape development proposed by King (1948, 1966, 1975) and his theory of bornhardt evolution, but given the apparent structural control on the location of bornhardts in the Namib, support for King's theory is weak. Although, small-scale processes may be sensitive to surface slope and produce a relative difference between the rates calculated from flank and summit samples, large-scale sheeting, thought to be controlled by pre-existing parallel sheeting structures, is unlikely to preserve the differential.

5.7.2 Comparisons with Other Cosmogenic Denudation Rate Data

A study of inselberg denudation in the Eyre Peninsula, south-central Australia using cosmogenic ^{10}Be and ^{26}Al has been carried out by Bierman and Turner (1995). Of all the erosion rate studies reviewed in section 2.5.3, this is the only one that is directly comparable because of the similar geomorphic setting of the sampling locations. Data from the summits of six granite inselbergs (one sample per inselberg) yielded an average summit lowering rate of 0.7 ± 0.1 m Ma^{-1} ranging from 0.56 to 0.96 m Ma^{-1}. The reasons for the order of magnitude difference between the rates reported here for the central Namib and those from very similar features in Australia are not clear. The distribution and overall strategy of their samples appears to be directly comparable to those from the Namib. It is reasonable to expect subtle lithological differences between the two types of granite but these are unlikely to have had a profound effect on the measured rates particularly given that within the Namibian samples crystal size was variable but exerted no apparent control on the rates. Of the factors that may control denudation at each location, climate shows the greatest contrast. The climate of the Eyre Peninsula was described as semi-arid by Bierman and Turner (1995) but is significantly more humid than the central Namib. Mean annual rainfall in their sampling area is >350 mm a^{-1} (29 year record), a large majority of which

falls in the winter (Gentilli, 1971). Temperatures range from a daily maximum of ~25°C in January to a mean daily minimum in July of ~5°C but rarely drop below 0°C. It is perhaps surprising therefore that cosmogenic rates from the Namib, which has been more consistently arid, are all significantly higher than rates from the Eyre Peninsula.

A possible explanation for the large difference in measured rates between this study and that of Bierman and Turner (1995) involves fog precipitation. As discussed in section 5.2.3, fog is a distinctive feature of the climate of the Namib Desert but occurs, on average, less than one day a year in the Eyre Peninsula (Gentilli, 1971). In Namibia, fog precipitation occurs much more frequently than rain and reaches a maximum ~50 km inland in the vicinity of the study area (Lancaster *et al.*, 1984). Due to high evaporation rates, wetting and drying cycles from fog events are very frequent. Fog has been implicated as a principal controlling factor of aggressive salt weathering conditions found in the central Namib by supplying a frequent source of both salts and moisture (Goudie and Viles, 1997). High rock disintegration rates from salt crystallisation have been measured in the coastal Namib and granite is generally thought of a sensitive to salt attack (Goudie, 1972; Goudie *et al.*, 1997). Other physical weathering processes that speed up in the presence of a frequent moisture input and wetting and drying cycles include hydration and insolation. Although no salt precipitates were obvious in the samples analysed from the bornhardts, it is possible that fog precipitation enhances the effectiveness of weathering processes that rely on a regular supply of moisture. This relationship may be reflected in high denudation rates of granite in the Namib of ~5 m Ma^{-1} compared with much lower rates measured in samples from the Eyre Peninsula, Australia where the moisture input regime is more sporadic.

To date, there are no other studies that have used cosmogenic isotope analysis in such a directly comparable setting or in any other areas of southern Africa to estimate erosion rates or otherwise. However, the comparison outlined above had led to an interesting insight into possible controls on the rate of denudation processes on a set of classic landforms. This example paves the way for further work in this vein and demonstrates the potential to use cosmogenic isotope analysis to tackle basic geomorphologic questions. However, the importance of thorough geomorphological understanding of the sites and the need for compatibility of variables such as climate, lithology and geomorphic setting for comparative purposes cannot be over emphasised.

5.7.3 *Implications for Landscape Evolution in the Central Namib*

Given the apparent persistence of arid climatic conditions in the central Namib for at least the past 10-12 Ma and possibly throughout much of the Cenozoic (5.3.4; Ward *et al.*, 1983), it is likely that a mean rate of granite bornhardt lowering of ~5 m Ma^{-1} has applied over this period. Temporal extrapolations of denudation rate data in many cases can be misleading (section 1.3), but denudation rate estimates from cosmogenic isotope analysis are necessarily integrated over geologically significant periods of time (in this case over the past 10^3-10^5 a). Extrapolation, therefore, becomes less problematic if the average climatic conditions over the past 10^3-10^5 a can be assumed to have characterised the preceding time period. Denudation rates from cosmogenic isotope analysis combined with the almost unique stability of the central Namib environment probably provides one of the few locations on Earth, outside Antarctica, where it is reasonable to infer a single, characteristic rate over such a long period of time.

A consistently low rate of ~5 m Ma^{-1} for granite bedrock exposures in the central Namib since the early Tertiary is fully compatible with longer term assessments of margin denudation from fission track thermochronology (Brown *et al.*, 1990, 1994, 1998), analysis of the offshore sedimentary record (Rust and Summerfield, 1990) and other indirect methods using stratigraphic information on the coastal plain of Namibia (Gilchrist *et al.*, 1994b; Pickford *et al.*, 1995). These studies have already been reviewed and discussed in detail in Chapter 4 and the overall implication for the Namibian passive margin was rapid denudation of ~3-5 km soon after rifting at ~130 Ma BP, formation of the coastal platform by the late Cretaceous and a significant reduction in the amount of denudation occurring from the start of the Tertiary throughout the Cenozoic. Low rates after the beginning of the Tertiary mostly <20 m Ma^{-1} and within an order of magnitude of cosmogenic isotope analysis estimates are proposed in every case. Possible reasons for a slowing down of denudation rates in the Tertiary for the coastal plain in general have been previously speculated upon in section 4.8. Although climate appears to have a profound effect on the rates measured by cosmogenic isotope analysis on bornhardts in the coastal plain, it is not the controlling factor at the larger, margin-scale. The decline in rates is more likely to be a function of the configuration of relief on the passive margin after several million years of evolution, i.e. the relative proximity and possible pinning of the escarpment by the drainage divide and the low relief coupled with low elevation of the coastal plain.

It can be inferred that because the granite bornhardts in the study area form positive relief they must be the most resistant components of the landscape and that their rate of summit lowering

has therefore been less than that of the surrounding landscape. If this were not the case, the bornhardts would not exist as even relatively large inselbergs could be denuded in a matter of a few million years. This implies that the denudation rate for the Namib platform overall has been higher than ~5 m Ma^{-1} for at least the time period applicable to the cosmogenic data (~10^5 a) and probably much longer. The fact that the estimate of 5 m Ma^{-1} for bornhardt summits is somewhat lower than other regional estimates for the coastal plain since the Tertiary is therefore fully explained. If the rate of bornhardt lowering is extrapolated over the past 10 Ma-phase of arid climatic stability, then a total amount of denudation during this period of more than 50 m is inferred; in addition, but perhaps less certainly, extrapolation over the whole of the Cenozoic suggests a total depth of denudation of >300 m. These depths of denudation are not particularly spectacular but they demonstrate that even the most resistant components of the central Namib landscape are undergoing significant active denudation and have not been preserved unmodified even under prolonged hyper-arid conditions.

Bornhardts have traditionally been thought of as old landforms (Twidale, 1988; Thomas, 1994; Oberlander, 1997). Now, the survival time of bornhardts in the Namib Desert can be predicted quantitatively for the first time using empirical data from cosmogenic isotope analysis. If the landforms are being denuded at ~5 m Ma^{-1}, and the rate of pediment lowering and the climate of the coastal plain of Namibia is assumed to remain broadly constant into the future, it is likely that Vogelfederberg, Blutkopje and Mirabib will remain prominent features of the central Namib landscape for at least the next 15 Ma.

5.8 Conclusions

Denudation rates calculated from concentrations of *in-situ* cosmogenic ^{10}Be and ^{26}Al on the summits of granite bornhardts Blutkopje, Vogelfederberg and Mirabib in the central Namib Desert range from 2.51 ± 0.5 m Ma^{-1} to 7.43 ± 1.6 m Ma^{-1}. A mode of bornhardt mass wasting at two contrasting scales with small-scale laminar sheeting and granular disintegration and larger-scale spallation of sheets >0.5 m thick can explain the apparent complexity in exposure history indicated for some samples in Fig. 5.12. An average rate of ~5 m Ma^{-1} is inferred to have characterised the rate of granite bornhardt lowering in the central Namib for at least the past 10^3-10^6 Ma. Comparable rates from similar features in Australia have yielded cosmogenic denudation rates estimates on the order of ~0.7 m Ma^{-1} (Bierman and Turner, 1995). The reason proposed for the unexpected order of magnitude difference in measured rates is the persistent presence of coastal fogs in the Namib and high rates of fog precipitation which may significantly

increase the effectiveness of weathering processes such as salt weathering and hydration in the central Namib. The remarkable persistence of arid climatic conditions throughout the Cenozoic in the central Namib in the vicinity of the sampling sites, supports the idea that a rate of ~5 m Ma^{-1} has characterised the rate of bornhardt denudation during the past 10-12 Ma and possibly since the early Tertiary. This rate is fully compatible with other data from techniques such as fission track thermochronology and analysis of the offshore sedimentary record which also suggest a rate of <<20 m Ma^{-1} after the beginning of the Tertiary (Brown *et al.*, 1990). Bornhardts in the central Namib are long-lived features of the landscape but are also actively denuding and are not preserved unmodified even under hyper-arid climatic conditions.

Chapter 6:

In-Situ-Produced Cosmogenic ^{10}Be, ^{26}Al and ^{21}Ne Denudation Rate Estimates from the Dry Valleys Region of the Transantarctic Mountains, Antarctica

---

6.1 Introduction

Denudation rate estimates from *in-situ* cosmogenic isotope analysis of ^{10}Be, ^{26}Al and ^{21}Ne in samples from contrasting landscape elements in the Dry Valleys region of the Transantarctic Mountains in southern Victoria Land, Antarctica are presented in this chapter. The overall rationale and aim of the work described here are similar to the previous two chapters; namely, to quantify denudation rates in order to understand landscape evolution and to investigate modes of change by constraining rates on contrasting landscape elements. A knowledge of denudation rates and modes of landscape modification in the Dry Valleys region is important for several reasons (Summerfield *et al.,* 1998a, b): First, there is a long-standing debate over the stability of the East Antarctic Ice Sheet and an understanding of the antiquity of the landscape in the Transantarctic Mountains is crucial to the argument. The unstable ice sheet model (Webb *et al.,* 1984; Barrett *et al.,* 1992) suggests that the ice sheet has responded dramatically to climatic fluctuations in the past and as recently as the Pliocene experienced significant melting. Associated with periods of ice sheet collapse and re-growth, rates of glacial and periglacial processes and landscape change in the Transantarctic Mountains would have been much greater than today. On the other hand, the stable ice sheet model proposes long-term ice sheet and associated landscape stability under a prevailing hyper-arid polar climate over the last 15 Ma (Clapperton and Sugden, 1990; Denton *et al.,* 1993; Sugden, 1992, 1996). Secondly, over the last 2-3 Ma at least, it is generally agreed that the Dry Valleys landscape has developed under a cold hyper-arid regime in the virtual absence of running water, a situation unique to Antarctica. The Transantarctic Mountains have not been subject to the same Quaternary glacial/interglacial climatic oscillations which have affected most other parts of the globe. Finally, there is a range of existing data from other geochronological techniques as well as morphological and stratigraphic information, principally in the Dry Valleys region of the Transantarctic Mountains,

that suggest very low rates of landscape change, possibly the lowest on Earth. Examining rates in the Dry Valleys could therefore permit a lower limit to be placed on possible rates of denudation. Quantification of minimum global rates is important not only as a benchmark with which to compare other rates from different environments but also to assess the notion of assigning an 'age' to a landform or landsurface under the assumption that it has not been modified since its creation. With respect to long-term aridity, the Dry Valleys region has similarities with the central Namib (section 5.2.4). Comparison of cosmogenic data from each region will demonstrate the contrast between denudation in long-lived warm and cold deserts.

To date, there have been a number of studies that have used *in-situ* cosmogenic isotopes to estimate denudation rates and ages of landsurfaces in the Transantarctic Mountains, a few of which have been specifically concerned with the debate over East Antarctic stability (Nishiizumi *et al.*, 1991; Ivy-Ochs *et al.*, 1995; Brook *et al.*, 1995a; Bruno *et al.*, 1997). Other work using *in-situ* cosmogenic isotope analysis has also been carried out in Antarctica. The work includes early pioneering work on ^{10}Be and ^{26}Al (Nishiizumi *et al.*, 1986), studies of ^{21}Ne systematics (Graf *et al.*, 1991; Hudson *et al.*, 1991), production rate measurement and depth profile analysis of ^{10}Be, ^{26}Al and ^{21}Ne (Brown *et al.*, 1991; Brown *et al.*, 1992), several applications concerning glacial chronology in the Dry Valleys area using ^{3}He, ^{10}Be and ^{26}Al (Brown *et al.*, 1991; Brook, 1993; Brook and Kurz, 1993; Brook *et al.*, 1993; Brook *et al.*, 1995b) as well as other kinds of applications including *in-situ* produced cosmogenic isotopes in ice (Lal *et al.*, 1987) and cosmogenic isotopes in meteorites found in Antarctica (Nishiizumi *et al.*, 1989b). The are a number of reasons for a concentration of work in Antarctica. Cosmic ray research was initially concerned with meteorites, many of which have been collected from ice fields in Antarctica, and it was therefore an obvious place to collect and test terrestrial samples. In general, Antarctica is ideal for sampling and testing of the *in-situ* technique because of the presence of exposed bedrock in apparently stable geomorphic settings with, by inference, exceptionally low erosion rates. Because of its high latitudinal position and high mountainous elevations it has high cosmogenic isotope production rates compared to other parts of the Earth. These factors result in high nuclide concentrations that require small sample sizes and are easier to measure. Early studies (e.g. Nishiizumi *et al.*, 1986) used these locational advantages to investigate the technique without paying particular attention to the geomorphic significance of the sampling sites. Recent studies have been more selective but have, in general, sampled for specific dating purposes such as determining the age of glacial deposits and moraines (Brook and Kurz, 1993; Brook *et al.*, 1995a; Ivy-Ochs *et al.*, 1995; Bruno *et al.*, 1997). There have been no studies that have been designed to explicitly assess denudation rates on different landscape components and this is the

first study to specifically address rates of landscape change in Dry Valleys using multiple *in-situ* cosmogenic isotopes.

Use of *in-situ* ^{10}Be and ^{26}Al as well as ^{21}Ne provides a rare opportunity to compare data from three isotopes and stable/radioactive pairs. Using only one isotope to assess denudation can be problematic because whether or not the isotope system has reached secular equilibrium or has been subject steady-state denudation cannot be tested (section 2.4). If only ^{10}Be and ^{26}Al had been used, an erosion-island plot would provide a check on the validity of the steady-state erosion/secular equilibrium model but the longest period of time over which a steady-state denudation rate could be definitely extrapolated would be over the period of time that ^{10}Be takes to reach saturation; i.e. a measured steady-state ^{10}Be denudation rate that is matched by a measured steady-state ^{26}Al denudation rate can only be assumed to have been active over the time it takes for ^{10}Be to reach secular equilibrium with that denudation rate. (^{26}Al has a shorter half-life than ^{10}Be and will therefore reach saturation sooner.) Use of stable ^{21}Ne coupled with ^{10}Be extends the time range over which a measured steady-state rate can be assumed to have been operating provided the rates are similar and the model of steady-state denudation is supported. This is because ^{21}Ne requires more time to reach secular equilibrium without the influence of radioactive decay. (^{21}Ne does not reach secular equilibrium except in the presence of denudation.) In theory, ^{3}He would provide the same benefit but probable diffusive loss from quartz limits it application (Trull *et al.*, 1991; Brook *et al.*, 1993). Diffusive loss of ^{21}Ne in quartz is minimal, particularly at the low temperatures experienced in the Antarctic (Graf *et al.*, 1991; Hudson *et al.*, 1991). Set against a background of inferred long-lived landscape stability, it is advantageous to have this potential extension to the time frame over which measured cosmogenic denudation rates can be extrapolated.

6.2 East Antarctic Ice Sheet Stability

The question over the stability or otherwise of the East Antarctic Ice Sheet is by now well documented but remains a hotly debated subject (see Denton *et al.*, 1993 and Sugden, 1996 for reviews). New evidence, such as the possible influence of a large meteorite impact on critical pieces of evidence, is still forthcoming (e.g. Gersonde *et al.*, 1997). The principal point of contention is whether or not the ice sheet experienced significant melting and was therefore much smaller under warmer Pliocene climates, ~3 Ma BP. The controversy is important because of the apparent significance of the ice sheet in influencing global climate and the potentially catastrophic consequences of large-scale melting under an anthropogenically induced global

warming scenario of a few degrees; the equivalent water volume of the present ice accumulation would amount to a 60 m rise in global sea level (Drewry, 1982).

The present day Antarctic Ice Sheet is the largest accumulation of ice on Earth and consists of about 30 x 10^6 km^3 over an area of 13.6 x 10^6 km^2 (Fig. 6.1; Denton *et al.*, 1993). It is divided by the Transantarctic Mountains into the West and East Antarctic Ice Sheets. The East Antarctic Ice Sheet is the larger of the two and is over 4 km thick in places. Its western edge is dammed by the Transantarctic Mountains but other remaining edges terminate directly into the Southern Ocean or in floating ice shelves such as the Filchner-Ronne Ice Shelf. Major outlet glaciers pass through the Transantarctic Mountains (e.g. Beardmore Glacier) and between some of these, local ice domes feed further outlet glaciers, some of which terminate in the Dry Valleys region (Figs. 6.2 and 6.3). The Dry Valleys region is bounded by the Mackay Glacier in the north and Ferrar Glacier to the south and contains the largest expanse of ice free land in the Transantarctic Mountains. Ice Major ice-free valley systems are flanked by the Quartermain Mountains and Asgard and Olympus Ranges. Taylor Dome, a local dome of the East Antarctic Ice Sheet, feeds ice into Wright and Taylor Glaciers which terminate in ice-free valleys.

The unstable ice sheet hypothesis is critically dependent on the inferred age and origin of marine diatoms in outcrops of the Sirius Group deposits at high elevations in the Transantarctic Mountains. The Sirius Group are terrestrial glacial deposits that include tills and gravels indicative of a melting ice-margin (Sugden, 1996). By correlation with diatoms from marine cores, Webb *et al.* (1984) assigned a maximum age of ~3 Ma for the deposition of the Sirius Group. They proposed that the diatoms originated in exposed inland marine basins that were subsequently overridden and covered by an expanding East Antarctic Ice Sheet that reworked marine sediments and deposited them as the Sirius Group as the ice sheet spread up the inland slope of the Transantarctic Mountains. In order for marine diatoms to exist in the centre of Antarctica, the ice sheet must have been small enough to expose the Wilkes and Penascola Subglacial Basins which are at present beneath the East Antarctic Ice Sheet directly to the east of the Transantarctic mountains (Fig. 6.1). The discovery of *Nothofagus* fragments (Southern Beech) in the Sirius Group implied temperate mid-latitude conditions in the Transantarctic Mountains with temperatures up to 30°C higher than present during the deposition of the Sirius. Such a high temperature difference at the current Sirius elevations of 2000 m seemed unlikely but suggestions of late Pliocene uplift on the order of 0.5 - 1 km Ma^{-1} significantly reduces the temperature differential required (Behrendt and Cooper, 1991). Support for periodic collapse of the East Antarctic Ice Sheet has come from the discovery of high Pliocene shorelines in the

eastern USA and New Zealand (Dowsett and Cronin, 1990) and evidence for warm climates from marine isotope and biogenic productivity records in some deep sea cores.

A stable view of the East Antarctic Ice Sheet was originally based on the oxygen isotope record of carbonates in deep sea cores around Antarctica (Sugden, 1996). The record showed progressive climatic cooling during the Cenozoic and that a large ice sheet over East Antarctica first developed ~14 Ma BP (Shackleton and Kennett, 1975; Kennett, 1977). Since the development of the unstable ice sheet hypothesis, a wide variety of other evidence has been collected to support and demonstrate stability of the ice sheet since the mid-Miocene and to constrain the morphological evolution of the Transantarctic Mountains (Sugden *et al.,* 1993; Denton *et al.,* 1993; Sugden, 1996). Geomorphological evidence from the Dry Valleys has been used to argue that the region is a relict fluvial landscape with very little subsequent glacial modification (Denton *et al.,* 1993). $^{40}Ar/^{39}Ar$ dating of *in-situ* volcanic ash deposits at elevations over 1000 m in the Dry Valleys indicates slope stability and a lack of significant fluvial or glacial erosion since at least 15.15 (± 0.02) Ma (Nibelungen Valley ash) (Marchant *et al.,* 1983a, b, 1996). Together with the discovery of buried 8 Ma old glacier ice preserved in Taylor Valley (Sugden *et al.,* 1995b), further geomorphic mapping and interpretation of the Dry Valleys topography (Denton *et al.,* 1993) and glaciogenic modelling of ice sheet response to climatic change, a convincing argument has been put forward against significant climatic change, tectonic uplift or warm based ice advance in the Dry Valleys prior to or during the Pliocene and probably as far back as the Miocene.

Although the stable and unstable ice sheet hypotheses have largely relied on independent lines of evidence, counter arguments from both sides have been an integral part of the debate. Against the instability hypothesis, it has been argued that the Penascola and Wilkes marine basins that were thought to act as a source of the Sirius Group diatoms (Webb *et al.,* 1984) would have been above sea level if the crust is isostatically compensated for the removal of East Antarctic ice (Denton *et al.,* 1993). It has also been shown the diatoms in the Sirius Group consist of a wide range of ages and are only found in the top layers of the deposits and could have been deposited from above, either windblown or in fallout from an meteorite impact, into their present positions (Burkle and Potter, 1996; Kellogg and Kellogg, 1996; Gersonde *et al.,* 1997). Cosmogenic isotope analysis of ^{10}Be and ^{26}Al, and, ^{3}He and ^{21}Ne concentrations in samples fringing and within the Sirius Group have indicated minimum deposition ages of greater than the late Pliocene at ~5Ma (Ivy-Ochs *et al.,* 1995; Bruno *et al.,* 1997). Against the stable ice sheet hypothesis, it has been argued that ash deposits used to infer landscape stability in the Dry Valleys are not *in*

were incorporated into their present locations in sand wedges, avalanche deposits and desert pavements after initial eruption either by aeolian or fluvial/slope processes and therefore cannot be used for dating. It has also been postulated that the Dry Valleys have had a unique tectonic history and are not representative of other tectonic blocks of the Transantarctic Mountains and therefore cannot be used to argue against hypothesis that has implications for a much larger area (van der Wateren and Hindmarsh, 1995).

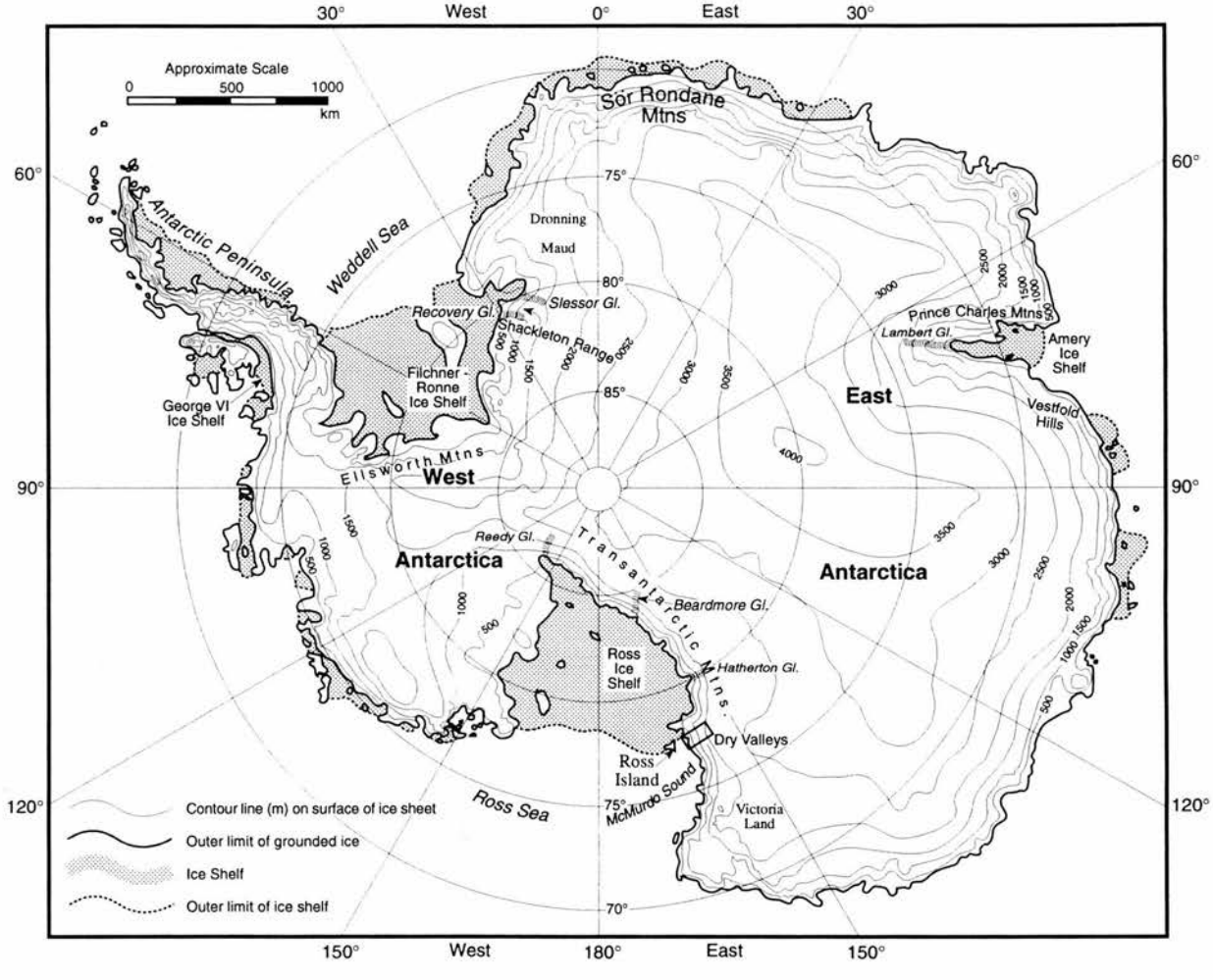

Figure 6.1: Map of Antarctica showing the division into East and West by the Transantarctic Mountains and the present-day extent of the East Antarctic Ice Sheet. The location of the Dry Valleys region is also shown.

In an attempt to corroborate evidence that implies low rates of change in the Dry Valleys region over the past few million years which relate to the ice sheet stability debate and, to extend knowledge about the evolution of the landscape, concentrations of *in-situ* cosmogenic isotopes have been measured in samples from contrasting landscape elements. Cosmogenic isotope analysis provides an independent means of testing the stable/unstable ice sheet hypothesis by providing direct quantification of denudation rates and landscape change. As such, cosmogenic isotope data should not only be less equivocal than inferred slow rates of landscape change based on the correlation of $^{40}Ar/^{39}Ar$ dated ash deposits with landforms but the data will also be able to test whether or not an *in-situ* origin for the ash deposits is likely. Measurement of three cosmogenic isotopes enables thorough testing of the steady-state denudation assumption and of the exposure history of the sites and has the capacity to provide potentially unambiguous denudation rates for different landscape components over the maximum time range of the cosmogenic technique.

6.3 Physical Setting

6.3.1 Morphotectonic Evolution of the Transantarctic Mountains

The Transantarctic Mountains extend for more than 3000 km in a broad arc that separates East from West Antarctica (Fig. 6.1). The major structural elements were created by asymmetric intracontinental rifting in the Eocene (~55-50 Ma BP) with the lower plate forming the Ross Sea Embayment. The Transantarctic Mountains are therefore not strictly a mountain range but a large amplitude (2-4 km), short wavelength (50-200 km) upwarp that forms the rim of an extensive plateau that rises from the interior of East Antarctica (Fitzgerald *et al.,* 1986). Tilting of individual tectonic blocks and lithospheric flexure produced an inland dip to the upwarp that is clearly visible in the exposed strata of the Transantarctic Mountains. The outer flank of the mountains comprises a major escarpment or series of smaller escarpments which fall off dramatically into the basins of the Ross Embayment.

Fission track evidence from a transect through the Dry Valleys suggests that a total of 4-5 km of denudation has occurred along the Ross Sea coast since rifting at ~55 Ma BP (Gleadow and Fitzgerald, 1987). A pulse of denudation soon after rifting, characteristic of passive margin development, indicates that significant relief must have existed in the Dry Valleys at ~50 Ma and the rift flank must have been elevated with respect to sea level either due to tectonic uplift of the rift flank or subsidence of the Ross Embayment (Gleadow and Fitzgerald, 1987). Surface uplift

rates of ~1 km Ma^{-1} since the Pliocene have been proposed for the Dry Valleys to support the unstable ice sheet hypothesis (Behrendt and Cooper, 1991). However, this argument has been refuted on basis of the present-day elevations of sub-aerially erupted Pliocene lava deposits which indicate a maximum possible uplift over the last ~2.5 Ma of only ~300m (Wilch *et al.,* 1993a, b). It has also been demonstrated that high cosmogenic nuclide concentrations in rocks from the Dry Valleys are inconsistent with rapid recent surface uplift of the magnitude suggested by Behrendt and Cooper (1991), if the Sirius Group deposits are also held to be of Pliocene age (Brook *et al.,* 1995a, Ivy-Ochs, 1996; Bruno *et al.,* 1997).

6.3.2 Morphology and Geology of the Dry Valleys Area

The Dry Valleys region consists of three major largely ice-free transverse valley systems in the Transantarctic Mountains, the Taylor, Wright and Victoria systems, separated by the ice-free Asgard and Olympus ranges (1500 - 2400 m high; Figs. 6.2 and 6.3). It represents a 4000 km^2 ice-free area from 77° 15'S to 77° 45'S and 160° E to 164° E located between McMurdo Sound in the Ross Sea Embayment and Taylor dome on the flank of the East Antarctic Ice Sheet. These valleys were carved by major outlet glaciers similar to the nearby Ferrar and McKay Glaciers but they are now starved of ice flow (Denton *et al.,* 1993; Summerfield *et al.,* 1998a, b). The Dry Valleys region is thought to be separated from the Royal Society Range to the south and from the Convoy Range to the north by major east west trending transverse faults across the marginal upwarp of the Transantarctic Mountains. To the south, the Ferrar fault runs along the trough formed by the Ferrar Glacier although it precise location is uncertain (Sugden *et al.,* 1998).

Figure 6.2 (on pull out page overleaf): Geomorphological map of Beacon, Taylor and Wright valleys showing the location of cosmogenic samples in Arena Valley, on Mount Fleming and adjacent to the Sollas Glacier (after Summerfield et al., 1998a).

Figure 6.3 (on pull out page overleaf): Satellite image map of the area shown in Figure 6.2. The distinction between ice covered and ice free areas is clearly visible (from United States Geological Survey McMurdo Dry Valleys 1:100 000 satellite image map).

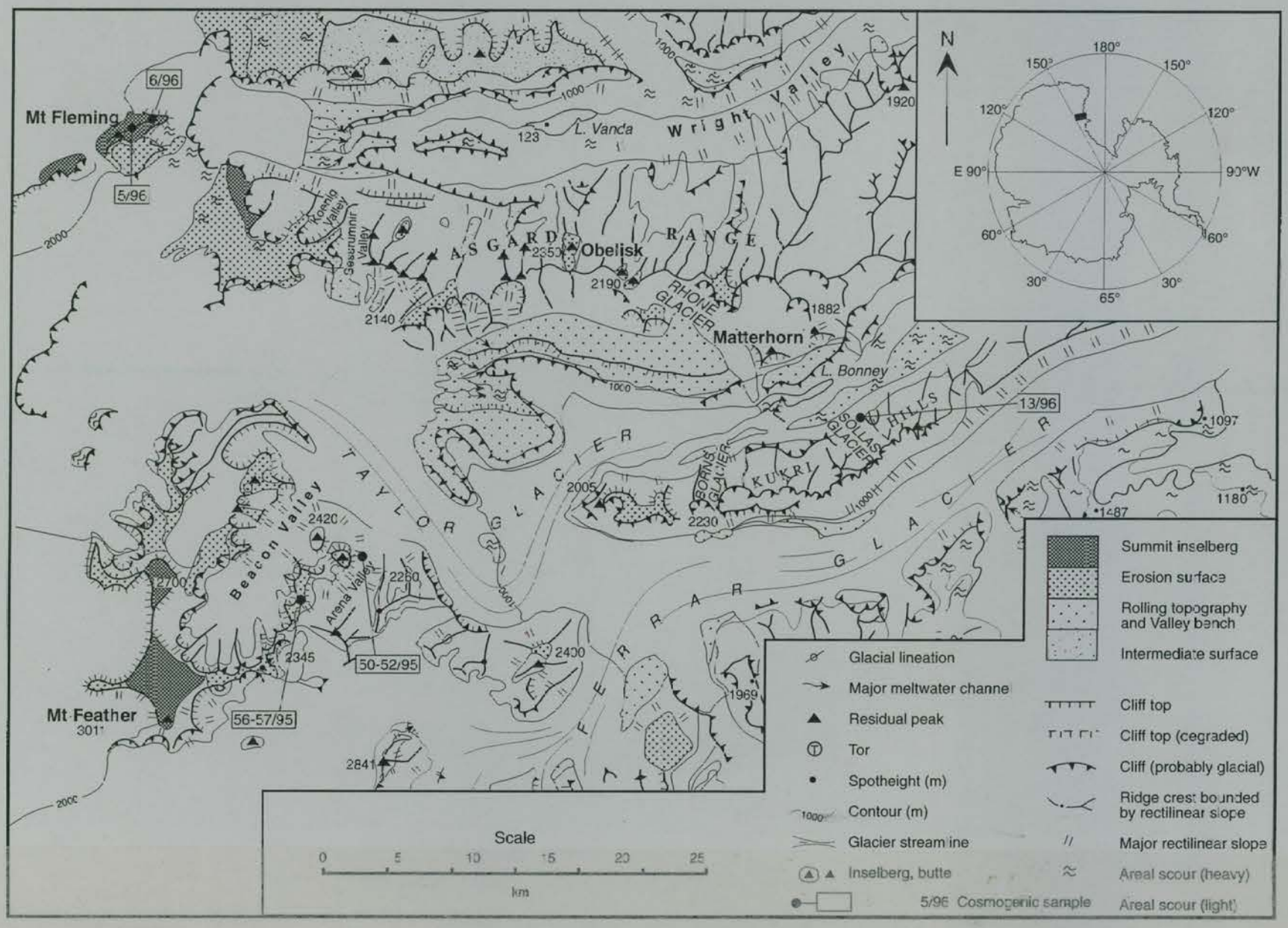
Mt Fleming
6/96
5/96
Mt Feather
3017
56-57/95
50-52/95
13/96
Obelisk
2350
2190
Matterhorn
1882
L. Vanda
L. Bonney
Wright Valley
Asgard Range
Rhone Glacier
Taylor Glacier
Ferrar Glacier
Solitude Glacier
Kukri Hills
Beacon Valley
Arena Valley
Roaring Valley
Seasurumir Valley
Scale
0 5 10 15 20 25
km
N
180°
150°
120°
90°W
60°
30°
65°
Summit inselberg
Erosion surface
Rolling topography and Valley bench
Intermediate surface
Glacial lineation
Major meltwater channe
Residual peak
Tor
Spotheight (m)
Contour (m)
Glacier streamline
Inselberg, butte
5/96 Cosmogenic sample
Cliff top
Cliff top (cegraded)
Cliff (probably glacial)
Ridge crest bounded by rectilinear slope
Major rectilinear slope
Areal scour (heavy)
Areal scour (light)

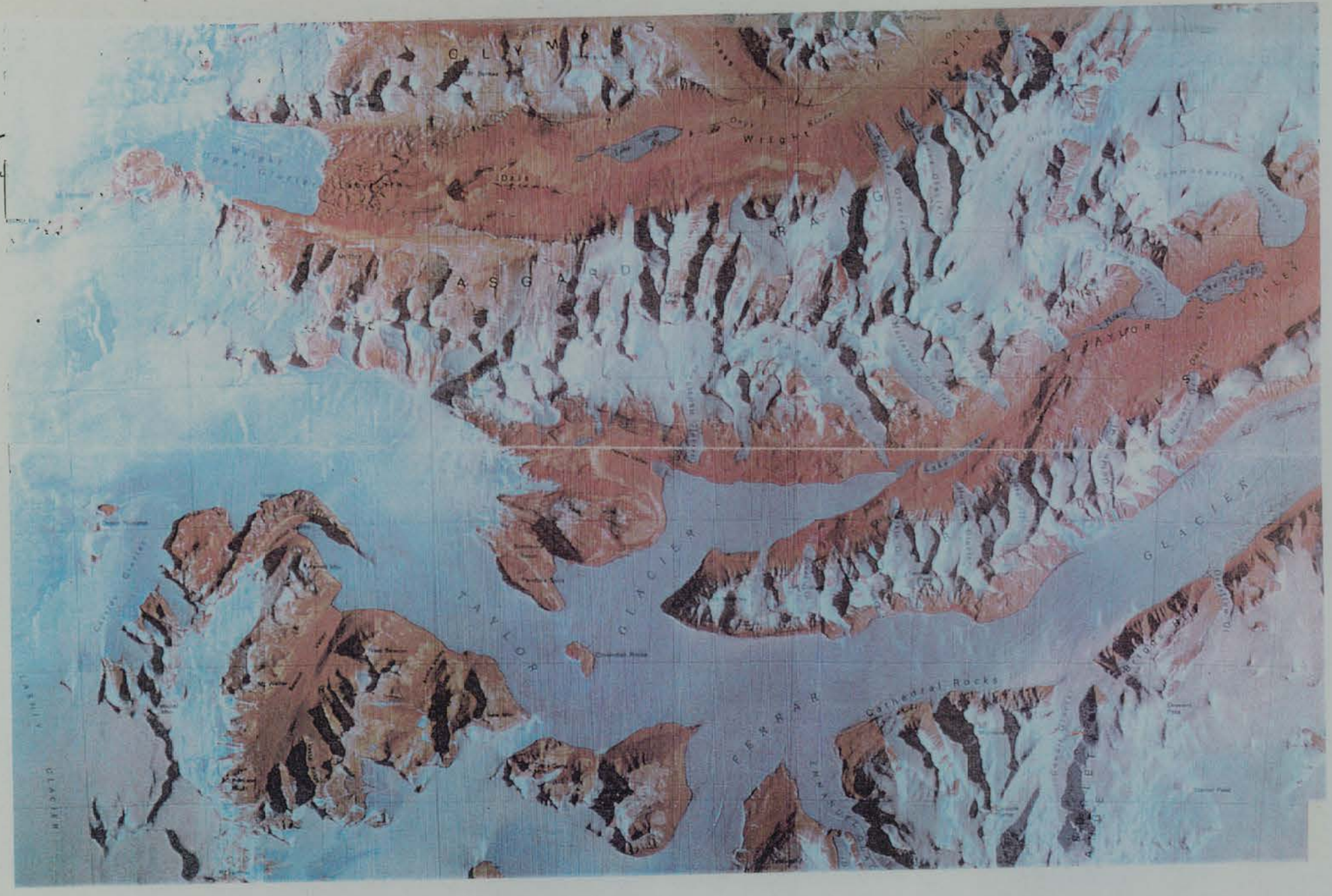
Olympus
Asgard Range
Taylor Glacier
Ferrar Glacier
Wright Valley
Cathedral Rocks

Exposed bedrock in the Dry Valleys region consists of a basement complex of Precambrian igneous and meta-igneous rocks which are overlain by gently dipping sandstones, siltstones and conglomerates of the Devonian-Triassic Beacon Supergroup including Beacon Sandstone and Arena Sandstone. Extensive Jurassic dolerite intrusions (Ferrar Supergroup) form sills up to several hundred metres thick throughout the basement and overlying sedimentary strata. Localised surfical deposits include glaciogenic sediments as well as Late Cenozoic volcanic cones and ash deposits. (Summerfield *et al.,* 1998a, b).

Sugden *et al.* (1995a) identified five major landscape elements in the Dry Valleys region. The two most areally significant of these are high-elevation (>1800 m), low-relief (<30m) surfaces and rectilinear slopes which flank the upland surfaces at angles of ~33°-37° (see Sugden *et al.,* 1995a, figure 4, p. 9954). An upper surface at 2000-2400 m surrounds the heads of the main valleys separating the Dry Valleys from the Polar Plateau. Large residuals on this surface form the highest summits in the area such as Mount Feather (2985 m) and Mount Fleming (2400 m). A lower intermediate surface (~1800 m) forms extensive sections in the western parts of the Asgard and Olympus ranges between Taylor, Wright and Victoria Valleys. These surfaces are formed predominantly on dolerite sills and near-horizontal Beacon Supergroup sedimentary rocks, respectively, and exhibit some structural control. Rectilinear slopes characterise the flanks of both the upper and lower surface and form a significant proportion of valley sides in the Dry Valleys (Selby, 1971, 1974). In the eastern portion of the Dry Valleys where the lower surface is absent, rectilinear slopes still characterise the valley sides but meet as sharp edged interfluves. The rectilinear slopes are cut into bedrock and are partly covered by a thin (~1 m thick) veneer of coarse rock debris.

6.3.3 Present and Past Climates of the Dry Valleys

The present climate of the Dry Valleys region is cold and hyper-arid (Summerfield *et al.,* 1998a, b). Mean annual temperatures at lower elevations in the eastern sections of the valleys are about -20°C although summer noon temperatures may exceed +5°C for several days. Active debris and mud flows and stream channels below ~800 m indicate that liquid water and temperatures above 0°C are common at lower elevations near the coast. Data for higher, inland locations are sparse, however, assuming a lapse rates of 10°C km^{-1}, mean annual temperatures at higher elevations in the western Asgard and Olympus Ranges, the Quartermain Mountains and on high elevation surfaces in the Polar Plateau drop to -30°C to -40°C (Marchant and Denton, 1996). Mean annual precipitation ranges from ~100 mm water equivalent near the coast to <10 mm at high elevations

in the west. Winds blow through the Dry Valleys from both the Ross Sea in the east and the inland Polar Plateau in the west. Easterly winds have a mean relative humidity of 65-75% and snow precipitation reaches a maximum of ~100 mm a^{-1} in the eastern ends of the Dry Valleys. Westerly katabatic winds blow from the Polar Plateau with a lower relative humidity of 5-60% and in summer these winds are largely confined to the western end of the Dry Valleys and the valley bottoms. Accumulation of wind-blown snow in the lee of topographic barriers sustains small cold based glaciers on the sides of Taylor, Wright and Victoria Valleys. Meltwater seems to be absent at high altitudes inland but can be found at progressively higher altitudes near the coast. This trend probably results from a combination of more active katabatic winds in the upper parts of the Dry Valleys and a maritime influence near the coast (Marchant and Denton, 1996).

Consensus about past climates in the Dry Valleys is contested within the context of the East Antarctic Ice Sheet Stability debate described in section 6.2. The unstable ice sheet model implies higher temperatures at about ~3 Ma BP. It has been argued that deglaciation of East Antarctic and exposure of sub-glacial basins could be achieved with a modest increase in temperature compared to the present assuming rapid surface uplift after deglaciation and a low temperature tolerance of shrub-type *Nothofagus* trees (Webb and Harwood, 1991). However, ice-sheet modelling studies indicate that temperatures 17-20°C above those of the present would be required to remove ice from sub-glacial basins (Huybrechts, 1993). The stability hypothesis, based on a range of evidence, supports a hyper-arid, polar climatic regime similar to that of the present for at least the past 15 Ma (Denton *et al.,* 1993; Sugden, 1996). Irrespective of the veracity of the two contrasting interpretations of past climates, there is overall agreement that there has been remarkable climatic stability in the Dry Valleys area for at least the last 2-3 Ma with only with only modest fluctuations in the extent of ice cover in outflow and valley-side glaciers resulting from climatic change during this period (Summerfield *et al.,* 1998b). (There has been significant variation in the extent of ice cover as a result of changes in sea-level due to grounding of ice shelf areas.) As previously mentioned, this morphoclimatic regime contrasts starkly with the large magnitude and frequent climatic fluctuations driven by glacial-interglacial oscillations that have characterised virtually all other morphoclimatic zones on Earth throughout the Quaternary (Summerfield, *et al.,* 1998b.)

6.4 Sampling Strategy and Sites

Samples were collected by D. Sugden and M. Summerfield according to a previously agreed strategy of assessing rates of denudation in the contrasting morphological settings of high-elevation surfaces and rectilinear slopes in the Dry Valleys region. Sample locations were chosen with particular attention paid to identifying representative sites from which useful extrapolations could be made. Sampling sites on the rectilinear slopes were chosen to provide comparisons with existing independent evidence of rates of landscape change from dated lava and volcanic ash deposits (Wilch *et al.,* 1993a, b; Marchant *et al.,* 1996). In total, eight samples were analysed, four from each type of site (Table 6.1)

Four samples consisting of Beacon Sandstone were analysed from two high-elevation (>2000m), low-relief surfaces (5-6/96, 56-57/95). Samples 5/96 and 6/96 were collected from the eastern flank of Mount Fleming at the head of Wright Valley overlooking Wright Upper Glacier (Fig. 6.2). 5/96 came from a broad, low-relief ridge just below the summit and 6/96 from a lower elevation on a flat-topped spur from an iron stained bedrock surface scattered with dolerite boulders and cobbles (Summerfield *et al.,* 1998a) (Fig. 6.4). Samples 56/95 and 57/95 were collected less than 2 m apart from a low relief, iron-stained bedrock surface on the flat-topped interfluve between Beacon Valley and Arena Valley (Figs. 6.2 and 6.5). All four samples were taken from within 50 mm of the surface. At all the high-elevation sites, bedrock surfaces exhibited evidence of some rock disintegration in the form of cavernous weathering and tafoni features. At the time of sample collection, the higher sampled surface on Mount Fleming (5/96) was covered by a thin (<100 mm), discontinuous layer of snow. However, lying snow is rare due to the extremely exposed and windy nature of the site and it is unlikely that any of the high-elevation surface sites have been subject to significant shielding from cosmic radiation (Summerfield *et al.,* 1998a).

Figure 6.4: Sampling site 5/96 on the high elevation surface of Mount Fleming. Wright Upper Glacier can be seen in the middle distance (photo: D. Sugden)

Figure 6.5: Sampling site 56/95 and 57/95 on the high elevation surface between Arena and Beacon Valleys (photo: D. Sugden)

Three samples consisting of Arena Sandstone were collected and analysed from a 10 m^2 area on a 36-38° rectilinear slope in the Quartermain Mountains on the western side of Arena Valley overlooking Taylor Glacier (50-51/95). The three samples were collected at an elevation of 1572 m on a rectilinear slope on the western side of Arena Valley (Fig. 6.2). Near-horizontal sandstone beds protrude from the slope forming a series of cavernously weathered steps with localised undercutting and slumping and relief of up to 4 m. Sample 50/95 was collected from the surface of a characteristic rock step (Fig. 6.6), sample 51/95 from a 0.4 m boulder on the same rock step and 52/95 from the slumped front of the step. Although 52/95 was from a detached section of a step, it could unequivocally be seen to have been previously a part of the step and to have slumped less than 2 m down the slope. However, sample 51/95 was from a loose boulder on the surface of a step which could have fallen from a significantly higher elevation. The site was selected because it is close to an avalanche deposit located 100 m south of the cosmogenic sampling site. The avalanche deposit consists of sandstone and dolerite clasts, quartz sand and granite grus and cobbles mixed with volcanic ash. There is a sharp contrast between the debris cover of the rectilinear slope and the avalanche deposit which rises up to 3 m above the slope surface. The avalanche deposit contains *in-situ* $^{40}Ar/^{39}Al$ dated volcanic ash of 11.3-12.9 Ma old (Marchant *et al.*, 1993a). The deposit therefore suggests minimal geomorphic activity on the slope. Additional evidence for low rates of landscape change is provided by a thin granite till located 30 m below the site which has been dated by its association with volcanic ash in a nearby valley to >13.6 Ma BP (Marchant *et al.*, 1993a).

Sample 13/96 was collected from a north-facing, 33° rectilinear slope in the lower Taylor valley immediately to the east of the Sollas Glacier at an elevation of 810 m (Fig. 6.7). The slope is formed on granite basement and is characterised by protruding bedrock outcrops and a discontinuous mantle of coarse talus. The sample comprised thin surface fragments (<10 mm thick) from an exfoliating bedrock granite exposure inclined at 25°. The site was selected because it is immediately adjacent to a partially eroded lava flow deposit, $^{40}Ar/^{39}Ar$ dated to 2.19 Ma BP (Wilch *et al.*, 1993a, b).

Figure 6.6: Sampling site 50/95 on a bedrock step on the rectilinear slope on the western side of Arena Valley (photo D. Sugden).

Figure 6.7: Sampling site 13/96 to the east of the Sollas Glacier, Taylor Valley. The sample location is indicated by the figure on the left. the view is to the west along Taylor Valley (photo M. Summerfield).

Table 6.1: Sample and field data for Antarctic samples (from Summerfield *et al.*, 1998a).

Sample Number	Sample Site	Location Long. & Lat.	Altitude (m)	Lithology	Surface Slope (°)	*Exposure Geometry
High-elevation Surfaces						
5/96	Mount Fleming	77° 33' S 160° 08' E	2427	Beacon Sandstone	0	full exposure
6/96	Mount Fleming	77° 32' S 160° 16' E	2038	Beacon Sandstone	0	full exposure
56/95	Beacon/Arena interfluve	77° 53' S 160° 44'E	2050	Beacon Sandstone	0	partial shielding
57/95	Beacon/Arena interfluve	77° 53'S 160° 44' E	2050	Beacon Sandstone	0	partial shielding
Rectilinear Slopes						
50/95	Arena Valley	77° 46' S 160° 51' E	1572	Arena Sandstone	2	partial shielding
51/95	Arena Valley	77° 46'S 160° 51' E	1572	Arena Sandstone	0	partial shielding
52/95	Arena Valley	77° 46'S 160° 51' E	1572	Arena Sandstone	38	partial shielding
13/96	Lower Taylor Valley	77° 43'S 162 ° 38E	810	Granite	25	partial shielding

* For complete exposure geometry data see Appendix A.

6.5 Analysis, Results and Interpretation

Cosmogenic ^{10}Be and ^{26}Al were measured in the five samples collected in Arena Valley (50-57/95), one of which, 51/95, was prepared and analysed twice in order to test the reproducibility of the results. Cosmogenic ^{21}Ne concentrations were measured in all eight samples selected for analysis at the Vrije Universiteit, Amsterdam according to the methodology described in section 3.4 (Appendix B, Batch 2). He isotopes, including a cosmogenic component, were therefore also measured in all eight samples as an integral part of cosmogenic ^{21}Ne determination (section 3.4.2). Pure quartz separates were prepared for ^{10}Be, ^{26}Al and ^{21}Ne analysis according to the methodology described in section 3.3; sample masses are shown in Tables 6.3 and 6.4. ^{10}Be and ^{26}Al was extracted in a clean laboratory at the Scottish Universities Research and Reactor Centre (SURRC) using a chemical protocol similar to that shown in Figure 3.3 but included an acetylacetone extraction (section 3.3.2). The resultant quantities of BeO and Al_2O_3 were small but probably much purer than the oxides prepared from Namibian samples discussed in Chapters 4 and 5 using the final methodology described in Chapter 3 that did not include an acetylacetone extraction. Total Al analysis was performed by graphite furnace atomic absorption spectrometry (GFAAS) at the Department of Geology and Geophysics at the University of Edinburgh (Table

6.3). ^{10}Be and ^{26}Al targets were prepared and isotopic ratios were measured by accelerator mass spectrometry at the Eidgenössische Technische Hochschule/Paul Scherrer Institut (ETH/PSI) tandem accelerator facility in Zurich (section 3.3.3.2, Appendix B, Batch 2).

Production rates in quartz and at sea level and high latitude (>60°) of 6 atoms g^{-1} a^{-1} and 36.8 atoms g^{-1} a^{-1} were used for ^{10}Be and ^{26}Al respectively (Nishiizumi *et al.*, 1989a). Likewise, production rates of 21 atoms g^{-1} a^{-1} (Niedermann *et al.*, 1994) and 115 atoms g^{-1} a^{-1} (Cerling and Craig, 1994; Brook *et al.*, 1995a) were used for ^{21}Ne and ^{3}He respectively. Although there have been recent attempts to refine the production rates of ^{10}Be and ^{26}Al (Clark *et al.*, 1995; Nishiizumi *et al.*, 1996) the original estimates have been retained to facilitate comparison with other cosmogenic work in Antarctica which has conventionally used the original rates. Production rates for ^{3}He are subject to large uncertainties (Brook and Kurz, 1993; Brook *et al.*, 1995a); however, as will be seen, diffusion effects in quartz preclude meaningful interpretation of the data and therefore the choice of production rate is not critical. Production rates were corrected for the effects of altitude using the nuclear disintegration rates of Lal (1991) (section 2.2.7). Production rates were also corrected for the dip of the sampled surface and the effects of topographic shielding and in every case corrections were less than 2% (section 2.2.6, Table 6.2). Production rates have not been corrected for depth; where thicker samples had been collected only the top 20 mm were used for analysis. Because of current levels of uncertainty in production rate values for all isotopes an error of 20% has been included on all production rate estimates (Table 6.2).

Table 6.2: Production rates for Antarctic samples corrected for altitude, latitude and the exposure geometry of the site, (atoms $g^{-1}SiO_2$ a^{-1}).

Sample Number	Exposure Correction	*Corrected Production Rate Including 20% Error			
High-elevation Surfaces		^{10}Be	^{26}Al	^{21}Ne	^{3}He
5/96	-	-	-	158.22 ± 31.64	460.4 ± 92.1
6/96	-	-	-	120.58 ± 24.12	460.4 ± 92.1
56/95	-	31.63 ± 6.33	191.26 ± 38.25	121.62 ± 24.32	451.2 ± 90.2
57/95	-	31.63 ± 6.33	191.26 ± 38.25	121.62 ± 24.32	246.1 ± 49.1
Rectilinear Slopes					
50/95	0.987	22.14 ± 4.43	134.08 ± 26.82	84.07 ± 16.81	666 ± 133.2
51/95	0.987	22.14 ± 4.43	134.08 ± 26.82	84.07 ± 16.81	666 ± 133.2
52/95	0.967	21.69 ± 4.34	131.40 ± 26.28	82.38 ± 16.48	866.5 ± 173
13/96	0.984	-	-	44.94 ± 8.99	660.3 ± 132

*Slightly different production rates and correction factors from those used by Summerfield *et al.*, (1998a) for ^{21}Ne and ^{3}He have been used here. As a result, calculated ages and rates (Tables 6.5 and 6.6) will differ very slightly. However, these alterations do not affect the similarity of the overall interpretation and conclusions drawn here compared to Summerfield *et al.* (1998a) where appropriate.

Table 6.3: Be and Al data for Antarctic samples.

Sample Number	Quartz Mass (g)	Al content (ppm)[1]	Background Corrected $^{10}Be/^{9}Be$[2] AMS ratio	Background Corrected $^{26}Al/^{27}Al$[2] AMS ratio	^{10}Be conc. (N)[3] (10^7 at.$^{-1}$ g^{-1} SiO_2)	^{26}Al conc. (N)[3] (10^7 at.$^{-1}$ g^{-1} SiO_2)
High-Elevation Surfaces						
56/95	15.01	176.69 ± 8.8	$2.84 \times 10^{-11} \pm 4.26 \times 10^{-13}$	$6.22 \times 10^{-11} \pm 1.31 \times 10^{-12}$	6.30 ± 0.32	24.3 ± 1.72
57/95	15.11	115.53 ± 5.78	$2.73 \times 10^{-11} \pm 3.55 \times 10^{-13}$	$6.89 \times 10^{-11} \pm 1.79 \times 10^{-12}$	6.03 ± 0.3	17.7 ± 1.25
Rectilinear Slopes						
50/95	15.01	105.58 ± 5.28	$7.19 \times 10^{-12} \pm 1.8 \times 10^{-13}$	$3.22 \times 10^{-11} \pm 9.98 \times 10^{-13}$	1.6 ± 0.08	7.56 ± 0.53
51/95	15.05	126.13 ± 6.31	$1.41 \times 10^{-11} \pm 1.97 \times 10^{-13}$	$4.59 \times 10^{-11} \pm 1.42 \times 10^{-12}$	3.12 ± 0.16	12.9 ± 0.91
51/95 #2	15.00	135.73 ± 6.79	$1.37 \times 10^{-11} \pm 4.67 \times 10^{-13}$	$4.48 \times 10^{-11} \pm 1.25 \times 10^{-12}$	3.05 ± 0.15	13.5 ± 0.92
52/95	10.02	110.97 ± 5.55	$1.32 \times 10^{-11} \pm 6.75 \times 10^{-13}$	insufficient current	2.94 ± 0.15	-

[1] GFAAS result with 5% 1 σ error, [2] 1 σ AMS measurement error only, [3] error includes 5% reproducibility, (with 5% GFAAS for Al) and is given at the 1 σ level.

Be and Al AMS isotopic data and concentrations of cosmogenic ^{10}Be and ^{26}Al for samples 50-57/95 are shown in Table 6.3. Errors shown for the AMS isotopic ratios include machine measurement error only. These are low because the concentrations of cosmogenic isotopes are high and probably do not reflect the true level of uncertainty in the results. The reproducibility of sample 51/95, which was measured twice, was within 3% for both ^{10}Be and ^{26}Al AMS ratios. This is good but is lower than levels commonly found when more samples are reproduced (e.g. Gosse *et al.*, 1995; Ivy-Ochs, 1996). Errors on the concentrations of ^{10}Be and ^{26}Al (N) have been calculated to include a 5% uncertainty in the Al content as well as a 5% reproducibility uncertainty at the 1 σ level. AMS isotopic ratios were normalised to ETH standards S555 and ZAL94 which have values of $^{10}Be/^{9}Be = 95.5 \times 10^{-12}$ and $^{26}Al/^{27}Al = 526 \times 10^{-12}$ respectively. The Be standard (S555) is a secondary standard calibrated to the original material used to determine the half life of Be of 1.51 Ma (Hofmann *et al.*, 1987; P. Kubik, *pers. com.*). The ratios have also been corrected for process blank measurements. For Be, the average process blank result from two standard samples was $1.15 \times 10^{-14} \pm 6.4 \times 10^{-15}$ and for Al, the process blank result was $2.6 \times 10^{-14} \pm 100\%$ from one sample. Current in the AMS from the Al samples was generally low (~30 nA compared to 150nA from the standard) because of the small amount of Al_2O_3 in the samples which could have been due to separation problems encountered during the acetylacetone extraction. It was not possible to determine whether Be and Al had been separated

fully during the extraction procedure. Sample 52/95 did not have enough current for AMS measurement of $^{26}Al/^{27}Al$ (Table 6.3).

Table 6.4: He and Ne isotope data for Antarctic samples (from Summerfield *et al.*, 1998a)

Sample Number	Quartz Mass (mg)	$^{4}He^{*}$ x 10^{12} atoms g^{-1}	R/R_a*	$^{3}He_c$** x 10^{8} atoms g^{-1}	$^{20}Ne^{*}$ x 10^{10} atoms g^{-1}	$^{21}Ne/^{20}Ne^{*}$ (x 10^{-3})	$^{21}Ne_c$** x 10^{8} (N) atoms g^{-1}
High-elevation Surfaces							
5/96	278	9.05 ± 0.01	32.78 ± 0.7	4.13 ± 0.18	7.39 ± 0.02	11.27 ± 0.06	6.19 ± 0.08
6/96	288	46.6 ± 0.02	11.94 ± 0.14	7.75 ± 0.18	6.29 ± 0.02	10.46 ± 0.06	4.51 ± 0.08
56/95	302	11.14 ± 0.03	25.1 ± 0.3	4.12 ± 0.9	3.45 ± 0.01	18.78 ± 0.06	5.65 ± 0.1
57/95	263	20.67 ± 0.04	1.75 ± 0.02	0.50 ± 0.02	3.19 ± 0.01	18.97 ± 0.08	5.22 ± 0.1
Rectilinear Slopes							
50/95	263	9.80 ± 0.01	9.39 ± 0.1	1.28 ± 0.04	0.08 ± 0.001	6.25 ± 0.06	0.88 ± 0.02
51/95	257	107.1 ± 0.3	1.58 ± 0.1	2.36 ± 0.06	3.27 ± 0.01	10.41 ± 0.04	1.51 ± 0.06
52/95	320	9.77 ± 0.08	4.69 ± 0.06	0.64 ± 0.04	3.83 ± 0.02	8.37 ± 0.04	2.11 ± 0.04
13/96	250	2.35 ± 0.01	0.65 ± 0.05	0.005 ± 0.002	1.31 ± 0.01	5.11 ± 0.06	0.38 ± 0.02

$^{21}Ne_c$ and $^{3}He_c$ = cosmogenic ^{21}Ne and ^{3}He respectively. * 1 σ error limits, ** 2 σ error limits. R/Ra = the ratio of $^{4}He/^{3}He$ (R) relative to the atmospheric ratio (R_a) 1.4 x 10^{-6}.

The isotopic composition of Ne and He including the cosmogenic ^{21}Ne and ^{3}He concentrations of all eight samples are presented in Table 6.4. All errors are quoted at the 1 σ level, except for the concentration values (N) which are at the 2 σ level, and include measurement uncertainty only. Blank measurements at 1400°C were ^{4}He: 2 x 10^{-11} cc STP and ^{20}Ne: 1 x 10^{-11} cc STP. ^{3}He was undetectable in the blank while the Ne blanks were indistinguishable from the atmospheric isotopic composition. Reproducibility of abundance measurements was ± 1.5%. Errors on Table 6.4 are propagated from the analytical errors and do not include reproducibility errors. The basis of cosmogenic neon interpretation has been discussed in section 2.3.1 and is briefly described here. Table 6.4 shows that in all cases, the measured $^{21}Ne/^{20}Ne$ ratios (0.00505 - 0.01905) are significantly greater than the atmospheric value of 0.00296 indicating an excess of ^{21}Ne from some other source (Niedermann *et al.*, 1993). The $^{21}Ne/^{20}Ne$ ratio of minerals is essentially a mixture of atmospheric (sometimes known as trapped) and cosmogenic contributions. However, (α,n)-reactions on ^{18}O can produce a nucleogenic ^{21}Ne ($^{21}Ne_n$) component throughout the lifetime

of the rock which may obscure the simple two component mixing (section 2.2.1). The radiogenic ^4He ($^4He_{rad}$) concentration of a sample is a monitor of the α-particle flux which is essential for $^{21}Ne_n$ production (Niedermann *et al.*, 1993). Thus the $^{21}Ne_n$ contribution to the measured excess ^{21}Ne may be estimated from the $^4He_{rad}$ content using the most recent determination of the $^{21}Ne_n/^4He_{rad}$ ratio of crustal rocks (4.5×10^{-8}; Yatsevich and Honda, 1997). Assuming that all the measured ^4He is radiogenic, and that at least 5% has been retained since cooling below the $^{21}Ne_n$ closure temperature, the contribution of $^{21}Ne_n$ to each samples can be calculated (Niedermann *et al.*, 1993). The contribution of $^{21}Ne_n$ is less than 5% in all but one samples (51/95 = 30%). This can be considered as a conservative estimate as, in all but one sample, more than 5% of the ^3He_c has been retained despite it being significantly more mobile in quartz than $^4He_{rad}$ (Trull *et al.*, 1991).

The cosmogenic ^{21}Ne concentrations shown in Table 6.4 have been calculated from the measured ^{21}Ne values assuming an atmospheric composition and corrected for the contribution of nucleogenic ^{21}Ne. $^3He/^4He$ ratios are in the range 0.65 - 32.8 Ra (Table 6.4). These are significantly in excess of radiogenic values and identify the presence of a high cosmogenic ^3He concentrations (^3He_c). The ^3He_c concentrations were calculated assuming that the inherited ^3He is radiogenic ($^3He/^4He = 0.02$ Ra). The ^3He concentration is insensitive to the precise value used for the radiogenic $^3He/^4He$ ratio because of the high ratio in the samples.

In order to investigate the relationship between cosmogenic ^{21}Ne and ^3He, exposure ages were calculated from the measured concentrations assuming no denudation had occurred (Summerfield *et al.*, 1998a but also see Table 6.6). The apparent ^{21}Ne exposure ages ranged from 4.65 ± 0.94 Ma for sample 56/95 to 846 ± 19 ka for sample 13/96 whereas the ^3He exposure ages ranged from 1.17 ± 0.24 Ma for sample 6/96 to 2 ± 1 ka for sample 13/96 (including a 20% production rate uncertainty and 2σ error on N). Because field observations indicated that the samples did not represent a specific exposure event and were undergoing progressive denudation, the concept of an exposure age has no apparent geomorphic meaning (section 6.6.1). However, comparison of the ^3He and ^{21}Ne ages clearly supports the notion that cosmogenic ^3He is lost from quartz via diffusion preferentially over ^{21}Ne (Trull *et al.*, 1991). The ^3He exposure ages vary between 2 and 416 times lower than those derived from ^{21}Ne abundances. The relative age differences appear unrelated to apparent exposure age, lithology, altitude or temperature. The absence of systematic behaviour clearly demonstrates the limitations of obtaining accurate exposure ages or denudation rates from ^3He in quartz (Graf *et al.*, 1991, Brook and Kurz, 1993; Bruno *et al.*, 1997). Comparison of the He and Ne data with other data from samples that had not been

prepared by selective chemical dissolution but had been run on the same mass spectrometer provided limited support for the notion that selective chemical dissolution promotes diffusive loss of cosmogenic ^{3}He in quartz (F. Stuart, *pers. com.*).

Table 6.5: Denudation rate data for Antarctic samples.

Sample Number	$^{26}Al/^{10}Be$	$^{21}Ne/^{10}Be$	$^{21}Ne/^{26}Al$	^{26}Al denudation rate (m Ma^{-1})	^{10}Be denudation rate (m Ma^{-1})	^{21}Ne denudation rate (m Ma^{-1})
High-Elevation Surfaces						
5/96	-	-	-	-	-	0.14 ± 0.03
6/96	-	-	-	-	-	0.15 ± 0.03
56/95	-	8.96 ± 0.91	-	-	0.02 ± 0.01	0.12 ± 0.02
57/95	2.94 ± 0.51	8.65 ± 0.88	2.95 ± 0.42	0.06 ± 0.02	0.03 ± 0.01	0.13 ± 0.03
Rectilinear Slopes						
50/95	4.73 ± 0.82	5.51 ± 0.56	1.16 ± 0.17	0.45 ± 0.16	0.51 ± 0.15	0.53 ± 0.11
51/95	4.12 ± 0.71	4.84 ± 0.52	1.17 ± 0.17	0.04 ± 0.01	0.14 ± 0.04	0.31 ± 0.07
51/95 #2	4.43 ± 0.77	-	-	0.01 ± 0.01	0.15 ± 0.04	-
52/95	-	7.19 ± 0.73	-	-	0.15 ± 0.04	0.22 ± 0.04
13/96	-	-	-	-	-	0.65 ± 0.15

NB: all errors are quoted at 2 σ and include a total of 20% uncertainty on the production rates.

Denudation rate estimates from ^{10}Be, ^{26}Al and ^{21}Ne are given in Table 6.5. Denudation rates were calculated assuming secular equilibrium has been reached for all isotopes and that denudation has been continuous and steady-state such that (Kurz, 1986b; Lal, 1991):

$$\varepsilon = \frac{\Lambda}{\rho}\left(\frac{P}{N} - \lambda\right) \quad \text{for } ^{10}Be \text{ and } ^{26}Al \qquad [6.1]$$

and

$$\varepsilon = \frac{\Lambda}{\rho}\left(\frac{P}{N}\right) \quad \text{for } ^{21}Ne \qquad [6.2]$$

where N is the concentration of the cosmogenic isotope (atoms g^{-1} SiO_2), P is the production rate (atoms g^{-1} SiO_2 a^{-1}), λ is the decay constant of the radionuclide (a^{-1}), Λ is the cosmic ray attenuation coefficient in quartz (150 g cm^{-2}), ρ is the rock density (2.7 g cm^{-3}) and ε is the

steady-state denudation rate (cm a^{-1}) (Lal, 1991, Brown *et al.*, 1992). Denudation rates shown in Table 6.5 have been converted to m Ma^{-1}. Propagated errors on the denudation rates include a 2 σ uncertainty on N (Table 6.3 and 6.4) as well as 20% uncertainty in the production rate values used in equations 6.1 and 6.2 (Table 6.2).

Modelled denudation rates for every sample are below 1 m Ma^{-1} with an overall average of 0.21 ± 0.5 m Ma^{-1}. Samples from the rectilinear slopes yield rates ranging from 0.01 ± 0.01 m Ma^{-1} (51/95 #2 from ^{26}Al) to 0.65 ± 0.15 m Ma^{-1} (13/96 from ^{21}Ne). Samples from the high-elevation surfaces yield rates ranging from 0.02 ± 0.01 m Ma^{-1} (57/95 from ^{26}Al) to 0.15 ± 0.03 m Ma^{-1} (6/96 from ^{21}Ne). In general, the rectilinear slope samples yield higher rates than those for the high-elevation surfaces. Within the rates from each isotope this is always true but rates from ^{21}Ne from the plateau surfaces are sometimes higher than slope rates from ^{10}Be and ^{26}Al. An average rate from all three isotopes for each type of sampling location is 0.29 ± 0.07 m Ma^{-1} for the slopes and 0.09 ± 0.02 m Ma^{-1} for the surfaces. There is better agreement between the rates modelled for the high-elevation sites than the slope sites. This is likely to reflect the closer similarity between the sites on the surfaces compared to the slopes.

Although ^{26}Al was measured in sample 56/95, no denudation rate for this sample has been quoted in Table 6.5. The reason being that equation 6.1 returns a negative answer ($P/N-\lambda$ = –ve for sample 56/95) and therefore is not shown. Causes of this could be underestimation of the production rate for the site, overestimation of the concentration of ^{26}Al or a combination of these two. At the upper limit of the bracket of error for the production rate (+20%), the erosion model still returns a negative answer and it therefore appears that the reason is more likely to be due to an overestimate of the concentration of ^{26}Al (N), or potentially a combination of the two. It is possible that the GFAAS measurement of total ^{27}Al in the sample aliquot was in error. (The concentration of ^{26}Al (N) is dependent on the AMS ratio, the mass of quartz used and the total ^{27}Al content of the sample (section 2.3.2)). Although, sample 56/95 had a significantly higher total ^{27}Al content compared to its neighbouring sample, 57/95 (Table 6.3), there is no guarantee that even closely spaced samples should yield similar results. Total Al content is variable and within the same lithology can vary even at the cm scale, it therefore cannot be ascertained unequivocally whether the anomalous result is attributable to an overestimate of the total Al content without further measurement. Other possible mechanisms for 'excess' ^{26}Al are discussed below.

Data for all three isotopes are available for samples 50/95, 51/95 and 57/95. Agreement in the rates calculated for sample 50/95 is good and is the same for all three isotopes within error. For the other two samples (51/95 and 57/95) the rates estimated from the ^{21}Ne concentrations are significantly higher (outside error limits). When only ^{10}Be and ^{21}Ne data are available (samples 56/95, 52/95), this trend is also apparent and ^{10}Be rates are always lower. Overall, the lowest modelled rates are from the ^{26}Al concentrations. Given that concentrations of three isotopes are only available for three samples in this study and the overall variation within the sample set is low, apparent trends in the data could be more coincidental than real. It is also important to note that ^{21}Ne measurements were performed on an aliquot of the quartz separate used for ^{10}Be and ^{26}Al measurement and some inconsistencies between the data could be attributed to slight initial variation between the samples. However, it is worthwhile to speculate on some potential mechanisms for relatively high ^{21}Ne rates and relatively low ^{26}Al rates. In general, the higher the measured concentration of cosmogenic nuclides then the lower the modelled denudation rate (section 2.4.3). Accepting the possibility of a small amount of diffusion of ^{21}Ne would mean that the measured concentrations are underestimates of the ^{21}Ne originally produced. An increase the amount of cosmogenic ^{21}Ne in the samples would lower the modelled denudation rates and bring them more in line the ^{26}Al and ^{10}Be rates. But, as previously mentioned, diffusion of ^{21}Ne is generally considered to be less problematic that diffusion of ^{3}He and has been shown to be quantitatively retained in Antarctic quartz (Hudson *et al.*, 1991; Graf *et al.*, 1991; Bruno *et al.* 1997). Enhanced concentrations of cosmogenic ^{26}Al compared to concentrations of other isotopes could be due to significant negative muon capture production in the surface layers of rock (section 2.2.1). Although this is generally thought to be insignificant for surface production, it may be more important for ^{26}Al than ^{10}Be (Brown *et al.*, 1991). Alternatively, enhanced ^{26}Al concentrations may be a result of radiogenic (non-cosmogenic) production mechanisms (section 2.2.1). Such production has been shown to be far more significant for ^{26}Al than ^{10}Be but requires a source of α-particles from uranium and thorium decay (Sharma and Middleton, 1989). Although a viable mechanism for producing a variable amount of excess ^{26}Al in a set of samples, Brown *et al.* (1991) showed that U and Th content of Beacon Supergroup rocks is generally too low to explain elevated concentrations of ^{26}Al.

Ratios between the measured concentrations of all three cosmogenic isotopes are shown in Table 6.5 and the data are plotted on ^{26}Al/^{10}Be, ^{21}Ne/^{10}Be and ^{21}Ne/^{26}Al erosion-island graphs in Figures 6.8, 6.9 and 6.10 respectively (Lal, 1991, Graf *et al.*, 1991). An erosion-island graph enables the assumptions of steady-state denudation and secular equilibrium, inherent in the erosion rate model of Lal (1991), to be tested (section 2.4.4). Data that plot within the erosion-

island support the assumption of steady-state denudation, and samples that plot on the lower (dotted) line of the $^{26}Al/^{10}Be$ island or upper (dotted) line of the $^{21}Ne/^{10}Be$ and $^{21}Ne/^{26}Al$ islands indicate that the isotopes have reached secular equilibrium. Samples that lie below the $^{26}Al/^{10}Be$ island or above the $^{21}Ne/^{10}Be$ and $^{21}Ne/^{26}Al$ islands indicate a complex exposure history that could have included phases of burial that would temporarily shield the sample from cosmic rays, or non-steady-state denudation involving the removal of rock layers thicker than the cosmic ray attenuation length of ~0.55 m (Lal, 1991; Small *et al.*, 1997). Samples plotting on the other side of the islands respectively are within the 'forbidden zone'. This could be a result of prior exposure at a site where production was higher, an inherited component of one isotope relative to another or possible some measurement error.

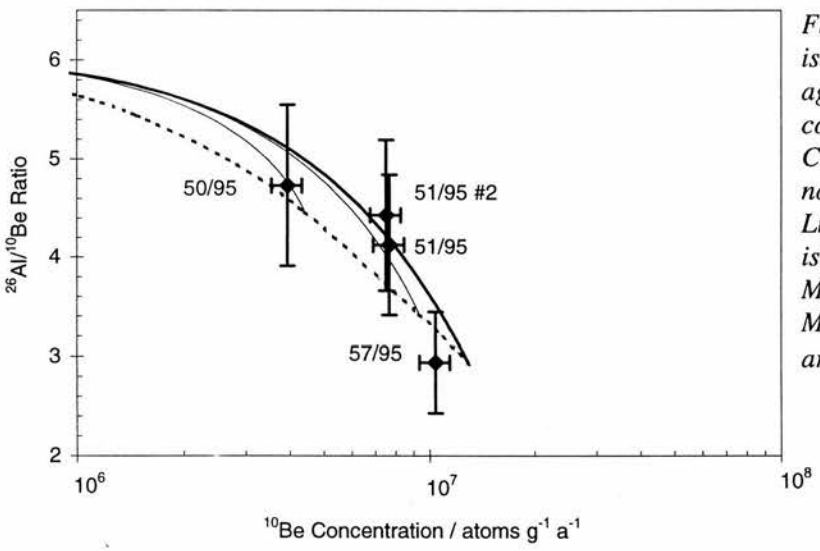

Figure 6.8: Erosion-island plot of $^{26}Al/^{10}Be$ against ^{10}Be concentration. Concentrations have been normalised to sea level. Lines within the erosion-island represent 0.1 m Ma^{-1} (longer) and 0.5 m Ma^{-1} (shorter). Error bars are for 2 σ.

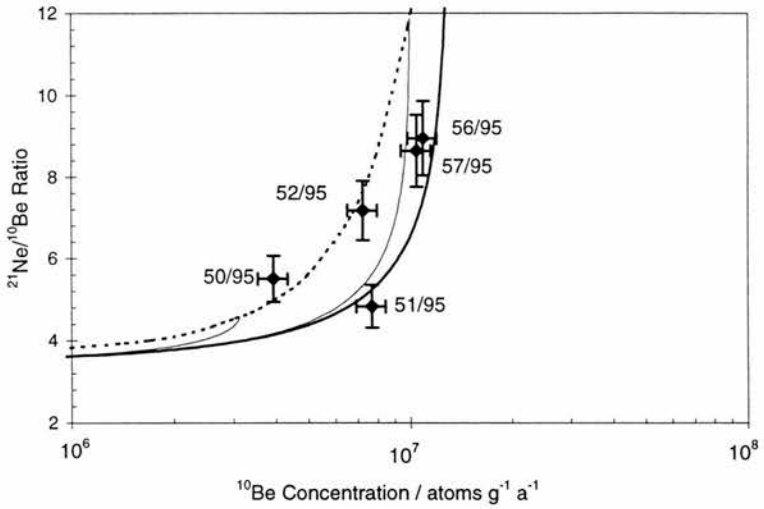

Figure 6.9: Erosion-island plot of $^{21}Ne/^{10}Be$ against ^{10}Be concentration. Concentrations have been normalised to sea level. Lines within the erosion-island represent 0.1 m Ma^{-1} (longer) and 1 m Ma^{-1} (shorter). Error bars are for 2σ.

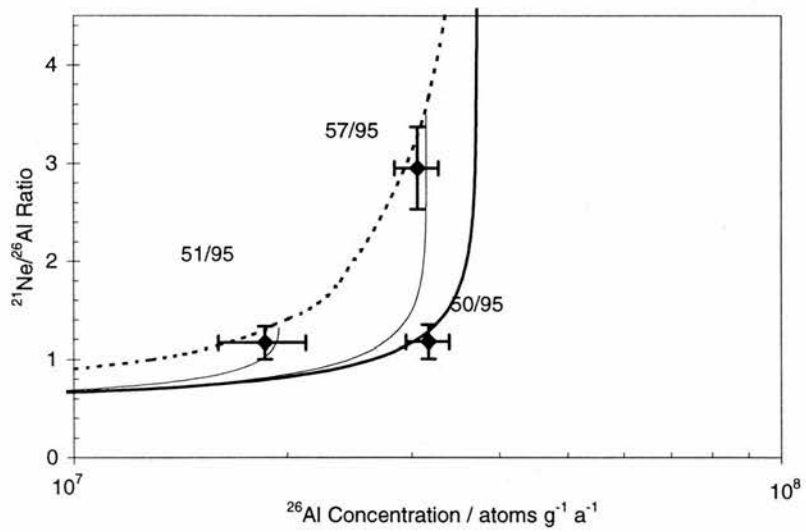

Figure 6.10: Erosion-island plot of $^{21}Ne/^{26}Al$ against ^{26}Al concentration. Concentrations have been normalised to sea level. Lines within the erosion-island represent 0.1 m Ma^{-1} (longer) and 0.5 m Ma^{-1} (shorter). Error bars are for 2σ.

In general, all the samples shown in Figs. 6.8, 6.9 and 6.10, plot very close to the respective erosion-islands. Within the error limits, no samples plot inside the forbidden zone. However, not all samples are showing unequivocal steady-state denudation or a saturation concentration at secular equilibrium. In addition, there appear to be conflicting indications from different isotope pairs in the same sample. High-elevation surface sample 57/95 indicates that both assumptions of the erosion model are satisfied by its position in Figs. 6.8 and 6.10. But in Fig. 6.9, in which neighbouring sample 56/95 is also plotted, although steady-state denudation is indicated, secular equilibrium is not. It is likely, given the similarity of the sampling sites and modelled rates that samples 5/96 and 6/96 would generally support a model of steady-state denudation, and most likely secular equilibrium, if paired isotopic data were available. Rectilinear slope samples (50/95, 51/95, 51#2/95) suggest steady-state denudation and possibly secular equilibrium in Fig.

6.8. Large error bars however, mean that this is not unequivocal and they also could be interpreted in terms of zero erosion. Comparison with the position of 50/95 and 51/95 in the other two graphs indicates that while 50/95 suggests saturation on the $^{21}Ne/^{10}Be$ graph, it suggests no erosion on the $^{21}Ne/^{26}Al$ graph. Conversely for sample 51/95, it indicates steady-state denudation or no erosion on the $^{21}Ne/^{10}Be$ graph but saturation on the $^{21}Ne/^{26}Al$ graph. Sample 52/95, that only appears in Fig. 6.9, supports a model of steady-state denudation as well as secular equilibrium.

Given that all the data do indicate, for some isotope combinations at least, that the exposure history of the samples has been characterised by steady-state denudation but that the samples may not be in secular equilibrium, the modelled rates should be treated as maxima. Although it has been recently shown that removal of thick layers of rock can mean that a modelled rate is in fact lower than the true rate, examination of denudational processes at the sites suggested that the predominate style of weathering would be the incremental removal of grains and thin layers of rock (Small *et al.*, 1997; Summerfield *et al.*, 1998a). Slight inconsistencies between the data shown in Figures 6.8, 6.9 and 6.10 for the rectilinear slope samples could reflect the relative morphological complexity of the sampling sites. Sample 51/95 was taken from a loose boulder resting on a bed rock step and therefore may have fallen from a higher elevation where production rates are higher, alternatively, it may have rolled or contain an inherited component. Previous analysis has shown that, unsurprisingly, non-bedrock samples are prone to giving inconsistent information regarding sample history due to a complex exposure history (Nishiizumi *et al.*, 1991; Graf *et al.*, 1991). Likewise, sample 50/95 was not strictly *in situ* having been taken from a slumped step. Although overall the samples from the slopes do no indicate very significant problems, they demonstrate the importance of simple sampling settings and well understood geomorphology for interpretation purposes.

Making the assuming that the denudation rates are steady-state in every case and the isotopes have reached secular equilibrium, the minimum length of time over which the modelled rate estimates are necessarily integrated is shown in Table 6.6. This is the minimum amount of time required for the isotope to reach secular equilibrium subject to the measured erosion rate. Denudation rates may have been operating for much longer than the periods shown in Table 6.6 but it is not possible to assign a maximum limit using the cosmogenic technique. As discussed in the introduction, the length of time represented by the ^{21}Ne rates is necessarily more than both the ^{26}Al and ^{10}Be rates because ^{21}Ne does not decay and therefore takes longer to reach secular equilibrium. In effect, the values in Table 6.6 are minimum apparent exposure ages for each

sample calculated using equation 2.5 (section 2.4.2), but field evidence indicates that an interpretation in terms of an single exposure event would be invalid (section 6.5.1). For samples 56-57/95, the erosion rates are so low that the minimum exposure times are almost at the upper limit of the time range for ^{10}Be and ^{26}Al when maximum secular equilibrium concentrations (assuming no erosion) are achieved (section 2.4.1). In light of the discussion above, the steady-state/secular equilibrium assumption is most likely to be valid for samples 52/95 and those from high elevation surfaces.

Table 6.6: Minimum length of time over which steady-state rates are integrated.

Sample Number	Minimum Time/Ma	Minimum Time/Ma	Minimum Time/Ma
	Al	Be	Ne
High-Elevation Surfaces			
5/96	-	-	3.78 ± 0.75
6/96	-	-	3.90 ± 0.78
56/95	-	5.49 ± 1.23	4.66 ± 0.93
57/95	2.34 ± 0.57	5.61 ± 1.03	4.30 ± 0.86
Rectilinear Slopes			
50/95	0.81 ± 0.20	0.88 ± 0.20	1.05 ± 0.21
51/95	2.72 ± 0.67	2.28 ± 0.51	1.80 ± 0.39
51/95 #1	3.83 ± 0.94	2.19 ± 0.49	-
52/95	-	2.13 ± 0.48	2.56 ± 0.52
13/96	-	-	0.85 ± 0.19

6.6 Discussion

Denudation rates based on concentrations of cosmogenic ^{10}Be, ^{26}Al and ^{21}Ne for rectilinear slopes and high-elevation plateau surfaces in the Dry Valleys presented in Table 6.5 indicate an average maximum modelled denudation rate of 0.21 ± 0.5 m Ma^{-1} over at least the past ~1 Ma. Plotting the data on erosion-island graphs in Figures 6.8, 6.9 and 6.10 has shown that the majority of rates can be considered as steady-state (i.e. have progressed by the removal of thin layers of rock) and that the sampling sites have had a simple exposure history with no evidence for non-steady-state denudation or phases of burial. However, for some samples the evidence from all three isotopes is inconsistent. Graf *et al.* (1991) is the only other study to have explicitly compared data from ^{10}Be, ^{26}Al and ^{21}Ne on erosion-island plots and here, too, evidence for complex exposure was found for some isotope pairings but not all three for individual samples.

6.6.1 Geomorphic Interpretation of Cosmogenic Isotope Data

All the ^{10}Be, ^{26}Al and ^{21}Ne isotopic concentrations have been interpreted in terms of maximum, steady-state denudation rates and have yielded consistently low values (Table 6.5). However, if the concentrations had been interpreted as minimum exposure ages instead of denudation rates (Table 6.6), older ages would have been associated with the high-elevation surfaces at higher altitudes than the rectilinear slopes. This trend of older ages inland at higher elevations than nearer the coast at lower altitudes has be noted elsewhere in the Transantarctic Mountains (Nishiizumi *et al.,* 1991; Geigengack *et al.,* 1994). One explanation for this trend could be that lowering of the East Antarctic Ice Sheet in the past progressively exposed bedrock at lower elevations. There are, however, compelling arguments against this mechanism as a general explanation of the data (Summerfield *et al.,* 1998a). Firstly, field observations of bedrock surfaces both at low and high altitudes reveal abundant evidence of cavernous weathering and rock degradation. Field evidence indicated that the predominant form of denudation on the high-elevation surfaces was through a continuous incremental detachment of clasts or thin slivers of rock, with some wind abrasion. On the rectilinear slopes detachment of thicker rocks was evident in Arena Valley although the granite basement at the Lower Taylor Valley site appeared to be exfoliating in sheets <20 mm thick. These observations indicate that at least some erosion has occurred since any hypothetical exposure event. But in addition, there are climatic reasons for expecting the observed gradient of rates (section 6.3.3) and other evidence to suggest that the East Antarctic Ice Sheet has been stable since the Miocene and has not fluctuated over the higher elevation sampling sites on the time scale of apparent ^{10}Be, ^{26}Al and ^{21}Ne exposure ages (see below).

Although the data indicate very low rates of denudation for all the sampling locations, the highest rate of 0.65 ± 0.15 Ma^{-1} was calculated at the low elevation site in lower Taylor Valley (13/95). Little can be inferred solely from a single sample, particularly with just one isotope, but the partially eroded form of the immediately adjacent 2.19 Ma old lava flow deposit (Wilch *et al.,* 1993a) supports the interpretation of a higher rate of geomorphic activity in the area. The presence of gelifluction lobes, patterned ground, debris flow and ephemeral stream channels in lower Taylor Valley also indicates a relatively high level of geomorphic activity reflecting the presence of meltwater, relatively high precipitation and humidity, and freeze-thaw cycles during the summer. With the absence of liquid water further inland and at higher elevations, the landscape is subject to extremely low rates of weathering and erosion and appears to be essentially relict (Marchant and Denton, 1996). The low denudation rates measured in Arena

valley by ^{10}Be, ^{26}Al and ^{21}Ne and on Mount Fleming by ^{21}Ne, probably reflect the exceedingly slow operation of salt weathering in conjunction with deflation and very rare mass movement events precipitated by rock failures on the rectilinear slopes and free faces (Selby 1971, 1974). The relative abundance of tafoni and cavernous weathering forms suggests that salt weathering is more active at lower elevations near the coast where both salt supply and humidity are at a maximum. Despite uncertainty in the precise role of various weathering and erosional processes, it is clear that they vary in efficacy across the Dry Valleys area and that rates of denudation estimated from cosmogenic isotopes vary in consequence, possibly in a gradient from the coast, even under the present climatic regime.

6.6.2 Comparison with Other Cosmogenic Isotope Data

The denudation rates calculated from ^{10}Be, ^{26}Al and ^{21}Ne (Table 6.5) can be compared with previously reported cosmogenic isotope data from sites in the Dry Valleys region and other areas of the Antarctica (Summerfield *et al.*,1998a, b). Nishiizumi *et al.*, (1991) published the first ever set of ^{10}Be and ^{26}Al denudation rates on nine samples from Allan Nunatak in the Allan Hills, 75 km north-west of Victoria Valley, and these ranged from 0.24 ± 0.02 m Ma^{-1} to 1.31 ± 0.07 m Ma^{-1}. Four samples from Wright Valley gave a range of 0.54 m Ma^{-1} to 1.31 m Ma^{-1} (Nishiizumi *et al.*, 1991). In the same study, five samples from the Sör Rondane Mountains provided simple exposure rates from 0.05 ± 0.02 m Ma^{-1} to 0.45 ± 0.02 m Ma^{-1}. The Sör Rondane Mountains are almost directly opposite the Dry Valleys on the other side of the continent (Fig. 6.1) and are part of the ancient craton rim of East Antarctica. They are similar to the Transantarctic Mountains in that they have ice free areas and are traversed by ice as it pushes its way out to the Southern Ocean. Nishiizumi *et al.* (1991) is the only study that has demonstrated that samples from different ice free areas in Antarctic yield similar rates although lithological influences and precise sampling details are unknown. Ivy-Ochs *et al.*, (1995) measured ^{10}Be and ^{26}Al mainly in sandstone from the Table Mountain plateau (11 samples) and in granites from within the margins of Sirius deposits (8 samples) to assess the age of the Sirius Group in the framework of the East Antarctic Ice Sheet stability debate. Although the data were principally interpreted in terms of minimum limiting exposure ages, denudation rates from the sandstone samples of 0 to 0.3 m Ma^{-1} were reported. Erosion rates on the granite samples were up to 0.7 m Ma^{-1}. Bruno *et al.* (1997) estimated exposure ages of >40 samples from Sirius Group deposits at Table Mountain and Mount Fleming including several samples from Ivy-Ochs *et al.* (1995), using ^{21}Ne and ^{3}He in quartz, pyroxene and whole rock. Although the emphasis of this work was similar to Ivy-Ochs *et al.* (1995) to date Sirius deposition, denudation rates of <0.1 m Ma^{-1} were reported for plateau

samples. Brook *et al.*, (1995a) estimated ^{10}Be and ^{26}Al erosion rates of ~0.78 m Ma^{-1} for large boulders in tills in Arena Valley that have been $^{40}Ar/^{39}Ar$ dated to >11 Ma BP by volcanic ash (Marchant *et al.*, 1993a). Existing cosmogenic denudation rate data are summarised below in Table 6.7.

Table 6.7: Previously reported cosmogenic isotope denudation rates for the Dry Valleys and other Transantarctic Mountains Areas.

Author/Year	Isotope	Site Location and Number of Samples	Average Rate
Nishiizumi *et al.*, 1991	^{10}Be and ^{26}Al	Allan Nunatak (9)	0.65 m Ma^{-1}
		Wright Valley (4)	0.93 m Ma^{-1}
		Sör Rondane Mountains (6)	0.19 m Ma^{-1}
Ivy-Ochs *et al.*, 1995	^{10}Be and ^{26}Al	Table Mountain Plateau (11)	~ 0.15 m Ma^{-1}
Brown *et al.*, 1991	^{10}Be and ^{26}Al	Arena Valley Tills (4)	~ 0.78 m Ma^{-1}

Overall, the studies shown in Table 6.7 and discussed above have estimated rates that are on average <1 m Ma^{-1} in accordance with the cosmogenic rates from this study (Table 6.5). Table 6.7 does not include 100% of published data on cosmogenic denudation rates from Antarctica; samples that revealed a complex exposure history were excluded (Nishiizumi *et al.*, 1991; Ivy-Ochs *et al.*, 1995) as well as some samples that did not correspond to comparable sites, such as moraine boulders or loose material (e.g. Brook *et al.*, 1993). However, it should be noted that nowhere in Antarctica have cosmogenic data indicated significantly higher rates of landscape change, regardless of their geomorphic setting. Lack of detailed information on the geomorphic setting of the sample sites in Table 6.7 makes direct comparison with the rates in Table 6.5 difficult, but clearly the rates from this study are supported by the very low overall denudation rates calculated in other studies.

6.6.3 Comparison with Other Evidence for Landscape Stability in the Dry Valleys

A range of morphological and depositional evidence has been collected from the Dry Valleys region that suggests the landscape has been essentially stable and subject to little modification since the formation or deposition of the features (Denton *et al.*, 1993; Summerfield, *et al.*, 1998b). The evidence includes cinder cones and lava flows, surficial forms such as avalanche deposits associated with *in-situ* volcanic ash falls, raised marine features, and glacial landforms. Geochronometric dating (mainly $^{40}Ar/^{39}Ar$) of this evidence indicates that surface geomorphic processes have operated at a very low level of activity over the past ~15 Ma. A summary of the evidence demonstrating slow rates of landscape change is shown in Table 6.8 (Summerfield *et al.*, 1998b). Much more extensive data from more sites can be found in the original references.

Table 6.8: Evidence demonstrating slow rates of landscape change in the Dry Valleys (after Summerfield *et al.*, 1998b)

Location	Site/Stratigraphy	Altitude (m)	$^{40}Ar/^{39}Ar$ age (Ma)	Comments
Volcanic rocks and cinder cones in Taylor Valley *(Wilch et al., 1993a, b)*				
E. Rhone	volcanic cone	671	1.5	intact cone
W. Sollas	feeder dyke	416	2.5	partially eroded volcanics
E. Sollas	lava flow deposit (Fig 6.5)	815	2.19	partially eroded volcanics
E. Borns	volcanic cone	587	2.53	partially eroded cone
Matterhorn	pyroclastic/lava flow deposit	828	3.74	eroded volcanic outcrop
Volcanic ash-avalanche deposits *(Marchant et al., 1993a)*				
Upper Arena Valley	ash-avalanche tongue 20 x 200m in size	1380	6.4	deposit survived intact for >6 Ma and inferred desert conditions since this time.
Lower Arena Valley	ash-avalanche tongue 50 x 350m in size (Fig. 6.4)	1625 - 1650	11.3	Preservation of tongue on steep slope and polar desert conditions for >11.3 Ma
Volcanic ash on buried desert pavements				
West central Arena Valley	ash overlies pavement and is covered by regolith	1800	4.3	minimal slope development/ desert conditions since 4.3 Ma BP (Marchant *et al.*, 1993a)
Nibelungen Valley	ash overlies pavement at base of rectilinear slope and is covered by till	1500	14.8	Rectilinear slope older than 14.8 Ma/desert conditions since (Marchant *et al.*, 1993b)
Wright Valley	ash overlies regolith and is overlain by till	378-526	3.9	minimum age of regolith is 3.9 Ma/ prolonged desert conditions (Hall *et al.*, 1993)
Volcanic ash in unconsolidated tills and regolith *(Marchant et al., 1993b, 1996)*				
Nibelungen Valley	ash in wedge in weathered regolith	1450	15.15	ancient sand wedge, regolith older than 15 Ma, prolonged cold desert conditions
Inland Forts	ash in wedge in weathered till	1650	13.6	till at foot of rectilinear slope older than 13.6 Ma/cold desert conditions
Koenig Valley	ash in wedge in till near edge of valley floor	1800	15.0	till at base of rectilinear slope has survived for 15.0 Ma/ cold desert conditions
Volcanic Ash above preserved glacier ice *(Sugden et al., 1995b)*				
Beacon Valley	ash in wedge overlying glacier ice	1380	8.1	glacier ice >8 Ma old and persistent cold conditions
Preservation of raised marine deposits *(Prentice et al., 1993)*				
Wright Valley	glacio-marine diamicton near Lake Vanda	3-250	9 ± 1.5 ($^{87}Sr/^{86}Sr$)	fjord sediments have survived in valley bottom for 9 Ma
Wright Valley	shells in growing position on valley floor	165	5.5 ± 0.4 ($^{87}Sr/^{86}Sr$)	details of fjord bed have survived for 5.5 Ma
Modification of Glacial Landforms				
Sessrumnir Valley	meltwater channels and potholes	1550	>13.6	cavernous weathering and undercutting of 4 m in >13.6 Ma (Sugden *et al.*, 1991)
Wright Valley	moraine ridges	400-800	>3.7 (on basalt erratic)	ridge forms intact for >3.7 Ma (Hall *et al.*, 1993)
Wright Valley	feather edge of Peleus till occurs on 25-35° slope	<1150	>3.8	upper till limit survived on steep slope for >3.8 Ma (Hall *et al.*, 1993)

The data and comments presented in Table 6.8 clearly attest to a remarkable degree of landscape preservation since the mid-Miocene. Cinder cones and outcrops of volcanic rocks >3 Ma at low elevations in Wright Valley have been eroded but younger, <3 Ma old volcanic rocks and cones are better preserved and demonstrate that erosion of these features is a slow process requiring millions of years (Wilch *et al.,* 1993a, b). $^{40}Ar/^{39}Ar$ dating of *in-situ* volcanic ash associated with avalanche deposits, sand wedges, desert pavements, tills, glacial features and preserved glacier ice at higher elevations has shown that these features have been preserved for many millions of years (Marchant *et al.,* 1993a, b). Their preservation provides evidence for prolonged hyper-arid climatic conditions and minimal landscape modification. Raised marine features in Wright Valley, including fjord bed characteristics, have been preserved since they emerged from the sea 5.5 Ma BP (Prentice *et al.,* 1993), also demonstrating slow rates of denudation even at low altitudes. Denudation rate estimates from cosmogenic isotope analysis presented in Table 6.5 support all of the evidence for low rates of landscape change. In particular, the rates from samples 50-52/95 from the rectilinear slope in Arena Valley are compatible with the preservation of the nearby >11Ma old ash avalanche and the somewhat higher rate from sample 13/96 in lower Taylor Valley is consistent with the partially degraded state of the adjacent 2.19 Ma old lava-flow deposit.

The cosmogenic estimates of denudation over the past few million years can also be compared with the very long-term regional estimates of denudation from fission-track thermochronology. Apatite fission track analysis of samples from profiles across the Dry Valleys suggest total denudation since rifting (50-55 Ma BP) of up to 5 km. Maximum amounts of denudation have occurred in the vicinity of the rift-flank axis on the seaward side of the Transantarctic Mountains and decline inland to the west (Gleadow and Fitzgerald, 1987; Fitzgerald, 1992). This gives a maximum mean denudation rate for the Dry Valleys over the past 50 Ma of ~100 m Ma^{-1}. Modelling of the track data indicates a period of accelerated denudation soon after rifting 50-55 Ma BP with elevated rates denudation of ~200 m Ma^{-1} for 10-15 Ma after the initiation of this accelerated denudation. A significant reduction in denudation rates is inferred after this time and a lower rate over the past ~30 Ma is compatible with the denudation rates presented in Table 6.5 and other geochronological data (Table 6.8) that demonstrates low rates of landscape change over the past several million years (Summerfield *et al.,* 1998a).

6.6.4 *Implications for Ice Sheet Stability and Landscape Modification in the Dry Valleys*

The cosmogenic data presented in this chapter suggest that a maximum of only a few metres of total denudation have occurred on the two key topographic elements of high-elevation surfaces and rectilinear slopes in the Dry Valleys over the last 0-5 Ma assuming that the sites are broadly representative of similar geomorphic settings close by. It is therefore clear that presently active geomorphic processes (salt weathering, cavernous weathering etc.) have led to only minimal landscape modification. They would not have been able to create the present day topography from an earlier landscape shaped by through-valley glaciation. As such, the data support the *in-situ* interpretation of volcanic ash used for dating and the view that the existing landscape is relict and must relate to a former period of higher activity, probably under warmer conditions in the Miocene (Denton *et al.*, 1993). Minimal landscape modification since the Miocene suggests that glaciers in the Dry Valleys are likely to have remained cold based throughout this time.

The cosmogenic data correlate with and support other data which imply landscape stability since the mid-Miocene (Table 6.8). As such, the cosmogenic results strongly support the scenario that the East Antarctic Ice Sheet has been essentially stable since the mid-Miocene (Sugden, 1996). They are incompatible with the opposing view of ice-sheet instability and major deglaciation during the Pliocene associated with much warmer conditions (Webb *et al.*, 1984; Barrett *et al.*, 1992) which would have promoted much higher rates of denudation than is indicated by the cosmogenic isotope concentrations reported here (Summerfield *et al.*, 1998a, b).

6.7 Conclusions

Strategically selected samples from contrasting landscape components in the Dry Valleys area yield cosmogenic ^{10}Be, ^{26}Al and ^{21}Ne concentrations that indicate extremely low rates of denudation on the order of 0.3 ± 0.23 for rectilinear slopes and 0.1 ± 0.06 for high-elevation surfaces over at least the past ~1 Ma. Measurement of more than one isotope has enabled thorough testing of the steady-state denudation and secular equilibrium assumptions using three erosion-island diagrams and the data support the steady-state assumption in almost every case. The data are in accordance with previously reported cosmogenic isotope data but are the first data set to be interpreted specifically for denudation rates using three isotopes. The denudation rates are consistent with a large body of independent geochronological data that implies minimal

landscape modification since the mid-Miocene. There is some support for an increase in rates with reduced elevation and proximity to the coast but further sampling is necessary to address this issue properly. The data are 2 - 3 orders of magnitude lower than a mean rate of 100 m Ma^{-1} estimated for the past 50 Ma from apatite fission track analysis thermochronology but are consistent with an inferred slowing down of denudation rates after an initial accelerated period soon after rifting that is characteristic of passive margin evolution. By supporting long-term landscape and climatic stability over the past few million years, the data are at variance with the hypothesis that the Dry Valleys were overrun by ice following a major deglaciation event as recently as the Pliocene. The data, in conjunction with other evidence, support a theory of ice sheet stability for at least the last 15 Ma.

Chapter 7:

Conclusions and Synthesis

7.1 Conclusions

The overall aim of this thesis has been to quantify denudation rates using *in-situ* cosmogenic isotope analysis in order to investigate landscape evolution in passive margin settings with contrasting arid climatic environments. To this end, field sites were selected in the contrasting hot and cold arid conditions of central Namibia and the Transantarctic Mountains, Antarctica. In total, 56 denudation rate estimates based on concentrations of *in-situ* cosmogenic ^{10}Be, ^{26}Al and ^{21}Ne have been presented for 28 separate samples in three field areas. Conclusions drawn from the data can be divided into two broad categories: 1) those concerning the specific objectives of the three specified studies, and 2) broader conclusions about the value of *in-situ* cosmogenic isotopes in geomorphology, especially in terms of determining denudation rates.

The conclusions concerning rates of denudation and landscape evolution drawn from the substantive applications detailed in Chapters 4, 5 and 6 are as follows:

- Denudation rates at the Gamsberg, a flat topped residual on the Great Escarpment of south-west Africa in central Namibia, based on analysis of *in-situ* cosmogenic ^{10}Be and ^{26}Al in quartz, range from 0.26 ± 0.06 to 0.49 ± 0.1 m Ma^{-1} for the summit and 2.15 ± 0.5 to 17.27 ± 4.08 m Ma^{-1} for two granite ridges. Interpretation of these data yield a rate of escarpment retreat of the order of 10 m Ma^{-1} for at least the past 1 Ma and possibly for the entire Quaternary period. An average rate of ~10 m Ma^{-1} is likely to be representative of the rest of the escarpment in Namibia given the overall similarity of lithology, climate and morphology at other locations as well as the consistent distance between the escarpment and the coast along its length. The rate is compatible with existing data from other approaches, such as fission track thermochronology, that indicate large amounts of denudation for the margin soon after rifting but lower amounts and, by implication, lower rates of escarpment retreat throughout the Cenozoic. However, a rate of 10 m Ma^{-1} is two orders of magnitude lower than commonly assumed rates of retreat for Great Escarpments and implies that some existing

models, for south-west Africa at least, should be rejected. Coupled with data from techniques which have a longer-term perspective, *in-situ* cosmogenic isotope analysis can provide much needed empirical constraints for quantitative models of margin evolution.

- Denudation rates calculated from concentrations of *in-situ* cosmogenic ^{10}Be and ^{26}Al on the summits of granite bornhardts Blutkopje, Vogelfederberg and Mirabib in the central Namib Desert range from 2.51 ± 0.5 m Ma^{-1} to 7.43 ± 1.6 m Ma^{-1}. A mode of bornhardt mass wasting at two contrasting scales with small-small laminar sheeting and granular disintegration and larger-scale spallation of sheets >0.5 m thick can explain the apparent complexity in exposure history indicated for some samples. An average rate of ~5 m Ma^{-1} is inferred to have characterised the rate of granite bornhardt lowering in the central Namib for at least the past 10^3-10^6 Ma. The reason proposed for an unexpected order of magnitude difference in ^{10}Be and ^{26}Al denudation rates from similar features in Australia is the persistent presence of coastal fogs in the Namib and high rates of fog-precipitation which may significantly increase the effectiveness of weathering processes such as salt weathering and hydration. The remarkable persistence of arid climatic conditions throughout the Cenozoic in the central Namib in the vicinity of the sampling sites, supports the idea that a rate of ~5 m Ma^{-1} has characterised the rate of bornhardt denudation during the past 10-12 Ma and possibly since the early Tertiary. This rate is fully compatible with other data from techniques, which also suggest denudation rates of <20 m Ma^{-1} for the coastal plain of Namibia during the Tertiary.

- Samples from contrasting landscape components in the Dry Valleys area of the Transantarctic Mountains, Antarctica, yield denudation rates based on concentrations of cosmogenic ^{10}Be, ^{26}Al and ^{21}Ne on the order of 0.3 ± 0.23 m Ma^{-1} for rectilinear slopes and 0.1 ± 0.06 m Ma^{-1} for high-elevation surfaces over at least the past ~1 Ma. The data are in accordance with previously reported cosmogenic isotope data but are the first data set to be interpreted specifically for denudation rates using three isotopes. The denudation rates are consistent with a large body of independent geochronological data that implies minimal landscape modification since the mid-Miocene. The data are two to three orders of magnitude lower than a mean rate of 100 m Ma^{-1} estimated for the past 50 Ma from apatite fission track analysis thermochronology but are consistent with an inferred slowing down of denudation rates after an initial accelerated period soon after rifting that is characteristic of passive margin evolution. By supporting long-term landscape and climatic stability over the past few million years, the data are at variance with the hypothesis that the Dry Valleys were overrun

by ice following a major deglaciation event as recently as the Pliocene. The data, in conjunction with other evidence, support a theory of ice sheet stability for at least the past 15 Ma.

The main conclusions concerning the application of *in-situ* cosmogenic isotope analysis are:

- *In-situ* cosmogenic isotope analysis of ^{10}Be, ^{26}Al and ^{21}Ne is useful for providing estimates of denudation over timescales from ~70 ka up to ~5 Ma in locations where other techniques are either not feasible or are not applicable on a suitable temporal or spatial scale. The technique, therefore, does offer great scope as an alternative approach to assessing landscape change on a time scale meaningful to studies of landscape evolution. The value of the technique in providing first order estimates of denudation rates in areas where no such data exist is not diminished by remaining uncertainties in production rates.

- Given the site-specific nature of the technique, the most critical factor for meaningful application is a well considered sampling strategy coupled with careful site selection in the field. This requires sound general understanding of geomorphic processes and modes of landscape change. The number of samples which can be analysed is necessarily limited due to the expensive and time consuming nature of sample preparation and measurement. Accurate interpretation of data requires that the many factors affecting production of cosmogenic isotopes and the exposure history of the sample be taken into account for each individual site.

- In order to assess the accuracy of denudation rates estimated, it is useful to use more than one isotope. This is particularly important where denudational processes appear to violate the assumption of steady-state. Limited by the models currently available for the interpretation of isotopic concentrations, the technique does not offer reliable estimates of denudation rates (retreat rates) for steeply angled surfaces.

7.2 Synthesis and Future Directions

Further lessons can be learnt from a synthesis of the principal findings of the thesis and such a synthesis provides a useful basis from which to suggest opportunities for further work. The conclusions of the thesis, cited above, clearly confirm the scope for more applications of *in-situ* cosmogenic isotope analysis to constrain denudation rates over spatial and temporal scales intermediate between short-term process studies and long-term estimates from techniques such as

fission track thermochronology. Although it is sensible to reiterate the importance of careful site selection and thorough assessment of the validity of the interpretative models, there are numerous geomorphic settings world-wide that remain without basic information on rates of processes, understanding of which would benefit from applications of *in-situ* cosmogenic isotope analysis. The data from Namibia presented here are among the first concentrations of cosmogenic isotopes measured in samples from the whole of Africa. Large regions characterised by arid conditions and bedrock exposures similar to central Namibia mean that there is almost no end to the sites which could be investigated on this continent alone. Specific locations for further work related to the applications of the thesis are discussed below.

With any sample based technique there will always be a limit on the number of analyses that can be carried out as a function of either time or money. These constraints, of time and funding, were reflected in the number of analyses carried out in this thesis. An 'allowance' of 28 samples was divided up on the basis of finding out as much as possible on the one hand and having enough data to be able to draw substantial conclusions for any one application on the other. In general, the number of samples required for any one application depends on the complexity of the problem being addressed and the nature of the sampling location. But even in seemingly simple settings, such as the summit of the Gamsberg, two or more samples should always be analysed in order to assess potential spatial variability and the possibility that an individual sample yields an anomalous result. One possible approach that was not explored in this thesis, is the amalgamation of quartz from several different samples into one sample for analysis. The rationale here is that such an amalgamated quartz separate would yield an average concentration for all the samples included and therefore would yield an average denudation rate for the area that was sampled. There are potential statistical problems with this approach (J. Stone, *pers. com.)*, and it may be difficult to interpret the geomorphological significance of an average concentration as the intricacies of each sampling site need to be accounted for. To overcome this, the individual sampling locations for all the samples would have to be kept as similar as possible. An interesting trial of this approach would be to amalgamate 10 g of each of the quartz separates from samples 14/94, 10/95 and 12/95 from the summit of the Gamsberg and compare the results for the modelled denudation rates. Whether such an approach could be used in the future without a preliminary assessment of the concentrations of the individual samples would depend on the outcome of further trials and the specific nature of the problem under investigation.

The main benefit of a larger number of samples in all three applications of this thesis would have been that in each case the representativeness of the results to the geomorphic phenomena under investigation could have been better assessed. In Chapter 4, a larger number of samples could have been split between two sites on the Great Escarpment in Namibia which would have be able to discover the true representativeness of the Gamsberg site. In Chapter 5, a greater number of samples could have been spread over more bornhardts across a wider area to further test the proposal that a rate of ~5 m Ma^{-1} characterises the majority of granite bornhardts in the central Namib. Inselbergs of different lithologies could also have been investigated. In Chapter 6, cosmogenic isotope data from another ice-free area, for example the Royal Society Range, could have determined whether the Dry Valleys region is atypical of the Transantarctic Mountains as a whole as has been suggested in the context of the East Antarctic Ice Sheet Stability debate.

In both Chapters 5 and 6, denudation rates appeared to be related to climatic influences that might vary with the proximity of sampling sites to the coast. In the central Namib Desert denudation rates appeared to be influenced by moisture and salt supply from coastal fogs, the occurrence of which decreases inland. In the Dry Valleys cosmogenic isotope analysis lent some support to the theory that rates of denudation decrease with elevation and distance from the coast due to the availability of water. In both regions, a larger number of analyses and a specific sampling strategy could test these hypotheses. In the central Namib, an increased number of samples from bornhardts spaced more uniformly in a profile from the coast to the foot of the escarpment may reveal a gradient of denudation that could be correlated with the occurrence of fog precipitation and salt supply. The data collected so far do not support such a hypothesis but are located within a relatively narrow zone. In the Transantarctic Mountains, a similar sampling strategy of samples from one particular morphological element in a profile from the coast would demonstrate the strength of any gradient in denudation rates from the effects of climate across the region.

In all of the proposals for further work mentioned above, a key requirement is that the type of site investigated be kept as similar as possible for all samples. In Chapter 5, comparison of the results for the bornhardts with similar data for granite inselbergs on the Eyre Peninsula in Australia revealed a rather surprising order of magnitude contrast between the overall rate of denudation in the two locations. This led to the proposal that denudation in the central Namib is exacerbated by fog precipitation. This conclusion demonstrates the usefulness of the techniques for determining the possible controlling factors on denudation rates but the hypothesis was entirely dependent on the compatibility of the sites for comparison. If the data from Australia

had not been for granite inselbergs then the comparison would have been of limited value. In order to investigate the effect of controlling variables on denudation rates estimated from cosmogenic isotope analysis, for example a climatic gradient, the geomorphic setting of the sampling sites and lithology of the samples should be kept similar. Conversely if the rate of denudation on contrasting morphological elements is to be investigated, then it is important to ensure variables such as climate as well as lithology are kept uniform throughout the sampling sites and it is only the geomorphic settings that vary. In general, comparison between sites requires that uncontrolled variables be kept to a minimum.

All three of the substantive applications of this thesis were carried out in arid environments. These proved to be particularly suitable for sampling for cosmogenic isotope analysis due to the lack of soil and vegetation cover and abundance of exposed bedrock. Given the generally poor preservation of datable material in sedimentary sequences in arid environments, cosmogenic isotope analysis offers a useful alternative for the direct assessment of denudation in areas which have hitherto been lacking in such data. Under hot and cold arid conditions, denudation was found to be actively occurring on flat plateau surfaces, the summits of bedrock ridges as well as the more traditionally active landscape element, slopes. It cannot be assumed therefore that any exposed bedrock features remain unaltered in even the most seemingly frigid environments over long periods of time. Rates of denudation in the cold, hyper-arid Dry Valleys were found to be significantly lower than those in the warmer hyper-arid conditions of the central Namib. The almost uniquely low availability of moisture at the relatively high elevations of the sampling sites in the Dry Valleys is likely to be the cause of this differential but further investigation into the contrast between other hot and cold arid environments could provide insights to the relative effectiveness of processes such as salt weathering or wind scouring with temperature.

It has been demonstrated that *in-situ* cosmogenic isotope analysis can provide data on the behaviour of escarpments, the key feature of many passive margins, over time scales up to 10^6 a. Given the central role that escarpment retreat plays in many generic conceptual and quantitative models of margin evolution, data of this kind is needed for full understanding of margin development in many other locations. There is a large scope for applications, similar to the one carried out here and presented in Chapter 4, on other passive margins which exhibit large scale escarpments. As previously mentioned, work is already being undertaken on the Drakensberg Escarpment in South Africa (A. Fleming, *pers. com.*) and work on the south-east Australian margin using cosmogenic ^{10}Be and ^{26}Al to estimates denudation rates is also in progress (M. Seidl, *pers. com.*). When these studies are complete it will be interesting to see how the data

compare for although many passive margins do exhibit similar topography, it is likely that their evolution has differed (Bishop and Goldrick, 1998).

This thesis has demonstrated that an important future direction for *in-situ* cosmogenic isotope analysis, in terms of understanding landscape evolution, is for it to be used in conjunction with other techniques to provide detailed denudation chronologies. The technique offers geomorphology, as a discipline, a crucial link between the more traditional short-term process studies and long-term, regional scale techniques that tend to obscure geomorphic detail (Sugden *et al.,* 1996; Summerfield, 1996a). Although the technique has been adopted in a range of institutions in the USA, and to a lesser extent in Australia, in the UK it has not yet become part of standard range of techniques considered to approach geomorphic problems. However, the clear potential for *in-situ* cosmogenic isotope analysis to answer long-standing geomorphological questions presents a challenge to the UK scientific community.

References

Albrecht, A., Herzog, G. F., Klein, J., Dezfouly-Arjomandy, B and Goff, F. (1993) Quaternary erosion and cosmic-ray-exposure history derived from ^{10}Be and ^{26}Al produced *in-situ* - an example from Pajarito plateau, Valles Caldera region. *Geology* 21, 551-554.

Allen, P.A. and Allen, J. R. (1990) *Basin Analysis, Principles and Applications.* Blackwell Scientific, Oxford.

Anderson, K. C. and Wells, S. G. (1997) Processes responsible for the development of accretionary desert pavements in the southwestern USA. *Supplimenti di Geografia Fisca e Dinamica Quaternaria,* Supplemento III, 51-52.

Barnard, W. S. (1997) Classics in physical geography revisited: Wellington, J. H. (1955), Southern Africa: a geographical study. Part 1, Physical Geography. Cambridge University Press. *Progress in Physical Geography* 21, 137-144.

Barrett, P. J., Adams, C. J., McIntosh, W. C., Swisher III, C. C. and Wilson, G. S. (1992) Geochronological evidence supporting Antarctic deglaciation three million years ago. *Nature* 359, 816-818.

Beaumont, C., Fullsack, P. and Hamilton, J. (1992) Erosional control of active compressional orogens. In, McClay, K. (eds) *Thrust Tectonics*. Chapman and Hall, New York, 1-18.

Beaumont, C., Kooi, H. and Willet, S. (1998) Progress in coupled tectonic-surface process models with application to rifted margins and collisional orogens. In, Summerfield, M. A. (ed) *Geomorphology and Global Tectonics*. Wiley, Chichester, *in press.*

Behrendt, J. C. and Cooper, A. K. (1991) Evidence of rapid Cenozoic uplift of the shoulder escarpment of the Cenozoic West Antarctic rift system and a speculation on possible climatic forcing. *Geology* 19, 315-319.

Besler, H. and Marker, M. E. (1979) Namib Sandstone: A distinct lithological unit. *Transactions of the Geological Society of South Africa* 82, 155-160.

Besler, H. (1996) The Tsondab Sandstone in Namibia and its significance for the Namib Erg. *South African Journal of Geology* 99, 77-87.

Besler, H. and Pfeiffer, L. (1993) The Tertiary proto-erg of the Namib: depositional environment of the Tsondab Sandstone in Namibia. *Journal of the Namibian Scientific Society* 44, 7-23.

Bierman, P. R. (1993) *Cosmogenic Isotopes and the Evolution of Granite Landforms.* Unpublished Ph.D. thesis, University of Washington.

Bierman, P. (1994) Using *in-situ* produced cosmogenic isotopes to estimate rates of landscape evolution: a review from the geomorphic perspective. *Journal of Geophysical Research* 99, 13,885-13,896.

Bierman, P., Gillespie, A. R. and Caffee, M. W. (1995) Cosmogenic ages for earthquake recurrence intervals and debris flow fan deposition, Owens Valley, California. *Science* 270, 447-450.

Bierman, P. and Turner, J. (1995) ^{10}Be and ^{26}Al evidence for exceptionally low rates of Australian bedrock erosion and the likely existence of pre-Pleistocene landscapes. *Quaternary Research* 44, 378-382.

Bierman. P. and Steig, E. J. (1996) Estimating rates of denudation using cosmogenic isotope abundances in sediment. *Earth Surface Process and Landforms* 21, 125-139.

Bierman, P, Marsella, K. A., Davis, P. T. and Caffee, M. W. (1996) Old Arctic upland bedrock surfaces have complex burial and cosmogenic exposure histories. *EOS, Transactions of the American Geophysical Union* 77, 192.

Birkenhauer, J. (1991) *The great escarpment of southern Africa and its coastal forelands - a re-appraisal.* Munchener Geographische Abhandlungen Band B11.

Bishop, P. (1988) The eastern highlands of Australia: the evolution of an intraplate highland belt. *Progress in Physical Geography* 12, 159-181.

Bishop, P. (1995) Drainage rearrangement by river capture, beheading and diversion. *Progress in Physical Geography* 19, 449-473.

Bishop, P. (1998) Griffith Taylor and the SE Australian Highlands: issues of data sources and testability in the interpretations of long-term drainage history and landscape evolution. *Australian Geographer* 29, 7-29.

Bishop, P. and Goldrick, G. (1998) Eastern Australia. In, Summerfield, M. A. (ed) *Geomorphology and Global Tectonics.* Wiley, Chichester, *in press.*

Bohannon, R. G., Naesser, C. W., Schmidt, D. L. and Zimmermann, R. A. (1989) The timing of uplift, volcanism and rifting peripheral to the Red Sea: a case for passive rifting? *Journal of Geophysical Research* 94, 1683-1701.

Bradley, W. C., Hutton, J. T. and Twidale, C. A. (1978) Role of salts in development of granite tafoni, South Australia. *Journal of Geology* 86, 647-654.

Brain, C. K. and Brain, V. (1977) Microfaunal remains from Mirabib: some evidence of palaeo-ecological changes in the Namib. *Madoqua* 10, 285-293.

Braun, J. and Beaumont, C. (1989) Dynamical models of the role of crustal shear zone in asymmetric continental extension. *Earth and Planetary Science Letters* 93, 405-423.

Bremmer, H. (1985) Randschwellen: a link between plate tectonics and climatic geomorphology. *Zeitschrift für Geomorphologie N. F., Supplement band* 54, 11-21.

Bremner, J. M. (1981) Shelf morphology and surficial sediment off central and northern South West Africa (Namibia). *Geo-Marine Letters* 1, 91-96.

Briner, J. B. and Swanson, T. W. (1998) Using inherited cosmogenic ^{36}Cl to constrain glacial erosion rates of the Cordilleran ice sheet. *Geology* 26, 3-6.

Brook, E. J. (1993) *Surface Exposure Geochronology Using Cosmogenic Nuclides: Applications in Antarctic Glacial Geology.* Unpublished Ph.D. thesis, MIT/WHOI.

Brook, E. J. and Kurz, M. D. (1993) Surface-exposure chronology using *in-situ* cosmogenic ^{3}He in Antarctic quartz sandstone boulders. *Quaternary Research* 39, 1-10.

Brook, E. J., Kurz, M. D., Ackert, R. P., Denton, G. H., Brown, E. T., Raisbeck, G. M. and Yiou, F. (1993) Chronology of Taylor Glacier advances in Arena Valley, Antarctica using *in-situ* cosmogenic ^{3}He and ^{10}Be. *Quaternary Research* 39 11-23.

Brook. E. J., Brown, E. T., Kurz, M. D., Ackert, R. P., Raisbeck, G. M. and Yiou, F. (1995a) Constraints on age, erosion and uplift of Neogene glacial deposits in the Transantarctic Mountians determined from *in-situ* cosmogenic ^{10}Be and ^{26}Al. *Geology* 23, 1063-1066.

Brook, E. J., Kurz, M. D., Ackert, R. P., Raisbeck, G. and Yiou, F. (1995b) Cosmogenic nuclide exposure ages and glacial history of the late Quaternary Ross Sea drift in McMurdo Sound, Antarctica. *Earth and Planetary Science Letters* 131, 41-56.

Brook, E. J., Nesje, A., Lehmann, S. J., Raisbeck, G. M. and Yiou, F. (1996) Cosmogenic nuclide exposure ages along a vertical transect in western Norway: implications for the height of the Fenno-Scandinavian ice sheet. *Geology* 24, 207-210.

Brown, E. T.; Edmond, J. M,. Raisbeck, G. M., Yiou, F., Kurz, M. D. and Brook, E. J. (1991) Examination of surface exposure ages of Antarctic moraines using *in-situ* produced ^{10}Be and ^{26}Al. *Geochimica et Cosmochimica Acta* 55, 2269-2283.

Brown, E. T, Brook, E. J., Raisbeck, G. M., Yiou, F. and Kurz, D. (1992) Effective attenuation lengths of cosmic rays producing ^{10}Be and ^{26}Al in quartz: implications for exposure dating. *Geophysical Research Letters* 19, 367-372.

Brown, E. T., Stallard, R. F., Larsen, M. C., Raisbeck, G. M. and Yiou, F. (1995a) Denudation rates determined from the accumulation of *in-situ* produced ^{10}Be in the Luquillo experimental forest, Puerto Rico. *Earth and Planetary Science Letters* 129, 193-202.

Brown, E. T., Bourles, D. L., Colin, F., Raisbeck, G. M., Yiou, F. and Desgarceaux, S. (1995b) Evidence for muon induced *in-situ* production of ^{10}Be in near surface rocks from the Congo. *Geology* 22, 703-706.

Brown, R. W. (1991) Backstacking apatite fission-track 'stratigraphy': a method for resolving the erosional and isostatic rebound components of tectonic uplift histories. *Geology* 19, 74-77.

Brown, R. W. (1992) *A Fission Track Thermochronological Study of the Tectonic and Geophysical Development of the Sub-Aerial Continental Margins of Southern Africa.* Unpublished Ph.D. thesis, La Trobe University.

Brown, R. W. and Summerfield, M. A. (1997) Some uncertainties in the derivation of rates of denudation from thermochronological data. *Earth Surface Processes and Landforms* 22, 239-248.

Brown, R. W., Rust, D. J., Summerfield, M. A., Gleadow, A. J. W. and De Wit, M. C. J. (1990) An early Cretaceous phase of accelerated erosion on the south-western margin of Africa: evidence from apatite fission track analysis and the off-shore sedimentary record. *Nuclear Tracks and Radiation Measurements* 17, 339-350.

Brown, R. W., Summerfield, M. A. and Gleadow, A. J. W. (1994) Apatite fission track analysis: its potential for the estimation of denudation rates and implications for models of long-term landscape development. In Kirkby, M. J. (ed) *Process Models and Theoretical Geomorphology*. Wiley, Chichester, 23-53.

Brown, R. W., Gallagher, K., Gleadow, A. and Summerfield, M. A. (1998) Morphotectonic evolution of the South Atlantic margins of Africa and South America. In, Summerfield, M. A. (ed) *Geomorphology and Global Tectonics*. Wiley, Chichester, *in press.*

Bruno, L. A., Baur, H., Graf, T., Schluchter, C., Signer, P. and Weler, R. (1997) Dating of the Sirius group tillites in the Antarctic Dry Valleys with cosmogenic ^{3}He and ^{21}Ne. *Earth and Planetary Science Letters* 147, 37-54.

Büdel, J. (1982) *Climatic Geomorphology*. (English translation of *Klima-Geomorphologie*, (1977)). Princeton University Press.

Buck, W. R. (1986) Small-scale convection induced by passive margin rifting: the cause for uplift of rift shoulders. *Earth and Planetary Science Letters* 77, 362-372.

Burbank, D. W., Leland, J., Fielding, E., Anderson, R. S., Brozovic, N., Reid, M. and Duncan, C. (1996) Bedrock incision, rock uplift and threshold in hillslopes in the northwestern Himalayas. *Nature* 379, 505-510.

Burckle, L. H. and Potter Jr., N. (1996) Pliocene-Pleistocene diatoms in Paleozoic and Mesozoic sedimentary and igneous rocks from Antarctica: A Sirius problem solved. *Geology* 24, 235-238.

Cerling, T. E. (1990) Dating geomorphological surfaces using cosmogenic ^{3}He. *Quaternary Research* 33, 148-156.

Cerling, T. E. and Craig, H. (1993) Cosmogenic production rates of ^{3}He from 36-46°N latitude, western USA and France. *Geochimica et Cosmochimica Acta* 58, 249-255.

Cerling, T. E. and Craig, H. (1994) Geomorphology and *in-situ* cosmogenic isotopes. *Annual Review of Earth and Planetary Science* 22, 273-317.

Cerling, T. E., Poreda, R. J. and Rathburn, S. L. (1994) Cosmogenic ^{3}He and ^{21}Ne age of the Big Lost River flood, Snake River Plain, Idaho. *Geology* 22, 227-230.

Chorley, R. J., Dunn, A. J. and Beckinsale, R. P. (1964) *History of the Study of Landforms*, vol. 1. Methuen, London.

Clapperton, C. M. and Sugden, D. E. (1990) Late Cenozoic glacial history of the Ross Sea Embayment, Antarctica. *Quaternary Science Reviews* 9, 253-272.

Clark, D. H., Bierman, P. R. and Larsen, P. (1995) Improving *in-situ* cosmogenic chronometers. *Quaternary Research* 44, 366-376.

Craig, H. and Poreda, R. J. (1986) Cosmogenic ^{3}He in terrestrial rocks: the summit lavas of Maui. *Proceedings of the National Academy of Science USA* 83, 1970-1974.

Coetzee, J. A. (1980) Tertiary environmental changes along the south-western African coast. *Palaeontologia Africana* 23, 197-203.

Cooke, R. U. and Smalley, I. J. (1968) Salt weathering in deserts. *Nature* 220, 1226-1227.

Cooke, R. U., Warren, A. and Goudie, A. S. (1993) *Geomorphology in Deserts.*

Davidson, I. (1997) Wide and Narrow margins of the Brazillian South Atlantic. *Journal of the Geological Society* 154, 471-476.

Davis, J. C., Proctor, I. D., Southon, J. R., Caffe, M. W., Heikkinen, D. W., Roberts, M. L., Moore, T. L., Turteltaub, K. W., Nelson, D. E., Loyd, D. H. and Vogel, J. S. (1990) LLNL/UC AMS facility and research program. *Nuclear Instruments and Methods in Physics Research B* 52, 269-272.

Davis, R. and Schaeffer, O.A. (1955) Chlorine-36 in nature. *Ann. N. Y. Acad. Sci.* 62, 105-122.

Davis, W. M. (1899) The geographical cycle. *Geographical Journal* 14, 481-504.

Davis, W. M. (1905) The geographical cycle in and arid climate. *Journal of Geology* 13, 381-407.

Denton, G. H., Sugden, D. E., Marchant, D. R., Hall, B. L. and Wilch, T. I. (1993) East Antarctic Ice Sheet sensitivity to Pliocene climatic change from a Dry Valleys perspective. *Geografiska Annaler* 75A, 155-204.

De Swardt, A. M. J. and Bennet, G. (1974) Structural and physiographic development of Natal since the Late Jurassic. *Transactions of the Geological Society of South Africa* 77, 309-322.

De Waal, S. A. (1966) *The Alberta Complex, a metamorphosed layered intrusion, north of Nauchas, South West Africa, the surrounding granites and repeated folding in the younger Damara System.* Unpublished Ph.D. thesis, University of Pretoria.

Dingle, R. V. and Hendy, Q. B. (1984) Late Mesozoic and Tertiary sediment supply to the Eastern Cape Basin (SE Atlantic) and palaeo-drainage systems in southwestern Africa. *Marine Geology* 56, 13-26.

Dingle, R. V., Siesser, W. G. and Newton, A. R. (1983) *Mesozoic and Tertiary Geology of Southern Africa.* Balkema, Rotterdam.

Dixey, F. (1938) Some observations on the physiographical development of central and southern Africa. *Transactions of the Geological Society of South Africa* 41, 113-172.

Donahue, D. J., Jull, A. J. T., Toolin, L. J. (1990) Radiocarbon measurements at the University of Arizona AMS Facility. *Nuclear Instruments and Methods in Physics B* 52, 224-228.

Doornkamp, J. C. and Abraham, H. A. M. (1990) Salt weathering. *Progress in Physical Geography* 14, 335-348.

Dorn, R. I. and Phillips, F. M. (1991) Surface exposure dating: Review and critical evaluation. *Physical Geography* 12, 303-333.

Dowsett, H. J. and Cronin, T., M. (1990) High eustatic sea level during the middle Pliocene Evidence from the southeastern U. S. Atlantic coast plain. *Geology* 18, 435-438.

Drewry, D. J. (1982) Ice flow, bedrock and geothermal studies from radio echo sounding inland of McMurdo Sound, Antarctica. In. Craddock, C. (ed), *Antarctic Geoscience*, University of Wisconsin Press, 977-983.

Du Toit, A. L. (1954) The Geology of South Africa. (Third Edition - edited by Haughton, S. H.) Oliver and Boyd, Edinburgh.

Eales, H. V., Marsh, J. S. and Cox, K. G. (1984) The Karoo igneous province: an introduction. In, Erlank, A. J. (ed) Petrogenesis of the Volcanic Rocks of the Karoo Province. *Special Publication of the Geological Society of South Africa*, 13, 1-26.

Eitel, B. and Zöller, L. (1996) Soils and sediments in the basin of the Dieprivier-Uitskot (Khorixas District, Namibia): Age, geomorphic and sedimentological investigation, paleoclimatic interpretation. *Palaeoecology of Africa* 24, 159-172.

Elmore, D. and Phillips, F. M. (1987) Accelerator mass spectrometry for measurement of long-lived radioisotopes. *Science* 236, 543-550.

Emery, K. O. and Uchupi, E. (1984) *The Geology of the Atlantic Ocean.* Springer Verlag, New York.

Etheridge, M. A., Symonds, P. A. and Lister, G. S. (1989) Application of the detachment model to reconstruction of conjugate passive margins. *Association of American Petroleum Geologists Memoir* 46, 23-40.

Evans, J. M., Stone, J. O. H., Fifield, L. K. and Cresswell, R. (1997) Cosmogenic chlorine-36 produced in K-feldspar. *Nuclear Instruments and Methods in Physics Research B* 125, 340-346.

Fabryka-Martin, J. T. (1988) *Production of radionuclides in the Earth and their hydrological significance with emphasis on chlorine-36 and iodine-129.* Unpublished Ph.D. thesis, University of Arizona.

Faure, G. (1986) *Principles of Isotope Geology,* Second Edition. Wiley, New York.

Fink, D., Klein, J., Middleton, R., Vogt, S. and Herzog, G. F. (1990) ^{41}Ca in ironfalls, Grant and Estherville, production rates and related exposure age calculations. *Earth and Planetary Science Letters* 107, 115-128.

Fink, D., Middleton, R., Klein, J. and Sharma, P. (1994) ^{41}Ca measurement by accelerator mass spectrometry and applications. *Nuclear Instruments and Methods in Physics Research B* 47, 79-96.

Finkel, R. C. and Suter, M. (1993) AMS in the Earth sciences: Techniques and Applications. *Advances in Analytical Geochemistry* 1, 1-114.

Finkel, R. C., Ryerson, F. J., Caffee, M. W., Tapponnier, P., Van der Woerd, J. and Meriaux, A. (1997) Dating deformation: application of cosmogenic exposure dating to active tectonics. *Geological Society of America Annual Meeting Abstracts with Programs*, A-170.

Fitzgerald, P. G. (1992) The Transantarctic Mountains of southern Victoria Land: The application of apatite fission track analysis to rift shoulder uplift. *Tectonics*, 11, 634-662.

Fitzgerald, P. G., Sandifor, M., Barrett, P. J. and Gleadow, A. J. W. (1986) Asymmetric extension associated with uplift and subsidence in the Transantarctic Mountains and Ross Embayment. *Earth and Planetary Science Letters* 81, 67-78.

Flohn, H. (1984) Climatic evolution in the southern hemisphere and the equatorial region during the late Cenozoic. In Vogel, J. C. (ed*) Late Cainozoic Palaeoclimates of the Southern Hemisphere* Balkema Rotterdam/Boston, 5-20

Gallagher, K. (1995) Evolving temperature histories from apatite fission-track data. *Earth and Planetary Science Letters* 136, 421-435.

Gallagher, K and Hawkesworth, (1994) Mantle plumes, continental tectonics and asymmetry in the South Atlantic. *Earth and Planetary Science Letters* 123, 105-117.

Gallagher, K. and Brown, R. (1997) The onshore record of passive margin evolution. *Journal of the Geological Society* 154, 451-457.

Gentilli, J. (1971) The main climatological elements. In, Gentilli, J. (ed) *Climates of Australia and New Zealand. World Survey of Climatology*, Vol. 13. Elsevier, Amsterdam, 119-184.

Gerrard, I and Smith, G. C. (1982) Post-Palaeozoic succession and structure of the south western African continental margin. In Watkins, J. S. and Drake, C. L. (eds) *Studies in Continental Margin Geology* AAPC Memoirs 34, 49-74.

Gersonde, R., Kyte, F. T., Bleil, U., Diekmann, B., Flores, J. A., Gohl, K., Grahl, G., Hagen, R., Kuhn, G., Sierro, F. J., Volker, D., Abelmann, A. and Bostwick, J. A. (1997) Geological record and reconstruction of the late Pliocene impact of the Eltanin asteroid in the Southern Ocean *Nature* 390, 357-363.

Gevers, T. W. and Westhysen, J. B. (1931) The occurrence of salt in the Swakopmund Area. *Transactions of the Geological Society of South Africa*, 34, 61-80

Gevers, T. W. (1936) The morphology of western Damaraland and the adjoining Namib desert of South West Africa. *South African Geographical Journal* 19, 61-79.

Gevers, T. W. (1937) The Etjo beds of northern Hereroland, South West Africa. *Transactions of the Geological Society of South Africa* 39, 317-329.

Giegengack, R., Macchiaroli, P. E., Klein, J., Lawn, B. R, and Middleton, R. (1994) Exposure Ages, erosion rates and burial histories of bedrock surfaces in and near the Dry Valleys, Antarctica: preliminary results from AMS measurement of selected cosmogenic radionuclides. In van der Watern, F. M., Verbers, A. L. L. M. and Tessensohn, F. (eds) *LIRA Workshop on Landscape Evolution: A Multidisciplinary Approach to the Relationship Between Cenozoic Climatic Change and Tectonics in the Ross Sea Area, Antarctica*. Rijks Geologishe Dienst., Haarlem, 137.

Gilchrist, A. R. (1995) On appraising classical models of landscape evolution for passive continental margins. In Slaymaker, O. (ed) *Steepland Geomorphology*. Wiley, Chichester, 7-26.

Gilchrist, A. R. and Summerfield, M. A. (1990) Differential denudation and flexural isostasy in formation of rifted margin upwarps. *Nature* 246, 739-742.

Gilchrist, A. R. and Summerfield, M. A. (1991) Denudation, isostasy and landscape evolution. *Earth Surface Process and Landforms* 16, 555-562.

Gilchrist, A. R. and Summerfield, M. A. (1994) Tectonic models of passive margin evolution and their implications for theories of long-term landscape development. In Kirkby, M. J. (ed) *Process Models and Theoretical Geomorphology.* Wiley, Chichester, 55-84.

Gilchrist, A. R., Summerfield, M. A. and Cockburn, H. A. P. (1994a) Landscape dissection, isostatic uplift and the morphological development of orogens. *Geology* 22, 963-966.

Gilchrist, A. R., Kooi, H. and Beaumont, C. (1994b) Post Gondwana geomorphic evolution of southwestern Africa: Implications for the controls on landscape development from observations and numerical experiments. *Journal of Geophysical Research* 99, 12,211-12,228.

Gleadow, A. J. W. and Fitzgerald, P. G. (1987) Uplift history and structure of the Transantarctic Mountains: New evidence from fission track dating of basement apatites in the Dry Valleys area, southern Victoria Land. *Earth and Planetary Science Letters* 82. 1-14.

Gosse, J. C., Evenson, E. B., Klein, J., Lawn, B. and Middleton, R. (1995a) Precise cosmogenic ^{10}Be measurements in western North America: Support for a global Younger Dryas cooling event. *Geology* 23, 877-880.

Gosse, J. C., Klein, J. Evenson, E. B., Lawn, B. and Middleton, R. (1995b) Beryllium-10 dating of the duration and retreat of the last Pinedale glacial sequence. *Science* 268, 1329-1333.

Gosse, J. C., Reedy, C. D., Harrington, and Poths, J. (1996) Overview of the workshop on secular variations in production rates of cosmogenic nuclides on Earth. *Radiocarbon* 38, 135-147.

Goudie, A. S. (1972) Climate, weathering crust formation, dunes and fluvial features of the central Namib Desert, near Gobabeb, South West Africa. *Madoqua* 1, 54-62.

Goudie, A. S. (1974) Further experimental investigation of rock weathering by salt and other mechanical processes. *Zeitschrift Für Geomorphology, Supplement Band* 21, 1-12.

Goudie, A. S. (1983) Calcrete. In, Goudie, A. S. and Pye, K. (eds) *Chemical Sediments and Geomorphology: Precipitates and Residua in the Near Surface Environment.* Academic Press, London, 93-132.

Goudie, A. S. (1989) Weathering processes. In Thomas, D. S. G. (ed) *Arid Zone Geomorphology.* Belhaven Press, London, 11-24.

Goudie, A. S. (1995) *The Changing Earth. Rates of Geomorphological Processes.* Blackwell, Oxford.

Goudie, A. S. (1996) The geomorphology of the seasonal tropics. In Adams, W. M., Goudie, A. S. and Orme, A. R. (eds) *The Physical Geography of Africa.* Oxford University Press, 148-160.

Goudie, A. S. and Migon, P. (1997) Weathering pits in the Spitzkoppe area, central Namib Desert. *Zeitschrift Für Geomorphologie N. F.* 41, 417-444.

Goudie, A. S. and Viles, H. (1997) *Salt Weathering Hazards*. Wiley, Chichester.

Goudie, A. S., Cooke, R. U. and Doornkamp, J. C. (1979) The formation of silt from quartz dune sand by salt weathering processes in deserts. *Journal of Arid Environments* 2, 105-112.

Goudie, A. S., Viles, H. A. and Parker, A. G. (1997) Monitoring of rapid salt weathering in the central Namib Desert using limestone blocks. *Journal of Arid Environments* 37, 581-598.

Gould, S. J. (1977) *Ever Since Darwin*. Burnett Books, London.

Graf, T., Kohl, C. P. Marti, K. and Nishiizumi, K. (1991) Cosmic ray produced neon in Antarctic rocks. *Geophysical Research Letters* 18, 65-73.

Graf, Th., Niedermann, S., and Marti, K. (1993) A calibration of the production rates of P_{21}/P_{26} by low energy secondary neutrons: Identification of Ne spallation components at 10^6 atoms g^{-1} level in terrestrial samples. Proceedings of the Lunar and Planetary Science Conference 24, 555-556..

Granger, D. E., Kirchner, J. W. and Finkel, R. C. (1996). Spatially average long-term erosion rates measured from *in-situ* produced cosmogenic nuclides in alluvial sediment. *The Journal of Geology* 104, 249-257.

Granger, D. E., Kirchner, J. W. and Finkel, R. C. (1997) Quaternary downcutting rate of the New River Virginia measured from differential decay of cosmogenic ^{26}Al and ^{10}Be in cave-deposited alluvium. *Geology* 25, 107-110.

Gunn, R. (1949) Isostasy extended. *Journal of Geology* 57, 263-279.

Hall, B. L., Denton, G. H., Lux, D. R. and Brockheim, J. G. (1993) Late Tertiary Antarctic paleoclimate and ice-sheet dynamics inferred from surficial deposits in Wright Valley. *Geografiska Annaler* 75A, 239-268.

Hallet, B. and Putkonen, J. (1994) Surface dating of dynamic boulders on aging moraines. *Science* 265, 937-940.

Heine, K. and Geyth, M. A. (1984) Radiocarbon dating of speleotherms from the Rossing Cave, Namib Desert, and palaeoclimatic implications. In, Vogel, J. C. (ed) *Late Cainozoic Palaeoclimates of the Southern Hemisphere*, Balkema, Rotterdam, 465-472.

Helgren, D. M. (1979) *Rivers of Diamonds: An Alluvial History of the Lower Vaal Basin, South Africa.* University of Chicago, Illinois.

Hofmann, H. J., Beer, J., Bonani, G., von Gunten, H. R., Raman, S., Suter, M., Walker, R. L., Wolfli, W. and Zimmerman, D. (1987) ^{10}Be: Half-life and AMS standards. *Nuclear Instruments and Methods in Physics Research B* 29, 32-36.

Honda, M. and Arnold, J. R. (1967) Effects of cosmic rays on Meteorites. *Handbuch der Physik* XLVI/2, Springer Verlag, Berlin, 613-635.

Hudson, B., Caffee, M, Beiriger, J., Ruiz, B., Kohl, C. P. and Nishiizumi, K. (1991) Production rate and retention properties of cosmogenic ^{3}He and ^{21}Ne in quartz. *EOS, Transactions of the American Geophysical Union* 72, Fall Meeting Supplement, 575.

Hüser, B. (1989) Die Südwestafrikanische Randstufe. Grundsätzliche Problemeiliner geomorphologische Entwichlung. *Zeitschrift für Geomrophologie N F, Supplement band* 74, 95-110.

Hutton, J. (1785) Theory of the Earth. *Transactions of the Royal Society of Edinburgh* 1, 209-304.

Huybrechts, P. (1993) Glaciological modelling of the Late Cenozoic East Antarctic ice sheet: stability or dynamism? Geografiska Annaler 75A, 221-238.

Ivy-Ochs, S. (1996) The dating of rock surfaces using in situ produced ^{10}Be, ^{26}Al and ^{36}Cl, with examples from Antarctica and the Swiss Alps. Unpublished Ph. D. thesis, ETH, Zurich.

Ivy-Ochs, S., Schluchter, C., Kubik, P. W., Dittrich-Hannen, B. and Beer, J. (1995) Minimum ^{10}Be exposure ages of early Pliocene for the Table Mountain plateau and the Sirius Group at Mt. Fleming, Dry Valleys, Antarctica. *Geology* 23, 1007-1010.

Ivy-Ochs, S., Schlutcher, C., Kubik, P. W., Synal, H. A., Beer, J., and Kerschner, H. (1996) The exposure ages of an Egesen moraine at Julier Pass, Switzerland measured with the cosmogenic radionuclides ^{10}Be, ^{26}Al and ^{36}Cl. *Eclogae Geol. Helv.* 89/3, 1-15.

Jackson, J. A. (1997) (ed) *The Glossary of Geology*, 4th Edition, American Geological Institution.

Jackson, L. E., Phillips, F. M., Snimamura, K. and Little, E. (1997) Cosmogenic ^{36}Cl dating of the Foothills erratics train, Alberta, Canada. *Geology* 25, 195-198.

Jacobson, P. J., Jacobson, K. M. and Seely, M. K. (1995) *Ephemeral Rivers and Their Catchments: Sustaining People and Development in Western Namibia*. Desert Research Foundation of Namibia, Windhoek.

Jaeger, F (1930) *Probleme der Großformen Afrikas*. Petermanns Mitt., Gotha.

Janse, A. J. A. (1975) Kimberlite and related rocks from the Nama plateau of south-west Africa. *Physics and Chemistry of the Earth* 9, 81-94.

Jessen, O. (1943) *Die Randschwellen der Kontinente.* Petermans Mitt., Gotha.

Jull, A. J. T., Wilson, A., Burr, G., Toolin, L. J. and Donahue, D. J. (1992) Measurements of the cosmogenic ^{14}C produced by spallation in high altitude rocks. *Radiocarbon* 34, 737-744.

Jull, A. J. T., Lifton, N., Phillips, W. M. and Quade, J. (1994) Studies of the production rate of cosmic-ray produced ^{14}C in rock surfaces. *Nuclear Instruments and Methods in Physics Research B* 92, 308-310.

Kellogg, D. E. and Kellogg, T. B. (1996) Diatoms in South Pole ice: Implications for eolian contamination of Sirius Group deposits. *Geology* 24, 115-118.

Kennett, J. P. (1977) Cainozoic evolution of Antarctic glaciation, the Circum-Antarctic Ocean, and their impact on global palaeooceanography. *Journal of Geophysical Research* 82, 3843-3860.

Kirkby, M. J. (ed) (1994) *Process Models and Theoretical Geomorphology.* Wiley, Chichester.

King, L. C. (1948) A theory of bornhardts. *Geographical Journal* 112, 83-87.

King, L. C. (1951) South African Scenery. 2nd Ed. (revised) Oliver and Boyd, Edinburgh.

King, L. C. (1955) Pediplanation and isostasy: an example from South Africa. *Quarterly Journal of the Geological Society* 111, 353-359.

King, L. C. (1962) *The Morphology of the Earth.* Oliver and Boyd, Edinburgh.

King, L. C. (1966) The origin of bornhardts. *Zeitschrift für Geomorphologie, N. F., Supplement Band* 10, 97-98.

King, L. C. (1975) Bornhardt landforms and what they teach. *Zeitschrift für Geomorphologie, N. F.* 19, 299-318.

King, L. C. (1983) *Wandering Continents and Spreading Sea Floors on an Expanding Earth.* Wiley, Chichester.

Klein, J., Middleton, R. and Tang, H. (1982) Modification of an FN tandem for quantitative ^{10}Be measurement. *Nuclear Instruments and Methods in Physics Research B* 193, 601-616.

Klein, J., Giegengack, R., Middleton, R., Sharma, P., Underwood, J. R and Weeks, R. A. (1986) Revealing histories of exposure using *in-situ* produced ^{26}Al and ^{10}Be in Libyan desert glass. *Radiocarbon* 28, 547-555.

Klein, J., Lawn, B., Gosse, J. and Harrington, C. (1997) Can terrestrial cosmogenic ^{10}Be be measured in whole rock samples to decipher surface exposure histories. *Geological Society of American Annual Meeting Abstracts with Programs*, A-346.

Koch, C. (1961) Some aspects of the abundant life in the vegetationless sand of the Namib Desert dunes. *Journal of the South West African Scientific Society* 15, 9-92.

Kohl, C. P. and Nishiizumi, K. (1992) Chemical isolation of quartz for measurement of *in-situ*-produced cosmogenic nuclides. *Geochimica et Cosmochimica Acta* 56, 3583-3587.

Kooi, H and Beaumont, C. (1994) Escarpment evolution on high-elevation rifted margins: insights derived from a surface processes model that combines diffusion, advection and reaction. *Journal of Geophysical Research* 99, 12,191-12,210.

Kooi, H. and Beaumont, C. (1996) Large scale geomorphology: classical concepts reconciled and integrate with contemporary ideas via a surface process model. *Journal of Geophysical Research* 101, 3361-3386.

Koons, P. O. (1989) The topographic evolution of collisional mountain belts: A numerical look at the Southern Alps, New Zealand. *American Journal of Science* 289, 1041-1069.

Kurz, M. D. (1986a) Cosmogenic helium in a terrestrial igneous rock. *Nature* 320, 435-439.

Kurz, M. D. (1986b) *In-situ* production of terrestrial cosmogenic helium and some applications to geochronology. *Geochimica et Cosmochimica Acta* 50, 2855-2862 (and Kurz, M. D. (1987) Correction to: *In-situ* production of terrestrial cosmogenic helium and some applications to geochronology. *Geochimica et Cosmochimica Acta* 51, 1019).

Kurz, M. D., Colodner, D., Trull, T. W., Moore, R. B. and O'Brien, K. (1990) Cosmic-ray exposure dating with *in-situ*-produced cosmogenic ^{3}He: results from young Hawaiian lava flows. *Earth and Planetary Science Letters* 97, 177-189.

Kurz, M. D. and Brook, E. J. (1994) Surface exposure dating with cosmogenic nuclides. In Beck, C. (ed) *Dating in Exposed and Surface Contexts* University of New Mexico Press, Albuquerque, 139-159.

Lao, Y., Anderson, R. F., Broecker, W. S., Trumbore, S. E., Hofmann, H. J. and Wolfli, W. (1992) Increased production of cosmogenic ^{10}Be during the Last Glacial Maximum. *Nature* 357, 576-578.

Lal, D. (1987) Production of ^{3}He in terrestrial rocks. *Chemical Geology* 66, 88-98.

Lal, D. (1988) *In-situ*-produced cosmogenic isotopes in terrestrial rocks. *Annual Reviews in Earth and Planetary Science* 16, 355-388.

Lal, D. (1991) Cosmic ray labelling if erosion surfaces: *in-situ* nuclide production rates and erosion models. *Earth and Planetary Science Letters* 104, 424-439.

Lal, D. (1995) On cosmic-ray exposure ages of terrestrial rocks: a suggestion. *Radiocarbon* 37, 889-898.

Lal, D. and Peter, B. (1967) Cosmic-ray produced radioactivity on the Earth. *Handbuch der Physik XLVI/2,* Springer Verlag, Berlin, 551-612.

Lal, D. and Arnold, J. R. (1985) Tracing quartz through the environment. *Proceedings of the Indian Academy of Science (Earth and Planetary Science)* 94, 1-5.

Lal, D., Nishiizumi, K., and Arnold, J. (1987) *In-situ* cosmogenic ^{3}H, ^{14}C and ^{10}Be for determining the net accumulation and ablation rates of ice sheets. *Journal of Geophysical Research* 92, 4947-4952.

Lancaster, N. (1984a) Palaeoenvironments in the Tsondab Valley, central Namib Desert. *Palaeoecology of Africa* 16, 411-419.

Lancaster, N. (1984b) Aridity in southern Africa: Age, origins and expression in landforms and sediments. In Vogel, J. C. (ed) *Late Cainozoic Palaeoclimates of the Southern Hemisphere*, Balkema, Rotterdam, 455-463.

Lancaster, N. (1989) *The Namib Sand Sea: Dune Forms, Processes and Sediments*. Balkema, Rotterdam.

Lancaster, J., Lancaster, N. and Seely, M. K. (1984) Climate of the central Namib Desert. *Madoqua* 14, 5-61.

Langbein, W. B. and Schumm, S. A. (1958) Yield of sediment in relation to mean annual precipitation. *Transactions of the American Geophysical Union* 39, 1076-1084.

Laughlin, A. W., Poths, J., Healey, H. A., Reneau, S. and Woldegabriel, G. (1994) Dating of Quaternary basalts using the cosmogenic ^{3}He and ^{14}C methods with implications for excess ^{40}Ar. *Geology* 22, 135-138.

Light, M. P. R., Maslanyj, M. P., Greenwood, R. J. and Banks, N. L. (1993) Seismic sequence stratigraphy and tectonics offshore Namibia. In Williams, G. D. and Dobb, A. (eds) Tectonics and Seismic Stratigraphy. *Geological Society Special Publication* 71, 163-191.

Linton, D. L. (1955) The problem of tors. *Geographical Journal* 121, 470-487.

Lister, G. S., Etheridge, M. A. and Symonds, P. A. (1986) Detachment faulting and the evolution of passive margins. *Geology*, 14, 246-250.

Lyell, C. (1830) *Principles of Geology, Vol 1.* John Murray, London.

McGreevy, J. P. and Smith, B. J. (1982) Salt weathering in hot deserts: Observations on the design of simulation experiments. *Geografiska Annalar* 64A, 161-170.

McKean, J. A., Dietrich, W. E., Finkel, R. C., Southon, J. R. and Caffee, M. W. (1993) Quantification of soil production and downslope creep rates from cosmogenic ^{10}Be accumulation on a hillslope profile. *Geology* 21, 343-346.

McKenzie, D (1978) Some remarks on the development of sedimentary basins. *Earth and Planetary Science Letters* 40, 25-32.

Mabutt, J. A. (1966) Mantle-controlled planation of pediments. *American Journal of Science* 64, 721-751.

Marchant, D. R. and Denton, G. H. (1996) Miocene and Pliocene paleoclimate of the Dry Valleys region, southern Victoria land: a geomorphological approach. *Mar. Macropaleont.* 27, 253-271.

Marchant, D. R., Denton, G. H. and Swisher III, C. C. (1993a) Miocene-Pliocene-Pleistocene glacial history of Arena Valley, Quartermain Mountains, Antarctica. *Geografiska Annaler* 75A, 269-302.

Marchant, D. R., Denton, G. H., Sugden, D. E. and Swisher III, C.C. (1993b) Miocene glacial stratigraphy and landscape evolution of the western Asgard Range, Antarctica, *Geografiska Annaler* 75A, 303-330.

Marchant, D. R., Denton, G. H., Swisher III, C. C. and Potter Jr., N. (1996) Late Cenozoic Antarctic paleoclimate reconstructed from volcanic ashes in the Dry Valleys region of southern Victoria Land. *Geological Society of America Bulletin* 108, 181-194.

Marker, M. E. (1977) Aspects of the geomorphology of the Kuiseb River, South West Africa. *Madoqua* 10, 199-206.

Marti, K. and Craig, H. (1987) Cosmic-ray-produced neon and helium in the summit lavas of Maui. *Nature* 325, 335-337.

Martin, H. (1953) Notes on the Dwyka succession and on some pre-Dwyka valleys in South West Africa. *Transactions of the Geological Society of South Africa* 56, 37-41.

Martin, H. (1981) The late Palaeozoic Dwyka Group of the South Kalahari Basin in Namibia and Botswana and the subglacial valleys of the Kaokoveld in Namibia. In: Hambrey, M. J. and Harland, W. B. (eds) *Earth's Pre-Pleistocene Glacial Record.* Cambridge University Press, Cambridge, 61-66.

Martin, H. (1982) Die Trias im Südlichen Afrika. *Geologische Rundschau* 71, 937-947.

Masarik, J. and Reedy, R. C. (1995) Terrestrial cosmogenic nuclide production systematics calculated from numerical simulations. *Earth and Planetary Science Letters* 136, 381-395.

Maslanyj, M. P., Light, M. P. R., Greenwood, R. J. and Banks, N. L. (1992) Extension tectonics offshore Namibia and evidence for passive rifting in the South Atlantic. Marine and Petroleum Geology 9, 590-601.

Meigs, P. (1966) *Geography of Coastal Deserts.* UNESCO Arid Zone Research 28.

Merritts, D. J. and Ellis, M. (1994) Introduction to the special section on tectonics and topography. *Journal of Geophysical Research* 99, 12,135-12,141.

Middleton, R. and Klein, J. (1987) ^{26}Al: Measurement and applications. *Philosophical Transactions of the Royal Society of London* 323, 121-143.

Middleton, R., Klein, J., Raisbeck, G. M. and Yiou, F. (1983) AMS with ^{26}Al. *Nuclear Instruments and Methods in Physics Research B* 218, 430-438.

Miller, R. McG. (1983) *Evolution of the Damara Orogen of South West Africa/Namibia.* Geological Society of South Africa Special Publication 11.

Miller , R. McG. and Schalk, K. E. L. (1980) 1: 1000000 Geological Map of Namibia, Geological Survey of Namibia.

Molnar, P. and England, P. (1990) Late Cenozoic uplift of mountain ranges and global climate change chicken or egg? *Nature* 346, 29-34.

Molnar, P., Brown, E. T., Burchfiel, B. C., Qidong, D., Xianyue, F., Yun, L., Raisbeck, G. M., Jianbang, S., Zhangming, W., Yiou, F. and Huichuan., Y. (1994) Quaternary climate change and the formation of river terraces across growing anticlines on the north flank of the Tien Shan, China. *The Journal of Geology* 102, 358-602.

Moon B. P. and Selby, M. J. (1983) Rock mass strength and scarp forms in southern Africa. *Geografiska Annaler* 65A, 135-145.

Moore, M. E., Gleadow, A. J. W. and Lovering, J. F. (1986) Thermal evolution of rifted continental margins: new evidence from fission tracks in basement apatites in southeastern Australia. *Earth and Planetary Science Letters* 78, 255-270.

Moss, J. R. (1977) The formation of pediments: scarp retreat backwearing or surface downwasting. In Doehring, D. O. (ed) *Geomorphology in arid regions.* 8th Annual Geomorphological Symposium, Binghampton, New York, 51-78.

Muller, R, A. (1977) Radioisotope dating with a cyclotron. *Science* 196, 489-494.

Neidermann, S., Graf, Th., Marti, K. (1993) Mass spectrometric identification of cosmic-ray-produced neon in terrestrial rocks with multiple neon components. *Earth and Planetary Science Letters* 118, 650-73.

Neidermann, S., Graf, Th., Kin, J. S., Kohl, C. P., Marti, K. and Nishiizumi, K. (1994) Cosmic-ray-produced ^{21}Ne in terrestrial quartz: the neon inventory of Sierra Nevada quartz separates. *Earth and Planetary Science Letters* 125, 341-355.

Nishiizumi, K., Elmore, D. and Ma, X. Z., (1984) ^{10}Be and ^{36}Cl depth profiles in an Apollo drill core. *Earth and Planetary Science Letters* 70, 157-63.

Nishiizumi, K., Lal, D., Klein, J., Middleton, R. and Arnold, J. R. (1986) Production of ^{10}Be and ^{26}Al by cosmic rays in terrestrial quartz *in-situ* and implications for erosion rates. *Nature* 319, 134-136.

Nishiizumi, K., Elmore, D. and Kubik, P. W. (1989b) Update on the terrestrial ages of Antarctic Meteorites. *Earth and Planetary Science Letters* 93, 299-313.

Nishiizumi, K., Winterer, E. L., Kohl, C. P., Klein, J., Middleton, R., Lal, D., and Arnold, J. R. (1989a) Cosmic-ray production rates of ^{10}Be and ^{26}Al in quartz from glacially polished rocks. *Journal of Geophysical Research* 94, 17907-17915.

Nishiizumi, K., Klein, J., Middleton, R. and Craig, H. (1990) Cosmogenic ^{10}Be, ^{26}Al and ^{3}He in olivine from Maui lavas. *Earth and Planetary Science Letters* 98, 263-266.

Nishiizumi, K., Kohl, C. P., Arnold, J. R., Klein, J., Fink, D. and Middleton, R. (1991) Cosmic-ray produced ^{10}Be and ^{26}Al in Antarctic rocks: exposure and erosion history. *Earth and Planetary Science Letters* 104, 440-454.

Nishiizumi, K., Kohl, C. P., Arnold, J. R., Dorn, R., Klein, J., Find, D., Middleton, R. and Lal, D. (1993) Role of in-situ cosmogenic nuclides ^{10}Be and ^{26}Al in the study of diverse geomorphic processes. *Earth Surface Processes and Landforms* 18, 407-425.

Nishiizumi, K., Finkel, R. C., Klein, J. and Kohl, C. P. (1996) Cosmogenic production of ^{7}Be and ^{10}Be in water targets. *Journal of Geophysical Research* 101, 22,225-22,232.

Nott, J., Young, R. and McDougall, I. (1996a) Wearing down, wearing back, and gorge extension in the long-term denudation of a highland mass: Quantitative evidence from the Shoal Haven catchment, SE Australia. *Journal of Geology* 104, 224-232.

Nott, J. and Roberts, R. G. (1996b) Time and process rates over the past 100 m.y: A case for dramatically increased landscape denudation rates during the late Quaternary in northern Australia. *Geology* 24, 883-889.

Oberlander, T. M. (1974) Landscape inheritance and he pediment problem in the Mojavi Desert of southern California. *American Journal of Science* 274, 849-875.

Oberlander, T. M. (1997) Slope and pediment systems. In, Thomas, D. S. G. (ed) *Arid Zone Geomorphology: process, form and change in drylands*. Wiley, Chichester, 135-164.

Obst, E. and Kayser, K. (1949) *Die Gross Randstufe auf der Ostseite Süd-afrikas und ihr Vorland: ein Beitrag zur Geschichte der Jungen Aushebung des Subkontinents.* Geogr. Ges. Hannover.

Ochs, M. and Ivy-Ochs, S. (1997) The chemical behaviour of Be, Al, Fe, Ca and Mg during AMS target preparation from terrestrial silicates modeled with chemical speciation calculations. *Nuclear Instruments and Methods in Physics Research B* 123, 235-240.

Olivier, J. (1992) Some spatial and temporal aspects of fog in the Namib. *South African Geographer* 19, 106-126.

Ollier, C. D. (1978) Inselbergs of the Namib Desert: processes and history. *Zeitschrift für Geomorphology, N. F., Supplement Band* 31, 161-176.

Ollier, C. D. (1985) Morphotectonic of continental margins with great escarpments. In, Morisawa, M. and Hack, J. T. (eds) *Tectonic Geomorphology*, Allen and Unwin, Boston.

Ollier, C. D. and Marker, M. E. (1985) The Great Escarpment of southern Africa. *Zeitschrift für Geomorphologie N. F., Supplement Band* 54, 37-56.

Ollier, C. D. and Pain, C. F. (1997) Equating the basal unconformity with the palaeoplain: a model for passive margins. *Geomorphology* 19, 1-15.

Partridge, T. C. and Maud, R. R. (1987) Geomorphic evolution of southern Africa since the Mesozoic. *South African Journal of Geology* 90, 179-208.

Partridge, T. C. and Maud, R. R. (1988) The geomorphic evolution of southern Africa: a comparative review. In Dardis, G. F. and Moon, B. P. (eds) *Geomorphological Studies in Southern Africa*. Balkema, Rotterdam, 5-15.

Penck, A. (1908) Der Drakensberg und der Quatlambabruch. *Sitz. ber. d. Kgl. Preuß. Akademie d. Wiss.* 9, 230-258.

Phillips, F. M., Leavy, B. D., Jannik, N. O., Elmore, D. and Kubik, P. W. (1986) The accumulation of cosmogenic chlorine-36 in rocks: a method for surface exposure dating. *Science* 231, 41-43.

Phillips, F. M., Zreda, M. G., Smith, S. S., Elmore, D., Kubik, P. W. and Sharma, P. (1990) Cosmogenic chlorine-36 chronology for the glacial deposits at Bloody Canyon, Eastern Sierra Nevada. *Science* 248, 1529-1532.

Phillips, F. M., Zreda, M. G., Elmore, D. and Sharma, P. (1996a) A reevaluation of cosmogenic ^{36}Cl production rates in terrestrial rocks. *Geophysical Research Letters* 23, 949-952.

Phillips, F. M., Zreda, M. G., Benson, L. V., Plummer M. A., Elmore, D., Sharma, P. (1996b) Chronology for fluctuations in late Pleistocene Sierra Nevada glaciers and lakes. *Science* 274, 749-751.

Pickford, M. and Dauphin, Y. (1993) *Diamantornis wardi* nov. gen., nov. sp., giant extinct bird from Roilepel, lower Miocene, Namibia. *C. R. Acad. Sci. Paris, Series II* 316, 1643-1650.

Pickford, M., Senut, B. and Dauphin, Y. (1995) Biostratigraphy of the Tsondab Sandstone (Namibia) based on gigantic avian eggshells. *Geobios* 18, 85-98.

Poag, C. W. and Sevon, W. D. (1989) A record of Appalachian denudation in postrift Mesozoic and Cenozoic sedimentary deposits of the U. S. middle Atlantic margin. *Geomorphology* 2, 119-157.

Poreda, R. and Cerling, T. (1992) Cosmogenic neon in recent lavas from the western United States. *Geophysical Research Letters* 19, 1863-1866.

Potts, P. J. (1987) *A Handbook of Silicate Rock Analysis.* Blackie and Son Ltd, Glasgow.

Prentice, M. L., Bockheim, J. C. Wilson, S. C., Burckle, L. H., Hodell, D. A., Schluchter, C. and Kellogg, D. E. (1993) Late Neogene Antarctic Glacial History: Evidence from central Wright Valley. *American Geophysical Union, Antarctic Ressearch Series* 60, 207-250.

Proctor, I. D., Southon, J. R., Roberts, M. L., Davis, J. C., Heikkinen, D. W., Moore, T. L,. Garibaldi, J. L and Zimmerman, T. A. (1990) The LLNL ion source - past, present and future. *Nuclear Instruments and Methods in Physics Research B* 52, 334-337.

Pugh, J. C. (1955) Isostatic readjustment in the theory of pediplanation. *Quarterly Journal of the Geological Society of London* 111, 361-369.

Raisbeck, G. M., Yiou, F., Fruneau, M., Loiseaux, J. M., Lieuvin, M., Ravel, J. C. and Lorius, C. (1981) Cosmogenic Be concentrations in Antartcic ice during the past 30,000 years. *Nature* 292, 825-826.

Raisbeck, G. M., Yiou, F., Bourlés, J., Lestrinuez, J. and Deboffle, D. (1987) Measuerments of ^{10}Be and ^{26}Al with a Tandetron AMS facility. *Nuclear Instruments and Methods in Physics Research B* 29, 22-26.

Rama and Honda, M. (1961) Cosmic-ray-induced radioactivity in terrestrial materials. *Journal of Geophysical Research* 66, 3533-3539.

Reedy, R. C. and Arnold, J. R. (1972) Interaction of solar and galactic cosmic-ray particles in solar system matter. *Journal of Geophysical Research* 77, 537-555.

Reedy, R. C., Arnold, J. R. and Lal, D. (1983) Cosmic ray record in solar system matter. *Annual Review of Earth and Planetary Science* 33, 505-537.

Renne, P. R., Glen, J. M., Milner, S. C. and Duncan, A. R. (1996) Age of the Etendeka flood volcanism and associated intrusions in southwestern Africa. *Geology* 24, 659-662.

Repka, J. L., Anderson, R. S. and Finkel, R. C. (1997) Cosmogenic dating of fluvial terraces, Fremont River, Utah. *Earth and Planetary Science Letters* 152, 59-73.

Ritz, J. F., Brown, E. T., Bourles, D. L., Enktuvshin, B., Phila, H., Galsan, P., Raisbeck, G. M., Yiou, Y. and Chery, J. (1995) Slip rates along active faults estimated with cosmic-ray exposure dates: application to the Bogd fault, Gobi-Altai, Mongolia. *Geology* 23, 1019-1022.

Roberts, M. L., Bench, G. S., Brown, T. A., Caffee, M. W., Finkel, R. C., Freeman, S. P. H. T., Hainsworth, L. J., Kashgarian, M., McAninich, J. E., Proctor, I. D., Southon, J. R. and Vogel, J. S. (1997) The AMS facility at Lawrence Livermore National Laboratory. *Nuclear Instruments and Methods in Physics Research B* 123, 57-61.

Rogers, A. W. (1920) Geological survey and its aims; and a discussion on the origin of the Great Escarpment. *Transactions of the Geological Society of South Africa* 23, 14-33.

Royden, L. and Keen, C. E. (1980) Rifting processes and thermal evolution of the continental margin of eastern Canada determined from subsidence curves. *Earth and Planetary Science Letters* 51, 343-361.

Rust, U. and Wieneke, F. (1980) A reinvestigation of some aspects of the evolution of the Kuiseb River valley up stream of Gobabeb, South West Africa. *Madoqua*, 12, 163-173.

Rust, U. and Vogel, J. C. (1988) Late Quaternary environmental changes in the northern Namib Desert as evidenced by fluvial landforms. *Palaeoecology of Africa* 19, 127-137.

Rust, U., Schmidt, H. H. and Dietz, (1984) Palaeoenvironments of the present day arid south western Africa 30 000-5000 BP: Results and problems. *Palaeoecology of Africa* 16, 109-148.

Rust, D. J. and Summerfield, M. A. (1990) Isopach and borehole data as indicators of rifted margin evolution in southwestern Africa. *Marine and Petroleum Geology* 7, 277-287.

Sandelowsky, B. H. (1977) Mirabib - an archaeological study in the Namib. *Madoqua* 10, 221-283.

Sante Fe Workshop Abstracts (1995) *Radiocarbon* 38, 149-173.

Sarda, P., Staudacher, T., Allegre, C. J. and Lecomte, A. (1993) Cosmogenic neon and helium at Reunion: measurement of erosion rate. *Earth and Planetary Science Letters* 199, 405-417.

Saunders, I. and Young, A. (1983) Rates of surface process on slopes, slope retreat and denudation. *Earth Surface Processes and Landforms* 8, 473-501.

Schalk, K. E. L. (1983) Geologishe geschichte des Gamsberggebrietes. *SWA Wissenschaftliche Gesellschaft Journal* 37, 7-15.

Schultz, S. A. and McGee, O. S. (1978) Climatic indices and classifications in relation to the biogeography of southern Africa. In, Werger, M. (ed) *Biogeography and Ecology of southern Africa, Part 1.* W. Junk, The Hague, 19-52.

Schmidt, K-H. (1987) Factors influencing structural landform dynamics on the Colorado Plateau - about the necessity of calibrating theoretical models by empirical data. *Catena Supplement Band* 10, 51-66.

Schmidt, K-H. (1989) The significance of scarp retreat for Cenozoic landform evolution on the Colorado Plateau, U. S. A. *Earth Surface Processes and Landforms* 14, 93-105.

Schumm, S. A. (1979) Geomorphic thresholds: the concept and its applications. *Transactions of the Institute of British Geographers* NS 4, 485-504.

Seely, M. K. (1978) The Namib Dune Desert: an unusual ecosystem. *Journal of Arid Environments* 1, 117-128.

Seidl, M. A. (1993) *Form and Process in Channel Incision of Bedrock*. Unpublished Ph. D. thesis, University of California at Berkeley.

Seidl, M. A., Dietrich, W. E. and Kirchener, J. K. (1994) Longitudinal profile development into bedrock: An analysis of Hawaiian channels. *Journal of Geology* 102, 457-474.

Seidl, M. A., Weissel, J. K. and Pratson, L. F. (1996) The kinematics and pattern of escarpment retreat across the rifted continental margin of SE Australia. *Basin Research* 8, 301-316.

Seidl, M. A., Finkel, R. C., Caffee, M. W., Hudson, G. B. and Dietrich, W. E. (1997) Cosmogenic isotope analysis applied to river longitudinal profile evolution: problems and interpretations. *Earth Surface Processes and Landforms* 22, 195-209.

Selby, M. J. (1971) Slopes and their development in an ice-free, arid area of Antarctica. *Geografiska Annaler* 53A, 235-245.

Selby, M. J. (1974) Slope evolution in an Antarctic oasis. *New Zealand Geographer* 30, 18-34.

Selby, M. J. (1977a) Bornhardts of the Namib Desert. *Zeitschrift für Geomorphologie N. F.*, 21, 1-13.

Selby, M. J. (1977b) On the origin of sheeting and laminae in granitic rocks: evidence from Antarctica, the Namib Desert and the central Sahara. *Madoqua* 10, 171-179.

Selby, M. J. (1982a) Rock mass strength and the form of some inselbergs in the central Namib Desert. *Earth Surface Processes and Landform,* 7, 489-498.

Selby, M. J. (1982b) Form and origin of some bornhardts of the Namib Desert. *Zeitschrift für Geomorphologie* 26, 1-15.

Selby, M. J. (1993) *Hillslope Materials and Processes*. 2nd Edition, Oxford University Press, Oxford.

Selby, M. J., Hendey, C. H. and Seely, M. K. (1979) A late Quaternary lake in the central Namib Desert, southern Africa and some implications. *Palaeogeography, Palaeoclimatology and Palaeoecology* 26, 37-41.

Senut, B and Pickford, M. (1995) Fossil eggs and Cenozoic continental biostratigraphy of Namibia. *Palaeontologica Africana* 32, 33-37.

Senut, B., Pickford, M. and Ward, J. (1994) Biostratigraphie des eolianites neogenes de la Sperrgebiet (Sud de la Namibie) *C. R. Acad. Sci. Paris* 318, 1001-1007.

Shackleton, J. N. and Kennett, J. P. (1975) Palaeotemperature history of the Cenozoic and the initiation of Antarctic glaciation: Oxygen and carbon isotope analyses in DSCP sites 277, 279 and 281. In, Kennett, J. P. and Houtz, R. (eds) *Initial Reports of the Deep Sea Drilling Project* 29, 743-755.

Sharma, P. and Middleton, R. (1989) Radiogenic production of ^{10}Be and ^{26}Al in uranium and thorium ores: implications for studying terrestrial samples containing low levels of ^{10}Be and ^{26}Al. *Geochimica et Cosmochimica Acta* 53, 709-716.

Shepherd, M. K., Arvidson, R. E., Caffee, M., Finkel, R and Harris, L (1995) Cosmogenic exposure ages of basalt flows: Lunar Crater volcanic field, Nevada. *Geology* 23, 21-24.

Siesser, W. G. (1978) Aridification of the Namib Desert: evidence from oceanic cores. In Van Zinderen Bakker (ed) *Antarctic Glacial History and World Palaeoenvironments*. Balkema, Rotterdam, p. 105-113.

Siesser, W. G. (1980) Late Miocene origin of the Benguela upwelling system off northern Namibia. *Science* 208, 283-285.

Smith, B. J. and McGreevy, J. P. (1983) A simulation study of salt weathering in hot deserts. *Geografiska Annaler* 65A, 127-133.

Small, E. E., Anderson, R. S., Repka, J. L. and Finkel, R. (1997) Erosion rates of alpine bedrock summit surfaces deduced from *in-situ* ^{10}Be and ^{26}Al. *Earth and Planetary Science Letters* 150, 413-425.

Southon, J. R., Caffee, M. W., Davis, J. C., Moore, T. L., Proctor, I. D., Schumacher, B. and Vogel, J. S. (1990) The new LLNL AMS spectrometer. *Nuclear Instruments and Methods in Physics Research B* 52, 301-305.

Spönemann, J. and Brunotte, E. (1989) Zur reliefgeschichte der Südwestafrikanishen Randschwelle zwischen Huab und Kuiseb. *Zeitschrift für Geomorphologie, N.F. Supplement Band* 74, 111-125.

Staudacher, T. and Allégre, C. J. (1991) Cosmogenic neon in ultramafic nodules from Asia and quartzite from Antarctica *Earth and Planetary Science Letters* 106, 87-102.

Staudacher, T. and Allégre, C. J. (1993) Ages of the second caldera of Piton de la Fournaise volcano (Reunion) determined by cosmic ray produced ^{3}He and ^{21}Ne. *Earth and Planetary Science Letters* 119, 395-404.

Steckler, M. S. (1985) Uplift and extension at the Gulf of Suez: indications of induced mantle convection. *Nature* 317, 135-139.

Steckler, M. S. and Omar, G. I. (1994) Controls on erosional retreat of uplifted rift flanks at the Gulf of Suez and northern Red Sea. *Journal of Geophysical Research* 99, 12159-12173.

Stokes, S., Thomas, D. S. G. and Washington, R. (1997) Multiple episodes of aridity in southern Africa since the last interglacial period. *Nature* 388, 154-158.

Stone, J. O, Allan, G. L., Fifield, L. K., Evans, J. M. and Chivas, A. R. (1994) Limestone erosion measurements with cosmogenic chlorine-36 in calcite - preliminary results from Australia. *Nuclear Instruments and Methods in Physics Research B* 92, 311-316.

Stone, J. O., Allan, G. L., Fifield, L., K. and Cresswell, R. G. (1996a) Cosmogenic chlorine-36 from calcium spallation. *Geochimica et Cosmochimica Acta* 60, 679-692.

Stone, J. O., Lambeck, K., Fifield, L. K., Evans, J. M. and Cresswell, R. G. (1996b) A late glacial age for the Main Rock Platform, Western Scotland. *Geology* 24, 707-712.

Strack, E., Heisinger, B., Dockhorn, B., Hartmann, F. J., Korgchiner, G., Nolte, E., Morteani, G., Petitjean, C. and Newmaier, S. (1994) Determination of erosion rates with cosmogenic ^{26}Al. *Nuclear Instruments and Methods in Physics Research B* 92, 317-320.

Stuvier, M. and Reimer, P. J. (1993) Extended ^{14}C database and revised CALIB radiocarbon calibration program. *Radiocarbon* 35, 215-230.

Sugden, D. E. (1992) Antarctic ice sheets at risk? *Nature* 359, 775-776.

Sugden, D. E. (1996) The East Antarctic Ice Sheet: unstable ice or unstable ideas? *Transactions of the Institute of British Geographers NS* 21, 443-454.

Sugden, D. E., Marchant, D. R. and Denton, G. H. (1993) The case for a stable East Antarctic Ice Sheet: the background. Geografiska Annaler 75A, 151-154,

Sugden, D. E., Denton, G. H. and Marchant, D. R. (1995a) Landscape evolution of the Dry Valleys, Transantarctic Mountains: Tectonic implications. *Journal of Geophysical Research* 100, 9949-9967.

Sugden, D. E., Marchant, D. R., Potter Jr., N., Souchez, A., Denton, G. H., Swisher III, C. C. and Tison, J-L. (1995b) Preservation of Miocene glacier ice in East Antarctica. *Nature* 376, 412-414.

Sugden, D. E., Summerfield, M. A. and Burt, T. P. (1997) Editorial: Linking short-term geomorphic processes to landscape evolution. *Earth Surface Processes and Landforms* 22, 193-194.

Sugden, D. E., Summerfield, M. A., Denton, G. H., Marchant, D. R., Wilch, T. I. and McIntosh, W. C. (1998) Landscape development in the Royal Society Range, southern Victoria Land, Antarctica. submitted to *Geomorphology.*

Summerfield, M. A. (1985) Plate tectonics and landscape development on the African continent. In Morisawa, M. and Hack, J. T. (eds) *Tectonic Geomorphology.* Allen and Unwin, Boston, 27-51.

Summerfield, M. A. (1991a) *Global Geomorphology.* Longman, London.

Summerfield, M. A. (1991b) Sub-aerial denudation of passive margins: regional elevation versus local relief models. *Earth and Planetary Science Letters* 102, 460-469.

Summerfield, M. A. (1996a) Understanding landscape development: the evolving interface between geomorphology and other earth sciences. *Area* 28, 211-220.

Summerfield, M. A. (1996b) Tectonics, geology, and long-term landscape development. In Adams, W. M., Goudie, A. S. and Orme, A. R. (eds) *The Physical Geography of Africa.* Oxford University Press, 1-17.

Summerfield, M. A. and Hulton, N. J. (1994) Natural controls of fluvial denudation rates in major world drainage basins. *Journal of Geophysical Research* 99, 13,871-13,883.

Summerfield, M. A., Stuart, F. M., Cockburn, H. A. P., Sugden, D. E., Denton, G. H., Dunai, T. and Marchant, D. R. (1998a) Long-term rates of denudation in the Dry Valleys region of the Transantarctic Mountains, southern Victoria Land, Antarctica: Preliminary results based on *in-situ*-produced cosmogenic ^{21}Ne. *Geomorphology*, in press.

Summerfield, M. A., Sugden, D. E., Denton, G. H., Marchant, D. R., Cockburn, H. A. P., and Stuart, F. M. (1998b) Cosmogenic isotope data support previous evidence of extremely low rates of denudation in the Dry Valleys region, southern Victoria Land, Antarctica. *Geological Society Special Publication,* in press

Sweeting, M. M. and Lancaster, N. (1982) Solutional and wind erosion forms on limestone in the central Namib. *Zeitschrift für Geomorphologie, N. F.* 26, 197-207.

Synal, H. A., Bonani, G., Dobeli, M., Ender, R. M., Gartenmann, P., Kubik, P., Schnabel, C. and Suter, M. (1997) Status report of the PSI/ETH AMS Facility. *Nuclear Instruments and Methods in Physics Research B* 123, 62-68.

Syres, J. K. *et al.,* (1968) Quartz isolation from rocks, sediments and soils for the determination of oxygen isotope composition. *Geochimica et Cosmochimica Acta* 32, 1022-1025.

Tankard, A. J. and Rogers, J. (1978) Late Cenozoic palaeoenvironments on the west coast of Africa. *Journal of Biogeography* 5, 319-337.

Tankard, A. J., Jackson, M. P. A., Eriksson, K. A., Hobday, D. K., Hunter, D. R. and Minter, W. E. L. (1982) *Crustal Evolution of Southern Africa: 3.8 Billion Years of Earth History.* Springer-Verlag, New York.

Thomas, D. S. G. and Shaw, P. A. (1990) The deposition and development of the Kalahari Group Sediments, central Southern Africa. *Journal of African Earth Sciences* 10, 187-197.

Thomas, D. S. G. and Summerfield, M. A. (1987) Long-term landform development: Key theme and research problems. In Gardiner, V. *et al.,* (eds) *International Geomorphology 1986: Proceedings of the 1st International Conference on Geomorphology, Part ii.* Wiley, Chichester, 935-956.

Thomas, M. F. (1978) The study of inselbergs. *Zeitschrift für Geomorphologie, N. F., Supplement Band* 31, 1-41.

Thomas, M. F. (1994) *Geomorphology in the Tropics.* Wiley, Chichester.

Trull, T. W., Kurz, M. D. and Jenkins, W. J. (1991) Diffusion of cosmogenic ^{3}He in olivine and quartz: implications for surface exposure dating. *Earth and Planetary Science Letters* 103, 241-256.

Trull, T. W., Brown, E. T., Marty, B., Raisbeck, G. M. and Yiou, F. (1995) Cosmogenic ^{10}Be and ^{3}He accumulation in Pleistocene beach terraces in Death Valley, California, USA: implications for cosmic-ray-exposure dating of young surfaces in hot climates. *Chemical Geology* 119, 191-207.

Tucker, G. E. and Slingerland, R. L. (1994) Erosional dynamics, flexural isostasy, and long-lived escarpments: A numerical modeling study. *Journal of Geophysical Research*, 99, 12,229-12,245.

Turner, S., Regelous, M. Kelley, S., Hawkesworth, L. and Mantovani, M. (1994) Magmatism and continental break-up in the South Atlantic: high precision $^{40}Ar/^{39}Ar$ geochronology. *Earth and Planetary Science Letters* 121, 333-348.

Twidale, C. R. (1976) On the survival of palaeoforms. *American Journal of Science* 276, 77-95.

Twidale, C. R. (1988) Granitic Landscapes. in, Moon, B. P. and Dardis, G. F. (eds) *The Geomorphology of Southern Africa*, 198-230.

Twidale, C. R. (1992) King of the plains: Lester King's contributions to geomorphology. *Geomorphology* 5, 491-509.

Twidale, C. R. and Bourne, J. A. (1975) Episodic exposure of inselbergs. *Bulletin of the Geological Society of America* 86, 1473-1481.

Tyson, P. D. (1986) *Climate Change and Variability in Southern Africa*. Oxford University Press.

Van der Beek, P. A. (1995) *Tectonic Evolution of Continental Rifts: inferences from numerical modelling and fission track thermochronology*. Unpublished Ph.D. thesis, Vrije Universiteit te Amsterdam.

Van der Wateren, D. and Hindmarsh, R. (1995) Stabilists strike again. *Nature* 376, 389-391.

Van Zinderen Bakker, E. M. (1975) The origin and palaeoenviroment of the Namib Desert biome. *Journal of Biogeography* 2, 65-73.

Van Zinderen Bakker, E. M. (1984a) Aridity along the Namibian Coast. *Palaeoecology of Africa* 16, 149-160.

Van Zinderen Bakker, E. M. (1984b) A late- and post-glacial pollen record from the Namib Desert. *Palaeoecology of Africa* 16, 421-428.

Visser, J. N. J. (1987) The palaeogeography of part of southwestern Gondwana during the Permo-Craboniferous glaciation. *Palaeogeography, Palaeoclimatology, Palaeoecology* 61, 205-219.

Vogel, J. C. (1982) The age of the Kuiseb River silt at Homeb. *Palaeoecology of Africa* 15, 201-209.

Vogel, J. C. and Visser, E. (1981) Pretoria radiocarbon dates II. *Radiocarbon* 23, 43-80.

Vogel, J. C., Rogers, J. and Seely, M. K. (1981) Ancient climates and the age of the Namib: Summary of the SASQUA Congress May 1981. *South African Journal of Science* 77, 435-436.

Watson, A. (1988) Desert gypsum crusts as palaeoenvironmental indicators: a mirco-petrographic study of crusts from southern Tunisia and the central Namib Desert. *Journal of Arid Environments* 15, 19-42.

Ward, J. D. (1984) A reappraisal of the Cenozoic stratigraphy in the Kuiseb valley of the central Namib Desert. In, Vogel, J. C. (ed) *Late Cainozoic Palaeoclimates of the Southern Hemisphere*, Balkema, Rotterdam, 455-463.

Ward, J. D. (1987) The Cenozoic succession in the Kuiseb Valley, central Namib Desert. *Geological Survey of Namibia Memoir* 9.

Ward, J. D., Seely, M. K. and Lancaster, N. (1983) On the antiquity of the Namib. *South African Journal of Science* 79, 175-183.

Webb, P. N. and Harwood, D. M. (1991) Late Cenozoic glacial history of the Ross Embayment, Antarctica. *Quaternary Science Reviews* 10, 215-223.

Webb, P. N., Harwood, D. M., McKelvey, B. C., Mercer, J. H. and Stott, L. D. (1984) Cenozoic marine sedimentation and ice-volume variation on the East Antarctic craton. *Geology* 12, 287-291.

Weissel, J. K. and Karner, G. D. (1989) Flexural uplift of rift flanks due to mechanical unloading of the lithosphere during extension. *Journal of Geophysical Research* 94, 13,919-13,950.

Wellington, J. H. (1955) *Southern Africa: A Geographical Study, Vol 1: Physical Geography*. Cambridge University Press.

Wells, S. G., McFadden, L. D., Poths, J. and Olinger, C. T. (1995) Cosmogenic ^{3}He surface exposure dating of stone pavements: Implications for landscape evolution in deserts. *Geology* 23, 613-616.

Wilch, T. I., Denton, G. H. Sugden, D. E. and Swisher III, C. C. (1993a) Limited Pliocene glacier extent and surface uplift in Middle Taylor Valley, Antarctica. *Geografiska Annaler* 75A, 331-351.

Wilch, T. I., Lux, D. R., Denton, G. H. and Mcintosh, W. C. (1993b) Minimal Pliocene-Pleistocene uplift of the Dry Valleys sector of the Transantarctic Mountains: A key parameter in ice-sheet reconstructions. *Geology* 21, 841-844.

Wilkinson, M. J. (1990) Palaeoenvironment in the Namib Desert: The lower Tumas Basin in the late Cenozoic. *University of Chicago Geography Research Paper No. 231.*

Willis, B. (1934) Inselbergs. *Annals of the Association of American Geographers* 24, 123-129.

Wittig, R. (1976) Die Gamsberg-Spalten (SW-Afrika) - Zeugen Karroo-zeitlicher Erdbeben. *Geologische Rundschau* 65, 1019-1035.

White, R. and McKenzie, D. (1989) Magmatism at rift zones: the generation of volcanic continental margins and flood basalts. *Journal of Geophysical Research* 94, 7685-7729.

Yaalon, D. H. and Ward, J. D. (1982) Observations on calcrete and recent calcic horizons in relation to landforms in the central Namib Desert. *Palaeoecology of Africa* 15, 183-186.

Yasevitch, I. and Honda, M. (1997) Production of nucleogenic neon in the Earth from natural radioactive decay. *Journal of Geophysical Research* 102, 10291-10298.

Yokoyama, Y, Reyss J. and Guichard, F. (1977) Production of radionuclides by cosmic rays at mountain altitudes. *Earth and Planetary Science Letters* 36, 44-56.

Young, R. W. (1983) The tempo of geomorphological change: evidence from southeastern Australia. *Journal of Geology* 91, 221-230.

Young, R. W. and McDougall, I. (1982) Basalts and slitters on the coast near Ulladulla, southern N. S. W. *Journal of the Geological Society of Australia* 29, 425-430.

Zreda, M. G. (1994) *Development and calibration of the ^{36}Cl surface exposure dating method and its application to the chronology of Late Quaternary glaciations.* Unpublished Ph.D. thesis, New Mexico Institute of Mining and Technology.

Zreda, M. G., Phillips, F. M., Elmore, D., Kubik, P. W., Sharma, P. and Dorn, R. (1991) Cosmogenic chlorine-36 production rates in terrestrial rocks. *Earth and Planetary Science Letters* 105, 94-109.

Zreda, M. G., Phillips, F. M., Kubik, P., Sharma, P. and Elmore, D. (1993) Cosmogenic ^{36}Cl dating of a young basaltic eruption complex, Lathrop Wells, Nevada. *Geology* 21, 57-60.

Personal Communications

R. Brown:	School of Earth Sciences, La Trobe University, Victoria, Australia.
K. Gallagher:	Dapartment of Geology, Imperial College, London.
S. Ivy-Ochs:	Teilchenphysik, ETH Hoenggerberg, Zurich, Switzerland.
P. Kubik:	Paul Sherrer Institut, ETH Hoenggerberg, Zurich, Switzerland.
M. McCartney:	Department. of Chemistry, Scottish Universities Research and Reactor Centre, East Kilbride.
T. Neckel:	Max-Plank-Institut für Astronomie, Heidelberg, Germany.
M. Seidl:	Department of Geological Sciences, Rutgers University, USA.
J. Stone:	Department of Geological Sciences, University of Washington, USA.
F. Stuart:	Isotope Geoscience, Scottish Universities Research and Reactor Centre, East Kilbride.
R. Thompson:	Department. of Geology and Geophysics, University of Edinburgh.

Appendix A

Sample Details

Appendix A: Sample Details

Two tables of sample information are included in Appendix A. Table A.1 below shows all the samples prepared and those analysed during the preparation of this thesis. It includes information about the location and lithology of the samples, preparation laboratory, sample size and the isotopes measured. It also provides an indication of who was involved at each stage from initial sample collection (shown under sampling location) through pre-treatment and isotope extraction (shown under preparation laboratory), target preparation and AMS or MS measurement (shown under AMS/MS facility). Acknowledgement for total Al measurements are also shown (under Al content measurement method). 37 samples were prepared in five batches at three different laboratories. 63 Be, Al and Ne isotopic ratios were measured in 31 completely prepared samples at three different AMS/MS facilities. Table A.2 provides details of the exposure geometry recorded at each sampling site location the exposure geometry correction applied to the production rate scaled to the site.

Table A.1: Samples Prepared and Analysed.

Sample Number	Sampling Location	Preparation Laboratory	AMS/MS Facility	Isotopes Measured	Lithology	Sample Size, g SiO_2	Al Content Measurement Method	Chapter Discussed/ Outcome
BATCH 1								
3/94	Gamsberg (HAPC)	LDEO (MS/HAPC)	-		Gamsberg Quartzite	50.04	-	Incomplete Preparation
4/94	Gamsberg (HAPC)	LDEO (MS/HAPC)	LLNL (RCF)	^{10}Be, (^{26}Al)	Gamsberg Quartzite	50.03	-	4
7/94	Gamsberg (HAPC)	LDEO (MS/HAPC)	-		Gamsberg Quartzite	50.09	-	Incomplete Preparation
8/94	Gamsberg (HAPC)	LDEO (MS/HAPC)	-		Gamsberg Quartzite	50.02	-	Incomplete Preparation
11/94	Gamsberg Pass (HAPC	LDEO (MS/HAPC)	-		Quartz Vein	50.08	-	Incomplete Preparation
14/94	Gamsberg (HAPC)	LDEO (MS/HAPC)	LLNL (RCF)	^{10}Be, (^{26}Al)	Gamsberg Quartzite	50.02	-	4
17/94	Gaub River (HAPC)	LDEO (MS/HAPC)	LLNL (RCF)	^{10}Be, (^{26}Al)	Quartz Vein	50.01	-	4
28/94	Fish Riv. Canyon (HAPC)	LDEO (MS/HAPC)	-		Granite Gneiss	40.04	-	Incomplete Preparation
29/94	Fish Riv. Canyon (HAPC)	LDEO (MS/HAPC)	-		Granite Gneiss	35.06	-	Incomplete Preparation

BATCH 2								
50/95	Arena Valley (DES, DRM)	SURRC (HAPC)	VUA (FMS, TD) ETH (SIO, PWK, HAPC)	^{21}Ne, ^{10}Be, ^{26}Al	Arena Sandstone	0.25, 15.00613	ICPMS (MM, HAPC), GFAAS (AM, HAPC)	6
51/95	Arena Valley (DES, DRM)	SURRC (HAPC)	VUA (FMS, TD) ETH (SIO, PWK, HAPC)	^{21}Ne, ^{10}Be, ^{26}Al	Arena Sandstone	0.25, 15.04979	ICPMS (MM, HAPC), GFAAS (AM, HAPC)	6
51/95 #2	Arena Valley (DES, DRM)	SURRC (HAPC)	ETH (SIO, PWK, HAPC)	^{10}Be, ^{26}Al	Arena Sandstone	15.00241	ICPMS (MM, HAPC), GFAAS (AM, HAPC)	6
52/95	Arena Valley (DES, DRM)	SURRC (HAPC)	VUA (FMS, TD) ETH (SIO, PWK, HAPC)	^{21}Ne, ^{10}Be, ^{26}Al	Arena Sandstone	0.25, 15.00193	ICPMS (MM, HAPC), GFAAS (AM, HAPC)	6
56/95	Arena Valley (DES, DRM)	SURRC (HAPC)	VUA (FMS, TD) ETH (SIO, PWK, HAPC)	^{21}Ne, ^{10}Be, ^{26}Al	Beacon Sandstone	0.25, 15.00857	ICPMS (MM, HAPC), GFAAS (AM, HAPC)	6
57/95	Arena Valley (DES, DRM)	SURRC (HAPC)	VUA (FMS, TD) ETH (SIO, PWK, HAPC)	^{21}Ne, ^{10}Be, ^{26}Al	Beacon Sandstone	0.25, 15.01689	ICPMS (MM, HAPC), GFAAS (AM, HAPC)	6
5/96	Mt. Fleming (MAS, DES)	EDIN (HAPC)	VUA (FMS, TD)	^{21}Ne	Beacon Sandstone	0.25	-	6
6/96	Mt. Fleming (MAS, DES)	EDIN (HAPC)	VUA (FMS, TD)	^{21}Ne	Beacon Sandstone	0.25	-	6
13/96	Taylor Valley (MAS, DES)	EDIN (HAPC)	VUA (FMS, TD)	^{21}Ne	Granite	0.25	-	6
BATCH 3								
2/95	Gamsberg (HAPC)	EDIN (HAPC)	LLNL (RCF)	^{10}Be, ^{26}Al	Gamsberg Granite	45.02106	DCPMS (MS)	4
3/95	Gamsberg (HAPC)	EDIN (HAPC)	LLNL (RCF)	^{10}Be, ^{26}Al	Quartz Vein	45.00417	DCPMS (MS)	4
6/95	Gamsberg (HAPC)	EDIN (HAPC)	LLNL (RCF)	^{10}Be, ^{26}Al	Gamsberg Granite	44.59402	DCPMS (MS)	4
8/95	Gamsberg (HAPC)	EDIN (HAPC)	LLNL (RCF)	^{10}Be, ^{26}Al	Gamsberg Quartzite	35.00454	DCPMS (MS)	4
10/95	Gamsberg (HAPC)	EDIN (HAPC)	LLNL (RCF)	^{10}Be, ^{26}Al	Gamsberg Quartzite	30.01181	DCPMS (MS)	4
11/95	Gamsberg (HAPC)	EDIN (HAPC)	LLNL (RCF)	^{10}Be, ^{26}Al	Gamsberg Quartzite	35.03961	DCPMS (MS)	4

BATCH 4								
15A	Blutkopje (HAPC)	EDIN (HAPC)	LLNL (RCF)	^{10}Be, ^{26}Al	Donkerhuk Granite	29.44153	GFAAS (AM)	5
15B	Blutkopje (HAPC)	EDIN (HAPC)	LLNL (RCF)	^{10}Be, ^{26}Al	Donkerhuk Granite	30.10317	GFAAS (AM)	5
16A	Vogelfederberg (HAPC)	EDIN (HAPC)	LLNL (RCF)	^{10}Be, ^{26}Al	Donkerhuk Granite	28.42626	GFAAS (AM)	5
16B	Vogelfederberg (HAPC)	EDIN (HAPC)	LLNL (RCF)	^{10}Be, ^{26}Al	Donkerhuk Granite	25.35027	GFAAS (AM)	5
17A	Mirabib (HAPC)	EDIN (HAPC)	LLNL (RCF)	^{10}Be, ^{26}Al	Donkerhuk Granite	25.75000	GFAAS (AM)	5
17B	Mirabib (HAPC)	EDIN (HAPC)	LLNL (RCF)	^{10}Be, ^{26}Al	Donkerhuk Granite	21.02916	GFAAS (AM)	5
BATCH 5								
1/95	Gamsberg (HAPC)	EDIN (HAPC)	LLNL (RCF)	^{10}Be, ^{26}Al	Gamsberg Granite	42.05750	ICPMS (XRAL)	4
4/95	Gamsberg (HAPC)	EDIN (HAPC)	LLNL (RCF)	^{10}Be, ^{26}Al	Gamsberg Granite	42.34084	ICPMS (XRAL)	4
5/95	Gamsberg (HAPC)	EDIN (HAPC)	LLNL (RCF)	^{10}Be, ^{26}Al	Gamsberg Granite	41.42633	ICPMS (XRAL)	4
7/95	Gamsberg (HAPC)	EDIN (HAPC)	LLNL (RCF)	^{10}Be, ^{26}Al	Gamsberg Quartzite	32.13122	ICPMS (XRAL)	4
9/95	Gamsberg (HAPC)	EDIN (HAPC)	LLNL (RCF)	^{10}Be, ^{26}Al	Gamsberg Quartzite	28.9971	ICPMS (XRAL)	4
10/95 #2	Gamsberg (HAPC)	EDIN (HAPC)	LLNL (RCF)	^{10}Be, ^{26}Al	Gamsberg Quartzite	14.96368	ICPMS (XRAL)	4
12/95	Gamsberg (HAPC)	EDIN (HAPC)	LLNL (RCF)	^{10}Be, ^{26}Al	Gamsberg Quartzite	25.91193	ICPMS (XRAL)	4

Individuals: HAPC=Hermione Cockburn, MS=Michele Seidl, DES=David Sugden, MAS=Michael Summerfield, FMS=Fin Stuart, TD=Tibor Dunai, DRM=David Marchant, RCF=Bob Finkel, SIO=Susan Ivy-Ochs, PWK=Peter Kubik, MM=Martin McCartney, AM=Ann Mennin.

Laboratories: LDEO=Lamont-Doherty Earth Observatory of Columbia University, SURRC=Scottish Universities Research and Reactor Centre, EDIN=Department of Geography, University of Edinburgh, XRAL=XRAL Laboratories, Ontario, Canada.

AMS/MS Facilities: LLNL=Lawrence Livermore National Laboratory, VUA=Vrije Universiteie Amsterdam, ETH=Swiss Federal Institute of Technology Zurich.

Measurement techniques: AMS: Accelerator mass spectrometry, MS: Mass spectrometry: GFAAS: Graphite furnace atomic absorption spectrometry, ICPMS: Inductively coupled plasma mass spectrometry, DCPMS: Doubly coupled plasma mass spectrometry.

Table A.2: Exposure Geometry Details

Sample Number	[1]Dip and orientation of dip		[2]Angle to Horizon Quadrant 1 0 to 90°						[2]Angle to Horizon Quadrant 2 90° to 180°						[2]Angle to Horizon Quadrant 3 180° to 270°						[2]Angle to Horizon Quadrant 4 270°-360°						[3]Exposure Geometry Correction
Gamsberg Samples																											
1/95	37	336	1	1	1	0	7	17	23	22	21	13	6	2	0	5	6	0	0	0	0	0	0	0	0	0	0.981
2/95	47	343	0	0	0	0	8	26	40	45	45	46	42	40	40	28	6	3	0	0	0	0	0	0	0	0	0.946
3/95	33	354	0	0	0	6	17	13	43	47	50	50	43	40	30	15	0	0	0	0	0	0	0	0	0	0	0.951
4/95	0	-	29	26	17	24	4	0	0	1	0	0	0	1	0	0	0	2	3	7	12	13	12	22	27	29	0.985
5/95	0	-	14	23	17	8	0	3	0	0	0	0	0	0	0	0	0	0	1	0	4	6	8	11	11	17	0.998
6/95	0	-	28	19	6	1	0	0	0	0	0	0	0	0	0	0	0	0	1	2	2	7	15	19	25	27	0.995
7/95	88	330	0	0	0	0	0	90	90	90	90	90	90	90	90	90	90	40	17	9	5	0	0	0	0	0	0.578
8/95	65	350	0	0	6	8	17	43	68	68	70	68	64	46	40	32	35	28	0	0	0	0	0	0	0	0	0.826
9/95	70	320	0	0	0	0	0	12	48	66	80	80	66	74	54	19	6	0	0	0	0	0	0	0	0	0	0.836
10/95	0	-	-	-	-	-	-	-	-	-	-	-	-	-	-	-	-	-	-	-	-	-	-	-	-	-	1
11/95	80	180	88	82	17	0	0	0	0	0	0	0	0	0	0	0	0	0	0	0	0	39	17	82	88	88	0.766
12/95	0	-	-	-	-	-	-	-	-	-	-	-	-	-	-	-	-	-	-	-	-	-	-	-	-	-	1
14/94	0	-	-	-	-	-	-	-	-	-	-	-	-	-	-	-	-	-	-	-	-	-	-	-	-	-	1
15/94	80																										0.601

Bornhardt Samples																											
15A	0	-	-	-	-	-	-	-	-	-	-	-	-	-	-	-	-	-	-	-	-	-	-	-	-	-	1
15B	0	-	-	-	-	-	-	-	-	-	-	-	-	-	-	-	-	-	-	-	-	-	-	-	-	-	1
16A	0	-	-	-	-	-	-	-	-	-	-	-	-	-	-	-	-	-	-	-	-	-	-	-	-	-	1
16B	0	-	-	-	-	-	-	-	-	-	-	-	-	-	-	-	-	-	-	-	-	-	-	-	-	-	1
17A	28	20	0	0	0	0	0	0	4	0	6	19	21	36	17	20	25	21	14	20	20	15	13	7	0	0	0.988
17B	55	30	0	0	0	0	0	0	0	0	7	25	40	51	55	49	49	35	31	23	17	7	0	0	0	0	0.936
Antarctic Samples																											
50/95	2	105	1	0	0	1	0	1	6	6	3	3	4	2	10	21	23	27	33	33	33	28	24	15	6	1	0.987
51/95	0	-	1	0	0	1	0	1	6	6	3	3	4	2	10	21	23	27	33	33	33	28	24	15	6	1	0.987
52/95	38	105	1	0	0	1	0	1	6	6	3	3	4	2	10	21	23	27	33	33	33	28	24	15	6	1	0.967
56/95	0	-	-	-	-	-	-	-	-	-	-	-	-	-	-	-	-	-	-	-	-	-	-	-	-	-	1
57/95	0	-	-	-	-	-	-	-	-	-	-	-	-	-	-	-	-	-	-	-	-	-	-	-	-	-	1
5/96	0	-	-	-	-	-	-	-	-	-	-	-	-	-	-	-	-	-	-	-	-	-	-	-	-	-	1
6/96	0	-	-	-	-	-	-	-	-	-	-	-	-	-	-	-	-	-	-	-	-	-	-	-	-	-	1
13/96	25	330	5	6	3	7	18	25	28	28	35	33	32	25	19	19	12	8	5	1	1	2	5	5	6	6	0.984

Notes:

1: Dip and Orientation of Dip = The dip angle of the surface of the samples *in-situ* and the orientation of the down slope component relative to 0° N.

2: Angle to Horizon = Angle from the sample site to the nearest horizon at 15° intervals. Quadrant 1 = 0-15°, 15°-30°, 30°-45°, 45°-60°, 60°-75°, 75°-90°; Quadrant 2 = 90°-105°, 105°-120°, 120°-135°, 135°-150°, 150°-165°, 165°-180°; Quadrant 3 = 180°-195°, 195°-210°, 210°-225°, 225°-240°, 240°-255°, 255°-270°; Quadrant 4 = 270°-285°, 285°-300°, 300°-315°, 315°-330°, 330°-345°, 345°-360°.

3: Exposure Geometry Correction = Factor applied to production rate at each site to account for shield effect of surrounding topography and dip angle of sample. For details on how this is calculated see 2.2.6.

Appendix B

Publications

This appendix contains two manuscripts resulting from the analysis of *in-situ* cosmogenic ^{21}Ne in Antarctica presented in Chapter 6. Both papers are currently in press. The first, Summerfield *et al.* (1998a) will be published in a special publication of the Geological Society and the second, Summerfield *et al.* (1998b) will be published in a special issue of *Geomorphology* on the application of *in-situ* cosmogenic isotope analysis.

Long-term rates of denudation in the Dry Valleys region of the Transantarctic Mountains, southern Victoria Land, Antarctica: Preliminary results based on *in-situ*–produced cosmogenic ^{21}Ne

M.A. Summerfield[1], F.M. Stuart[2], H.A.P. Cockburn[1], D.E. Sugden[1], G.H. Denton[3], T. Dunai[4] and D. R. Marchant[5]

[1] Department of Geography, University of Edinburgh, Edinburgh EH8 9XP, UK

[2] Isotope Geosciences Unit, Scottish Universities Research and Reactor Centre, East Kilbride, G75 0QF, UK

[3] Department of Geological Sciences, Institute for Quaternary Studies, University of Maine, Orono, Maine 04469, USA

[4] Vrije Universiteit Amsterdam, Faculteit der Aardwetenschappen, De Boelelaan 1085, 1081 HV Amsterdam, The Netherlands

[5] Department of Earth Sciences, Boston University, 675, Commonwealth Avenue, Boston, Massachusetts 02215, USA

Abstract

Cosmogenic ^{21}Ne ($^{21}Ne_c$) concentrations measured in quartz have been used to estimate long-term denudation rates for contrasting landscape components in the Dry Valleys area of the Transantarctic Mountains, southern Victoria Land, Antarctica. Samples of Beacon Supergroup sandstones and granitic basement were collected from two contrasting landscape elements – low-relief, high-elevation surfaces and rectilinear slopes – in order to assess variations in rates of denudation with topographic position. The rectilinear slope sample sites were selected because of their proximity to $^{40}Ar/^{39}Ar$–dated lavas and ash-avalanche deposits. All $^{21}Ne/^{20}Ne$ ratios are significantly greater than the atmospheric value, and $^{21}Ne_c$ concentrations were calculated from the measured ^{21}Ne values assuming an atmospheric composition for the trapped component. Apparent exposure ages calculated from $^{21}Ne_c$ concentrations, assuming no denudation since exposure, range from 3.78–4.66 Ma for the high-elevation plateau surface samples, and 0.61–2.48 Ma for the rectilinear slope samples. Exposure ages for $^{3}He_c$ were 2 to 42 times lower than those derived from $^{21}Ne_c$ abundances due to preferential diffusive loss of $^{3}He_c$ from the quartz lattice; $^{3}He_c$ concentrations were therefore not used in the calculation of denudation rates. We interpret the $^{21}Ne_c$ abundances as reflecting variations in denudation rates rather than exposure age in view of independent evidence for prolonged exposure (>15 Ma) of bedrock surfaces at the sample sites. Calculated maximum denudation rates range from 0.26–1.02 m Ma^{-1} for the rectilinear slopes, down to only 0.133–0.164 m Ma^{-1} for the high-elevation surface sites. These rates are comparable to other denudation rate estimates for the Dry Valleys area derived from cosmogenic isotope analyses, but are around two orders of magnitude lower than the long-term mean rate over the past ~50 Ma estimated from fission-track thermochronology. Combined with the preservation of volcanic deposits dating back to the mid-Miocene, our $^{21}Ne_c$ data demonstrate that only minimal landscape modification has occurred in the Dry Valleys area over at least the past ~15 Ma. This conclusion supports the view that the East Antarctic Ice Sheet has been essentially stable over this period rather than experiencing significant fluctuations as late as the Pliocene, as has previously been suggested.

Key words Denudation rates, cosmogenic isotopes, landscape evolution, paleoclimatology, Antarctica

1. Introduction

We report here quantitative estimates of rates of denudation derived from measurements of *in-situ*–produced cosmogenic ^{21}Ne for contrasting landscape elements in the Dry Valleys region of the Transantarctic Mountains in southern Victoria Land, Antarctica. A knowledge of rates of landscape modification in this area is important for several reasons. First, the current debate about the stability of the East Antarctic Ice Sheet has involved contrasting interpretations of the antiquity of the landscape of the Transantarctic Mountains. The unstable ice sheet model (Webb *et al.*, 1984; Webb and Harwood, 1991; Barrett *et al.*, 1992) requires much warmer conditions, with temperatures 20 – 25°C higher than those of the present, as recently as 3 Ma BP, and such a climatic environment implies significant rates of glacial and periglacial geomorphic processes and landscape change. By contrast, those advocating long-term ice sheet stability for the past 15 Ma or more have viewed the present landscape as being essentially relict with minimal change under a hyper-arid polar climate similar to that of the present (Clapperton and Sugden, 1990; Denton *et al.*, 1993; Marchant *et al.*, 1993a; Sugden *et al.*, 1995a) . Secondly, irrespective of these conflicting interpretations of the late Cenozoic climatic history of Antarctica, the landscape of the Dry Valleys area has experienced stable climatic conditions for, at the very least, the past 2-3 Ma ; this is in contrast to the glacial-interglacial–driven oscillations in temperature and precipitation that have affected virtually every other morphoclimatic zone. Thirdly, during this period of climatic stability, much of the landscape has developed under an extreme hyper-arid, frigid regime in the virtual absence of running water, a situation encountered nowhere else on Earth. Finally, various lines of evidence, including the preservation of volcanic deposits of known age and already published data from *in-situ* –produced cosmogenic isotopes, suggest that rates of denudation in this area are the lowest for any terrestrial environment, and therefore represent a benchmark against which denudation rates in areas of greater geomorphic activity elsewhere can be compared.

Over the past decade, measurements of *in-situ*–produced cosmogenic nuclides in bedrock exposures and surface deposits have begun to provide both chronological information on Quaternary, and in some cases, Pliocene events, and valuable site-specific and basin-scale estimates of long-term rates of denudation (Bierman and Turner, 1995; Nishiizumi *et al.*, 1991). The majority of applications of cosmogenic nuclide analyses in previous studies have involved surface exposure ages, the calculation of which are based on the assumption of zero denudation since an exposure event. This assumption can be constrained in some cases by independent evidence, or can be reasonably assumed for certain very young surfaces, such as those exposed by the most recent episode of deglaciation in the mid-latitudes. In most situations, however, there is geomorphological evidence for progressive denudation, albeit at an extremely low rate in some cases, and therefore it is generally more appropriate to interpret cosmogenic isotope data in terms of denudation rates rather than 'exposure

ages'. Here we use measurements of *in-situ*–produced cosmogenic ^{21}Ne in quartz to provide preliminary estimates of rates of denudation in the Dry Valleys region (Fig. 1). More specifically, we attempt to characterize differences in rates of denudation between high-elevation surfaces and rectilinear valley-side slopes, the two most significant landscape components in this geomorphologically unique environment.

^{21}Ne has particular advantages as a cosmogenic isotope for use in environments with potentially extremely slow rates of denudation since, as a stable nuclide, it does not have an upper limit to its accumulation as a result of losses through radioactive decay. Even in the case of ^{10}Be, which has the longest half-life (~1.5 Ma) of presently used cosmogenic radionuclides, the maximum exposure age attainable assuming zero denudation is ~5-6 Ma. Whereas the diffusion rate of cosmogenic ^{3}He in quartz limits its ability to determine denudation rates (Trull *et al.*, 1991), diffusive loss of cosmogenic ^{21}Ne from quartz is minimal and ^{21}Ne can therefore be used to determine denudational histories on timescales of 10^6–10^7 a (Graf *et al.*, 1991).

2. Physical setting

2.1 Morphotectonics of the Transantarctic Mountains

The Transantarctic Mountains extend for more than 3000 km in a broad arc from northern Victoria Land on the Pacific coast to the Theron Mountains which terminate near the South Atlantic Ocean. Rather than being a mountain range *sensu stricto*, they consist of a large amplitude (~2000–4000 m), short wavelength (50–200 km) upwarp forming the rim of an extensive plateau that rises from the interior of East Antarctica (Kerr *et al.*, in press). The outer flank of this upwarp is marked by a significant topographic discontinuity comprising either a major escarpment, or a stepped series of minor scarps. This escarpment landscape is most dramatically developed where it fringes the structural basins forming the Ross Embayment.

The main elements of the present structural setting of the Transantarctic Mountains in the Dry Valleys area can apparently be traced to asymmetric rifting in the Eocene, with extension in the lower plate represented by the Ross Embayment, and block tilting, or flexure, of the upper-plate margin producing a gentle inland dip in Devonian–Triassic age sedimentary units (Fitzgerald *et al.*, 1986; Fitzgerald, 1992). The amount of surface uplift in the Dry Valleys area associated with this rifting event is uncertain; however, results from apatite fission-track thermochronology, which reveal a major denudational episode initiated about 50 Ma BP, indicate that significant local relief must have existed in the early Cenozoic (Gleadow and Fitzgerald, 1987; Brown *et al.*, 1994). A total of ~5 km of

denudation has occurred since this time along the Ross Sea coast, with somewhat lesser amounts inland. This phase of denudation could have been precipitated by tectonic uplift along the rift flank, by the creation of a new, lower base level through subsidence of the Ross Embayment adjacent to a rift flank with some residual elevation, or by a combination of these two factors (Brown *et al.*, 1994).

Although 3 km of surface uplift at a mean rate of ~1 km Ma^{-1} since the early of middle Pliocene has been suggested for the Transantarctic Mountains (Behrendt and Cooper, 1991), there is compelling evidence from the present elevations of sub-aerially erupted volcanics (Wilch *et al.*, 1993a), from the variation of cosmogenic nuclide production rate with altitude (Brook *et al.*, 1995; Bruno *et al.*, 1997), and from geophysical evidence (ten Brink *et al.*, 1993) that surface uplift in the Dry Valleys region over the past few million years has been minimal, with *maximum* possible uplift over the past ~2.5 Ma being limited to only ~300 m.

2.2 Geology and morphology of the Dry Valleys area

The Dry Valleys region represents a 4000 km^2 ice-free area of the Transantarctic Mountains from 77°15'S to 77°45'S and 160°E to 164°E, located between the Ross Sea embayment and the Taylor Dome on the flank of the East Antarctic Ice Sheet (Fig. 1). Along the length of the Transantarctic Mountains the plateau periphery is cut by numerous major transverse valleys carved by outlet glaciers draining from the Polar Plateau formed by the East Antarctic Ice Sheet. Along the western coast of McMurdo Sound three of these valleys – the Taylor, Wright and Victoria systems – are currently largely ice free as a result of being starved of flow from the Polar Plateau through the influence of the Taylor Dome lying immediately inland. Known collectively as the Dry Valleys, these valley systems are separated from each other by the 1500–2400 m high Asgard and Olympus Ranges.

Bedrock exposures in the Dry Valleys area consist of a basement complex of Precambrian igneous and meta-igneous rocks overlain by Devonian-to-Triassic–age sandstones, siltstones and conglomerates of the Beacon Supergroup, which dip gently inland away from the Ross Sea coast. Highly localized Cenozoic volcanics and associated intrusions occur throughout the area, while Jurassic dolerites (Ferrar dolerites) extensively intrude both the basement and overlying sedimentary sequence forming sills up to several hundred metres thick.

Several landscape elements can be distinguished in the Dry Valleys region (Sugden *et al.*, 1995a). Here we focus on the two areally most significant components, namely: 1) the high-elevation, low-relief surfaces that generally lie above about 1800 m and are the main landform in the interior sector of the Dry Valleys area; and 2) the rectilinear slopes that flank these upland surfaces and also constitute the predominant landform element of the Dry Valleys. The most extensive low-relief

surface elements occur in the high terrain between 2000 and 2400 m which overlooks the heads of the Dry Valley systems and runs along high-level interfluves such as that formed by the Asgard Range between Wright and Taylor Valleys. These surfaces rest on near-horizontal dolerite sills and Beacon Supergroup sedimentary rocks and are, at least to some extent, structurally controlled. Sufficiently prominent to be commented upon by the early explorers of the region (Taylor, 1914), rectilinear slopes at a typical angle of 33°–37° characterize both the flanks of the high surfaces fringing the Polar Plateau and a significant proportion of the valley sides of the Dry Valleys. Across the higher, western part of the region rectilinear slopes generally occur below free faces with an angle of more than 60° and lead down into a colluvium-mantled footslope at an angle of around 18° (Selby, 1971). At lower elevations to the east free faces are less common and rectilinear slopes of adjacent valleys meet to form sharp-edged interfluves. The rectilinear slope forms are cut in bedrock and have been recognized as Richter denudational slopes (Selby, 1971, 1974, 1993). They are partly covered by a thin veneer of generally coarse rock debris which appears not to exceed a thickness of 1 m even at the base of the rectilinear slope segment. Some boulders show evidence of weathering and degradation through surficial iron oxide staining and the development of cavernous weathering forms and tafoni.

2.3 Climate of the Dry Valleys area

The Dry Valleys area presently experiences a hyper-arid, polar climate. A mean annual temperature of –19.8°C at an elevation of 123 m in Wright Valley is indicative of conditions at low elevations in the bottom of the Dry Valleys (Schwerdtfeger, 1984), although mid-summer temperatures exceeding +5°C over several days have been recorded in middle Wright Valley (Bull, 1966) and the distribution of debris flows, mudflows and channels demonstrates that liquid water is common below ~800 m under the present climate. Assuming a lapse rate of 10°C km^{-1}, mean annual temperatures at higher elevations in the Asgard and Olympus Ranges, the Quatermain Mountains and along the high-elevation surfaces fringing the Polar Plateau drop to –30°C to –40°C, and mean annual precipitation is <10 mm water equivalent (Schwerdtfeger, 1984; Fortuin and Oerlemans, 1990). Easterly winds carry moist air with a relative humidity of around 65–75% inland from the Ross Sea, and snow precipitation reaches a mean maximum of around 100 mm per annum at the eastern ends of the Dry Valleys. Strong katabatic winds with a generally low relative humidity of 5–60% drain from the Polar Plateau through the Dry Valleys towards towards the Ross Sea, although in the summer they are largely confined to the western part of the area and to the valley bottoms. The accumulation of wind-blown snow in the lee of topographic barriers sustains small, cold-based glaciers on the sides of Taylor, Wright and Victoria Valleys. Meltwater seems to be absent at high altitudes inland, although it is present at progressively higher elevations towards the coast . This trend probably results from a combination of the maritime influence near the coast and more active katabatic winds in the upper parts of the Dry Valleys (Marchant and Denton, 1996).

3. Sample site characteristics

Sample sites were chosen in order to assess rates of denudation in the contrasting morphological settings of high-elevation surfaces and rectilinear slopes (Table 1). In selecting specific sample locations particular attention was paid to identifying representative sites from which useful extrapolations about denudation rates could be made and that would yield the maximum geomorphologically useful information. Although in sampling from discrete bedrock outcrops there is always the possibility of recording atypical denudation rates, the landform elements from which we sampled are relatively homogeneous over lateral distances of hundreds of metres and thus some spatial extrapolation of site-specific data is justified. We sampled bedrock outcrops in preference to regolith or colluvium as the exposure history of the latter under the highly episodic transportational regime operating in the Dry Valleys is much more uncertain. Rectilinear slope locations were chosen to provide comparisons with existing independent evidence of rates of landscape change from dated lava and ash deposits (Wilch *et al.*, 1993b; Marchant *et al.*, 1996). Our sampling strategy therefore differed significantly from previous cosmogenic isotope studies in Antarctica which have focussed on the dating of particular deposits or exposure events rather than characterizing variations in rates of landscape modification. Sample locations were recorded using GPS equipment and elevations were determined to ±20 m using altimeters calibrated daily to field camp elevation in lower Taylor Valley.

Four samples were analyzed from high-elevation (>2000 m), low-relief surfaces, all consisting of Beacon Sandstone (Beacon Supergroup). Two of these were collected from the eastern flank of Mount Fleming at the head of Wright Valley overlooking Wright Upper Glacier (Fig. 2), one on a broad, low-relief ridge just below the summit (5/96) (Fig. 3), and the other from a lower elevation on a flat-topped spur from an iron-stained bedrock surface scattered with dolerite boulders and cobbles (6/96). The other two high-elevation samples (56/95 and 57/95) were collected from the flat-topped interfluve between Beacon Valley and Arena Valley above Taylor Glacier. Bedrock surfaces at all the high-elevation surface sampling sites exhibit evidence of some rock disintegration in the form of cavernous weathering and the development of tafoni. A thin (<100 mm), discontinuous snow cover was observed at the higher sample site at Mount Fleming (5/96), although significant shielding by snow of the bedrock surface from exposure to cosmic radiation on the high-elevation surfaces is unlikely since the very high wind speeds characteristic of these extremely exposed locations retard snow accumulation.

Analyses were undertaken of three samples (50-52/95) of Arena Sandstone (Beacon Supergroup) from within a 10 m^2 area on a 36-38° rectilinear slope in the Quartermain Mountains on the western side of Arena Valley overlooking Taylor Glacier. The samples were collected at an elevation of ~1570 m, on a rectilinear slope ~500 m below the high-elevation surface sample site (56-57/95) located on the

adjacent interfluve (Fig. 4). Near-horizontal sandstone beds protrude from the slope forming a series of cavernously weathered steps with localized undercutting and slumping. Sample 50/95 was taken from one of the bedrock steps which characterize the slope and which have a relief of up to 4 m. Sample 51/95 is from a ~0.4 m boulder on the same bedrock step, while sample 52/95 was collected from the slumped front of the step. The site was selected because of its proximity to an avalanche deposit (one of two identified on the slope) located 100 m to the south which contains $^{40}Ar/^{39}Ar$–dated (11.3–12.9 Ma BP) volcanic ash, and which had been previously used to infer minimal rates of landscape change in this area over the past several million years (Marchant *et al.*, 1993b, 1996). This ash-avalanche deposit extends two-thirds of the way down the rectilinear slope from a bedrock couloir and comprises sandstone and dolerite clasts, quartz sand and dolerite grus with minor granite erratics chaotically mixed with a phonolitic ash incorporating glass shards and euhedral anorthoclase crystals. There is a sharp contact between the debris cover of the rectilinear slope and the avalanche deposit which rises up to ~3 m above the surrounding talus mantle. Additional evidence of minimal geomorphic activity on the slope is provided by a thinly distributed granite till located only 30 m downslope from the sample site for 50-52/95 which has been dated by its association with volcanic ash to > 13.6 Ma BP (Denton *et al.*, 1993).

Analysis was undertaken of one further sample (13/96) collected from a north-facing ~33° rectilinear slope in lower Taylor Valley immediately to the east of Sollas Glacier (Fig. 5). The slope is formed in granite basement and is characterized by protruding bedrock outcrops with a discontinuous mantle of coarse talus. The sample comprised fragments from a ~10 mm thick exfoliating sheet of granite on an *in situ* bedrock exposure inclined at ~25°. The site was chosen because it is immediately adjacent to a $^{40}Ar/^{39}Ar$–dated (2.2 Ma BP) partially eroded pyroclastic and lava-flow deposit (Wilch *et al.*, 1993b). This site is at a sufficiently low elevation to have been temporarily covered by expansion of Taylor Glacier during the Quaternary.

4. Analytical methods

The samples were crushed and sieved, and the 250-500 mm fractions were selected for analysis. Mono-minerallic quartz was prepared by magnetic separation and selective chemical dissolution following the procedure described by Kohl and Nishiizumi (1992). Aliquots were set aside for future ^{10}Be and ^{26}Al analysis. The dissolution process etches up to 15 mm from the surface of the quartz crystals and this effectively removes a large proportion of implanted alpha particles produced in adjacent minerals. Samples were then ultra-sonically cleaned in deionised water to remove traces of HF from mineral surfaces. Two samples (5/96 and 6/96) contained a small proportion of darker grains (possibly those with zircon inclusions) and these were removed by hand picking.

Approximately 250 mg of each sample was wrapped in aluminium foil and loaded into the extraction system and evacuated to $<10^{-8}$ torr for 48 hours prior to analysis.

Noble gases were extracted by heating samples for 15 minutes to 1400°C in a double vacuum resistance furnace with a tungsten heating element and a molybdenum crucible. The extracted gas was cleaned on two Ti-getters (at 250°C and 800°C) and a SAES-getter (at room temperature). The heavy noble gases (Ar, Kr and Xe) were separated from He and Ne by successive absorption on two charcoal traps cooled with liquid nitrogen. Neon was then absorbed on to a charcoal trap at –228°C and He isotope determinations were made on the residual gas. Subsequently Ne was released from the charcoal at -173°C and the isotopic composition analysed after the He isotope measurements. All measurements were made on a VG 5400 noble gas mass spectrometer. This has an ion source with a modified Nier-type geometry and is equipped with an axial electron multiplier and an off-axial Faraday cup. The amplifiers of the multiplier and the Faraday cup have switchable resistors (multiplier 10^8 and 10^9; Faraday cup 10^9, 10^{10} and 10^{11}).

Noble gas abundances were determined by peak height comparison with known amounts of gas. ^{3}He-enriched geothermal gas (^{3}He/^{4}He = 14.3 ± 0.1 Ra, where Ra is the atmospheric ratio of 1.39×10^{-6}) was used for the He calibrations. The He elemental and isotopic abundances in the geothermal standard were determined by repeated cross-calibrations with 0.25 cc STP air. Neon calibrations were made on 95.2 ± 0.5 µcc STP air. The reproducibility of noble gas abundances was better than ±1.5% and isotopic ratios of replicate calibrations were better than 0.5%. ^{20}Ne and ^{22}Ne were corrected for interfering $^{40}Ar^{2+}$ and CO_2^{2+}, respectively, using values of $^{40}Ar^{2+}/^{40}Ar^{+}$ and CO_2^{2+}/CO^{2+} determined previously. The abundances of H_2 and $H_2{}^{16}O$ were routinely measured but displayed no significant variation through the week of analysis. Blanks at 1400°C were ^{4}He: 2×10^{-11} ccSTP and ^{20}Ne 1×10^{-11} ccSTP. ^{3}He was undetectable in the blank and the Ne blanks were indistinguishable from the atmospheric isotopic composition.

5. Results and interpretation

The isotopic composition of Ne and He, and the ^{21}Ne and ^{3}He concentrations are presented in Table 2. In all cases the measured ^{21}Ne/^{20}Ne (0.00489 - 0.0183) are significantly greater than the atmospheric value (0.00296). At its simplest, the ^{21}Ne/^{20}Ne of minerals are a mixture of atmospheric and cosmogenic contributions. However, nuclear reactions on ^{18}O produce nucleogenic ^{21}Ne ($^{21}Ne_n$) throughout the lifetime of the rock which may obscure the simple two component mixing. The radiogenic ^{4}He ($^4He_{rad}$) concentration of a sample is a monitor of the a-particle flux (Niedermann *et al.*, 1993) which is essential for $^{21}Ne_n$ production (Wetherill, 1954). Thus the $^{21}Ne_n$

contribution may be estimated from the $^{4}He_{rad}$ content using the most recent determination of the $^{21}Ne_{n}/^{4}He_{rad}$ of crustal rocks (4.5×10^{-8} (Yatsevich and Honda, 1997)). Assuming that all the measured ^{4}He is radiogenic, and that at least 5% has been retained since cooling below the $^{21}Ne_{n}$ closure temperature, then the contribution of $^{21}Ne_{n}$ is less than 5% in all but one sample (51/95 = 30%). This can be considered as a conservative estimate as, in all but one sample, more than 5% of the $^{3}He_{c}$ has been retained despite it being significantly more mobile in quartz than the $^{4}He_{rad}$ (Trull *et al.* 1991).

The $^{21}Ne_{c}$ concentrations displayed in Table 2 have been calculated from the measured ^{21}Ne values assuming an atmospheric composition and corrected for the contribution of nucleogenic ^{21}Ne. $^{3}He/^{4}He$ are in the range 0.65 - 32.8 Ra (Table 2). These ratios are significantly in excess of radiogenic values and they identify the presence of high cosmogenic ^{3}He concentrations ($^{3}He_{c}$). The $^{3}He_{c}$ concentrations have been calculated assuming that the inherited ^{3}He is radiogenic ($^{3}He/^{4}He$ = 0.02 Ra). $^{3}He_{c}$ concentrations are insensitive to the precise value used for the radiogenic $^{3}He/^{4}He$ because of the high ratio of the samples. Errors in $^{21}Ne_{c}$ and $^{3}He_{c}$ abundances are propagated from the analytical errors and do not include uncertainties in the reproducibility of abundance measurements (±1.5%).

The minimum apparent exposure ages of all samples can be calculated from the measured $^{21}Ne_{c}$ and $^{3}He_{c}$ abundances assuming no denudation (Table 3). $^{21}Ne_{c}$ and $^{3}He_{c}$ production rates in quartz have not been measured directly but estimated by calibration against cosmogenic ^{26}Al abundances. This procedure yields production rates of 21 atoms $^{21}Ne_{c}\,g^{-1}\,a^{-1}$ (Niedermann *et al.*, 1994) and 85 atoms $^{3}He_{c}\ g^{-1}\ a^{-1}$ at sea level at high latitude (Brown *et al.*, 1992). The production rates have been adjusted to the altitudes of our sample sites using the nuclear disintegration data of Lal (1991). Corrections were also made to the production rates for the effect of topographic shielding and the dip of the sampled surface. These were calculated on the basis of the angular dependence of cosmic radiation, $F(q) = \sin^{2.3} q$, and in all cases were less than 3%. The resulting $^{21}Ne_{c}$ minimum apparent exposure ages range from 610 ka on a rectilinear slope (13/96) to 4.66 Ma on a high-elevation surface.

The $^{3}He_{c}$ apparent exposure ages are between 2 and 42 times lower than those derived the from the $^{21}Ne_{c}$ abundances (Table 3) (Fig. 6) due to preferential diffusive loss of $^{3}He_{c}$. The relative age differences are unrelated to apparent exposure age, lithology, altitude or temperature. The absence of any systematic behavior clearly confirms the limitations of obtaining accurate exposure chronologies from $^{3}He_{c}$ in quartz (eg Graf *et al.*, 1991). $^{3}He_{c}$ exposure ages of coarse quartz chips from the Antarctic which have not been treated by the chemical cleaning procedure used here are significantly closer to the $^{21}Ne_{c}$ age (Dunai and van der Wateren, unpublished data). This suggests that laboratory handling procedures may promote the diffusive loss of $^{3}He_{c}$ in quartz.

Concentrations of stable cosmogenic nuclides reach an equilibrium state with respect to production and loss through denudation assuming a finite, constant denudation rate and continuous, long-term exposure (Lal, 1995). Although we cannot fully verify these two assumptions, field evidence indicates that the predominant form of denudation on the high-elevation surfaces is through a continuous incremental detachment of clasts or thin slivers of rock, with some wind abrasion. These conditions also satisfy the assumption that the increments of denudation are very small in relation to the mean cosmic-ray absorption length (attenuation length) of ~0.5 m (~150 g cm^{-2}) (Lal, 1991). On the rectilinear slopes the detachment of thicker rock masses is evident in the case of the Arena Valley site, although the granitic basement at the lower Taylor Valley site appears to be exfoliating in sheets <20 mm thick at the point where it was sampled. For reasons discussed below, the assumption of long-term exposure of bedrock surfaces at our sample sites is supported by independent geochronological and stratigraphic data. We therfore consider it more appropriate to interpret our $^{21}Ne_c$ concentrations as representing long-term denudation rates rather than apparent exposure ages (Table 3). Although we regard the possibility as being excluded by existing cosmogenic isotope data (Brook *et al*., 1995; Bruno *et al.*, 1997) as well as independent geochronology from volcanic deposits (Wilch *et al*., 1993a), any significant surface uplift at our sample sites during exposure would cause an over-estimation of denudation rates because $^{21}Ne_c$ production rate increases with altitude.

Modifying the equation given by Kurz (1986) for stable cosmogenic nuclides in rock surfaces which have been exposed for short times relative to the formation age of the rock (clearly the case for our samples), we can interpret the measured concentration (N, atoms g^{-1}) of a stable cosmogenic isotope, i, in terms of a maximum constant denudation rate (e, g cm^{-2} a^{-1}), such that:

$$e = (P \times l)/N_i$$

where P is the production rate (atoms g^{-1} a^{-1}) and l is the cosmic-ray attenuation length (g cm^{-2}). To convert denudation rates into cm a^{-1} for a specific site, the result can be divided by the density of the sample (g cm^{-3}). The denudation rates displayed in Table 3 have been calculated using a $^{21}Ne_c$ attenuation length of 165 g cm^{-2} (Sarda *et al*., 1993), and a mean rock density of 2.7 g cm^{-3}. All rates reported here have been converted to m Ma^{-1}.

The highest denudation rate of 1.02 m Ma^{-1} is for sample 13/96 from a rectilinear slope in lower Taylor Valley, although this is probably an overestimate given the possibility of temporary burial of this site under an expanded Taylor Glacier during the Quaternary. All four samples from the high-elevation surfaces above 2000 m display much lower rates of 0.133 – 0.164 m Ma^{-1}. Samples from the rectilinear slope on the western side of Arena Valley (50-52/95) yielded intermediate denudation

rates of 0.26 – 0.60 m Ma^{-1}. Assuming prolonged steady-state denudation, and given the residence time of the samples in the cosmic-ray attenuation zone (~2 m depth), these rates apply over time scales of >1 Ma for the highest rate of 1.02 m Ma^{-1}, and >4 Ma for the lowest rate of 0.133 m Ma^{-1}.

6. Discussion

Our data elucidate various aspects of the morphological evolution of the Dry Valleys sector of the Transantarctic Mountains and the late Cenozoic history of the East Antarctic Ice Sheet. The issues we consider here are: 1) the interpretation of the measured $^{21}Ne_c$ concentrations as indicative of denudation rates rather than exposure ages; 2) the observed variations in rates of denudation between sample sites and their interpretation in terms of weathering and erosional processes, and the magnitude of late Cenozoic landscape modification; 3) the implications of the $^{21}Ne_c$ data for existing interpretations of late Cenozoic lavas and volcanic ash deposits; 4) the comparison of denudation rates reported here with previous estimates for the Dry Valleys and denudation rates for contrasting morphoclimatic regimes; and 5) the implications of our data for the ice-sheet stability debate.

6.1 Geomorphological interpretation of cosmogenic ^{21}Ne data

When expressed as apparent surface exposure ages (Table 3), the older ages reported here tend to be associated with the higher elevation sites. Old apparent exposure ages for high-altitude, inland locations compared with somewhat younger ages at lower elevations towards the coast have been noted elsewhere in the Transantarctic Mountains (Nishiizumi *et al.*, 1991; Geigengack *et al.*, 1994). A potential explanation for this trend is that lowering of the East Antarctic Ice Sheet progressively exposed bedrock surfaces at lower elevations. There are, however, compelling arguments against this mechanism as a general explanation of the data. For instance, there are climatic reasons for expecting a gradient of decreasing weathering and erosion rates inland from the coast, and from low to higher elevations, in the Dry Valleys sector of the Transantarctic Mountains which could account for the trend observed in apparent exposure ages. In addition, independent paleooceanographic, geochronometric, stratigraphic and geomorphological evidence for the history of the East Antarctic Ice Sheet (Denton *et al.*, 1993; Kennett and Hodell, 1993) indicates stability since the Miocene and argues against the $^{21}Ne_c$ data being interpreted as a record of the timing of progressive bedrock exposure from beneath a wasting ice mass. Apart from a modest expansion of glaciers in the Pliocene, Marchant *et al.* (1993b) have argued that there has been no significant change in the extent of glaicers lying above an elevation of 1500 m in the western Dry Valleys area since the deposition of a granite-rich drift by East Antarctic outlet glaciers more than 13.6 Ma ago. This interpretation has been further supported by the discovery of a preserved remnant of granite-bearing glacier ice at the

mouth of Beacon Valley overlooking Taylor Glacier (Sugden *et al.*, 1995b). The ice has a minimum age of 8 Ma BP on the basis of ^{40}Ar-^{39}Ar dating of overlying *in situ* volcanic ash. Any significant thickening of Taylor Glacier at the mouth of the valley, or of the East Antarctic Ice Sheet, would have caused this remnant ice to have been overridden and removed by normal processes of ice deformation. The fact that the ice preserves detailed characteristics from the time of initial deposistion demonstrates that there has been no such overriding.

6.2 Denudational processes and degree of late Cenozoic landscape modification

Although our data indicate very low rates of denudation for all the sample locations, a somewhat higher rate of denudation of around 1 m Ma^{-1} is indicated for the low elevation site in lower Taylor Valley (13/96). Little can be inferred soley from this single sample, but the partially eroded form of the immediately adjacent 2.2 Ma old lava-flow deposit (Wilch *et al.*, 1993) supports the interpretation of a higher rate of geomorphic activity in this area. Indeed, the presence of gelifluction lobes, patterned ground, debris flows and ephemeral streams channels in the lower Taylor Valley indicates some level of geomorphic activity reflecting the presence of meltwater, relatively high precipitation and humidity, and freeze-thaw cycles during the summer. However, with the absence of liquid water further inland and at higher elevation, the western Dry Valleys landscape appears to be essentially relict (Marchant and Denton, 1996). The low denudation rates reported here for the rectilinear slope in Arena Valley (samples 50-52/95) and the even lower rates of <0.2 m Ma^{-1} on the high-elevation surfaces (samples 5-6/96 and 56-57/95) probably reflect the exceedingly slow operation of salt weathering in conjunction with deflation, and very rare mass movement events precipitated by rock failures on rectilinear slopes and free faces (Augustinus and Selby, 1990; Selby, 1971, 1974). The relative abundance of tafoni and cavernous weathering forms suggests that salt weathering is more active at lower elevations near the coast where both salt supply and humidity are at a maximum. More uncertain is the role of cryptoendolithic microorganisms which can currently survive in the Dry Valleys up to an elevation of about 2000 m in the vicinity of Mount Fleming (Friedmann *et al.*, 1994), as they may promote case hardening of bedrock surfaces through silicification as well as rock breakdown through biochemical processes (Weed and Norton, 1991). Irrespective of the precise role of these various weathering and erosional processes, it is clear that they vary in their efficacy across the Dry Valleys area and that rates of denudation vary in consequence even under the present climatic regime.

Amounts of denudation since the most recent episode of wet-based glacial erosion of the Dry Valleys have been sufficient to allow differential rates of weathering and erosion of contrasting lithologies to produce relief of a few metres. As noted by Selby (1974), fine-grained rocks such as lamprophyre and finely crystalline dolerites form positive relief forms where they intrude less resistant granites.

However, our $^{21}Ne_C$ data, in combination with the survival of dated volcanic deposits, indicate that a maximum of only a few metres of total denudation has occurred throughout most of the Dry Valleys region during the past several million years. It is therefore clear that the presently active geomorphic processes have led to only minimal landscape modification in these areas during this extended period of time and have not been capable of creating the present topography from an earlier landscape shaped by through-valley glaciation.

These extremely slow rates of landscape change of ~0.2 – 1.0 m Ma^{-1} can be compared with estimates of longer term denudation rates from fission-track thermochronology. In the Dry Valleys area there is clear evidence of a period of accelerated denudation rates initiated in the early Cenozoic (50-55 Ma BP) associated with rifting, with a less certain phase of Cretaceous denudation being identified inland (Gleadow and Fitzgerald, 1987; Fitzgerald, 1992). The amount of denudation since the early Cenozoic is at a maximum of ~5 km in the vicinity of the rift-flank axis and Ross Sea coastal zone, and declines inland to the west. This gives a maximum mean denudation rate for the past ~50 Ma of ~100 m Ma^{-1}, although thermal modelling of fission-track age and track length data indicates that crustal cooling (denudation) rates were higher (~200 m Ma^{-1}) for a period of about 10-15 Ma after the initiation of this late Cenozoic phase of accelerated denudation. Although such fission-track data do not provide information on more recent denudation of the upper ~1 km of the crust, the reduction in denudation rates evident after the initial pulse associated with rifting ~55 Ma ago is fully compatible with our $^{21}Ne_C$ results and other geochronological data demonstrating extremely low denudation rates over the past several million years.

6.3 Correlations with lava and volcanic ash deposits

The ~1 m Ma^{-1} rate of denudation for the lower Taylor Valley slope site (13/96) is fully consistent with the partially eroded nature of the immediately adjacent 2.2 Ma old lava-flow deposit (Fig. 5) (Wilch *et al.*, 1993). Potentially more equivocal, however, is the interpretation of the ash-avalanche deposits on the slopes of Arena Valley as truly *in situ*, especially given their late Miocene age. These deposits are of considerable importance given their significance to the debate about the late Cenozoic history of the East Antarctic Ice Sheet (Marchant *et al.*, 1993b). One view might be that they represent pods of volcanic ash originally deposited within hollows on the summit surface that have subsequently avalanched down the slope when intersected by slope retreat. Another interpretation might be that they have been emplaced at some time after original eruption by aeolian processes. In both these scenarios the radiometric age of the ash would provide no information on the rate of landscape change in Arena Valley. By contrast, evidence that these deposits represent avalanching essentially contemporaneous with intial airfall includes physical characteristics of the ash that are diagnostic of primary ash falls, with limited subsequent reworking. These characteristics include poor

sorting (bi-modal grain-size distribution of glass shards), intact bubble vesicles, and angular glass shards. That each ash-avalanche deposit is composed of material from a single eruption is also supported by a distinct geochemistry and the consistency in radiometric age of individual crystals (Marchant *et al.*, 1996). It has therefore been inferred that these ash-avalanche deposits formed shortly after times of eruption, with strong katabatic winds deflating ash exposed at the surface but being unable to detach material incorporated within the slope-mantling talus (Marchant *et al.*, 1996).

Our $^{21}Ne_c$ data for the Arena Valley slope site (samples 50-52/95) located close to the 11.3–12.9 Ma dated ash-avalanche support the interpretation of its formation essentially contemporaneously with initial deposition. If extrapolated, the estimated denudation rates of ~0.2–0.6 m Ma^{-1} imply minimal slope retreat of only about 3-4 m over the past 11 Ma under the present hyper-arid, polar climatic regime. These would be sufficiently low to preserve the ash-avalanche deposit. Such low denudation rates would also be compatible with preservation without significant disturbance of moraine ridges of Pliocene age which cross the lower parts of the avalanche cone. Volcanic ash might be expected to survive such limited slope retreat through progressive infiltration into voids created by mechanical weathering of the slope-mantling talus and underlying bedrock. Survival would also be expected if the original avalanche deposit was originally more than 3–4 m thick.

6.4 Comparison of denudation rates

Our maximum denudation rates of <1 m Ma^{-1} are within the range previously reported for cosmogenic isotope studies from sites in the Dry Valleys sector and adjacent areas of the Transantarctic Mountains. For instance, Nishiizumi *et al.* (1991) have modelled maximum denudation rates based on cosmogenic ^{10}Be and ^{26}Al concentrations for nine samples from the Allan Nunatak (Allan Hills), 75 km north-west of Victoria Valley, and these range from 0.24 m Ma^{-1} to 1.31 m Ma^{-1} (mean = 0.65 m Ma^{-1}). In the same study four samples from Wright Valley gave a range of 0.54 m Ma^{-1} to 1.31 m Ma^{-1} (mean = 0.93 m Ma^{-1}). Similarly low rates of 0.06 – 0.27 m Ma^{-1} over the past 2–3 Ma, based on cosmogenic ^{10}Be concentrations, have been recorded by Brook *et al.* (1995) for quartz arenite boulders and cobbles in glacial deposits in the Quartermain Mountains and Asgard Range in the Dry Valleys area. Extremely low maximum denudation rates based on cosmogenic ^{26}Al and ^{10}Be concentrations and ranging up to 0.7 m Ma^{-1} have also been reported by Ivy-Ochs *et al.* (1995) for Beacon Supergroup sandstones, granite from glaciogenic Sirius Group deposits from Table Mountain at the head of Ferrar Glacier, and sandstone boulders from a Sirius Group deposit at Mount Fleming. Denudation rates of less than 0.1 m Ma^{-1} have also been reported by Bruno *et al.* (1997) from cosmogenic ^{21}Ne concentrations for some of their pyroxene, quartz and whole-rock dolerite samples from Sirius Group tillites and associated bedrock samples from the Dry Valleys.

Lack of detailed information on the geomorphic setting of the sampled sites in these studies makes direct comparison with our own results difficult, but clearly the low overall denudation rates reported are comparable with the estimates from our $^{21}Ne_c$ data. Together with existing results, our data support the contention that the Dry Valleys sector of the Transantarctic Mountains have the lowest recorded denudation rates for any terrestrial environment, especially in the case of the high-elevation surfaces. They only appear to be matched by the maximum denudation rates of as low as 0.6 m Ma^{-1} reported by Bierman and Turner (1995) on the basis of ^{26}Al and ^{10}Be concentrations in samples from granitic domes in the Eyre Peninsula, South Australia. By contrast, much higher denudation rates of 5–11 m Ma^{-1} have been derived from cosmogenic ^{26}Al and ^{10}Be concentrations for rhyolitic volcanic ash-flow tuffs in New Mexico, USA (Albrecht *et al.*, 1993) and of ~3.2 m Ma^{-1} for a flat interfluve in Réunion (Sarda *et al.*, 1993). Mean denudation rates for large drainage basins estimated from modern sediment and solute load data range from 5 m Ma^{-1} to 688 m Ma^{-1} and show that rates for the Dry Valleys area lie well below the average for low relief basins (Summerfield and Hulton, 1994). Mean denudation rates for individual catchments may be as low as 1 m Ma^{-1} (Summerfield, 1991), but these figures include large areas of net deposition, and thus underestimate local rates of denudation comparable to the site-specific rates provided by cosmogenic isotope analysis.

6.5 Implications for ice-sheet stability debate

By supporting the *in-situ* interpretation of the Arena Valley ash-avalanche deposits, and by demonstrating the extremely low rates of denudation for various sites in the Dry Valleys area, our $^{21}Ne_c$ data strongly support the scenario that the East Antarctic Ice Sheet has been essentially stable since the mid-Miocene (Marchant *et al.*, 1993a, b; Sugden *et al.*, 1995). Our $^{21}Ne_c$ data certainly seem incompatible with the opposing view of ice-sheet instability and major deglaciation during the Pliocene associated with much warmer conditions (Webb *et al.*, 1984; Barrett *et al.*, 1992) which would have promoted significantly higher rates of denudation than is indicated by the $^{21}Ne_c$ concentrations reported here. Our results, and interpretation of long-term climatic stability, are also in accord with other cosmogenic isotope studies (Brook *et al.*, 1995; Ivy-Ochs *et al.*, 1995) that demonstrate a minimum late Miocene age for key Sirius Group deposits representing the most recent significant ingress of glacial ice into the Dry Valleys area.

6. Conclusions

Our strategically selected samples from constrasting landscape components in the Dry Valleys area yield cosmogenic ^{21}Ne concentrations that indicate extremely low rates of denudation of ~0.15 m Ma^{-1} on low relief, high-elevation surfaces and ~0.20–1.00 m Ma^{-1} on rectilinear slopes. Field evidence and independent geochronological data support the interpretation of the $^{21}Ne_c$ concentrations as reflecting denudation rates rather than ages since exposure from beneath an ice cover. Our estimated rates are comparable to those established from cosmogenic isotope concentrations for other Dry Valleys locations and confirm that denudation rates in this hyper-arid polar environment are the lowest of any terrestrial environment, and are around two orders of magnitude lower than mean rates over the past ~50 Ma estimated from fission-track thermochronology. Such slow rates of geomorphic activity, even on high angle rectilinear slopes, largely involving salt weathering, deflation and limited mass movement, mean that only minimal landscape modification has occurred in the Dry Valleys area since the most recent phase of extensive glaciation around 15 Ma ago. This interpretation is supported by the survival of volcanic deposits extending back to the mid-Miocene, and our estimated rates of denudation for the slopes in Arena Valley are compatible with the *in-situ* survival of ash-avalanches dating back to more than 11 Ma BP. Our data are at variance with the hypothesis that the Dry Valleys were overrun by glacial ice following a major deglaciation event as recently as the late Pliocene; rather, when considered in conjunction with related field and geochronometric data our results support the view that the East Antarctic Ice Sheet has been essentially stable for at least the past 15 Ma.

Acknowledgements

This research was supported by the UK Natural Environment Research Council (grant no. GR3/9128 (DES/MAS) and research studentship no. GT4/93/8/G (HAPC)). Field support was provided by the Division of Polar Programs of the National Science Foundation of the USA through grants to the University of Maine. Alun Hubbard provided assistance with the exposure geometry corrections to production rates.

References

Albrecht, A., Herzog, G.F., Klein, J., Dezfouly-Arjomandy, B. and Goff, F., 1993. Quaternary erosion and cosmic-ray-exposure history derived from ^{10}Be and ^{26}Al produced in situ – An example from Pajarito plateau, Valles caldera region. Geology, 21: 551-554.

Augustinus, P.C. and Selby, M.J., 1990. Rock slope development in McMurdo Oasis, Antarctica, and implications for interpretations of glacial history. Geogr. Ann., 72A, 55-62.

Barrett, P.J., Adams, C.J., McIntosh, C.J., Swisher III, C.C. and Wilson, G.S., 1992. Geochronological evidence supporting Antarctic deglaciation three million years ago. Nature, 359: 816-818.

Behrendt, J.C. and Cooper, A., 1991. Evidence of rapid Cenozoic uplift of the shoulder escarpment of the Cenozoic West Antarctic rift system and a speculation on possible climate forcing. Geology, 19: 315-319.

Bierman, P. and Turner, J., 1995. ^{10}Be and ^{26}Al evidence for exceptionally low rates of Australian bedrock erosion and the likely existence of pre-Pleistocene landscapes. Quat. Res., 44: 378-382.

Brook, E.J., Brown, E.T., Kurz, M.D., Ackert, R.P. Jr, Raisbeck, G.M. and Yiou, F., 1995. Constraints on age, erosion, and uplift of Neogene glacial deposits in the Transantarctic Mountains determined from in situ cosmogenic ^{10}Be and ^{26}Al. Geology, 23: 1063-1066.

Brown, E.T., Brook, E.J., Raisbeck, G.M., Yiou F. and Kurz, M.D., 1992. Effective attenuation of cosmic rays producing ^{10}Be and ^{26}Al in Quartz: Implications for exposure dating. Geophys. Res. Lett., 19: 369-372.

Brown, R.W., Summerfield, M.A. and Gleadow, A.J.W., 1994. Apatite fission track analysis: Its potential for the estimation of denudation rates and implications for models of long-term landscape development. In M.J. Kirkby (Editor), Process Models and Theoretical Geomorphology. Wiley, Chichester, pp. 23-53.

Bruno, L.A., Baur, H., Graf, T., Schlüchter, C., Signer, P. and Wieler, R. 1997. Dating of Sirius Group tillites in the Antarctic Dry Valleys with cosmogenic ^{3}He and ^{21}Ne. Earth Planet. Sci. Lett., 147: 37-54.

Bull, C., 1966. Climatological observations in ice-free areas of southern Victoria Land, Antarctica. Amer. Geophys. Un., Antarctic Res. Ser., 9: 177-194.

Clapperton, C.M. and Sugden, D.E., 1990. Late Cenozoic glacial history of the Ross Sea embayment, Antarctica. Quat. Sci. Rev., 9: 253-272.

Denton, G.H., Sugden, D.E., Marchant, D.R., Hall, B.L. and Wilch, T.I., 1993. East Antarctic ice sheet sensitivity to Pliocene climatic change from a Dry Valleys perspective. Geogr. Ann., 75A: 155-204.

Fitzgerald, P.G., 1992. The Transantarctic Mountains of southern Victoria Land: The application of apatite fission track analysis to a rift shoulder uplift. Tectonics, 11: 634-662.

Fitzgerald, P.G., Sandiford, M., Barrett, P.J. and Gleadow, A.J.W., 1986. Asymmetric extension associated with uplift and subsidence of the Transantarctic Mountains and Ross Embayment. Earth Planet. Sci. Lett., 81: 67-78.

Fortuin, J.P.F. and Oerlemans, J., 1990. Paramaterization of the annual surface temperature and mass balance of Antarctica. Ann. Glaciol., 14: 78-84.

Friedmann, E.I., Druk, A.Y. and McKay, C.P., 1994. Limits of life and microbial extinction in the antarctic desert. Antarctic Jour. Rev., 00: 000-000.

Giegengack, R., Macchiaroli, P.E., Klein, J., Lawn, B. and Middleton, R., 1994. Exposure ages, erosion rates, and burial histories of bedrock surfaces in and near the Dry Valleys, Antarctica: preliminary results from AMS measurement of selected cosmogenic radionuclides. In F.M. van der Wateren, A.L.L.M. Verbers and F. Tessensohn (Editors), LIRA Workshop on Landscape Evolution: A Multidisciplinary Approach to the Relationship Between Cenozoic Climate Change and Tectonics in the Ross Sea Area, Antarctica. Rijks Geologische Dienst., Haarlem, p. 137.

Gleadow, A.J.W. and Fitzgerald, P.G., 1987. Uplift history and structure of the Transantarctic Mountains: New evidence from fission track dating of basement apatites in the Dry Valleys area, southern Victoria Land. Earth Planet. Sci. Lett., 82: 1-14.

Graf, T., Kohl, C.P, Marti, K. and Nishiizumi, K., 1991. Cosmic ray produced neon in Antarctic rocks. Geophys. Res. Lett., 18: 65-73.

Ivy-Ochs, S., Schlüchter, C., Kubik, P.W., Dittrich-Hannen, B. and Beer, J., 1995. Minimum ^{10}Be exposure ages of early Pliocene for the Table Mountain plateau and the Sirius Group at Mount Fleming, Dry Valleys, Antarctica. Geology, 23: 1007-1010.

Kennett, J.P. and Hodell, D.A., 1993. Evidence for relative climatic stability of Antarctica during the early Pliocene: A marine perspective. Geogr. Ann., 75A: 205-220.

Kerr, A., Sugden, D.E. and Summerfield, M.A., in press. Linking tectonics and landscape development in a passive margin setting: The Transantarctic Mountains. In M.A. Summerfield (Editor), Geomorphology and Global Tectonics. Wiley, Chichester.

Kohl, C.P. and Nishiizumi, K., 1992. Chemical isolation of quartz for measurement of in-situ-produced cosmogenic nuclides. Geochim. Cosmochim. Acta, 56: 3583-3587.

Lal, D., 1991. Cosmic ray labeling of erosion surfaces: *in situ* nuclide production rates and erosion models. Earth Planet. Sci. Lett., 104: 424-439.

Lal, D. 1995. On cosmic-ray exposure ages of terrestrial rocks: a suggestion. Radiocarbon, 37: 889-898.

Marchant, D.R. and Denton, G.H., 1996. Miocene and Pliocene paleoclimate of the Dry Valleys region, Southern Victoria land: a geomorphological approach. Mar. Micropaleont., 27: 253-271.

Marchant, D.R., Denton, G.H., Swisher, C.C. III and Potter, N. Jr, 1996. Late Cenozoic Antarctic paleoclimate reconstructed from volcanic ashes in the Dry Valleys region of southern Victoria Land. Geol. Soc. Amer. Bull., 108: 181-194.

Marchant, D.R., Swisher, C.C. III, Lux, D.R., West, D.P. Jr, 1993a. Pliocene paleoclimate and east Antarctic ice-sheet history from surficial ash deposits. Science, 260: 667-670.

Marchant, D.R., Denton, G.H. and Swisher, C.C.III, 1993b. Miocene–Pliocene–Pleistocene glacial history of Arena Valley, Quatermain Mountains, Antarctica., Geogr. Ann., 75A: 269-302.

Niederman, S., Graf, T., Kim, J.S., Kohl, C.P., Marti, K. and Nishiizumi, K., 1994. Cosmic ray produced ^{21}Ne in terrestrial quartz: the neon inventory of Sierra Nevada quartz separates. Earth Planet. Sci. Lett., 125: 341-355.

Niederman, S., Graf, T. and Marti, K., 1993. Mass spectrometric identification of cosmic-ray-produced neon in terrestrial rocks with multiple neon components. Earth Planet. Sci. Lett., 118: 65-73.

Nishiizumi, K., Kohl, C.P., Arnold, J.R., Klein, J., Fink, D. and Middleton, R. 1991. Cosmic ray produced ^{10}Be and ^{26}Al in Antarctic rocks: exposure and erosion history. Earth Planet. Sci. Lett., 104: 440-454.

Sarda, P., Staudacher, T., Allègre, C.J. and Lecomte, A., 1993. Cosmogenic neon and helium at Réunion: measurement of erosion rate. Earth Planet. Sci. Lett., 119: 405-417.

Schwerdtfeger, W., 1984. Weather and Climate of the Antarctic. Elsevier, Amsterdam.

Selby, M.J., 1971. Slopes and their development in an ice-free, arid area of Antarctica. Geogr. Ann., 53A: 235-245.

Selby, M.J., 1974. Slope evolution in an Antarctic oasis. New Zealand Geogr., 30: 18-34.

Selby, M.J., 1993. Hillslope Materials and Processes. 2nd edition. Oxford University Press, Oxford.

Sugden, D.E., Denton, G.H. and Marchant, D.R., 1995a. Landscape evolution of the Dry Valleys, Transantarctic Mountains: Tectonic implications. J. Geophys. Res., 100: 9949-9967.

Sugden, D.E., Marchant, D.R., Potter, N.L. Jr, Souchez, R.A., Denton, G.H., Swisher, C.C. III and Tison, J-L., 1995b. Preservation of Miocene ice in East Antarctica. Nature, 376: 412-414.

Summerfield, M.A., 1991. Global Geomorphology. Longman, Wiley.

Summerfield, M.A. and Hulton, N.J., 1994. Natural controls of fluvial denudation rates in major world drainage basins. J. Geophys. Res., 99: 13871-13883.

Taylor, G., 1914. Physiography and glacial geology of east Antarctica. Geogr. J., 44: 365-382, 452-467, 553-571.

ten Brink, U.S., Bannister, S., Beaudoin, B.C. and Stern, T.A., 1993. Geophysical investigations of the tectonic boundary between East and West Antarctica. Science, 261: 45-50.

Trull, T., Kurz, M.D. and Jenkins, W., 1991. Diffusion of cosmogenic ^{3}He in olivine and quartz: implications for surface exposure dating. Earth Planet. Sci. Lett., 103: 241-256.

Webb, P.N. and Harwood, D.M., 1991. Late Cenozoic glacial history of the Ross Embayment, Antarctica. Quat. Sci. Rev., 10: 215-223.

Webb, P.N., Harwood, D.M., McKelvey, B.C., Mercer, J.H. and Stott, L.D., 1984. Cenozoic marine sedimentation and ice-volume variation on the East Antarctic craton. Geology, 12: 287-291.

Weed, R. and Norton, S.A., 1991. Siliceous crusts, quartz rinds and biotic weathering of sandstones in the cold desert of Antarctica. Proc. Int. Symp. Environ. Biogeochem. Elsevier, Amsterdam, 327-340.

Wetherill, G.W., 1954. Variations in the isotopic abundance of neon and argon extracted from radioactive minerals. Phys. Rev., 96: 679-683.

Wilch, T.I., Lux, D.R., Denton, G.H. and McIntosh, W.C., 1993a. Minimal Pliocene-Pleistocene uplift of the dry valleys sector of the Transantarctic Mountains: A key parameter in ice-sheet reconstructions. Geology, 21: 841-844.

Wilch, T.I., Denton, G.H., Lux, D.R. and McIntosh, W.C., 1993b. Limited Pliocene glacier extent and surface uplift in middle Taylor Valley, Antarctica. Geogr. Ann., 75A: 331-351.

Yatsevich, I. and Honda, M., 1997. Production of nucleogenic neon in the Earth from natural radioactive decay. J. Geophys. Res., 102: 10291-10298.

Figure captions

Fig. 1 Map of the Dry Valleys area of the Transantarctic Mountains showing sampling sites for cosmogenic isotope analysis. Locations and $^{40}Ar/^{39}Ar$ ages for volcanic deposits are also shown.

Fig. 2 Oblique air photo showing the location of sampling sites 5/96 and 6/96 on the east flank of Mount Fleming at the head of Wright Valley. Sampling sites 50-52/95 and 56-57/95 are in Arena Valley. Locations of the glaciogenic Sirius Group deposits are also shown.

Fig. 3 Sample site 5/96 on the east flank of Mount Fleming at an elevation of ~2400 m. Note the thin snow cover at this highly exposed location. Wright Upper Glacier can be seen in the middle distance.

Fig. 4 Rectilinear slopes on the western side of Arena Valley, Quatermain Mountains. Free faces are evident above the rectilinear segment which terminates upslope in the dark dolerite sill. The location of samples 50-52/95 is marked by a cross.

Fig. 5 Site of sample 13/96 immediately to the east of Sollas Glacier, Taylor Valley. The sample site is indicated by the silhouetted figure on the left and the view is to the west across the Sollas Glacier and along Taylor Valley towards the Quatermain Mountains and Arena Valley (sample site 50-52/95). The dated lava-flow (arrowed) can be seen on the slope to the right resting on the lighter granitic bedrock. There is no evidence that this originally extended as far as the sample site.

Fig. 6 ^{21}Ne apparent exposure age for the analyzed samples plotted against the ratio of $^{3}He/^{21}Ne$ age illustrating the variable diffusive loss of ^{3}He.

Table 1 Sample and field data

Sample No.	Area	Location	Elevation	Lithology	Surface slope	Exposure geometry
50/95	Arena Valley	S77°46' E160°51'	1572 m	Arena sandstone	2°	Partially shielded
51/95	Arena Valley	S77°46' E160°51'	1572 m	Arena sandstone	0°	Partially shielded
52/95	Arena Valley	S77°46' S77°51'	1572 m	Arena sandstone	38°	Partially shielded
56/95	Beacon/Arena interfluve	S77°53' E160°44'	2050 m	Beacon sandstone	0°	Partially shielded
57/95	Beacon/Arena interfluve	S77°53' E160°44'	2050 m	Beacon sandstone	0°	Partially shielded
5/96	Mount Fleming	S77°33' E160°08'	2427 m	Beacon sandstone	0°	100% exposure
6/96	Mount Fleming	S77°32' E160°16'	2038 m	Beacon sandstone	0°	100% exposure
13/96	Lower Taylor Valley	S77°43' E162°38'	810 m	Granite	25°	Partially shielded

Table 2. He and Ne isotope data for Antarctic quartz samples.

Sample	Weight (mg)	^4He 10^{12} atoms g^{-1}	R/R_a	^3He_c 10^8 atoms g^{-1}	^{20}Ne 10^{10} atoms g^{-1}	$^{21}Ne/^{20}Ne$ (x 10^{-3})	$^{21}Ne_c$ 10^8 atoms g^{-1}
Rectilinear slopes							
50/95	263	9.80 ± 0.01	9.39 ± 0.1	1.28 ± 0.02	0.08 ± 0.001	6.25 ± 0.06	0.88 ± 0.01
51/95	257	107.1 ± 0.3	1.58 ± 0.1	2.36 ± 0.03	3.27 ± 0.01	10.41 ± 0.04	1.51 ± 0.03
52/95	320	9.77 ± 0.08	4.69 ± 0.06	0.64 ± 0.02	3.83 ± 0.02	8.37 ±0.04	2.11 ± 0.02
13/96	250	2.35 ± 0.01	0.65 ± 0.05	0.005 ± 0.001	1.31 ± 0.01	5.11 ± 0.06	0.38 ± 0.01
Plateau surfaces							
56/95	302	11.14 ± 0.03	25.1 ± 0.3	4.12 ± 0.45	3.45 ± 0.01	18.78 ± 0.06	5.65 ± 0.05
57/95	263	20.67 ± 0.04	1.75 ± 0.02	0.50 ± 0.01	3.19 ± 0.01	18.97 ± 0.08	5.22 ±0.05
5/96	278	9.05 ± 0.01	32.78 ± 0.7	4.13 ± 0.09	7.39 ± 0.02	11.27 ± 0.06	6.19 ± 0.04
6/96	288	46.6 ± 0.02	11.94 ± 0.14	7.75 ± 0.09	6.29 ± 0.02	10.46 ± 0.06	4.51 ± 0.04

$^3He/^4He$ (R) are expressed relative to the air ratio (R_a) 1.4 x 10^{-6}. See text for method of calculation of $^{21}Ne_c$ and ^3He. The quoted errors are those of individual measurements at the 1σ level. Abundance measurements have a reproducibility of ±1.5%.

Table 3. He and Ne isotope exposure age and denudation rate data for Antarctic quartz samples.

Sample	$^{3}He_{C}$ age (ka)	$^{21}Ne_{C}$ age (Ma)	$^{21}Ne_{C}$ denudation rate (m Ma^{-1})
Rectilinear slopes			
50/95	373	1.04	0.6
	± 4	± 0.01	± 0.006
51/95	687	1.79	0.35
	± 6	± 0.03	± 0.002
52/95	186	2.48	0.26
	± 2	± 0.02	± 0.02
13/96	11	0.61	1.02
	± 3	± 0.006	± 0.01
Plateau surfaces			
56/95	791	4.66	0.133
	± 9	±0.04	± 0.001
57/95	102	4.30	0.142
	± 1	± 0.04	± 0.002
5/96	647	3.90	0.159
	± 14	± 0.01	± 0.003
6/96	1,594	3.78	0.164
	± 19	± 0.01	± 0.001

Errors in exposure ages and erosion rates are errors propogated from experimental measurements. They do not include those from uncertainties from reproducibility of abundance measurements (±1.5%) and in production rates (± 20%; Niederman et al., 1994).

Summerfield *et al.* (1998a) - Figure 1

Summerfield *et al.* (1998a) - Figure 2

Summerfield *et al.* (1998a) - Figures 3 and 4

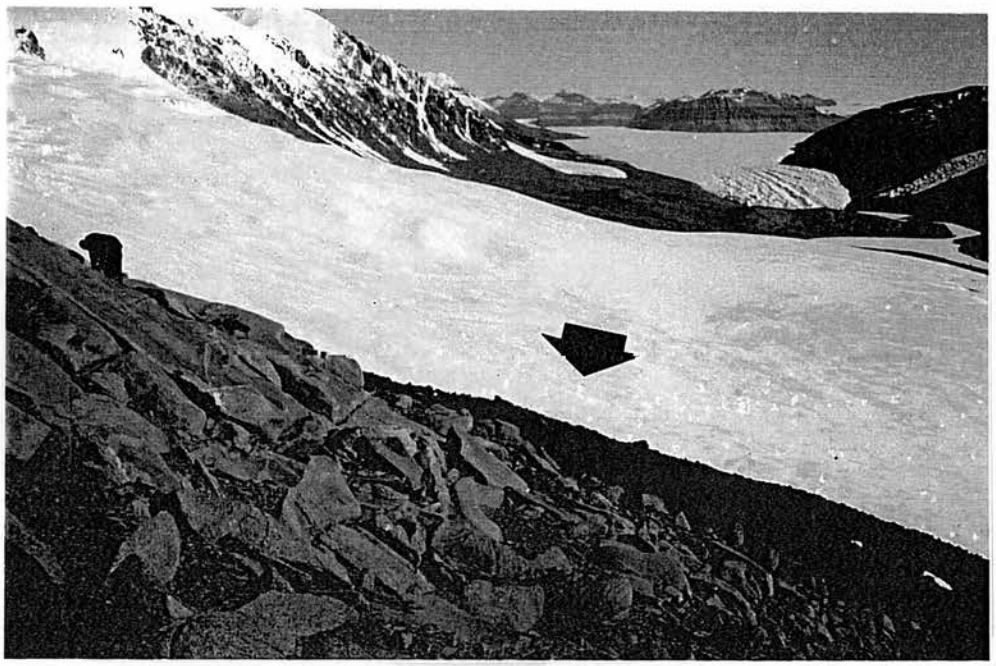

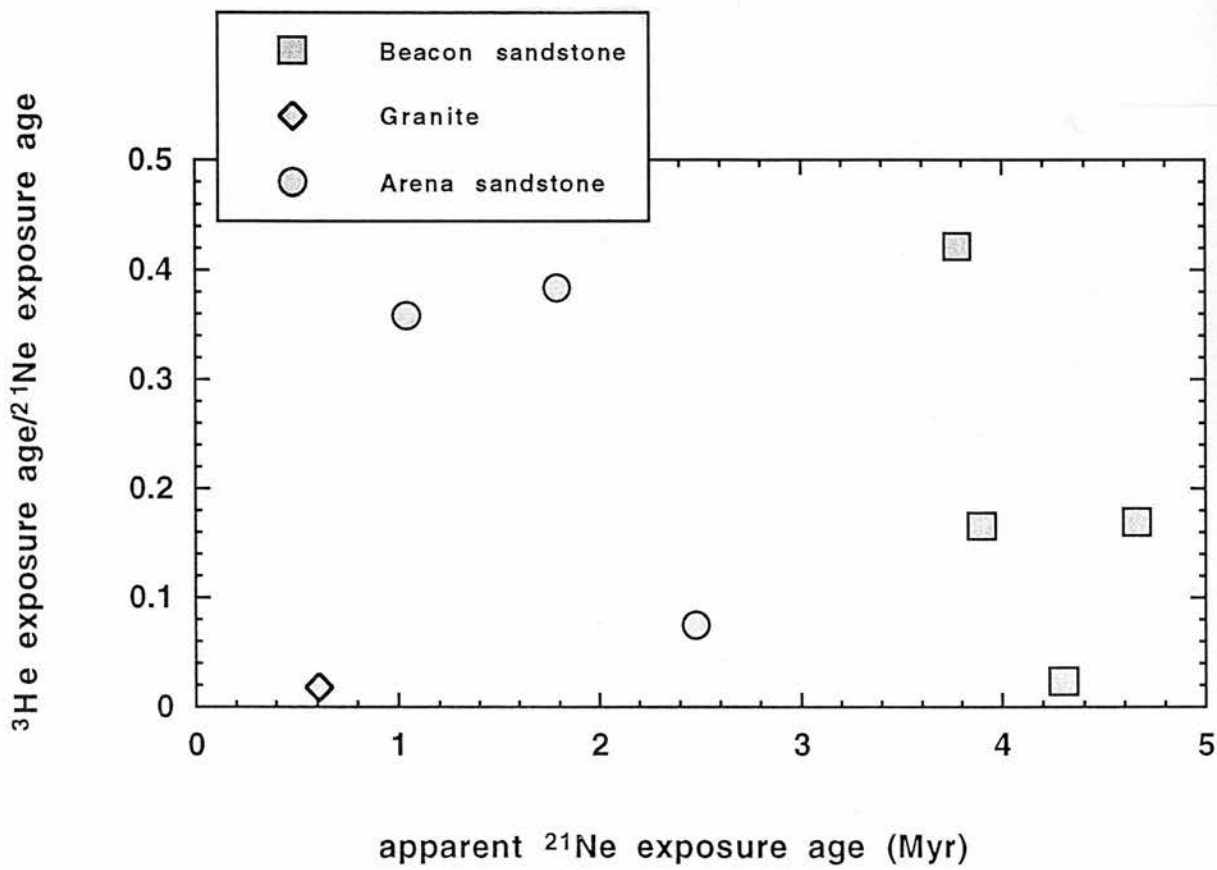

Summerfield *et al.* (1998a) - Figures 5 and 6

Cosmogenic isotope data support previous evidence of extremely low rates of denudation in the Dry Valleys region, southern Victoria Land, Antarctica

M.A. Summerfield [1], D.E. Sugden [1], G.H. Denton[2], D.R. Marchant [3], H.A.P.Cockburn [1] and F.M. Stuart [4]

[1] Department of Geography, University of Edinburgh, Edinburgh EH8 9XP, UK

[2] Department of Geological Sciences, Institute for Quaternary Studies, University of Maine, Orono, Maine 04469, USA

[3] Department of Earth Sciences, Boston University, 675, Commonwealth Avenue, Boston, Massachusetts 02215, USA

[4] Isotope Geosciences Unit, Scottish Universities Research and Reactor Centre, East Kilbride, G75 0QF, UK

Abstract

Quantitative estimates of denudation rates in different tectonic and climatic environments are of fundamental importance to an understanding of long-term landscape development. Little quantitative information is currently available on minimum denudation rates, although this is important in placing constraints on the maximum survival potential of individual landforms or erosion surfaces in terrestrial environments . The persistence for up to >15 Ma of a hyper-arid, polar climate in the ice-free Dry Valleys area of southern Victoria Land, Antarctica makes this a highly probable environment for minimum terrestrial denudation rates. $^{40}Ar/^{39}Ar$ dating constraints on the mimimum formation ages of individual landforms indicates generally little modification of even minor features over the past few million years. Relatively, the highest rates of denudation occur at low elevations near the Ross Sea coast. By contrast, rates of landscape change are exceedingly slow at elevations above ~1500 m in the western Dry Valleys where even landforms with a relief of a only a few metres have survived with minimal modification since the mid-Miocene. Measurements of *in-situ*–produced cosmogenic isotopes indicate that even on rectilinear slopes maximum denudation rates may be only ~1 m Ma^{-1}, with rates falling to <0.2 m Ma^{-1} at some locations on low relief surfaces at high elevation.

Introduction

Quantifying rates of denudation is a prerequisite to the comprehensive understanding of landscape evolution. Over the past decade a range of new geochronological techniques have been applied to the problem of rates of long-term landscape change and there are now increasing opportunities to compare this growing body of data with estimates of modern denudation rates based on sediment and solute load data (Summerfield & Hulton 1994). Although the data now available indicate that long-term, natural denudation rates can range up to ~10000 m Ma^{-1} in active orogenic belts, such as over parts of the Southern Alps of New Zealand (Tippett & Kamp 1995), the lower limit for denudation rates in terrestrial environments is rather poorly constrained. Obviously in some environments long-term deposition has occurred, and the net excess of sedimentation over denudation may persist over extensive areas for tens of millions of years in cratonic basins in continental interiors, such as the Kalahari Basin of southern Africa. However, quantitative data on mimimum rates of denudation in environments not subject to significant or persistent sediment accumulation are important because the idea of the 'age' of a landform or landsurface is predicated upon the notion of minimal modification by denudational processes since its creation.

The combination of persistent low temperatures and hyper-aridity suggests that the ice-free 'oasis' of the Dry Valleys area of southern Victoria Land, Antarctica is a prime candidate for an environment

that has experienced very low rates of denudation and extreme landscape stability. Previous work on tors, rock slopes and associated landforms in this region (Selby 1971, 1974) has indicated low rates of landscape change, an interpretation which echoed ideas of some of the early explorers of the Dry Valleys and adjacent ice-free areas within the Transantarctic Mountains (Priestley 1909; Taylor 1922). However, none of these studies was able to call upon an adequate body of geochronological data to support their interpretations of rates of landscape change which were derived largely from morphological and stratigraphic relationships in the landscape. Here we review a range of geochronological data which, in combination with information from morphological and depositional evidence, have provided quantitative estimates of rates of denudation and landscape change in the Dry Valleys region. We also show how data from cosmogenic isotope analysis can provide a means, hitherto unavailable, of constraining site-specific denudation rates in this extreme morphoclimatic environment.

Field setting

The Dry Valleys region consists of a number of ice-free, or partially ice-free, transverse valleys and intervening mountain ridges in the Transantarctic Mountains flanking McMurdo Sound in the Ross Sea embayment between 77°15'S and 77°45'S and 160°E to 164°E (Fig. 1). Inland lies the Polar Plateau formed by the East Antarctic Ice Sheet from which outlet glaciers have drained at various times in the past through the Dry Valleys. The majority of the 4000 km^2 ice-free area is accounted for by the Taylor, Wright and Victoria Valleys and the intervening 1500–2400 m high Asgard and Olympus Ranges. These transverse valleys cut across the compound escarpment that marks the Ross Sea margin of the topographic upwarp on the rift-flank uplift forming the Transantarctic Mountains.

Geological and tectonic setting

Exposed bedrock in the Dry Valleys region comprises a basement complex of Precambrian igneous and meta-igneous rocks overlain by gently dipping sandstones, siltstones and conglomerates of the Devonian–Triassic Beacon Supergroup. Both the basement and overlying sedimentary strata are intruded by dolerites of Jurassic age (Ferrar dolerites) which form extensive sills up to several hundred metres thick. Highly localized volcanic cones and ash deposits of late Cenozoic age are also extensively distributed across the region. The major structural components of the Transantarctic Mountains in the Dry Valleys area were established by asymmetric rifting in the Eocene, with the lower plate forming the Ross Sea Embayment and a combination of block-tilting and flexure in the upper-plate margin producing an upwarped rim to the extensive interior plateau and the modest inland dip observed in the Beacon Supergroup strata (Fitzgerald *et al.* 1986; Fitzgerald 1992).

Morphology of the Dry Valleys region

The Dry Valleys region is characterized by two major landscape components – high-elevation, low-relief surfaces, and rectilinear slopes (Sugden *et al*. 1995a). The high-elevation surfaces in general lie above an elevation of 1800 m and occur both as flat-topped ridges in the western sectors of the Asgard and Olympus Ranges and, more extensively, on the more elevated terrain between 2000 and 2400 m lying at the head of the Dry Valleys and separating them from the ice-cover of the Polar Plateau. Rectilinear slopes, typically at angles of 26°–37°, are prominent both on the flanks of the high surfaces adjacent to the Polar Plateau and on the sides of the Dry Valleys themselves. At higher elevations in the western sector of the Dry Valleys the rectilinear slopes lead up to strength-equilibrium free face slopes at angles of >60° and merge down slope into colluvium-mantled footslopes at an angle of around 18° (Selby 1971). At lower elevations in the eastern part of the Dry Valleys free faces are less common and the rectilinear slopes of adjacent valleys meet as sharp-edged interfluves. These rectilinear forms have been interpreted as Richter denudation-slopes by Selby (1971, 1974, 1993). They are cut in bedrock but partly covered by a thin veneer of generally coarse rock debris up to 1 m thick.

Present and past climates

The present climate of the Dry Valleys region is cold and hyper-arid. Mean annual temperatures at lower elevations in the central and eastern sectors of the valleys are around –20°C, although midday temperatures in summer may exceed +5°C for several days (Bull 1966; Schwerdtfeger 1984). The presence of active debris and mud flows, together with episodic flow in stream channels, attests to temperatures above 0°C below elevations of ~800 m under the present climatic regime. Meteorological data for higher inland locations are limited, but on the assumption of a lapse rate of 10°C km^{-1} mean annual temperatures at high elevations fringing the Polar Plateau and in the western Asgard and Olympus Ranges must drop to –30°C to –40°C (Schwerdtfeger 1984; Fortuin & Oerlemans 1990). Mean annual precipitation ranges from around 100 mm water equivalent near the coast to <10 mm at high elevations in the west, and this trend is mirrored by relative humidity which drops from around 75% immediately inland from the Ross Sea to as low as 5% on the Polar Plateau. Throughout the year strong, low humidity (5–60%) katabatic winds blow from the Polar Plateau, but during the summer they are largely confined to the western ends of the Dry Valleys and to the valley bottoms. Snow accumulation is sufficient to sustain small, cold-based glaciers which flow down the sides of Taylor, Victoria and Wright Valleys.

The systematic trend in climatic conditions in response to altitude and distance from the coast suggests three morphoclimatic zones based on temperature, precipitation, relative humidity and soil-moisture content (Marchant & Denton, 1996). In the coastal zone, with a mean annual temperature of ~−17°C and mean relative humidity of ~75%, there are active gelifluction terraces and lobes, streams, levées, debris and mud flows and subxerous soils. In the intermediate zone between ~40 and 55 km inland, where the mean annual temperature is ~−27°C and mean relative humidity is ~45%, there is little evidence of active slope processes, with streams, gelifluction lobes and debris flows being mostly confined to warmer north-facing slopes with more prolonged availability of liquid water on the surface and in the immediate substrate. Slope forms indicative of liquid water are essentially absent from the third morphoclimatic zone distributed across the elevated terrain of the western Dry Valleys in the Quartermain Mountains and the higher, western sectors of the Asgard and Olympus Ranges.

Late Cenozoic climates in the Dry Valleys region are a subject of dispute. According to one view, based primarily on the interpretation of Pliocene-age marine diatoms present in glaciogenic Sirius Group deposits located in the Transantarctic Mountains, the East Antarctic Ice Sheet experienced deglaciation in the early Pliocene (~4.5 Ma BP), with deglacial conditions probably continuing into the mid-Pliocene (Webb *et al*. 1984; Webb & Harwood 1991; Barrett *et al.* 1992; Harwood 1994). This model postulates the existence of seaways across the Wilkes-Pensacola Basin in the interior of Antarctica during this period, with these marine incursions providing the source of the diatoms found in the Sirius Group tills. Although it has been argued that such dramatic changes in the extent of the East Antarctic Ice Sheet could be achieved with a modest increase in temperature compared with the present (Webb & Harwood 1991; Harwood 1994), ice-sheet modelling studies indicate that temperatures 17-20°C above those of the present would be required to remove ice from the Wilkes-Pensacola Basin (Huybrechts 1993). Furthermore, there is a growing consensus that the marine diatoms that have been used to date the Sirius Group deposits are allogenic contaminants emplaced by aeolian deposition (Burckle & Potter 1996; Kellogg & Kellogg 1996), or possibly derived from fall-out from a bolide impact Gersonde *et al*., 1997), and that they are therefore not capable of constraining the age of deposition to the Pliocene.

A contrasting interpretation of the history of the East Antarctic Ice Sheet is that it has experienced long-term stability under a hyper-arid, polar climatic regime similar to that of the present for at least the past 15 Ma (Clapperton & Sugden 1990; Denton *et al.* 1993; Marchant *et al.* 1993a; Sugden *et al.* 1995a). This view is based on a range of evidence including marine stratigraphic data from the Southern Ocean (Kennett & Hodell 1993), modelling studies of ice-sheet dynamics (Huybrechts 1993), and morphological, stratigraphic and $^{40}Ar/^{39}Ar$ data from the Dry Valleys region and neighbouring areas (Denton *et al.* 1993; Marchant *et al.* 1993a; Marchant *et al.* 1996). Irrespective

of the veracity of these contrasting interpretations of the longer term climatic history of Antarctica, there is agreement that there has been remarkable climatic stability in the Dry Valleys area for the last 2–3 Ma, with only modest fluctuations in the extent of ice cover in the outflow and valley-side glaciers during this period. This morphoclimatic regime contrasts starkly with the large magnitude climatic fluctuations driven by glacial-interglacial oscillations that have characterized virtually all other morphoclimatic zones on Earth throughout the Quaternary.

Morphological and depositional evidence of rates of landscape change

The last few years have seen significant progress in the geochronometric dating of landforms in the Dry Valleys area and this has greatly enhanced our knowledge of the glacial history and long-term landscape evolution of the area (Denton *et al.* 1993). The main conclusion arising from this programme of landform dating is that a number of minor landforms, including small cinder cones, surficial forms associated with volcanic ash falls, raised marine features, and glacial forms, have survived without significant modification since the mid-Miocene. The implication of this is that surface geomorphic processes have operated at a very low level of activity over the past ~15 Ma. Here we collate observations on these various landforms and deposits in order to assess rates of landscape change; a summary of observations is presented in Table 1 and site locations are shown in Figure 1.

Cinder cones

In central Taylor Valley the glacially-moulded basement surface is dotted with a series of small cinder cones, typically 200 - 1000 m across, and associated lava flows (Wilch *et al*. 1993). Fourteen flows have been dated by whole-rock $^{40}Ar/^{39}Ar$ analysis, and have been shown to range in age from 1.5 - 3.9 Ma BP. Some of the cones retain their original form, whereas others have been partially eroded. In the latter cases, trails of dark volcanic rocks may be seen in the regolith extending 10^1–10^2 m directly downslope of the volcanic outcrop. There is insufficient evidence to quantify precisely the amount of denudation involved, but there is a relationship between the date of eruption and degree of erosion (Wilch *et al*.1993) . For example, the youngest 1.5 Ma old cone east of Rhone Glacier has essentially retained its initial form, whereas the older West Matterhorn cone at 3.0-3.5 Ma BP is heavily eroded (Table 1). The East Borns cone, with an age of 2.53 Ma BP, shows an intermediate degree of erosional modification. Within the altitudinal range of the cinder cones in Taylor Valley (209 to 828 m) denudational processes have been capable of eroding small cinder cones, but only slowly and over time scales of millions of years. A further point is that all the cones

have been erupted sub-aerially, and their age and altitudinal relationships demonstrate recent tectonic stability and constrain surface uplift in central Taylor Valleys to less than ~300 m in the last 2.57 Ma (Wilch *et al*. 1993).

Volcanic ash deposits

Volcanic ash falls, often of considerable antiquity, are intimately related to several types of deposit in the Dry Valleys area (Table 1). In Arena Valley at the western extremity of Taylor Valley there are two avalanche tongues where 30% of the matrix consists of volcanic ash (Marchant *et al.* 1993a). The unconsolidated ash is covered by a protective lag of pebbles, cobbles and boulders. One avalanche tongue, containing ash 11.3 Ma old, forms an elongated mound rising 3 m above the surrounding slope, the overall angle of which is 28°. In the western Dry Valleys area volcanic ashes are found at high altitudes in association with relict frost wedges (Marchant *et al*. 1993a,b), the ash having collected in the polygonal cracks much as snow does today (Fig. 2). The high concentration of ash and its uniform geochemistry, together with the bimodal grain-size distribution of glass shards, stratification by grain size, intact bubble vesicles and angular glass shards point to deposition by primary air falls with minimum subsequent disturbance. As the crack patterns have evolved, ash has become preserved in pockets in relict wedges (Fig. 3). Some 50 ashes associated with tills, slope regolith, lag deposits, lake sediments and, in one case, a moraine overlying relict glacier ice (Table 1), have been dated by $^{40}Ar/^{39}Ar$ single/multiple crystal analysis, the oldest yielding an age of ~15.0 Ma BP. In a number of other locations, such as in Wright, Arena and Nibelungen valleys, ashes ranging in age from 3.9 to 14.8 Ma BP have been located overlying old desert pavement surfaces (Table 1).

Various inferences concerning surface geomorphic processes can be drawn from this preservation of volcanic ashes dating back up to 15 Ma BP. For instance, it is evident that regolith, particularly at high altitudes, has undergone little weathering or transport since the mid-Miocene. This is particularly true of the ash-filled wedges which have retained their essential integrity for millions of years, thereby demonstrating that during this period there has been little disturbance or differential movement of the parent material in which they lie, be it till, slope regolith or moraine-covered glacial ice. This point is further supported by an avalanche tongue in the Arena Valley, which has retained its form on a slope of 28° for 11.3 Ma (Fig. 4). It follows from this that the rectilinear slopes on which the ashes are preserved must also be old. Volcanic ashes occur on valley floors and, in one case, in a lake deposit associated with a glacially-scoured rock basin (Table 1). The age and spatial extent of the ashes imply that the landsurface, at least at higher altitudes, is essentially relict

from pre–mid-Miocene times. In areas with a protective layer of regolith there has been minimal bedrock lowering in the last 15 Ma.

The preservation of landforms with which the ashes are associated is itself evidence of a remarkable degree of climatic stability at higher elevations in the Dry Valleys area since at least the mid-Miocene. Buried lag deposits reflect arid conditions as long ago as 14.8 Ma BP, while the presence of frost cracks to trap the ashes suggests that the temperatures have been typical of a cold polar climate since the mid-Miocene. In Beacon Valley at the head of Taylor Valley, the preservation of glacier ice beneath a thin moraine cover incorporating 8 Ma old volcanic ash deposits is difficult to explain unless a polar climate similar to that of today has persisted since this time (Sugden *et al.* 1995). The very freshness of the ash, which permits its dating, also demonstrates the lack of chemical weathering (Marchant *et al.* 1993b), and this, in turn, implies the absence over the past several million years of conditions significantly milder and moister than those of the present . In Arena Valley the clay content of ashes up to 11.3 Ma old is less than 5%, and this can be compared to a figure of 60% attained in just 50 ka under the temperate climate of New Zealand through highly active chemical weathering (Birrell & Pullar 1973). More generally, the lack of gelifluction lobes and terraces, rills and stream channels in dated Miocene and Pliocene deposits above ~1200 m in the far western Dry Valleys area demonstrates that the temperature and moisture conditions characteristic of lower elevations closer to the Ross Sea to the east have not extended into these high elevation areas over the past 15 Ma or so.

Raised marine features

Miocene and Pliocene raised marine deposits in the bottom of Wright Valley demonstrate slow rates of denudation even at low altitudes in the Dry Valleys region. The Jason glacio-marine diamicton occurs at an altitude of 3 to 250 m on the northern shore of Lake Vanda in Wright Valley, and $^{87}Sr/^{86}Sr$ dating of shell fragments demonstrates a late Miocene (9.5±1.5 Ma) age for this deposit. In the vicinity of Prospect Mesa, a few kilometres along the valley to the east, there is a shell fauna with $^{87}Sr/^{86}Sr$ ages of 5.5±0.4 Ma which, remarkably, is exposed in growth positions on parts of the present floor of the valley. The implication here is that the bed of a former fjord has survived since emerging from the retreating sea around 3.4 Ma ago (Hall *et al.* 1993), although there are some uncertainties surrounding the significance of these raised shell deposits for estimating rates of landscape change. The date of emergence is based on extrapolation from a marine core in an adjacent valley (Ishman & Rieck 1992) and Wright Valley fjord would have been isolated as a lake of unknown size and for an unknown duration before finally drying out. Indeed, the present Lake Vanda is a direct descendant of the isolated fjord and is known to have varied in extent sufficiently

to cover both sites on different occasions in the past. Furthermore, one cannot exclude the possibility that the fjord bed, including the *in situ* shells, was buried by sediment that has subsequently been eroded. Nonetheless, it remains clear that unconsolidated marine sediments have remained intact in the bottom of one of the larger of the Dry Valleys for ~9 Ma. Furthermore, the preservation of fragile shells in growth positions on the valley floor is consistent with minimal amounts of landscape modification over this period.

Glacial landforms

The modification of glacial landforms of known age can also be used to estimate rates of landscape change. For example, weathering has affected the walls of meltwater channels and associated potholes at an altitude of 1550 m in the Asgard Range (Table 1). Cavernous weathering forms are common on former glacial surfaces, and in places fine-grained sandstone beds have been exploited to form overhangs up to 4 m high (Sugden *et al.* 1991). This represents the sum of sub-aerial denudation in the > 13.6 Ma since the last warm-based glaciers overrode the mountains (Marchant *et al.* 1993b). Another example concerns Alpine IV moraines flanking the glaciers flowing into the side of Wright Valley at altitudes of 400-800 m. Ages for basalt clasts show the moraines to be over 3.7 Ma old and yet they retain their ridge form. There is evidence of some weathering; former upstanding boulders have been planed off and shattered and cavernously weathered, and ventifacts mantle the surface. Soils are oxidized to a depth of 0.42 m and contain visible salt horizons (Hall *et al.* 1993). Finally, one can point to the presence of Peleus Till in Wright Valley, whose upper feather edge is preserved on slopes of 25°–35°. This deposit is at least 3.8 Ma old, and could well be the equivalent of the Asgard Till which is at least 13.6 Ma old (Hall *et al.* 1993). The implication here is that surface geomorphic process acting over several million years have been unable to remove a till deposit from slopes of 25°–35° at an altitude of 1150 m in Wright Valley and that therefore rates of denudation have been extremely slow.

Denudation rate estimates from cosmogenic isotope data

The semi-quantitative estimates of rates of landscape change for the Dry Valleys area outlined above can be supplemented by denudation rates estimated from the accumulation of *in-situ*–produced cosmogenic isotopes in surface rock samples (Bierman 1994; Kurz & Brook 1994). A number of studies have previously reported denudation rate estimates for sites in the Dry Valleys and neighbouring ice-free areas in the Antarctic 'oasis' based on cosmogenic nuclide measurements. Nishiizumi *et al.* (1991), for example, have modelled maximum denudation rates over the past few

million years on the basis of measurements of the cosmogenic radionuclides ^{10}Be and ^{26}Al. Nine samples from Allan Nunatak (Allan Hills), located about 75 km north-west of northern limit of the Dry Valleys area, yielded denudation rates of 0.24 m – 1.31 m Ma^{-1} (mean = 0.65 m Ma^{-1}), while four further samples from Wright Valley gave a range of 0.54 m – 1.31 m Ma^{-1} (mean = 0.93 m Ma^{-1}). Somewhat lower denudation rates of 0.06 – 0.27 m Ma^{-1} over the past 2–3 Ma, based on cosmogenic ^{10}Be measurements, have been reported by Brook *et al.* (1995) for quartz arenite boulders and cobbles in glacial deposits in the Quartermain Mountains and Asgard Range. Extremely low maximum denudation rates based on cosmogenic ^{26}Al and ^{10}Be data have also been reported by Ivy-Ochs *et al.* (1995). Their samples from boulders in Sirius Group deposits on Table Mountain at the head of Ferrar Glacier and at Mount Fleming at the western end of Wright Valley, together with high-elevation outcrop samples of Beacon Supergroup sandstone, yielded denudation rates ranging only up to 0.7 m Ma^{-1}. Denudation rates of less than 0.1 m Ma^{-1} over the past several million years have been also revealed by measurements of the cosmogenic ^{21}Ne in pyroxene, quartz and whole-rock dolerite samples from Sirius Group tillites and associated bedrock from high-elevation sites in the Mount Fleming and Table Mountain areas (Bruno *et al.* 1997).

In order to supplement these data and provide estimates of denudation rates in contrasting morphological settings, we have measured cosmogenic ^{21}Ne in quartz in samples from both low relief, plateau surfaces and rectilinear slopes in the Dry Valleys. Four samples from *in situ* bedrock outcrops of Beacon Sandstone (Beacon Supergroup) were collected from sites on high-elevation (>2000m) surfaces in the western Dry Valleys – two from the eastern flank of Mount Fleming (C5, C6), and two from the flat-topped interfluve between Arena and Beacon valleys at head of Taylor Glacier (C56, C57). Three further samples (C50-52), of Arena Sandstone (Beacon Supergroup), were collected from a 36°–38° rectilinear slope in the Quatermain Mountains on the western side of Arena Valley, this site being selected because of its proximity to the ^{40}Ar/^{39}Ar-dated ash avalanche deposits described above. The final sample analyzed (C13) comprised exfoliating fragments of granite from a rectilinear slope in lower Taylor Valley adjacent to a ^{40}Ar/^{39}Ar-dated partially eroded pyroclastic and lava-flow deposit. Further details of sample locations together with documentation of analytical methods and procedures for calculating denudation rates are given elsewhere (Summerfield *et al.* in press).

Of the eight samples analyzed, the highest denudation rate recorded of 1.02 m Ma^{-1} over at least the past 1 Ma was from a rectilinear slope in lower Taylor Valley at an elevation of ~800 m (C13) (Fig. 1). All four samples from the high-elevation surfaces (>2000 m) in the western Dry Valleys display much lower rates of 0.135 – 0.165 m Ma^{-1} (over at least the past 4 Ma). Samples from the rectilinear slope on the western side of Arena Valley (C50-52) yielded intermediate denudation rates of 0.23 – 0.60 m Ma^{-1} (over the past ~2–4 Ma). These rates accord with the range of morphological

and stratigraphic evidence outlined above; in particular, the rates for the rectilinear slope in Arena Valley are compatible with the preservation of the nearby >11 Ma old ash avalanche deposit, and the somewhat higher rate for the lower Taylor Valley site is consistent with the partially degraded state of the adjacent 3.57 Ma old pyroclastic and lava-flow deposit (Wilch *et al*. 1993).

Discussion and conclusions

The diverse range of data collated here creates a coherent picture of extremely low rates of denudation of the order of 1 m Ma^{-1} or less over the past several million years in the hyper-arid, polar environment of the Dry Valleys region. Rates in the relatively warmer environments at lower elevations nearer the Ross Sea appear to be somewhat higher than those on the elevated surfaces above 1500–2000 m in the western sector of the Dry Valleys, presumably due to the seasonal presence of liquid water and more active physical and biological weathering. These rates can be compared with a much higher mean denudation rate for the Dry Valleys region of 40-100 m Ma^{-1} over the past ~50 Ma derived from fission-track thermochronology (Fitzgerald 1992).

Direct comparison with rates over the past few million years for other morphoclimatic and tectonic environments is problematic since the extreme stability of the Dry Valleys region and the resulting long-term preservation of landforms and deposits means that average denudation rates here apply to extensive periods of several millions of years. In more active environments such features survive for much less time and, consequently, rates based on the degree of modification of minor landforms and deposits apply to shorter periods. This situation also applies to data from cosmogenic isotopes, since they effectively measure the residence time of the top ~2 m of the earth's surface. Two of the few sets of comparable cosmogenic isotope data are the estimate of maximum denudation rates as low as 0.6 m Ma^{-1} for granitic domes in the arid Eyre Peninsula in South Australia (Bierman & Turner 1995), and the much higher rate of 5–11 m Ma^{-1} reported for volcanic ash-flow tuffs in New Mexico, USA (Albrecht *et al.* 1993).

Mean denudation rates for large drainage basins estimated from modern sediment and solute load data range from 5 m Ma^{-1} to 688 m Ma^{-1} and show that rates for the Dry Valleys area lie well below the average for low relief basins (Summerfield & Hulton 1994). Mean denudation rates for individual catchments may be as low as 1 m Ma^{-1} (Summerfield 1991), but these figures include large areas of net deposition, and thus underestimate local rates of denudation comparable to the site-specific rates provided by cosmogenic isotope analysis and the modification of minor landforms and deposits.

We have demonstrated how limited modification of a range of landforms and deposits in the Dry Valleys area whose age of is constrained by associated radiometrically dated volcanic rocks indicate very slow rates of denudation and landscape change in this hyper-arid, polar environment, probably for the past 15 Ma or more. Cosmogenic isotope analyses of surface samples provide additional quantiative data on denudation rates and indicate that over the past several million years these have ranged from around 1 m Ma^{-1} down to 0.1 m Ma^{-1} with the lowest rates occurring at high elevations inland where temperatures appear to be always too low for liquid water or biological activity to exist.

We conclude that rates of denudation of 0.1–1.0 m Ma^{-1} represent a minimum in terrestrial sub-aerial environments. At such low rates not only major landforms, such as erosion surfaces, but also minor forms are able to survive for several million years. In environments where liquid water is present for at least some period of time each year it is likely that long-term denudation rates will be above these values. Further applications of cosmogenic isotope analysis in a range of other environments should provide valuable constraints on long-term rates of landscape change and the survival potential of erosion surfaces and other landforms used to reconstruct landscape history.

Acknowledgements

Field support for much of the work reported here was provided by the U.S. Division of Polar Programs of the National Science Foundation through grants to the University of Maine and the Berkeley Geochemistry Center. The cosmogenic isotope was supported by the Natural Environment Research Council through a grant (GR3/9128).

References

Albrecht, A., Herzog, G. F., Klein, J., Dezfouly-Arjomandy, B. & Goff, F., 1993. Quaternary erosion and cosmic-ray-exposure history derived from ^{10}Be and ^{26}Al produced in situ – An example from Pajarito plateau, Valles caldera region. *Geology*, **21**, 551-554.

Barrett, P. J., Adams, C. J., McIntosh, C. J., Swisher III, C. C. & Wilson, G. S. 1992. Geochronological evidence supporting Antarctic deglaciation three million years ago. *Nature*, **359**, 816-818.

Bierman, P. R. 1994. Using in situ cosmogenic isotopes to estimate rates of landscape evolution: A review from the geomorphic perspective. *Journal of Geophyscial Research*, **99**, 13885-13896.

Bierman, P. & Turner, J. 1995. ^{10}Be and ^{26}Al evidence for exceptionally low rates of Australian bedrock erosion and the likely existence of pre-Pleistocene landscapes. *Quaternary Research*, **44**, 378-382.

Birrell, K. S.& Pullar, W. A. 1973. Weathering of paleosols in Holocene and late Pleistocene tephras in central North Island, New Zealand. *New Zealand Journal of Geology and Geophysics*, **16**, 687-702.

Brook, E. J., Brown, E. T., Kurz, M. D., Ackert, R. P. Jr, Raisbeck, G. M. & Yiou, F. 1995. Constraints on age, erosion, and uplift of Neogene glacial deposits in the Transantarctic Mountains determined from in situ cosmogenic ^{10}Be and ^{26}Al. *Geology*, **23**, 1063-1066.

Bruno, L. A., Baur, H., Graf, T., Schlüchter, C., Signer, P. & Wieler, R. 1997. Dating of Sirius Group tillites in the Antarctic Dry Valleys with cosmogenic ^{3}He and ^{21}Ne. *Earth and Planetary Science Letters*, **147**, 37-54.

Bull, C. 1966. Climatological observations in ice-free areas of southern Victoria Land, Antarctica. *American Geophysical Union Antarctic Research Series*, **9**, 177-194.

Burckle, L. H. & Potter, N. Jr 1996 Pliocene-Pleistocene diatoms in Paleozoic and Mesozoic sedimentary and igneous rocks from Antarctica: A Sirius problem solved. *Geology* **24**, 235-238.

Clapperton, C. M. & Sugden, D. E., 1990. Late Cenozoic glacial history of the Ross Sea embayment, Antarctica. *Quaternary Science Reviews*, **9**, 253-272.

Denton, G. H., Sugden, D. E., Marchant, D. R., Hall, B. L. & Wilch, T. I. 1993. East Antarctic Ice Sheet sensitivity to Pliocene climatic change from a Dry Valleys' perspective. *Geografiska Annaler*, **75A**, 155-204.

Fitzgerald, P.G. 1992. The Transantarctic Mountains of southern Victoria Land: The application of apatite fission track analysis to a rift shoulder uplift. *Tectonics*, **11**, 634-662.

Fitzgerald, P. G., Sandiford, M., Barrett, P. J. & Gleadow, A. J. W. 1986. Asymmetric extension associated with uplift and subsidence of the Transantarctic Mountains and Ross Embayment. *Earth and Planetary Science Letters*, **81**, 67-78.

Fortuin, J.P.F. & Oerlemans, J. 1990. Paramaterization of the annual surface temperature and mass balance of Antarctica. *Annals of Glaciology*, **14**, 78-84.

Gersonde, R., Kyte, F.T., Bleil, U., Diekmann, B., Flores, J.A., Gohl, K., Grahl, G., Hagen, R., Kuhn, G., Sierro, F.J., Völker, D., Abelmann, A. and Bostwick, J.A. 1997. Geological record and reconstruction of the late Pliocene impact of the Eltanin asteroid in the Southern Ocean. *Nature*, **390**, 357-363.

Hall, B. L., Denton, G. H., Lux, D. R. & Bockheim, J. R. 1993. Late Tertiary Antarctic paleoclimate and ice-sheet dynamics inferred from surficial deposits in Wright Valley. *Geografiska. Annaler*, **75A**, 239-267.

Harwood, D. M. 1994. The continuing debate on Pliocene Antarctic deglaciation. *In*: van der Wateren, F.M., Verbers, A.L.L.M. and Tessensohn, F. (eds) *LIRA Workshop on Landscape Evolution: A Multidisciplinary Approach to the Relationship Between Cenozoic Climate Change and Tectonics in the Ross Sea Area, Antarctica.* Rijks Geologische Dienst., Haarlem, 101-105.

Ishman, S. E. & Rieck, H. J., 1992. A late Neogene Antarctic glacio eustatic record, Victoria Land basin margin, Antarctica. *In*: Kennett, J. P. and Warnke, D. A. (eds) *The Antarctic Paleoenvironment: A Perspective on Global Change*. Antarctic Research Series, **56**, 327-347.

Ivy-Ochs, S., Schlüchter, C., Kubik, P. W., Dittrich-Hannen, B. & Beer, J., 1995. Minimum ^{10}Be exposure ages of early Pliocene for the Table Mountain plateau and the Sirius Group at Mount Fleming, Dry Valleys, Antarctica. *Geology*, *23*, 1007-1010.

Huybrechts, P. 1993. Glaciological modelling of the late Cenozoic East Antarctic Ice Sheet: Stability or dynamism? *Geografiska Annaler*, **75A**, 221-238.

Kellogg, D. E. and Kellogg, T. B. 1996. Diatoms in South Pole ice: Implications for eolian contamination of Sirius Group deposits. *Geology*, **24**, 115-118.

Kennett, J. P. & Hodell, D. A. 1993. Evidence for relative climatic stability of Antarctica during the early Pliocene: A marine perspective. *Geografiska Annaler*, **75A**, 205-220.

Kurz, M. D. & Brook, E. J., 1994. Surface exposure dating with cosmogenic nuclides. *In*: Beck, C. (ed.) *Dating in Exposed and Surface Contexts*. University of New Mexico Press, Alberquerque, 139-159.

Marchant, D. R. & Denton, G. H., 1996. Miocene and Pliocene paleoclimate of the Dry Valleys region, Southern Victoria land: a geomorphological approach. *Marine Micropaleontology*, **27**, 253-271.

Marchant, D. R., Denton, G. H. & Swisher, C. C.III, 1993a. Miocene Pliocene Pleistocene glacial history of Arena Valley, Quartermain Mountains, Antarctica. *Geografiska Annaler*, **75A**, 269-302.

Marchant, D. R., Denton, G. H., Sugden, D. E. & Swisher, C. C.III, 1993b. Miocene glacial stratigraphy and landscape evolution of the western Asgard Range, Antarctica, *Geografiska Annaler*, **75A**, 303-330.

Marchant, D. R., Denton, G. H., Swisher, C. C. III & Potter, N. Jr, 1996. Late Cenozoic Antarctic paleoclimate reconstructed from volcanic ashes in the Dry Valleys region of southern Victoria Land. *Geological Society of America Bulletin*, **108**, 181-194.

Nishiizumi, K., Kohl, C. P., Arnold, J. R., Klein, J., Fink, D. & Middleton, R. 1991. Cosmic ray produced ^{10}Be and ^{26}Al in Antarctic rocks: exposure and erosion history. *Earth and Planetary Science Letters*, **104**, 440-454.

Prentice, M.L., Bockheim, J.G., Wilson, S.C., Burckle, L.H., Hodell, D.A., Schlüchter, C. and Kellogg, D.E. 1993. Late Neogene Antarctic glacial history: evidence from central Wright Valley. In: J.P. Kennett and D.A. Warnke (eds) *The Antarctic Palaeoenvironment: A Perspective on Global Change* Antarctic Research Series, **56**, 207-250.

Priestley, R. E. 1909. Scientific results of the western journey. In: E.H. Shackleton *The Heart of the Antarctic* vol. 2, Heinemann, London, 315-333.

Schwerdtfeger, W., 1984. *Weather and Climate of the Antarctic*. Elsevier, Amsterdam.

Selby, M.J., 1971. Slopes and their development in an ice-free, arid area of Antarctica. *Geografiska Annaler*, **53A**, 235-245.

Selby, M.J., 1974. Slope evolution in an Antarctic oasis. *New Zealand Geographer*, **30**, 18-34.

Selby, M.J., 1993. *Hillslope Materials and Processes*. 2nd edn., Oxford University Press, Oxford.

Sugden, D. E., Denton, G. H. & Marchant, D. R., 1991. Subglacial meltwater channel systems and ice sheet overriding, Asgard Range, Antarctica. *Geografiska Annaler*, **73A**, 109-121.

Sugden, D.E., Denton, G.H. & Marchant, D.R., 1995a. Landscape evolution of the Dry Valleys, Transantarctic Mountains: Tectonic implications. *J. Geophys. Res.*, 100: 9949-9967.

Sugden, D. E., Marchant, D. R., Potter, N. L. Jr., Souchez, R. A., Denton, G. H., Swisher, C. C.III & Tison, J-L. 1995b. Preservation of Miocene ice in East Antarctica, *Nature*, **376**, 412-414.

Summerfield, M.A., 1991. *Global Geomorphology*, Longman, London.

Summerfield, M. A. and Hulton, N. J., 1994. Natural controls of fluvial denudation rates in major world drainage basins. *Journal of Geophysical Research*, **99**, 13871-13883.

Summerfield, M. A., Stuart, F. M., Cockburn, H. A. P., Sugden, D. E., Dunai, T.,
Marchant, D. R. & Denton, G. H. in press. Long-term rates of denudation in the Dry Valleys region of the Transantarctic Mountains, southern Victoria Land, Antarctica: Preliminary results based on *in-situ*–produced cosmogenic ^{21}Ne. *Geomorphology*.

Taylor, G. 1922 The Physiography of McMurdo Sound and Granite Harbour Region *British Antarctic (Terra Nova) Expedition, 1910-1913*, Harrison, London.

Tippett, J. M. & Kamp, P. J. J. 1995 Geomorphic evolution of the Southern Alps, New Zealand. *Earth Surface Processes and Landforms*, **20**, 177-192.

Webb, P. N. & Harwood, D. M., 1991. Late Cenozoic glacial history of the Ross Embayment, Antarctica. *Quaternary Science Reviews*, **10**, 215-223.

Webb, P. N., Harwood, D. M., McKelvey, B. C., Mercer, J. H. & Stott, L. D., 1984. Cenozoic marine sedimentation and ice-volume variation on the East Antarctic craton. *Geology*, **12**, 287-291.

Wilch, T. I., Denton, G. H., Lux, D. R. & McIntosh, W. C. 1993. Limited Pliocene glacier extent and surface uplift in middle Taylor Valley, Antarctica. *Geografiska Annaler*, **75A**, 331-351.

Figure captions

Fig 1 Morphological map of Beacon, Taylor and Wright valleys showing the main geomorphological features and locations of landforms and surficial deposits dated by association with volcanic deposits together with cosmogenic ^{21}Ne sample sites.

Fig. 2 Polygonal cracks in regolith in McKelvey Valley, central Dry Valleys picked out by snow. The polygons range from 5 to 15 m across.

Fig. 3 Volcanic ash preserved in a relict wedge in till, Beacon Valley.

Fig. 4 Volcanic ash avalanche tongue (arrowed) in Arena Valley ^{40}Ar/^{39}Ar dated at 11.3 Ma BP. Moraines associated with an enlarged Taylor Glacier have been deposited on the tongue without deforming or displacing it.

Table 1 Evidence demonstrating slow rates of landscape change

Location	Site/stratigraphy	Altitude (m)	Basis of dating	$^{40}Ar/^{39}Ar$ age (Ma)	Comment
	Cinder cones in Taylor Valley (Wilch et al., 1993)				
East Rhone	volcanic cone	671	whole rock basalt	1.5	intact pristine cone
East Borns	volcanic cone	587	" " "	2.53	partially eroded cone
West Matterhorn	volcanic outcrop	602	" " "	3.0-3.5	heavily eroded volcanic outcrop
East Matterhorn	volcanic outcrop	828	" " "	3.74	eroded volcanic outcrop
	Volcanic ash avalanches (Marchant et al., 1993a)				
Upper Arena Valley	ash avalanche tongue, 20 x 200 m in size	1380	sanidine; 3 crystals	6.4	deposit survived intact for 6 Ma. 1-1.5m lowering of surrounding, exposed Arena sandstone.
Lower Arena Valley	ash avalanche tongue, 50 x 350m in size, standing 3m proud of slope of 28°	1625-1650	sanidine; 3 crystals	11.3	preservation of avalanche tongue morphology on steep rectilinear slope for >11.3 Ma.
	Volcanic ash in unconsolidated tills and regolith (Marchant et al., 1993b)				
Nibelungen Valley	ash in wedge in weathered regolith at foot of rectilinear slope	1450	sanidine; 5 crystals	12.1	ancient sand wedge; regolith older than 12 Ma.; cold desert climate shown by existence of wedge.
Inland Forts, Asgard Range	ash in wedge in weathered till	1650	glass	13.6	till and rectilinear slope older than 13.6 Ma.; cold desert conditions.
Koenig Valley, Asgard Range	ash in wedge in till on valley floor	1800	sanidine; 5 crystals	13.6	Asgard till has survived on rectilinear slope for >13.6 Ma.; cold desert climate.
Nibelungen Valley, Asgard Range	ash in wedge	1600	sanidine; 10 crystals	15.0	till at base of rectilinear slope has survived for 15.0 Ma.; cold desert climate
Njord Valley, Asgard Range	grey, stratified with drop stones	1600	sanidine; 3 crystals	14.6	small pond deposit and bedrock hollow survived 14.6 Ma
	Volcanic ash above glacier ice (Sugden et al., 1995)				
Beacon Valley, Quartermain Mountains	ash in wedge overlying glacier ice	1380	sanidine; 14 crystals	7.9, 8.1	glacier ice >8 Ma old; persistent cold conditions for 78 Ma.

	Volcanic ash burying desert pavements				
West Central Arena Valley, Quartermain Mountains	ash overlies pavement and covered by regolith	1800	anorthoclase	4.3	minimal slope development in 4.3 Ma.; desert conditions at the time (Marchant *et al*, 1993a)
Nibelungen Valley, Asgard Range	ash overlies desert pavement at base of steep rectilinear slope; covered by till	1500?	sanidine	14.8	rectilinear slope older that 14.8 Ma.; desert conditions at the time (Marchant *et al*, 1993b)
Wright Valley between Hart and Goodspeed glaciers	ash overlies oxidised regolith; overlain by till	378-526	glass	3.9	minimum age of regolith on side of Wright Valley; desert conditions at the time (Hall *et al*, 1993)
	Preservation of raised marine deposits (Prentice et al., 1993)				
Central Wright Valley	glacio-marine Jason diamicton near Lake Vanda	3 - 250	$^{87}Sr/^{86}Sr$ on shell fragments	9 ± 1.5	fjord sediments have survived in valley bottom since Miocene
Central Wright Valley	shells in growing position on valley floor and in Prospect Mesa section	165	$^{87}Sr/^{86}Sr$ on *Chlamys tuftsensis*	5.5 ± 0.4	details of bed of fjord have survived for 5.5 Ma
	Modification of glacial landforms				
Sessrumir Valley, Asgard Range	meltwater channels and potholes	1550	association with ash-dated till deposits	>13.6	cavernous weathering and undercutting of 4m in >13.6 Ma (Sugden *et al.*, 1991).
Central Wright Valley	Alpine IV moraine ridges	400-800	whole-rock basalt	>3.7	weathered stones but ridge forms intact for over 3.7 Ma (Hall *et al.*, 1993)
Central Wright Valley	feather edge of Peleus till occurs on 25-35° slope	<1150	minimum age of till	>3.8	upper till limit survived on steep slope for over 3.8 Ma (Hall *et al.*, 1993)
	Deflation basins				
Arena Valley, Quartermain Mountains	basins in Altar and Arena sandstone. Largest 200 x 500m and 3m deep	1600-1700	stratigraphic association with ash-dated tills	>11.3?	fine-grained sandstone bedrock stripped by ice has eroded by 3m in >11.3 Ma (Marchant *et al.*, 1993a)
Asgard Range	basins in several valleys in Altar and Arena sandstone; basins 10-50m wide, up to 500m long and 1-10m deep.	1600-1800?	stratigraphic association with ash-dated tills	>13.6?	maximum rates of bedrock deflation of 10m in >13.6 Ma in fine-grained sandstone (Marchant *et al.*, 1993b)

Summerfield *et al.* (1998b) - Figure 1

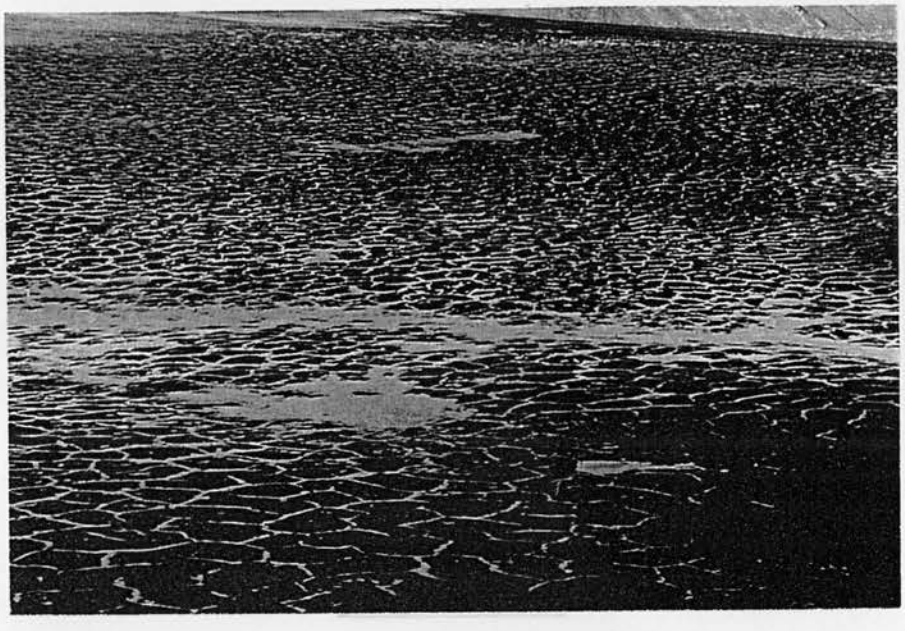

Summerfield *et al.* (1998b) - Figures 2 and 3

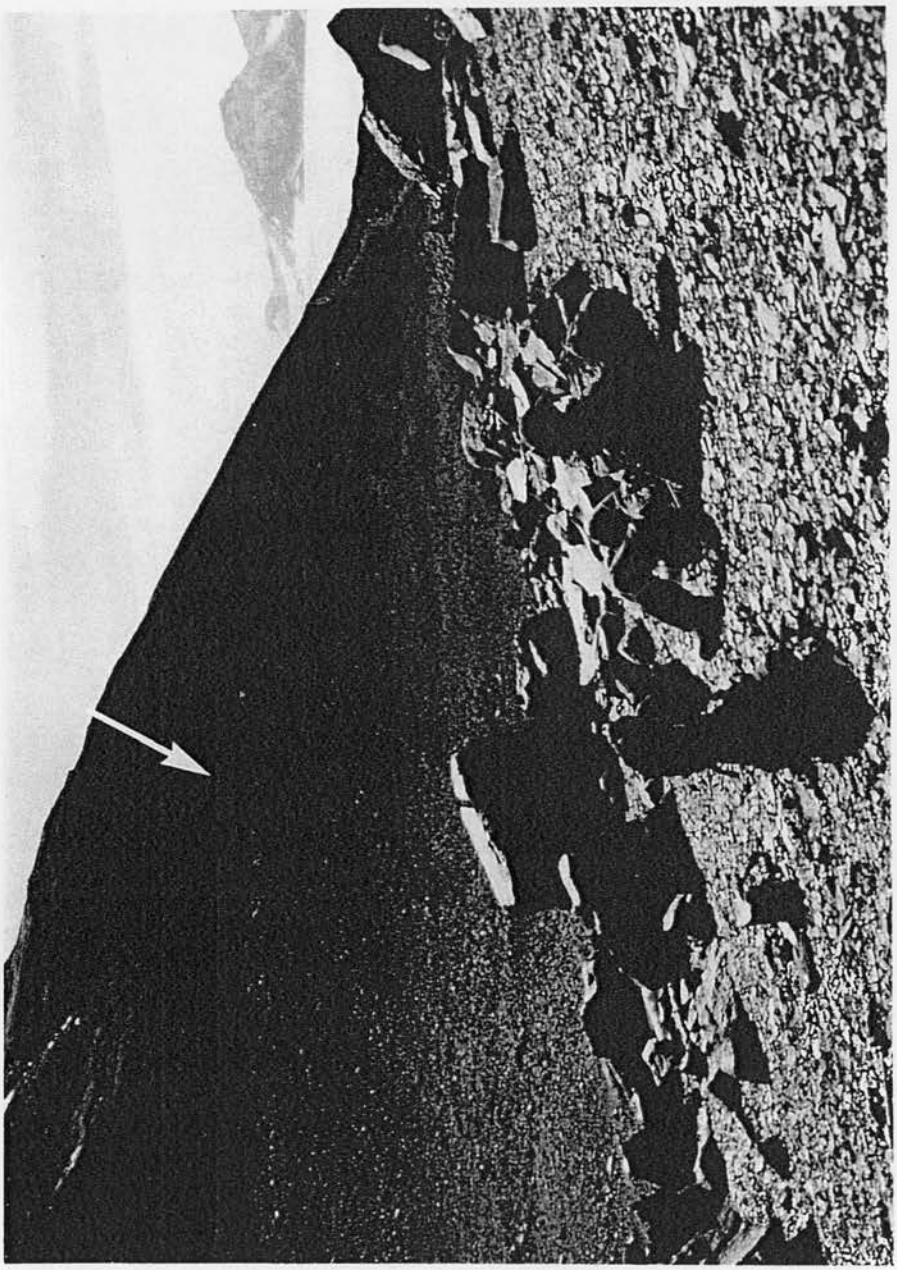

Summerfield *et al.* (1998b) - Figure 4